ENHANCEMENT OF SERVICE LIFE OF PRESTRESSED CONCRETE BRIDGE GIRDERS USING FRP COMPOSITES

By

Muhammad Shafqat Ali

Department of Civil Engineering and Applied Mechanics

McGill University, Montreal,

Quebec, Canada

March, 2014

A thesis submitted to McGill University in partial
fulfillment of the requirements of the degree of
Doctor of Philosophy.

ABSTRACT

This research aims at enhancing the service life of the prestressed concrete bridge girders, using fiber-reinforced polymer (FRP) composite shell on the lower flange to impede the ingress of deleterious elements into the concrete. The FRP shell would help to retard the resulting deterioration reactions and achieve more durable bridges for a considerably increased service life. The behavior of prestressed concrete bridge girders with FRP shells on the tension flange was investigated experimentally.

The flexural characteristics of FRP shell and concrete interface along with the effect of the steel reinforcement ratio were studied experimentally. This FRP shell was bonded around the lower part of the concrete beams, constructed with four different reinforcement ratios. The beam specimens with the FRP shell showed a significant enhancement in their strength, stiffness and energy absorption capacities, as compared with the associated control beams.

The flexural behavior of cast-in-place prestressed concrete beams with FRP shell was studied to examine the contribution of the bonded FRP shell to the strength, stiffness, ductility and energy absorption capacity of prestressed concrete beam specimens, for five different levels of prestressing. The initial cracking, yield and ultimate strengths of the beam specimens with FRP shell were significantly higher than those of the associated control beam specimens. The FRP shell and the prestressing force enhanced the strength and stiffness of the beams.

The long-term durability of the FRP shell to act as a barrier against ingress of aggressive elements, such as moisture and chlorides into the proposed FRP shell-concrete system, was examined experimentally in a preliminary manner. Detailed tests on concrete specimens reinforced

externally with FRP shells subjected to accelerated moisture and salt solution at control temperatures were performed. In addition, scanning electron microscopy (SEM) was used to determine the effects caused by aging, with time, temperature and chloride injection pressure. The FRP shell, acting as a barrier, showed a significant resistance against chloride ingress by significantly slowing down the chlorides ingress rate and the total amount of chlorides. For a prestressed concrete girder with an FRP shell, the accumulated time for chloride penetration and reaching the level of prestressing steel strands was predicted to be more than 135 years. These results suggest that the FRP shell is quite effective in improving the durability characteristics of prestressed concrete girders and can significantly extend their service life.

RÉSUMÉ

Cette recherche vise à améliorer la durée de vie des poutres de pont en béton précontraint à l'aide de coquilles de composite de polymères renforcés de fibres (FRP) appliquées à la semelle inférieure pour empêcher l'infiltration d'éléments nocifs dans le béton. La coque en FRP permettrait de retarder les réactions de détérioration et de réaliser des ponts plus durables ayant une durée de vie considérablement accrue. Le comportement de ces poutres de a été étudié expérimentalement.

Les caractéristiques en flexion de la coquille en FRP et de son interface de béton ainsi que de l'effet du pourcentage d'armature d'acier ont été étudiés expérimentalement. La coquille en FRP a été collée autour de la partie inférieure de poutres béton construites avec quatre pourcentages d'armature. Les spécimens de poutres avec la coquille de FRP ont montré une amélioration significative dans leurs résistances, rigidités et capacités d'absorption d'énergie par rapport aux poutres sans coquilles.

Le comportement en flexion de poutres de béton précontraint coulées en place avec la coquille de FRP a été étudié afin d'examiner la contribution de la coquille à la résistance, rigidité, ductilité et capacité d'absorption d'énergie pour cinq pourcentages de précontraintes. La limite de fissuration, la limite d'élasticité et la limite ultime des spécimens avec FRP étaient sensiblement supérieures à ceux des spécimens sans coquille. La coquille en FRP et la force de précontrainte a amélioré la résistance et la rigidité des poutres.

La contribution à la durabilité à long terme de la coquille de FRP contre les infiltrations d'éléments agressifs dans la coquille et le béton, tels que l'humidité et les chlorures, a été étudiée

expérimentalement de façon préliminaire. Des tests accélérés sur des échantillons de béton renforcés extérieurement avec des coquilles de FRP ont été effectuées en les soumettant à l'humidité et une solution saline à température contrôlées. La microscopie électronique (SEM) a aussi été utilisée pour déterminer les effets du vieillissement par rapport au temps d'exposition, à la pression d'injection, à la température et aux chlorures. La coquille de FRP, agissant comme une barrière, a augmenté significativement la résistance contre la pénétration des chlorures en réduisant significativement le taux de pénétration des chlorures et de la quantité totale d'ions chlorure. Pour une poutre en béton précontraint avec une coque en FRP, le temps total pour que les ions chlorure atteignent les câbles d'acier de précontrainte est estimé à 135 ans. Ces résultats suggèrent que la coquille de FRP est très efficace pour améliorer la longévité des poutres en béton précontraints et peut allonger considérablement leur durée de vie.

ACKNOWLEDGEMENTS

The author is grateful to Allah, the most gracious and merciful, for enabling him to complete this research program.

The author wishes to express his greatest gratitude to his both supervisors, Professor Saeed Mirza, Department of Civil Engineering and Applied Mechanics and Professor Larry Lessard, Department of Mechanical Engineering, McGill University. I am thankful to both my supervisors and have had a distinct honour working with them.

I would like to thank Professor Mirza for his everlasting encouragement, extensive guidance and support, and precious advice throughout my research program at McGill University. I feel greatly honoured that I was supervised by such a great and outstanding educator, visionary engineer, and dedicated and passionate infrastructure professional. I am thankful to him for being not only my best teacher ever and an outstanding supervisor but also a friend. I am also thankful to Professor Mirza because he taught me how to 'think' critically and 'write'.

The special involvement of Professor Lessard in the research activities by guiding and helping me in my research program, along with his knowledge and expertise in FRP composite materials, and valuable support by using his Structural Composite Laboratory, are gratefully acknowledged.

The author wishes to express his thankfulness to Professor Yixin Shao, Department of Civil Engineering and Applied Mechanics, McGill University, for his input and valuable suggestions to the research program.

The author is would like to thank BPDL International and their staff, specially Mr. Lino Pansieri (VP) and Guy Tremblay (Technical Director), for their generous donation of the prestressing strands and other accessories.

The author would like to thank Dr. M. Ehsani, President of QuakeWrap, Inc., for providing materials for FRP composite shells.

The author wishes to thank his parents and siblings for their support and encouragement during the course of this work.

I would like to thank Mrs. Brenda Silva-Mirza for her encouragement and appreciation throughout this research program.

I would like to thank my colleagues Ms. Emilie Hudon, Dr. Muhammad Sagheer Aslam, and Mr. Mani Balazadeh Minouei for all their help in the laboratory and moral support during this research. Also, sincere thanks and appreciation goes to Ms. Emilie Hudon for her assistance in translating the abstract into French.

The cordial assistance offered by the technical staff, noticeably Mr. Gerard Bechard, Mr. John Bartczak, Mr. Marek Pryzkorski, Mr. Ronald Sheppard, Dr. Bill Cook and Mr. Jorge Sayat in the Department Civil Engineering and Applied Mechanics at McGill University is thankfully acknowledged.

I would like to thank Ms. Monica Cornelia for her encouragement and assistance during this research work tenure.

Special thanks to Dr. Monica Nelea from Ecole Polytechnique, Montreal, Quebec for her assistance in SEM characterization of the FRP composites.

Finally, the author is also grateful for the financial support from the National Sciences and Engineering Research Council of Canada (NSERC) towards this research program and the McGill Engineering Doctoral Award (MEDA) to the author.

TABLE OF CONTENTS

LIST OF FIGURES

LIST OF TABLES

CHAPTER 1 INTRODUCTION

1.1 Introduction

Sustainable and durable civil infrastructure facilities, including bridges, require careful consideration during all project phases, such as planning, design (with diligent choice of materials and construction techniques), construction, maintenance, operations, repair and rehabilitation, and finally decommissioning and disposal of the debris at the end of their stipulated service life and beyond (Mirza 2013). Bridges are vital components of modern civil infrastructure; they are generally the most expensive part of the system. Prestressed concrete girder-reinforced concrete deck bridges are the most common type of bridge superstructure used presently; this form of construction is considered sufficiently durable and serviceable, provided it is adequately protected against various types of aggressive environments. Some of the present national codes and standards relate bridge durability directly to the severity of exposure to aggressive environments (JSCE 1997; ESCC 2005; CHBDC 2010). Reinforced concrete member(s) protected against aggressive environments can be sustainable and durable (Sarja and Veskari 1996; Mirza 2006). Durability of prestressed concrete girders can be enhanced by eliminating, or avoiding the various deterioration reactions, and/or by providing a multiple barrier protection against them, including protective coatings on steel, concrete cover to the reinforcement, and external protective coatings or barriers on the concrete surfaces.

New trends in construction of bridges involve innovations in the materials used, especially with application of fiber-reinforced polymer composites (FRPs). Current research has focussed on new durable and sustainable construction materials, with high strength and reliability, minimum flaws,

and easy applications in design, construction and maintenance (Mufti *et al.* 1996, GangaRao *et al.* 2007; Konecny 2007; Mufti 2007, Elmahdy *et al.* 2008; Wu and Shao 2008; Rosenboom *et al.* 2009). For the past two decades, application of FRPs for strengthening, rehabilitation and retrofitting, or construction of new bridges has become a recommended efficient solution for concrete bridges (Wu *et al.* 2003; Mukherjee and Arwikar 2007; Rosenboom *et al.* 2009; Zhuo *et al.* 2009). The Canadian Highway Bridge Design Code (CSA-S6-10) introduced a complete section (Section 16) dealing with the use of FRPs in bridges. Applications of FRPs can be classified into three main groups: rehabilitation of existing bridges, construction of new bridges and use of FRP composite profiles (sections) for new structural members of bridges.

The FRPs provide similar or superior mechanical, and chemical properties compared with conventional materials (steel, wood); however, the thermo-chemical properties of FRPs gradually deteriorate during their service life (Mufti *et al.* 2005,Subramaniam *et al.* 2007; Walker and Karbhari 2007; Brant 2008; Aldajah *et al.* 2009; Saadatmanesh *et al.* 2010; Benzarti *et al.* 2011). There are contradictory data regarding durability of FRPs from a variety of sources that may not be well understood by practicing engineers. These contradictions on durability of FRPs may be related to the reporting of the data, without adequate details of the materials used, processing techniques, and changes in the properties of material systems with time. Therefore, long-term durability of FRPs used in civil infrastructure and the development of an appropriate methodology capable of dealing with these materials in a variety of environments must be addressed (Karbhari 2007). Degradation and deterioration mechanisms of FRPs can result from the severe aggressive environment, exposure to moisture, high temperature (including fire), ultraviolet radiation, fatigue,

and creep. Figure 1.1 presents different factors which can influence the durability of the FRP-concrete system.

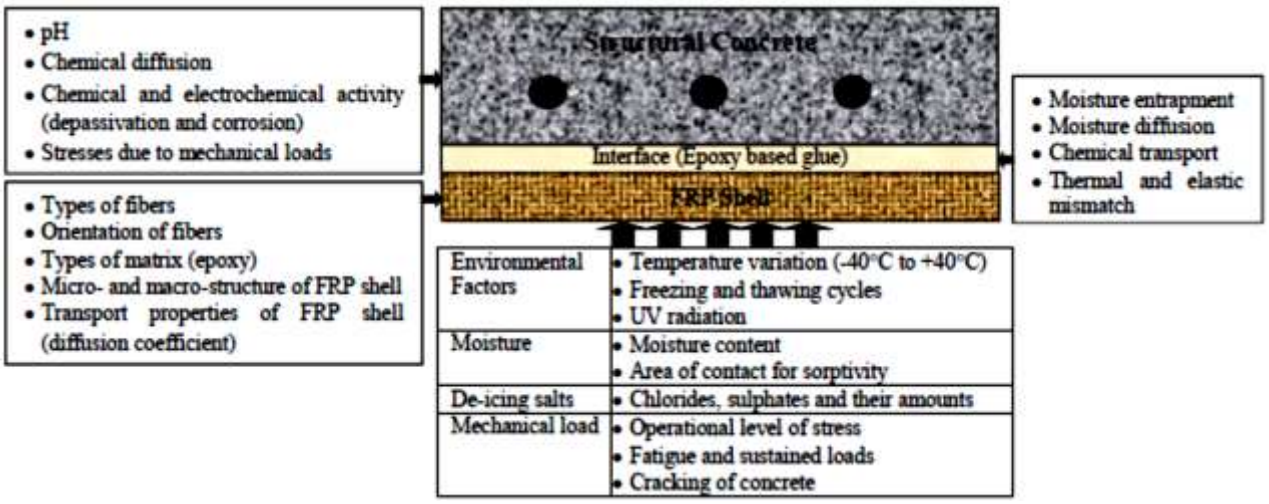

Figure 1.1 Influence of aggressive environment on FRP-reinforced structural concrete (fib 2001)

Barrier membranes are widely used by industries, such as food packaging, mining, paint and petroleum refining, to preserve contents or prevent degradation. The effectiveness of such barriers is gauged by their ability to prevent penetration and transmission of deleterious materials, which is typically characterized by the resistance against diffusion offered by the barrier material; effective barriers have small diffusion coefficients.

Several investigations confirmed that the rate of deterioration slowed down significantly when the FRP composite materials were used externally in reinforced concrete structural members (Mufti *et al.* 2005, Sheikh *et al.* 1997; Berver *et al.* 2001). Diffusion of chloride ions into the concrete and on to the reinforcing and prestressing steel level, results in the depassivation of the protective passive layer on the steel rebar, followed by the electrochemical reactions in the presence of oxygen and moisture, and subsequently corrosion of reinforcing and prestressing steel. The FRPs

can serve as a barrier to slow down the corrosion of reinforcing steel by preventing or slowing down the ingress of deleterious materials, such as chlorides, moisture and CO_2 (Figure 1.1).

1.2 Problem Statement

In cold climates, prestressed concrete girder-reinforced concrete deck bridges can deteriorate principally from moisture (wetting and drying cycles), freezing and thawing cycles, corrosion of the reinforcing and prestressing steel, alkali- aggregate reactivity, sulphate attack and other physical, mechanical, and chemical causes. Combination of these deterioration mechanisms results in serious durability problems in concrete bridges, and inhibits achievement of the code-specified design service life of 75 years (CHBDC 2010). Figure 1.2(a) shows the severely deteriorated exterior prestressed concrete girder of the Champlain Bridge in Montreal. This deterioration took place after only 28 years of service life of the bridge. Based on inspection of bridges operating in aggressive environments, the surface of concrete around the lower flange on the girders is more susceptible to deterioration due to corrosion of prestressing steel in comparison with other parts of the girders.

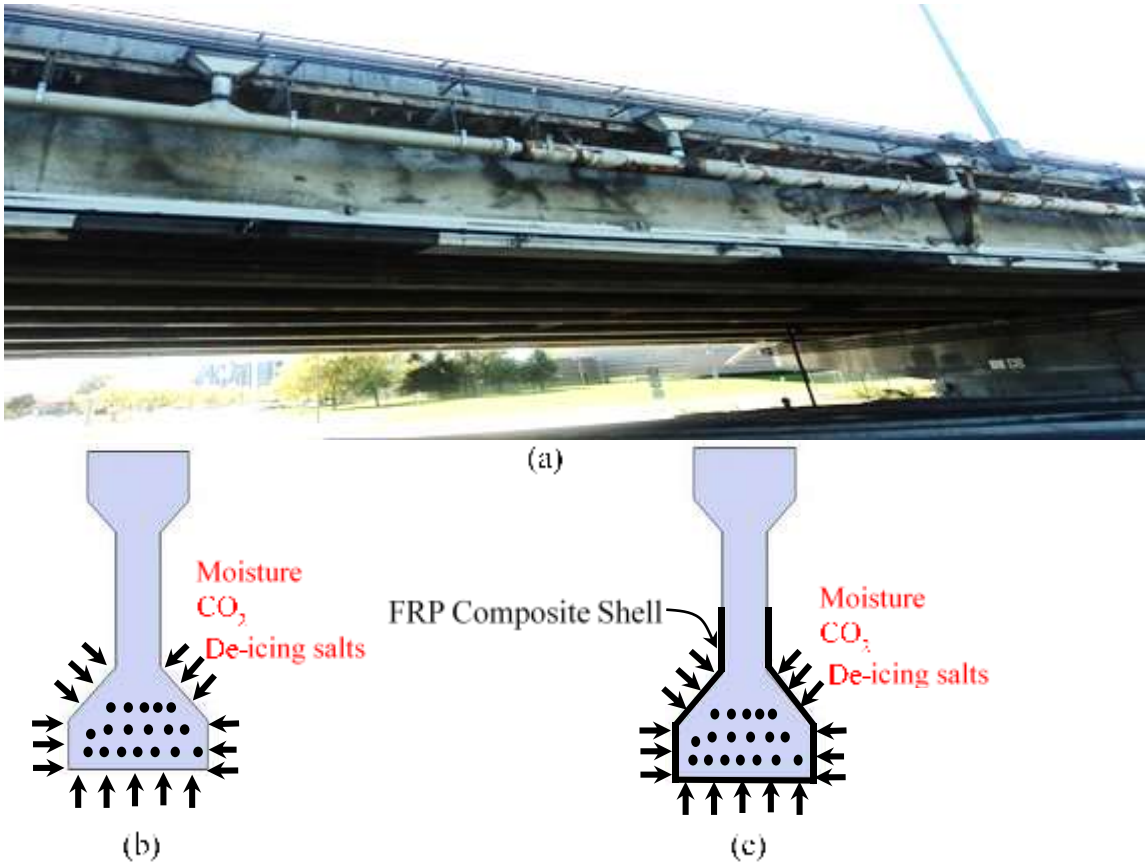

Figure 1.2 (a) Deteriorated prestressed concrete girder of the Champlain Bridge, Montreal (b) cross-section of prestressed concrete girder with ingress of harmful elements through permeable concrete (c) cross-section of prestressed concrete girder with an FRP shell on the lower flange

This research program was aimed at enhancing the durability of prestressed concrete girders by inhibiting (fully, or partially and considerably slowing down) the ingress of harmful elements, such as moisture, CO_2, chlorides (from de-icing salts), by providing an additional protective barrier, consisting of an exterior FRP composite layer (Fig. 1.2(c)) surrounding the bottom flange of the prestressed girder, which houses most of the prestressing tendons. Besides acting as "stay-in-place" formwork during the pre-casting operations, this FRP shell could assist with concrete confinement by wrapping and enhancing the member flexural and shear strengths.

1.3 Research Objectives

To evaluate the contribution of an FRP composite shell to structural strength and overall behaviour of a prestressed concrete bridge girder, this study focuses on the following objectives:

- The behaviour of hybrid FRP composite laminates.
- The bond characteristics between the FRP shell and cast-in-place concrete before and after prestressing.
- The overall behaviour of simple reinforced and prestressed concrete beams with FRP composite shell.
    - To establish construction procedures
    - To evaluate strength and stiffness characteristics
- Evaluation of durability of the proposed system for extended service life using a multiple barrier technique.

1.4 Methodology

Application of FRP composite materials to new prestressed concrete construction is a relatively new area of research with very limited information available in the literature; however, knowledge of prestressed concrete itself is well established. Evaluation of effectiveness of FRP composite shell in prestressed concrete construction includes the determination of material characteristics, their interaction at different load levels, and their durability against aggressive environment. The research program involved the following activities:

1. Selection, preparation and testing of materials for mechanical properties and durability of concrete, prestressing steel, and FRPs, including the various mechanical and durability tests.

2. An experimental program to investigate bond characteristics between FRP shell and freshly laid concrete substrate (with and without prestressing), which included the double-lap bond tests on concrete prisms and simple prestressed tension concrete members with externally-bonded FRP composite laminates

3. An experimental study of flexural characteristics of FRP composite shell-concrete system along with the actions at the FRP-concrete interface and effect of the steel reinforcement ratio.

4. The flexural and shear behaviours of FRP composite shell-reinforced prestressed concrete bridge girders.

5. Evaluation of durability of the proposed FRP shell and the entire FRP-concrete system. A preliminary research work aimed at enhancing the durability of prestressed concrete girders by inhibiting the ingress of harmful elements, such as moisture, chlorides (from de-icing salts), by provision of an additional protective FRP composites shell barrier.

1.5 Scope of Research Work

This thesis consists of eight chapters. Chapter 1 summarily introduces the use of FRP composite materials, problem statement, research objectives, scope of the study, and the layout of the thesis.

Chapter 2 reviews the various reinforcing fibers, epoxy resins and the processes used to manufacture FRPs. It also reviews some aspects of durability pertaining to the use of FRPs in

different civil infrastructure applications. Degradation and deterioration mechanisms of FRPs due to severely aggressive environment, exposure to moisture, ultraviolet radiation, fatigue, creep, are discussed briefly. The applications of FRPs can be classified into three main groups: application of FRPs to existing bridges, application of FRPs as reinforcement in construction of new bridges and FRP composite profiles (sections) for new structural members of bridges.

Chapter 3 presents the details of selection and preparation of materials used in the experimental program and the results of the double-lap bond tests on concrete prisms with externally-bonded FRP composite laminates.

In Chapter 4, the bond at the FRP composite shell and prestressed concrete interface was studied experimentally. Simple tension specimens, consisting of prestressed concrete prisms with externally-bonded FRP composite laminates, using pre-glued aggregates to the FRP composite laminates, with five levels of prestressing, were prepared and tested, and the test results were analysed.

The flexural characteristics of FRP composite shell-concrete system were studied experimentally along with the actions at the FRP-concrete interface and the effect of the steel reinforcement ratio. The results are analysed and presented in Chapter 5.

Chapter 6 describes the flexural and shear behaviours of FRP composite shell-reinforced prestressed concrete bridge girders.

Chapter 7 presents results of some preliminary research work aimed at enhancing the durability of prestressed concrete girders by inhibiting the ingress of harmful elements, such as moisture, chlorides (from de-icing salts), by provision of an additional protective FRP composites shell

barrier. The research results were used to predict long-term diffusion of chlorides into the system, and to estimate the service life of prestressed concrete girder with FRP composite shell.

Finally, Chapter 8 presents the summary and conclusions of this study, along with some recommendations for future research.

CHAPTER 2 LITERATURE REVIEW

2.1 Introduction

Prestressed concrete bridges are commonly used in modern transportation systems because they are considered to be more durable and serviceable as compared with other bridge types, provided that they are properly maintained and protected against various aggressive environments. As mentioned earlier, the deterioration manifested in different bridge components, such as deck slabs and girders, can range from superficial surface problems to significant disintegration of the concrete, resulting principally from wetting and drying, and freezing and thawing cycles, corrosion of reinforcing and prestressing steel, alkali- aggregate reactivity, sulphate attack and other physical, chemical, mechanical and biological deterioration mechanisms. Past experience has shown that deterioration of prestressed concrete bridges normally starts within first 15 to 20 years of service, resulting mostly from shortcomings or flaws in design, materials, construction and maintenance. It is not possible to completely eliminate the various deterioration mechanisms; however, they can be mitigated considerably by careful design for service life performance of the system, an appropriate choice of materials, high quality construction techniques and regular preventive and corrective maintenance (Mirza 2006).

Fiber-reinforced polymer composites (FRPs) have played a significant role in structural engineering applications (Karbhari and Zhao 2000, Mufti *et al.* 2005). The use of FRP has been studied extensively over the past two decades, as reinforcement in new concrete bridges, as an alternative for conventional steel reinforcing bars and prestressing tendons, and also for strengthening and rehabilitation of existing deteriorated concrete bridges.

The FRPs are an attractive alternative as a construction material because of several advantages over other conventional materials, such as structural steel, concrete, wood and others, because of their high specific stiffness and strength characteristics, low density, corrosion resistance, and durability against aggressive environments. Designers can improve or alter mechanical or other properties of FRPs, using different types of fibers and available matrices, according to the nature and requirements of the project. In addition, a wide variety of manufacturing processes enable fabrication of FRPs under highly controlled conditions, which results in very precise dimensional tolerances for pultruded FRP members and reinforcing bars. However, FRPs have a few drawbacks, such as their high cost, lack of ductility, relatively poor shear resistance, susceptibility to deformation under long-term loads, UV degradation, photo-degradation from exposure to light, poor resistance to fire and high temperatures, moisture effects and other durability related-issues, lack of practice-oriented design codes, guidelines and standards, and a general lack of awareness among practicing engineers (Meier *et al.* 1995; Homam 2000; Bank 2006; GangaRao *et al.* 2007; Karbhari 2007); these drawbacks have caused hesitation in their wider use in civil engineering applications.

Rebuilding of new infrastructure facilities and rehabilitation of ageing and severely deteriorated infrastructure presents a tremendous opportunity and challenge for the use of FRPs in various applications. The knowledge of available types of fibres, matrices, micro- and macro-structure, their mechanical properties, and interaction with an aggressive environment is quite important. There are several text books, technical papers and reports, and data sheets which detail the properties and uses of FRPs (Keller 2003; ACI-440 2004; Mufti *et al.* 2005, Bank 2006; GangaRao *et al.* 2007; Karbhari 2007).

2.2 Fiber-Reinforced Polymer Composites (FRPs)

Over the past two decades, there have been significant developments in the use of FRPs in civil engineering applications, for example, maintaining and upgrading of existing infrastructure facilities, such as buildings, bridges, transmission lines, and water supply and sewer lines. FRPs are also used in aerospace and automotive industries (Karbhari 2007).

2.2.1 Constituent Materials

Composite materials are commonly formed by combining two distinct phases, continuous reinforcing fibers and a polymeric matrix. Reinforcing fibers have high strength and stiffness with a relatively low density as compared with the matrix. Fibers define the mechanical properties of the material and act to resist the applied loads, while the function of the matrix is to transfer the loads to the fibers, protect them from damage and to control the setting properties of the FRP composite.

2.2.1.1 Reinforcing Fibers

The reinforcement component of FRPs consists of a number of individual long micro-fibers which constitute about 40 to 65% of the total volume of the material. There are three main types of fibers in structural engineering applications: glass, carbon and aramid fibers. The principal properties of the various types of fibers are summarized in Table 2.1.

Table 2.1 Approximate mechanical properties of common reinforcing fibers (Moy 2001; Bank 2006; GangaRao et al. 2007)

Fiber type	Typical diameter (μm)	Density (g/cm^3)	Tensile modulus (GPa)	Tensile strength (MPa)	Strain at failure (%)	Poisson's ratio
Glass	10	2.46-2.58	72-87	3445-4890	4.8	0.25
Carbon	7	1.74-2.20	220-900	2100-7100	1.4	0.20
Aramid	12	1.39-1.47	58-160	3150-3600	2.8	0.35

Glass fibers are used in the majority of large or low-cost composite applications. The main characteristics of glass fibers are their moderate strength, moderate elastic modulus, density, and low thermal conductivity. Silica (SiO_2) is the principal ingredient in all types of glass formulations, and it is about 50% to 70% by weight of the glass.

Carbon fibers are used in a variety of structural engineering applications in different forms and shapes, such as strengthening strips, sheets and fabrics, and in prestressing tendons. Carbon fibers, also known as graphite fibers, consist of more than 90% by weight of carbon. Carbon fibers have the highest elastic modulus of all reinforcing fibers, and have an advantage of an exceptionally high tensile strength-to-weight ratio along with a high tensile-modulus to weight ratio.

Aramid fibers consist of aromatic polyamide molecular chains. These are not as commonly used as the other two types of fibers, because of their relatively high price, difficulty in processing, high moisture absorption (up to 10% of the fiber weight), low melting temperatures, poor compression properties and sensitivity to UV rays, which indicate low durability over time as compared with other types of fibers. Their advantages include extremely high toughness, and lightness in weight, with a density of about 1.4 g/cm^3; other properties are summarized in Table 2.1.

2.2.1.2 MATRIX

In an FRP composite, fibers are encased in a tough polymer matrix, which serves to hold the fibers together in a structural unit and distributes the imposed loads to many neighboring fibers within the composite. The matrix also protects the fibers from environmental degradation due to moisture, ultraviolet radiation, corrosive chemicals, and to some extent from susceptibility to fire. Most of matrix materials are polymeric resins, which are used to cure and form the matrix. The properties of the matrix material depend on the type of resin used. These resins can be classified in several ways, based on their molecular structure, or their reactions to heating and cooling processes. The most common types of matrix materials and their properties are summarized in Table 2.2.

Table 2.2 Typical properties of common resin matrices (Bank 2006; GangaRao et al. 2007; Karbhari 2007).

Properties	Types				
	Polyester	Epoxy	Vinylester	Phenolic	Poly-propylene
Tensile strength (MPa)	50-75	60-85	75-95	60-80	30-37
Modulus of elasticity (GPa)	3.0	3.0	3.2	-	1.1-1.6
Strain at failure (%)	5	3-6	2-6.7	-	2-7
Density (kg/m3)	1200	1200	1120	1240	900- 9100

The main types of resins for FRPs in structural engineering applications are unsaturated polyesters and epoxies. The selection of a resin system for a matrix for an FRP depends on a number of characteristics; the most important among them are the adhesive properties, mechanical properties, and durability characteristics (micro-cracking resistance, fatigue resistance, moisture degradation and damage due to UV radiation).

Adhesive properties of a resin system are important in achieving the required mechanical properties of an FRP composite. Adhesive properties of a resin in FRPs, involving adhesion of the resin matrix to the fibers in an individual ply and within the subsequent plies of a lamina, are important. The matrix adhesive compatibility with other bonding agents is also very important to develop interfacial shear stresses between the FRP and other substrates (GangaRao *et al.* 2007). A polyester resin is normally used to manufacture pultruded FRP profiles/sections used in structural engineering applications. The strength and modulus of polyester resins are lower than those of epoxy resins. Vinyl-ester resins are unsaturated resins, and are produced by reactions between the epoxy resin and acrylic or methacrylic acids, which produce an unsaturated phase and render them very reactive. Vinyl-ester resins offer excellent corrosion resistance and higher fracture toughness than epoxy resins (GangaRao *et al.* 2007).

Epoxies normally consist of two separate parts - an epoxy resin and a hardener. These epoxy-based resins have excellent resistance to aggressive chemicals, and exhibit a low shrinkage of about 2 to 3% (Keller 2003), partial details are summarized in Table 2.2. Epoxies are used in high performance composites to achieve superior mechanical properties and resistance to corrosive environments (GangaRao *et al.* 2007), and are usually used for strengthening and repair applications, to attach FRP laminates to the existing under-strength concrete members, and for manufacturing of FRP tendons for prestressed concrete. However, due to the relatively higher cost of production and manufacturing difficulties, epoxy resins are not commonly used to produce large FRP structural members.

It is well established that the type of fiber and matrix used largely influence the overall mechanical properties of a composite; however, the final properties of FRPs produced from these materials

are also a function of their preparation and processing methods. In most cases, sheets or fabrics are saturated with the matrix and applied to the prepared surface (manual lay-up), and then allowed to cure. FRPs are also available in pre-formed, pre-cured sheets made of unidirectional carbon fibers with a much higher tensile strength, because of the fiber alignment and factory processing. These thin laminates are attached to the concrete surface using polymeric epoxies.

2.3 Durability of FRP Composites

The demand for FRPs, as an alternative construction material, has grown in a wide range of civil engineering infrastructure applications, particularly for bridges. These include reinforcing bars and prestressing tendons, wraps for strengthening and seismic retrofit of piers and abutments, externally bonded strips as reinforcement for strengthening of beams and deck slabs, composite bridge decks, and hybrid construction (FRPs in combination with conventional materials). Due to the limited research and engineering data on FRPs, there are serious concerns about the durability of FRPs, especially with respect to their long-term performance in harsh and rapidly changing environmental conditions, and heavy and dynamic loads.

Compared with conventional materials, FRPs provide similar or superior mechanical, thermal, and chemical properties; however, the thermo-chemical properties of FRPs gradually deteriorate during their service life (Springer 1977; Wu *et al.* 2006; GangaRao *et al.* 2007; Saadatmanesh *et al.* 2010). There is some evidence in the literature that some specific types of FRPs degrade rapidly when exposed to certain environmental conditions (AC1Committee440 2004), which seriously limits the confidence in the use of FRPs. In addition, there are contradictory data that may not be well understood by practicing engineers (Wu *et al.* 2006; GangaRao *et al.* 2007; Saadatmanesh, *et al.* 2010). These apparent contradictions about durability of FRPs are related to the reporting of

the data, without sufficient details of materials used, processing techniques, and changes occurring in the materials systems with time. The determination of long-term durability of FRPs used in civil infrastructure and the development of an appropriate methodology, capable of dealing with these materials in a variety of environments, must therefore be addressed urgently (Karbhari 2007).

2.3.1.1 Durability of FRPs – A definition

"*The ability of FRPs to resist the surrounding environmental factors such as, moisture, temperature, wetting and drying cycles, freezing and thawing cycles, ultra violet radiation and other factors, such as chemical attack, alkaline environment of concrete, creep, stress relief, fatigue and fire along with the age of the structure*" (Karbhari 2007). In case of an FRP subjected to any of the above factors separately, or in combination with one factor(s), the mechanical, physical or chemical properties will be negatively influenced with the passage of time (ESCC 2005).

FRPs can be affected by a variety of factors, including factors related to the natural and surrounding environment, and the effect of individual factors, or their combinations. The literature shows that durability of FRPs is a function of both the resin and the fiber. It should be reemphasized that durability of a material or structure should be defined as its "*ability to resist cracking, oxidation, chemical degradation, delamination, wear and/or the effects of foreign object damage for a specified period of time, under the appropriate load conditions, under specified environmental conditions*"(Karbhari *et al.* 2000).

2.3.2 Durability against Moisture

When FRPs are exposed directly to rain, humidity, moisture, and are partly or fully immersed, some moisture can diffuse into the composite which leads to changes in its thermo-physical,

mechanical and chemical characteristics. This can occur in the case of external column jackets used around bridge columns, or structures used in harbors, quality and service-life issues for composite decks that could be subjected to ponding or overflow in times of heavy rain. The absorption of moisture depends on the type of fiber and their orientation, the type of polymeric matrix, the matrix-fiber interface, the quality and composition of FRP sheets and the method of manufacturing. FRPs swell when they absorb moisture; the deterioration of a polymer matrix can occur when water molecules act as resin plasticizers and disrupt the van der Waals bonds in polymer chains, causing de-polymerization of the matrix (Bank *et al.* 1995).

The primary effect of absorption of moisture in the resin results from hydrolysis, plasticization and other mechanisms that cause both reversible and irreversible changes in the resin polymer structure. The effects of moisture absorption are plasticization, polymer matrix cracking due to swelling stresses, resulting in loss of integrity, reduction of glass transition temperature (T_g), strength and stiffness. Moisture and chemicals can cause degradation in aramid and glass fibers. In glass fibers, degradation is initiated by moisture extracting ions from the fiber, thereby altering its structure. The moisture contents and diffusion coefficients of composite materials can be determined by a variety of tests which have been reported in the literature (Springer 1977; Bank *et al.* 1995; Karbhari and Zhang 2003; Karbhari 2004; Wu *et al.* 2006; Saadatmanesh *et al.* 2010). However, it is possible to protect composite materials from rapid attack to a significant degree through the selection of appropriate resin systems, processing conditions, and the application of gel coats and protective coatings (Karbhari 2007). Since FRPs used in bridges come in contact with moisture and some solutions, either due to natural sources (rain and snow) or its location in

rivers or streams, it is essential that both the short-term and long-term effects of these preventive measures are well understood.

2.3.3 Durability against Freezing and Thawing Cycles

FRPs used in bridges can be subjected to a wide range of temperatures and moisture changes, along with the effects resulting from applied loads. Bridges exposed to cold environments must be assessed for the effects of freezing and thawing cycles, which can be more severe when FRPs are exposed directly to the environment. Low freezing and thawing cycles with the low variation in temperature appears to cause greater deterioration than constant immersion at below freezing temperatures (Karbhari 2004). Exposure to freezing and thawing cycles can cause damage to FRPs as a result of cyclic expansion and contraction of the entrapped water, which can also significantly affect the bond between the lamina, and the bond between the FRPs and the concrete substrate. The thermal characteristics of the constituents used in FRPs are different; both fibers and polymeric matrix have different thermal expansion characteristics due to notable difference in their coefficients of thermal expansion. Most of the epoxy resins, used as matrices in FRPs, have coefficients of thermal expansion ranging from 45×10^{-6}/°C to 65×10^{-6}/°C, while the coefficient of thermal expansion of glass fibers is 5×10^{-6}/°C and carbon fibers is in the range of -0.2×10^{-6}/°C to $+0.6 \times 10^{-6}$/°C. This large difference in expansion coefficient produces residual stresses. As a result of the difference in thermal expansion, FRPs can undergo a tensile strain, resulting in micro-cracking of the polymeric matrix. These micro-cracks in the polymeric matrix propagate when subjected to freezing and thawing cycles.

An experimental investigation was conducted by Oman and El-Hacha (2012) to study the effects of freezing and thawing cycles on large-scale reinforced concrete beams strengthened in flexure

with prestressed and non-prestressed FRP reinforcement. Five reinforced concrete beams, 5.15 m long, 200 mm wide and 400 mm deep, were tested under four-point transverse monotonically increasing loads at a rate of 1 mm/min rate of displacement. Before strengthening, these beams were cracked at a load of about 20 % above the analytical cracking load. Two out of four pre-cracked beams were strengthened with one 9.5 mm diameter sand coated CFRP rebar, and other two beams with two 2x16 mm rough textured CFRP strips, which were glued together and installed in a groove which was made on the tension face of the beams. These CFRP strips were prestressed to a level of 40% of their ultimate tensile strength. These beams were exposed to 500 freezing and thawing cycles at the rate of three cycles per day with temperature variation of +34°C to -34°C. The results indicated that the freeze-thaw exposure caused 13.4% decrease in the energy absorption characteristics in comparison with that in unexposed beams. The thermal incompatibility of the two materials caused development of residual stresses which led to the deterioration of concrete and the concrete-epoxy interface.

Combined effects of freezing and thawing cycles and sustained loading on flexural performance were studied by Brant (2008). Forty-five small-scale beams, 1220 mm long, with cross-sectional dimensions of 152 mm x 102 mm, longitudinally reinforced with 4-10M top and bottom bars and with external strengthening with glass and carbon FRP laminates were prepared in the laboratory. The beams were designed and strengthened to ensure that FRPs failed before the overall failure of beams. These beams were subjected to a sustained loading of 72% of design loads, along with freezing and thawing cycles according to ASTM Standard C 666-97 procedure (from +5°C to -18°C and back to +5°C within a period of 5 hours to complete a single freeze-thaw cycle). After 300 freezing and thawing cycles and about 3 months of sustained loading, the beams were tested

under flexural loading. It was found that the beams subjected to combined loads did not suffer a significant loss in their average ultimate strength; there was a strength reduction of 1.4% for the beams reinforced with GFRP sheets, 11.3% for the beams strengthened with CFRP sheets, and 7.6% for the beams strengthened with CFRP plates (Brant 2008). However, the greater inconsistency of the results for these beams relative to the control beams implies that lower guaranteed strengths should be used for situations with cyclic humidity and freezing/thawing conditions.

The effect of freeze–thaw cycling on durability of bond between FRP laminate reinforcement and concrete was studied by Green *et al.* (2000). An experimental investigation was conducted using both single lap pull-off and bond beam specimens, with uniaxial carbon FRP strips. For single lap pull-off tests, a total of 12 concrete prisms, of size, 150 mm × 150 mm × 400 mm and a specified 28-day concrete strength of 35 MPa were used. Once the concrete prisms were cast and moist-cured for 14 days, the CFRP strips were bonded to the exterior of the prism over a length of 300 mm; this length was chosen based on the results of preliminary studies which showed 300 mm to be the minimum bond length for which tensile failure of the CFRP strip was observed in pull-off tests. For bond beam tests, nine small scale (100 mm × 150 mm × 1220 mm) reinforced concrete beams were cast and cured, and then a single CFRP plate, 1020 mm long, was glued to the tension face of each beam. These plates were bonded only over a short length (300 mm) at either end of the beams and remained debonded in the central region. The specimens were exposed to 300 freezing and thawing cycles, consisting of 16 hours of freezing and 8 hours of thawing in a water bath. After this exposure, the specimens were tested to failure. Experimental results showed that

the bond between CFRP strips and the concrete was not significantly damaged by up to 300 freeze–thaw cycles (Green *et al.* 2000).

An investigation on the effects of freezing and thawing cycles on FRP-concrete interfacial bond behavior was carried out by Subramaniam *et al.* (2007). Concrete prismatic blocks, 330 mm in length and 125 mm square in cross-section, were used for direct shear tests. FRPs laminate was applied to the surface of the concrete specimens using the wet hand lay-up procedure. The width and the bonded length of the FRPs laminate attached to concrete were 46 mm and 150 mm, respectively. The specimens were subjected to two freezing and thawing cycles per day in an environmental chamber (from +5°C to -18°C for and back to +5°C within a period of 12 hours to complete a single freeze-thaw cycle). The results showed that the elastic modulus of the FRPs remained unchanged, whereas, with an increase in the number of freezing and thawing cycles, the load carrying capacity of the specimens decreased significantly along with a decrease in the fracture energy, which was noted to decrease as the number of freezing and thawing cycles was increased. The results revealed that freezing and thawing cycles produce significant decrease in the ultimate load capacity and interfacial fracture; these results are significantly different from the findings of Green *et al.* (2000).

Durability of FRPs for a bridge deck subjected to freezing and thawing cycles and low temperature conditions, was studied by Wu *et al.* (2006)**.** The selected composite panels were made of glass fiber and vinyl-ester resin. Twelve test specimen consisting of 381 mm x 813 mm size plates, with a thickness of 3.175 mm were extracted from selected panels. Each thin plate was made of two layers of fabric, with each layer made of four plies of unidirectional E-glass fiber bonded and stitched to a randomly oriented E-glass fiber, with a fiber volume fraction of about 50%. These

FRP specimens were then subjected to freezing and thawing cycles between 4.4°C and −17.8°C in media of dry air, distilled water, and saltwater and constant freeze at −17.8°C. The selected specimens were subjected to simultaneous environmental exposure conditions and sustained loading up to 25% of the ultimate strain of the FRPs. Test results on coupons (25.4 mm wide and 254 mm long) revealed that 625 freezing and thawing cycles (temperature range between 4.4°C and −17.8°C) caused insignificant reduction in the flexural strength of the FRP specimens, which were conditioned in dry air, distilled water and saltwater (Wu *et al.* 2006).

The experimental data available in the literature on durability of FRPs against freezing and thawing cycles and low temperature conditions are very contradictory. Presently, it is difficult to discern the effect of freezing and thawing cycles and low temperature conditions on durability of the FRPs. This variation in results can be due to many factors, such as the type of fibers and their orientation, type of polymeric matrix, the quality and composition of the FRPs, and the method of manufacturing. It can be concluded that the effect of freezing and thawing cycles and low temperature conditions on different types of FRPs can vary considerably, and cannot be generalized from any single type of study.

2.3.4 Durability against UV Radiation

FRPs can undergo photochemical damages near the exposed surface, because of UV radiation when exposed to the natural sunlight. The effects of ultraviolet exposure, or photo-degradation, are usually confined to the top few microns of the surface; however, this degradation at the component surface affects mechanical properties of the FRPs disproportionately. For example, flaws resulting from surface photo-degradation can serve as stress concentrators and initiate fracture at stress levels much lower than those for the unexposed specimens. The effect of

ultraviolet radiation is also compounded by the action of temperature, moisture, wind-borne abrasives, freezing and thawing cycles and other environmental phenomena. Homan (2000) noted that photochemical damage led to discoloration and reduction in molecular weight; however, there was no significant damage to the FRPs. The results showed (details presented in Section 3.6) that the UV radiation did not cause any change in the value of the modulus of elasticity and tensile properties of the laminates after an UV radiation exposure of 6000 to 12000 hours (Saadatmanesh, Tavakkolizadeh et al. 2010). A durable finish may be required for FRP forms exposed to UV rays to maintain color and gloss.

2.3.5 Durability against Alkalis

Alkalinity of the concrete protects embedded steel reinforcing bars in conventional reinforced concrete elements. FRPs can be adversely affected by this alkalinity, when exposed to the concrete. FRPs can come into contact with alkaline media through interaction with a variety of sources – including alkaline chemicals, soil and concrete. The main concern stems from the potential effects of degradation due to concrete pore water solution, which contains high hydrogen ion concentrations (pH of about 13.5). Over the last two decades, significant research has been conducted on degradation of bare glass fibers in contact with, or immersed in alkaline solutions, especially those derived from the concrete. It is well established that bare glass fibers in alkaline environment can get severely degraded due to a combination of mechanisms, ranging from pitting, hydroxylation, hydrolysis and leaching. The presence of resin as a matrix around an individual fiber in FRP can protect fibers from any such attack. The alkaline solutions can accelerate the degradation of the interface bond and of some resins themselves, especially if they are not fully cured.

The experimental investigation of the long-term behavior and environmental effects on mechanical properties of different types of FRP laminates produced, using a wet lay-up technique, was conducted by Saadatmanesh *et al.* (2010). A total 525 coupons, 25 mm wide and 400 mm long were tested under uniaxial tension. These tension test specimens were obtained from seven different types of FRPs laminates made of unidirectional loose glass, unidirectional glass, unidirectional carbon, unidirectional hybrid glass-carbon, bidirectional glass, bidirectional hybrid glass-carbon, and bidirectional hybrid glass aramid fibers. Nine different environments were implemented as exposure conditions, including fresh water, saturated $Ca(OH)_2$ solution with pH = 12.5, saturated $Ca(OH)_2$ solution with pH = 10.0, HCl solution with pH = 2.5, seawater, moist alkaline soil with micro-organisms, dry air at a temperature of 60°C, air temperature of 50°C and RH of 95% and UV radiation. The study revealed a significant loss (about 40% to 65%) in the strength and ultimate strain for GFRP in environments with high pH values (pH = 12.5), while carbon and hybrid glass-carbon laminates showed very little loss (< 10%) in their mechanical properties. The study also suggested that GFRP laminates are not recommended for application in environments with high pH values. Therefore, it is very important to select the appropriate constituents to manufacture FRP composites for both strength and durability requirements subjected to any specific environmental exposure.

2.3.6 Durability against Fatigue

Bridges are always subjected to a variety of loadings, including dynamic cyclic loading due to moving traffic. The fatigue phenomenon is important for durability and safety of bridges. Every cycle of loading, due to passing of trucks or other vehicles over the bridge results in a very small amount of permanent or residual strain in the constituent materials. Repeated loadings lead to

gradual accumulation of small amounts of damage with each cycle. FRPs can experience micro-cracking, delamination, fiber fracture, fiber/matrix decoupling, and micro-buckling under compressive loads. These damage modes can accumulate fatigue damage, and FRPs loses its resistance, which eventually results in fracture.

The fatigue performance of FRPs are influenced by properties of the constituents materials, both fibers and matrix, the fiber/matrix interface or the interphase region, the manufacturing process, loading parameters (such as frequency, stress range, and stress ratio of permissible stress to the stress at ultimate load), and in-service environmental conditions, such as hygrothermal, chemical and thermal-mechanical effects (Karbhari 2007). The fatigue performance of FRP laminate is affected significantly by the fiber type, its orientation and the lay-up scheme. The mechanical properties of the fibers play the most important role in fatigue performance. In general, composites made from fibers with a higher modulus have higher fatigue resistance. The matrix affects the transverse directional and shear properties, and axially loaded unidirectional fatigue properties. For unidirectional laminates, the effect of the matrix is reflected in the failure mode. Epoxy-based laminates tend to show very good fatigue resistance when compared with both polyester and vinyl-ester-based laminates (Bank 2006; GangaRao *et al.* 2007; Karbhari 2007).

2.3.7 Resistance against Creep and Long-Term Sustained Loading

For FRPs, creep or stress relaxation properties are governed by the resin matrix-dependent characteristics, rather than fiber or fiber-matrix interfacial properties. Under-cured resins are susceptible to significant creep and possible micro-crack initiation during the early stages of any service environmental exposure. The absorbed moisture and higher service environmental exposure temperatures both enhance the creep damage susceptibility; however, proper curing of

FRPs enhances durability against creep and long term sustained loading; details are not discussed here because of the scope of this thesis (Bank 2006; Karbhari 2007).

2.4 Applications of FRP Composites

The efficient use of an individual material or a combination of more than one material is always a key concern for efficiency and the level of performance of the composite system. The concept of advantageously combining materials to create a new system has been exploited in steel-reinforced and fiber-reinforced concrete, and prestressed concrete; the use of FRPs takes this concept one step further, enabling the interactive combination of reinforcing fibers, in a polymeric resin matrix. The ease of application of FRPs makes them extremely attractive for use in civil infrastructure applications, especially for bridges, because of the restrictions of dead weights and construction times. Furthermore, FRPs can have strength levels significantly higher than those of steel, and composites, such as CFRP have elastic moduli equal to or greater than the modulus of elasticity of steel; however, they have a significantly lower ultimate strain at failure. FRPs behave in a linear elastic manner until failure in a brittle mode, without any significant inelastic deformation, providing very limited amount of toughness, much smaller than from that steel or reinforced concrete.

The performance level of a prestressed concrete bridge is function of its load carrying capacity, serviceability, and durability over its service life. To ensure adequate performance, a bridge structure needs to be routinely maintained. Lack of maintenance lowers the performance level of a bridge and/or its components and appropriate upgrading or rehabilitation is then needed to upgrade it to an adequate performance level. (Hejll *et al.* 2005). Prestressed FRP plates bonded on the tensile face of flexural members improve both serviceability and the ultimate load carrying

capacity of reinforced concrete beams by providing additional strength (Wight *et al.* 2001). A literature survey revealed that some research work has been undertaken on the application of prestressing FRP tendon to replace the corrosion-prone prestressing steel tendons. Some codes and specifications are also available for practical application of FRPs in new construction and strengthening of existing bridges (AC1Committee440 2004, CHBDC 2010). There is very limited research work undertaken on the application of prestressed FRP laminates in any type of bridge construction; there is an urgent need for research to establish the effective application of FRP laminates as prestressing reinforcement for new construction.

FRPs have been used successfully in numerous structural applications in bridges. The review of applications of FRPs can be classified into three main groups: application of FRPs to existing bridges, application of FRPs as reinforcement in construction of new bridges and FRP composite profiles (sections) for new structural members of bridges. A brief review of these applications follows.

2.4.1 Application of FRP Composite in Existing Bridges

Application of FRPs for strengthening, rehabilitating and retrofitting of severely deteriorated, structurally deficient concrete bridge girders, or replacing of deteriorated bridge decks have become an efficient and a recommended solution for upgrading concrete bridges. The strength properties of FRPs are one of the primary reasons for their choice in such applications; these unique properties include the high tensile strength, the light weight, resistance to the electrochemical corrosion and formability (Mufti *et al.* 2005, Saadatmanesh *et al.* 2010). Through pre-tensioning of FRP sheets, significant enhancement in the flexural strength, stiffness, and crack resistance of

the strengthened structures can be achieved (Wu *et al.* 2003). FRP composite can be used in different ways for strengthening of bridges such as:

- FRP laminates glued to the soffit of girders to enhance and/or restore their flexural capacity.
- FRP laminates glued to the web of girders to enhance and/or restore their shear capacity.
- FRP composites wrapped around piers and abutments to enhance confinement and their compressive strength capacity.

The ACI 440.2 (2004) provides guidelines to avoid bond-related failures in glued FRP sheets or laminates; the details depend on the geometry of the structure, the soundness and quality of the substrate, and the levels of load to be sustained by the FRP sheets or laminates. For strengthening applications, CSA Standard S806 represents the first formalized design standard to deal with externally bonded FRP reinforcement for concrete; it considers all possible failure modes, including the limited FRP tensile strain, delamination and debonding of the FRP sheets and/or epoxy or resin. The Japanese Society of Civil Engineers (JSCE 1997) presented "JSCE Recommendations for the Upgrading of Concrete Structures with Use of Continuous Fiber Sheets" - a performance-based approach to the design of externally bonded FRP materials..

There are several practical examples of FRPs application in existing bridges for different purposes; few case studies are summarized here for completeness.

Spalling of the delaminated concrete cover due to corrosion of steel stirrups is very common in many prestressed I-section bridge girders. Demers *et al.* (2006) applied a GFRP laminate jacket to the girder bottom bulb to prevent the delaminated concrete cover from spalling. The falling of delaminated cover can damage vehicles moving and injure or kill pedestrians underneath the

bridge or overpass. Prestressed beams were retrieved from a bridge over an expressway in Montréal. The investigation was carried out in two phases. The first phase of the project was consisted of 25 laboratory tests conducted on GFRP jacketed segments of the prestressed beams (Figure 2.1). In the first step, 1.8-metre long full-section segments were used to investigate the various repair conditions, such as the type of GFRP wrapping, concrete surface preparation, and the curing conditions. In the second step, durability of repair was evaluated on 0.6-meter long half-section segments that were subjected to freezing and thawing cycles. The one-day freezing and thawing cycle consisted of a 16-hour dry period in a freezer at – 20°C followed by thawing in a water bath for 8 hours. No reduction in the strength of the FRP jacketing was observed after 300 freezing and thawing cycles. The second phase was involved installing this approved solution on in-service bridges in Montréal, Canada. The cost efficiency and service life expectation for bridge repair solutions were evaluated for field applications. The second phase involved installing of GFRP jackets on two edge beams on the Halpern Street Bridge over Autoroute Félix-Leclerc (A-40) in Montréal. Both laboratory and field test results indicated that jacketing was able to support many times (values are not given in the cited paper) the expected weight of the delaminated concrete, and suffered no significant deterioration after 300 freeze/thaw cycles, costing only 30% of the estimated replacement cost.

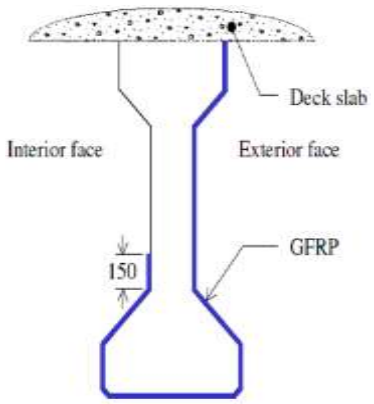

Figure 2.1 GFRP Jacketed cross-section of prestressed concrete bridge girder (Demers et al. 2006)

To restore the original structural capacity of an exterior prestressed concrete bridge girder, on the interchange of Interstate Highways 44 and 270 in St. Louis County, Missouri, USA, CFRP bonded laminates were used. The damaged I-section girder was initially prestressed using 20 low-relaxation 7-wire steel strands with a tensile strength of 1862 MPa; this girder had been damaged by accidental impact from an overloaded truck, which resulted in approximately 10% reduction in its flexural capacity. Two 45.7cm wide unidirectional plies of CFRP laminates (size 285 cm and 325 cm) prepared by hand lay-up, were installed on the bottom bulb of the girder, with fibers aligned along its longitudinal axis. To avoid the delamination of longitudinal plies, sixteen FRP strips, 10.2 cm wide and spaced at 20.4 cm on centers, were U-wrapped around the bottom bulb of the girder. The results showed that the factored capacity of the girder increased by 7% above that of the original girder capacity (Nanni *et al.* 2001).

2.4.2 FRP Applications to New Construction

FRPs are well known for strengthening and rehabilitation of existing bridges. Presently, there are a variety of FRP applications in new construction, such as FRP prestressing tendons for prestressed

concrete girders, FRP rebars for the deck and the railing reinforcement, and FRP stay-in-place forms for corrosion free bridge deck construction. FRP reinforced concrete bridge girders and beams are becoming common in bridge construction industry due to their advantage of light weight, easy installation, good durability and less maintenance requirements, as compared with the traditional materials, such as steel and concrete (Hejllet *et al.* 2005). A summary of the most common uses of FRPs in new construction follows:

2.4.3 FRP Stay-in-Place Forms for Concrete Structures

The structurally integrated stay-in-place FRP forms have been used in a number of applications, such as piles and structural supports for pier decks (Karbhari and Zhao 2000). The concept of stay-in-place forms is emerging as an effective and efficient method for concrete construction, with the advantages of being both the formwork, and through simplification of the construction procedure and reducing the construction time for a concrete member (ACI-440 2004). The FRPs are ideal materials for stay-in-place forms because of their high strength to self-weight ratio; these are also being used for bridge decks (Cheng and Karbhari 2008). Integrated FRP stay-in-place forms accommodate the concrete, act as external reinforcement, and in some cases, provide confinement for the concrete. Concrete-filled FRP tubes are another application that could be used as piles in corrosive marine environments and as bridge girders, piers, and columns (Fam and Rizkalla 2002)). The most common characteristics of integrated systems are as follow (Fam and Rizkalla 2002; ACI-440 2004; Cheng and Karbhari 2008; Wu and Shao 2008):

- The FRP shell acts as a permanent form for the concrete; as a result, it saves the cost of formwork involved in conventional cast-in-place or precast concrete.

- FRP shell acts as an external reinforcement, both for shear and flexure, using the multidirectional fiber orientation; additional reinforcement using other materials, such as steel may be provided internally.
- Closed FRP composite forms, such as tubes, provide passive confinement to the concrete, which significantly improves the strength and ductility of the core concrete (Fam and Rizkalla 2002).
- Depending on the nature of loading, the performance of a system may depend on the composite action between the concrete and the FRP shell. For example, under axial loads, it is desirable to debond the FRP tube from the concrete core, while under bending, it is essential to provide full composite action
- The hybrid system can be optimized based on material properties of each component; it enables the designers to choose several flexible parameters that can be controlled to achieve optimum design in individual applications, including the type of fibers, orientation of the fibers, number of layers in the composite shell, and the composite shell wall thickness.
- FRP stay-in-place forms act as a jacket, or a barrier against ingress of moisture and chemical substances that could otherwise deteriorate the concrete.

Along with the many advantages of stay-in-place forms, there are also a few limitations. When FRP stay-in-place forms are in contact with moisture, fire, exposed to UV rays and chemicals, the FRP shell can get degraded. Under such conditions, the durability of stay-in-place forms is uncertain. The bond between the FRP stay-in-place shell and the concrete core is very important,

especially, in flexural members because of slipping or sliding action between the inside concrete and the outer shell, than for axially loaded members (Bank 2006).

2.4.4 FRP Composite Structural Members

The light-weight FRPs offer a high tensile strength and excellent corrosion resistance; however, their low stiffness requires the design to be controlled by deflection. When FRPs are combined with the conventional material like concrete, their stiffness can be easily enhanced. This concept brings the idea of composite structural members in which FRP composites contribute the tensile and shear strength, whereas the concrete adds the compressive strength along with additional stiffness to the composite structural members. These composite members can be composite shell systems filled with concrete for columns, composite bridge decks, beams and girders with varying geometry. Other advantages of this type of composite members are their high quality and good dimensional stability because of automated manufacturing process, such as pultrusion and filament winding (Cheng and Karbhari 2006). FRP composite girders can be of different geometric shapes such as rectangular, I-shaped, or circular tubes, etc.; they act as external reinforcement that can be used to resist flexure and provide partial confinement to the concrete, and carry part of the applied shear force. The FRP composite beams can be made of GFRP composites, CFRP composites or hybrid CFRP-GFRP composites.

The concrete-filled FRP tube for columns simply replaces the steel tube with FRPs in conventional concrete-filled steel tube columns for better confinement and increased resistance to corrosion. These concrete-filled FRP tubes for columns are used in piers, beam-columns, and pile applications. Some research work has been undertaken by Mirmiran and Shahawy (1997); Mirmiran *et al.* (1998); Samaan *et al.* (1998); Fam and Rizkalla (2002) on concrete filled FRP

tubes for compression memebers. The scope of this review work is more toward the application of FRP composite for flexural members. Experimental results on concrete filled FRP tubes showed that concrete-filled FRP tubes have much higher ultimate strength capacity and ductility because of the high confining pressure provided by concrete-filled steel tubes (Mirmiran and Shahawy 1997; Mirmiran, Samaan et al. 1998; Samaan *et al.* 1998; Fam and Rizkalla 2002). Under uniaxial compression tests, the ultimate axial strength of the confined concrete could be 2 to 3 times higher than that of the unconfined concrete; the ultimate strains could be increased up to 10 to 15 times higher than those of the unconfined concrete.

Hybrid FRP-concrete members under transverse loadings, such as beams, slabs or bridge decks, have been investigated by Deskovic *et al.* 1995; Dieter *et al.* 2002; Fam and Rizkalla 2002; Banthia 2003; Ferreira *et al.* 2004; Hejll et al. 2005; Cheng and Karbhari 2008; Elmahdy et al. 2008; partial summary will be presented later in this chapter. In hybrid FRP-concrete members (or elements), the main function of the concrete is to resist the compressive loads and to improve the stiffness of the entire structure, and the FRP section carries the tensile loads and serves as permanent formwork to hold the wet concrete initially. Some of the sections used were FRP tubes, while the others were structural FRP shapes.

Full-scale prototype laboratory tests on an FRP stay-in-place forms deck and bidirectional grid concrete reinforcement system for a bridge were performed by Dieter *et al.* 2002. The objective of the research program was to develop design procedures and plans for construction of a two-span highway overpass. These overpasses were to be constructed on US-151 in the State of Wisconsin, with the required research being undertaken in the Department of Civil and Environmental Engineering, University of Wisconsin–Madison. The main purpose of this experimental research

program was to identify and understand the failure modes and fatigue performance, and to determine the ultimate and service load capacity of the FRP system. The FRP reinforced concrete system was composed of a top and a bottom layer of an FRP system; the bottom tensile reinforcement was composed of a pultruded FRP stay-in-place deck form spanning between two girders, but it was not continuous over the girders. The FRP deck form was analogous to the main positive steel reinforcement placed perpendicular to the girder system. Each deck form was 457 mm wide and overlapped with the adjacent deck forms. The stay-in-place forms were stiffened by two 76 mm square hollow corrugations, centered 229 mm apart. To ensure composite action through horizontal shear transfer between the deck form and the concrete, 6 mm aggregates were bonded to most of the horizontal surface area of the deck with epoxy (Fig. 6 (a) and (b)). Additional FRP grid and steel reinforcement were placed near the top of the slab and in the longitudinal direction. Two types of testing programs were undertaken: the first involved structural testing of the composite FRP reinforced slab and beam specimens, while the second consisted of investigation of physical and mechanical characteristics of the FRP composite material. Simply supported slab and beam specimens were tested with a concentrated load at mid-span and the two-span continuous beams were tested under four-point loading using an actuator to apply cycling loading to observe fatigue performance in the system. It was observed after failure that the deck panel exhibited an extraordinary capacity to hold a relatively large load through significant deflections. The FRP deck form strains indicated that the FRP reinforcement system fell short of being a fully composite section. The lack of a fully composite section may be attributed to the incomplete coverage of epoxy-coated gravel on the horizontal surfaces of the FRP deck form. The widths of the deck panel tests were found to range from 5% to 24% less than those in the

AASHTO's equation for live-load distribution. The mode of failure for these deck panels was punching shear, similar to the MTO research program at Queen's University, Kingston, Ontario. A significant increase in the load was observed by using external reinforcement. The load and deflection data, under accelerated flexural fatigue loading showed little relative stiffness loss, when specimens were subjected to over the 2 million loading cycles (Dieter *et al.* 2002). It was also observed that the accelerated flexural fatigue loading did not significantly decrease the stiffness of the reinforcement system, and performance of the FRP system was satisfactory.

Prefabricated composite tubes as girders filled with concrete for a bridge superstructure were studied by Karbhari *et al.* (2000). In this experimental program, six prefabricated FRP tubes with a 10 mm wall thickness and a 343 mm inside diameter were used; these are filled with cast-in-place concrete. The FRP composite deck system was integrated to form the prototype bridge superstructure system. This complete prototype system was tested for structural characterization of the girders, anchorages, and girder-deck assemblies for both serviceability and ultimate limit states. The carbon shell system technology was used for the superstructure components. The carbon/epoxy laminated shell with about 80% longitudinal and 20% transverse fiber reinforcement, with 80% fiber to matrix ratio were used. The concrete-filled carbon shell system for girders was tested for flexural response under four-point loading. The loading pattern consisted of 4 actuators applying a load of 56 kN each at a frequency of 1 Hz. This load level duplicates the shear force demand on the prototype bridge at the girder-deck interface under full service loads. The system failed at a total system load of 2136 kN due to compression buckling of the E-glass sheet on the deck top face. To observe the contact between the girders and the deck after the deck failure, the load was removed from the test unit and the system was loaded to a total load of one-

fifth of previously applied load for three cycles of loading. It was observed that the system responded linear-elastically with a reduced stiffness. It was also observed that the reloading stiffness after failure was approximately 75% of the initial stiffness. The bridge system showed good response under service, factored, and fatigue loads. The cyclic loading curve indicated that the structure suffered no structural degradation after completion of the 2 million fatigue cycles without any noticeable change in structural response (Karbhari *et al.* 2000).

2.5 Summary

In summary, most of the experimental investigations do not share any information about the life-time performance of the structural system under all kinds of mechanical and environmental loadings. There are other important issues, such as durability of FRPs and interfacial bond, sustainable development requirements, field application difficulties, and cost benefit analysis, which need to be addressed. The summary of the relevant literature review is also presented in each section of the thesis, for convenience of the readers to find relative information at the same place.

CHAPTER 3 BOND CHARACTERISTICS BETWEEN FRP LAMINATES AND CAST-IN-PLACE CONCRETE

3.1 Introduction

The interaction between FRP laminates and concrete surface is crucial to develop composite action, which is highly dependent on the quality of bond between three materials – the FRP laminates, the bonding agent and the concrete substrate, throughout the service life of the structural element. The bond behavior of FRP laminates and hardened concrete has been studied, mainly for structural repair and upgrading of existing concrete structures (Setunge 2002; Shao *et al.* 2005; Belingardi *et al.* 2006; Li *et al.* 2010). The pull-off tests (single or double lap), along with other methods are commonly used to evaluate the interfacial characteristics between the FRP laminates and the concrete substrate (Bank *et al.* 1995; Green *at al.* 2000; Shao *et al.* 2005; McSweeney and Lopez 2005).

The ACI design guidelines do not permit any type of bond failure between FRP repair and concrete substrate in FRP-concrete composite members (ACI-440.2R 2008); these bond failures can be extremely brittle and are normally accompanied by a large release of energy (McSweeney and Lopez 2005). There are several factors which can cause failure between FRP and concrete interface, such as poor distribution or lack of adhesion, existence of wider flexural cracks, or shearing cracks in the concrete member, coarse concrete surface, and fatigue loading (Wu and Shao 2008). Other factors that can also affect the bond quality are epoxy properties, environmental and concrete substrate humidity, temperature and stiffness of the FRP materials (Li 2007). Occasionally, the bonding agent, or epoxy can be incompatible either with the FRP matrix, or with

the concrete substrate. For example, polypropylene matrix-based FRPs are highly incompatible with any type of bonding agent, or epoxies, due to their non-cohesive or "slippery" surface behavior. Mechanical interlocking can be provided by increasing the surface roughness, or a grid of pockets on the inside of the FRP laminates to improve interfacial bonding. The mechanical interlocking can also be achieved by gluing a layer of coarse aggregates on the surface of the FRP laminate, which is examined in this study.

There are several studies available in the literature on the broad subject of bond characteristics of the FRP-concrete interface. These experimental and analytical studies mostly deal with the mechanism of load transfer and effect of the various parameters on interfacial bond quality Bank *et al.* 1995; Green *at al.* 2000; Shao *et al.* 2005; McSweeney and Lopez 2005; Li 2007). This chapter presents the details of the experimental and numerical modeling studies to evaluate the bond characteristics between the FRP laminates and cast-in-place concrete.

The FRP laminates were fabricated using wet lay-up method with vacuum molding, and bonded to the cast-in-place concrete. Eight double lap pull-off tests were conducted to evaluate the interfacial bond properties. The prefabricated FRP laminates with pre-glued aggregates were symmetrically placed in a mold, which was later filled with cast-in-place concrete. These specimens were then subjected to uniaxial tension, applied through the steel rod; the experimental load-pull-off displacement curves, shear stress and strain distributions were evaluated.

3.2 Materials

3.2.1 FRP Composites

FRP laminates were designed to act as a barrier against ingress of the various aggressive elements, such as moisture and chlorides into the concrete cover. It was assumed that the reinforcing fibers

are non-absorbent and polymeric matrix can absorb moisture only to a maximum value of 3.5%, with a constant diffusion coefficient value of 3×10^{-14} m/s^2, which found higher than experimental value. It was also assumed that after 365 days of exposure, the FRPs are completely dry and there will be no residual moisture at the end of one cycle. Also, it was assumed that moisture can evaporate from the salt- laden solution, leaving salt ions at a certain depth in the concrete cover, and progressing further with the next wetting cycle. These assumptions resulted in a total FRP shell thickness of 3.5 mm which can resist moisture from reaching the substrate after 100 years of exposure. The hybrid FRP composite laminates were fabricated in the Structures and Composites Laboratory of the Mechanical Engineering Department at McGill University. As mentioned earlier, the hybrid FRP composite laminates are a combination of glass fabric and carbon fabric saturated with epoxy, using the hand lay-up method with vacuum bagging, consisting of 2 plies of carbon and 2 plies of glass fabrics. After 24 hours of resin curing, the FRP plate was demolded and cut into 100 x 400 mm size plates. A 1.0 mm thick uniform epoxy resin film was applied on the surface of the FRP plate; coarse aggregates, size 10 mm, were evenly broadcast over the entire surface (Figure 3.1).The approximate mechanical properties of the hybrid FRP composite laminate were estimated using MLAM software, which is based on the classical laminate theory (CLT).

Figure 3.1 FRP laminates with broadcasted aggregates

Tension tests were also performed on FRP coupons to determine their mechanical properties; the results are presented in Table 3.1.

Table 3.1 Mechanical properties of hybrid FRP laminate

Properties	GFRP Lamina*	CFRP Lamina*	Hybrid FRP Laminate	
			Estimated†	Experimental‡
Tensile strength (MPa)	374	750	390	376
Tensile modulus (GPa)	22	44.4	34.5	24.4
Ultimate elongation (%)	2.1	1.0	---	3.5
Poisson's ratio	0.25	0.28	0.27	0.17
Thickness (mm)	1.02	1.27	3.6	3.56

***** Properties from manufacturer data sheet (QuakeWrap®)

†Estimated properties using MLAM

‡From coupon test using ASTM- D 3039

3.2.2 Epoxy-based Resin

The mechanical properties (tensile and shear strengths) of the epoxy-based resin, used for manufacturing of the FRP, and used as a glue to bond aggregates with the laminates, were determined experimentally, with tests on epoxy-based resin specimens.

The coupon specimens were prepared from the resin in steps, involving casting the resin into a mold, curing it in a controlled temperature and humidity environment for one week, removing from the mold, and cutting into rectangular specimens in required coupon dimensions. The coupons were then loaded in tension; a typical stress-strain curve for the epoxy sample is presented in Figure 3.2.

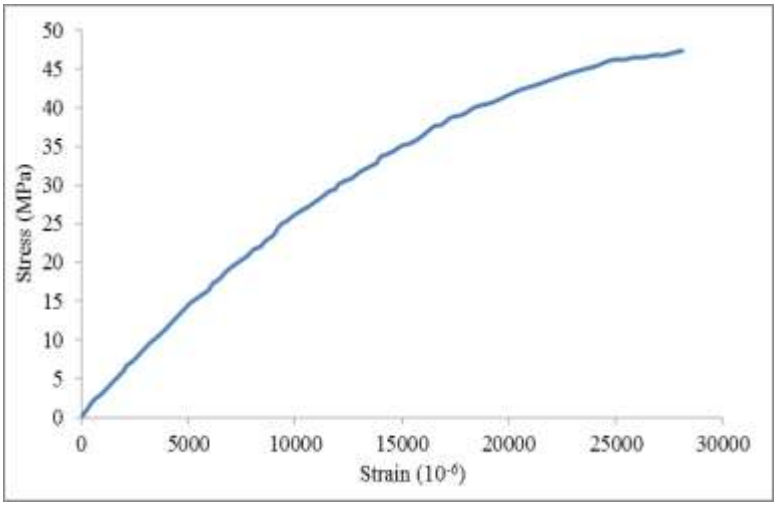

Figure 3.2 Tensile stress-strain curve for epoxy-based resin

The shear strength of the epoxy-based resin was determined according to standard procedure (ASTM D1002 - Standard test method for shear strength of single lap adhesively bonded specimens). In this method, two clean metal plates were attached to each other with an overlap of size 25 mm by 12.7 mm with the resin. After curing of resin, the specimens were tested until failure; Figure 3.3 presents a typical shear stress versus strain characteristics of the resin.

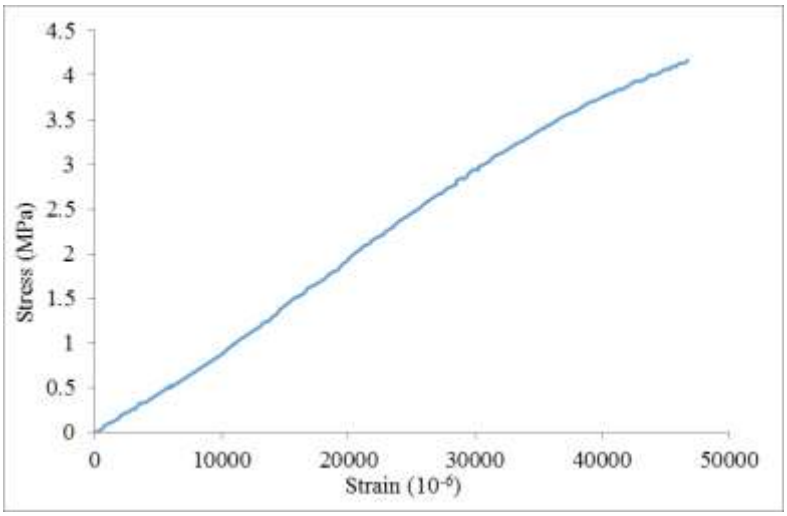

Figure 3.3 Shear stress-strain curve for epoxy-based resin

3.2.3 Concrete

The concrete mixture was designed for specific requirements, such as the small specimen size and a minimum compressive strength. The same mixture was used to construct specimens for other phases of this research project. The adopted concrete mixture had a slump of 75-100 mm, compressive strength of 50 MPa and one hour working time. After two weeks, the concrete cylinders were tested in compression, giving an average compressive strength of 55 MPa.

The tensile strength of concrete was determined in accordance with the standard method (ASTM C496/ C496 M-11), which provides details of the concrete cylinder splitting test, using Equation 3.1:

$$f_{st} = \frac{2P}{\pi LD} \qquad (3.1)$$

where P = splitting load (N)

L = length of the concrete cylinder (mm)

D = diameter of the concrete cylinder (mm)

f_{st} = tensile strength (MPa)

The average tensile strength of three concrete cylinders was 4.5 MPa, with a standard deviation of 0.13 and the coefficient of variation of 3%.

3.3 Experimental Work

3.3.1 Specimens Preparation

The double-lap pull-off bond test setup was used to determine the interfacial bond characteristics between the FRP laminate and the cast-in-place concrete. To develop effective bond, coarse aggregate particles were glued, using epoxy resin at the contact surface of the FRP laminates. Two sets of specimens were prepared by modifying the JSCE Cl.101 guidelines for pullout tests (JSCE 1997). The dimensions were modified to keep the prisms size to 150 x 150 mm in cross-section, and to provide clearance of 25 mm on both sides of the 100 mm wide FRP laminate to eliminate the edge effect. The FRP laminates were chosen to be 100 mm wide to accommodate at least 5 particles of 10 mm maximum aggregate size in one cross-sectional dimension. Two sets of specimens (4+4) were cast directly into the molds with symmetrically placed FRP plates. The test specimens consisted of two 250-mm long concrete prisms, 150 x 150 mm in cross-section, separated by a 2 mm thick wooden plate serving as a separator, and bonded with 100 mm wide by 400 mm long FRP laminates symmetrically placed on each side of the mold (Figure 3.4). In the first set of specimens, the concrete prisms were reinforced longitudinally using four 6 mm diameter steel bars and three 6 mm diameter ties at 55 mm spacing, acting as transverse reinforcement to

prevent any tension failure immediately upon (appearance of the first crack) in the concrete and to ensure that the final failure would occur either at the FRP-concrete interface, or over the depth of the bonded aggregates. The concrete prisms were unreinforced in the second set of the specimens, to allow the final failure to occur in the weakest link, which was the concrete subjected to tension. These specimens were tested by applying a uniaxial tensile force applied to the steel rod. The applied tensile force was transferred from the steel rod into the concrete, and then into the FRP laminates through the interfacial bond between the concrete and the FRP laminates, subjecting the FRP laminates to tension.

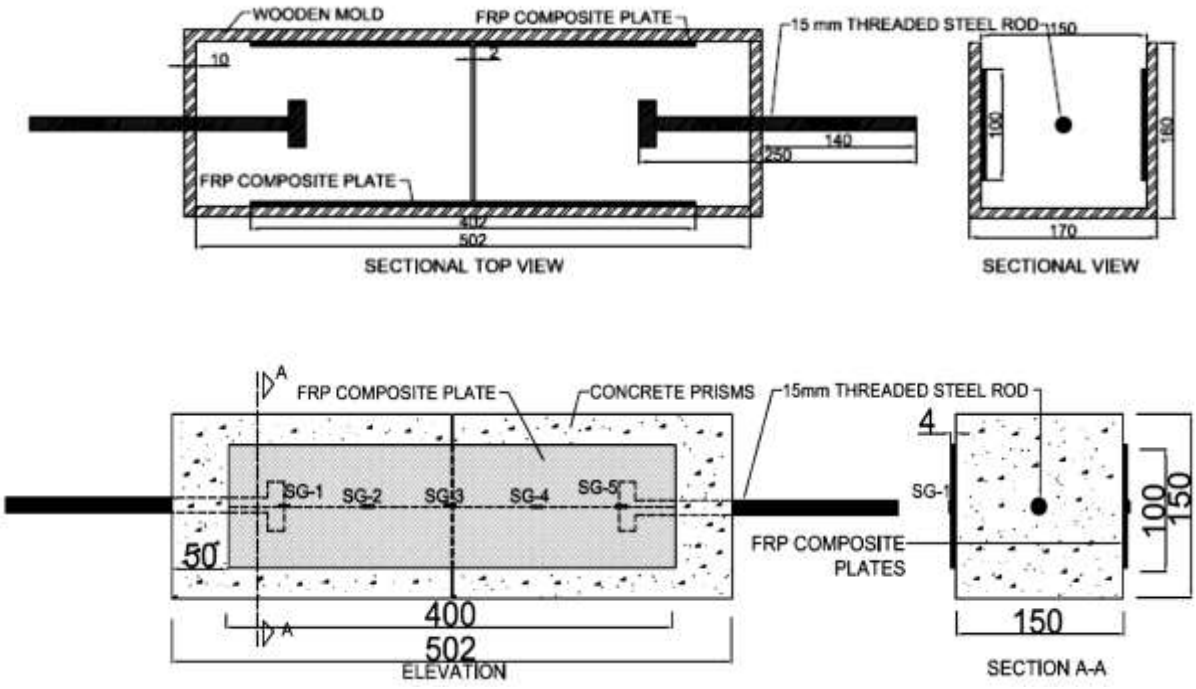

Figure 3.4 Double-lap pull-off bond test specimen details

3.3.2 Instrumentation and Testing

Each specimen was instrumented to measure the strain variation in 400 mm long FRP laminate; 10 mm long electrical resistance strain gauges, with gauge resistance of 120± 0.3 Ω (five on each

plate) were installed at the centerline at a spacing of 50, 125, 200, 275 and 350 mm along the length of the FRP laminate (Figure 3.5). The strain gauges SG-1 and SG-5 were installed at distance of 50 mm from each end of the FRP laminate, assuming that strain transfers gradually and commences from about 10 times the thickness of the FRP laminate. Strain gauge SG-3 was installed exactly at the middle of the plate, at the separation line. To record the average pull-out displacement at the separation line between the two concrete prisms, two 10V linear variable differential transformers (LVDT) sensors were installed on the opposite faces of the specimen. The instrumentation was connected to the data acquisition system (VISHAY 5100B series), which was connected to the computer to record the test data.

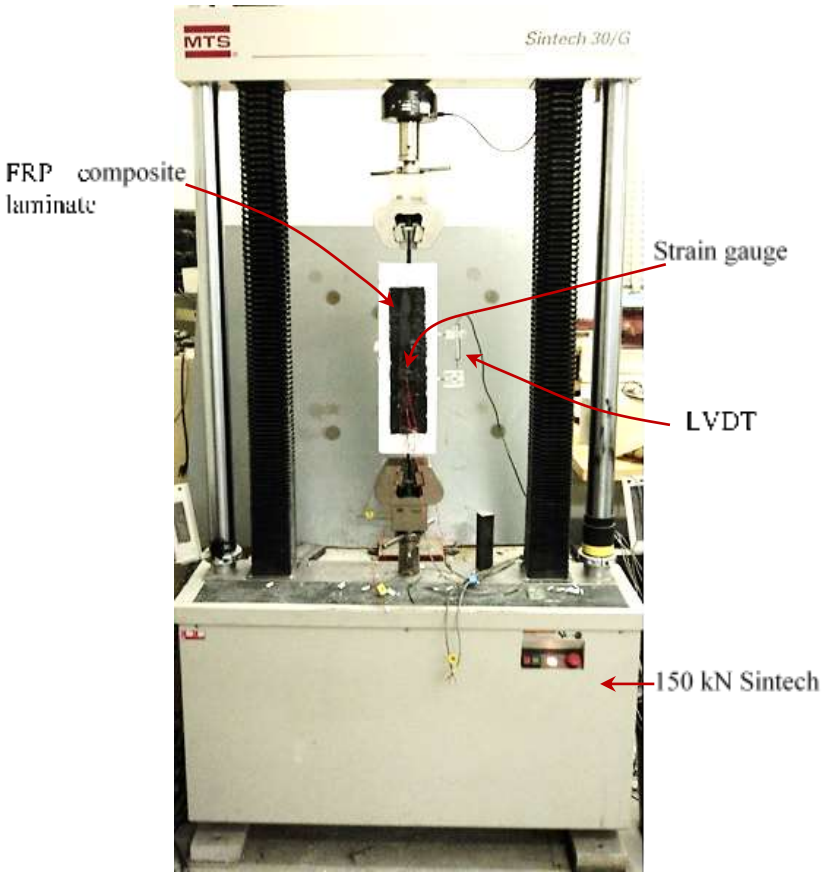

Figure 3.5 Double lap pull-off bond test setup

3.4 Experimental Results and Discussion

All of the specimens were tested under monotonically increasing uniaxial tension loading applied through the steel rod, using 150 kN SINTECH 30/G Universal Testing Machine (capacity = 150 kN), at a constant displacement rate of 0.5 mm/min, until failure of the specimens (Figure 3.5).

The test data were analyzed. The interfacial bond stress in Group-I of specimens was found to be 1.80 MPa, with a coefficient of variation (COV) of 3.26%, and 1.40 MPa with a COV of 3.97% in Group-II specimens. The test results are summarized in Table 3.2.

Table 3.2 Summary of double lap pull-off bond test results

Category		Maximum load (P_{max})	Interfacial shear stress		Slip	Maximum tensile strain in FRP	Interfacial fracture energy at failure
		(kN)	τ_{max} (MPa)	$\tau_{avg.}$ (MPa)	(mm)	$(\mu\varepsilon)_{max}$	G_f (N/mm)
Group-I	G1S1	70.66	1.77	1.80	1.090	2504	2.56
	G1S2	73.67	1.84		0.587	2713	2.78
	G1S3	73.59	1.84		1.159	2657	2.77
	G1S4	68.90	1.72		0.677	2396	2.43
Group-II	G2S1	57.91	1.45	1.40	0.478	2261	1.72
	G2S2	53.37	1.33		0.463	2063	1.46
	G2S3	54.16	1.35		0.472	2113	1.50
	G2S4	57.10	1.43		0.519	2210	1.67

The interfacial shear stress and slip characteristics were noted to be bi-linear, with a high value of bond stiffness (680 kN/mm) in the first part of the curve which is about 55% of the maximum load, and then gradually decreasing as the maximum load was approached (Figure 3.6 and Figure 3.7). This trend existed in the first part of the curve, where all three parameters (cohesion, friction and interlocking) contributed to the bond strength, and the bond stiffness reduced considerably after exhaustion of the interface cohesion in the second part of the curve. The trends observed in both groups of specimens were similar, despite the load at final failure; a comparison of all eight specimens is presented in Figure 3.8.

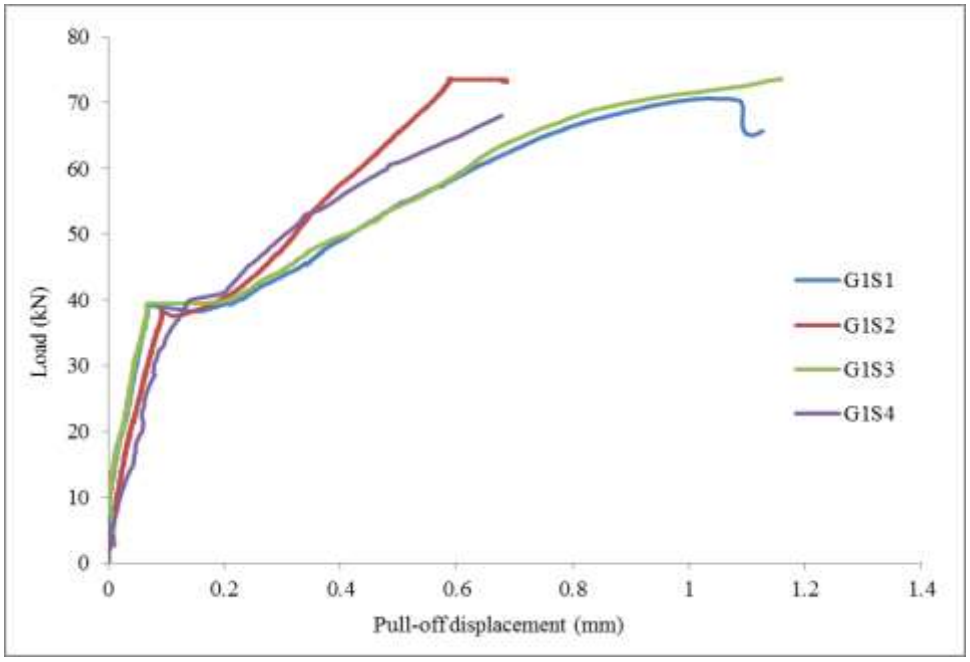

Figure 3.6 Load-pull off-displacement curves for Group-I specimens

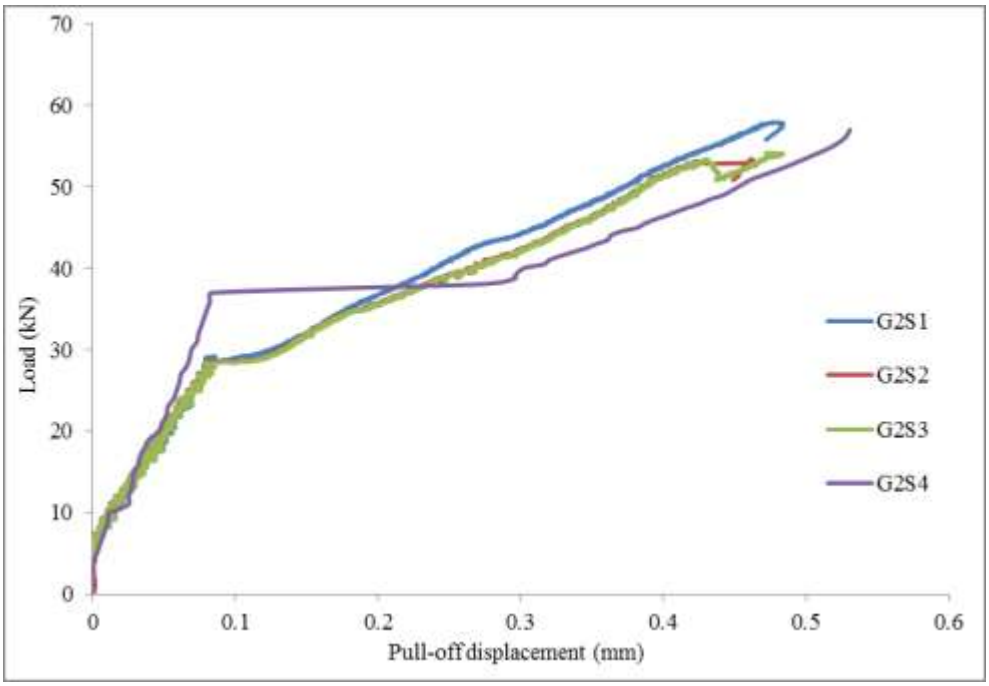

Figure 3.7 Load-pull off-displacement curves for Group-II specimens

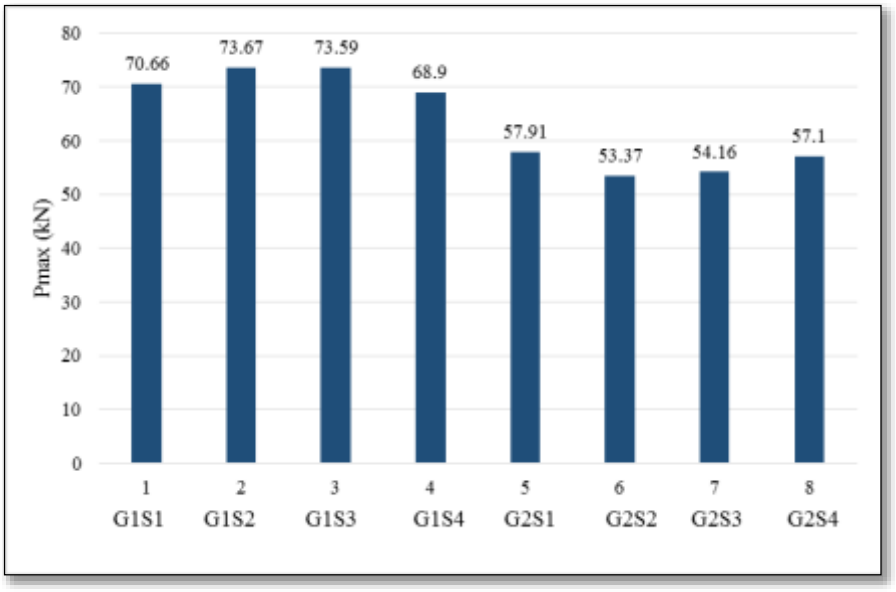

Figure 3.8 Maximum load comparison for all specimens

The trend of the tensile strain in the FRP laminates was found to be bi-linear, similar to the load – pull-off displacement distribution curves for the specimens; however, the strain distribution along the length of the FRP laminates was observed to be more variable (Figures 3.9, 3.10 and 11).

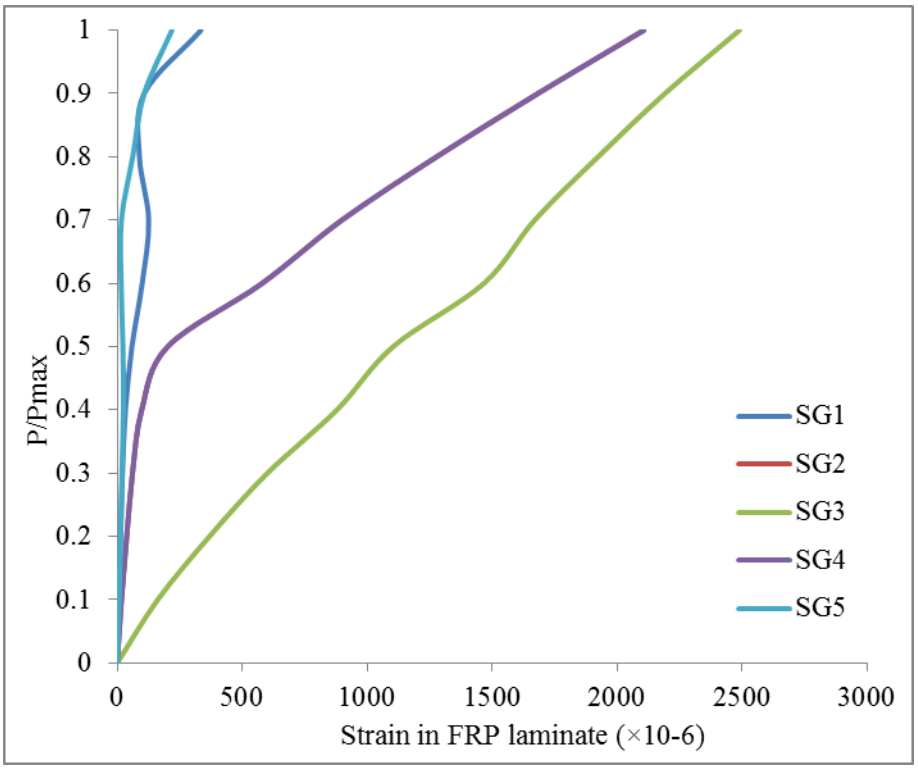

Figure 3.9 Strain variation in FRP laminate at different load stages in Group-I

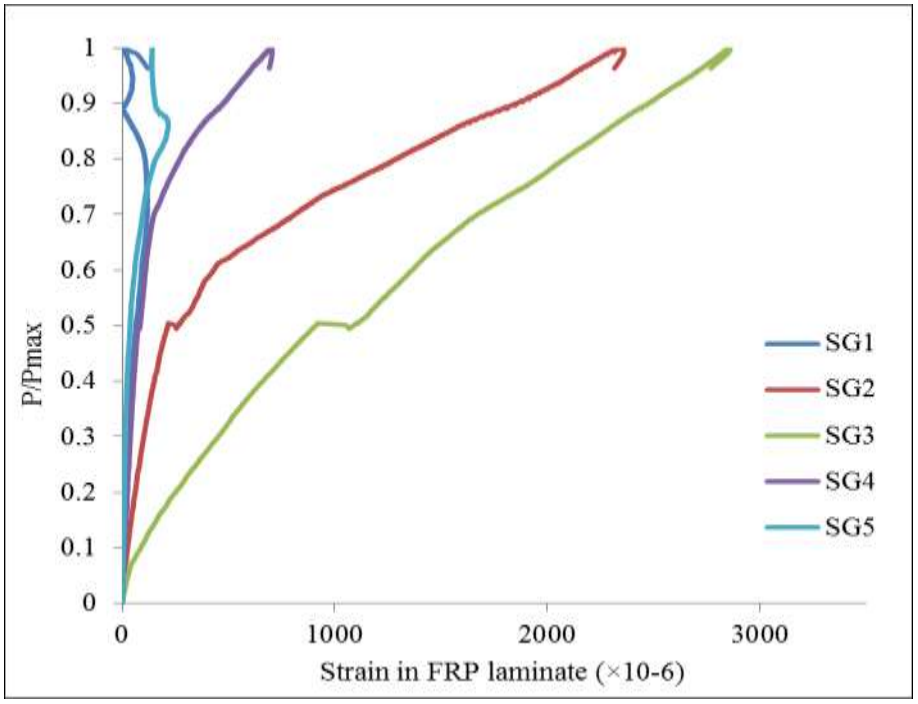

Figure 3.10 Strain variation in FRP laminate at different load stages in Group-II

The strain distribution along the FRP laminates can provide a clear picture of the load development along the laminate. Figure 3.11 represents the strain distribution along the FRP laminates at different load stages for the Specimen G1S1.

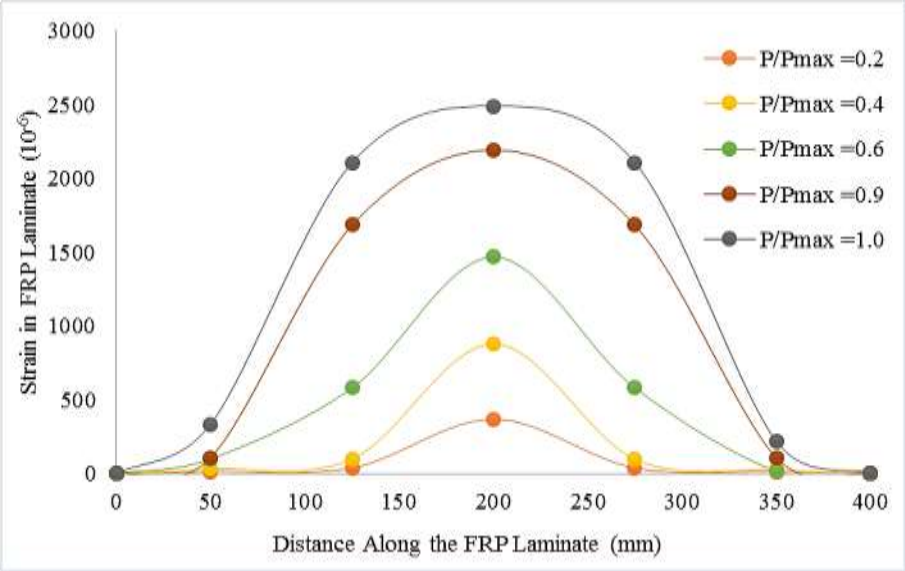

Figure 3.11 Typical strain distribution along the length of the FRP laminate in specimen G1S2

For the first 50 mm length of the FRP laminate, the strain does not change significantly; however, as the load increases the strain at the center of FRP laminate increases significantly, reaching a value of 2261×10^{-6} at ultimate load. The average ultimate strain for the second batch specimens is $2161\ 10^{-6}$. These values show that the data are close to each other with a COV of 4.2%.

The interfacial fracture energy, G_f, is the energy required to initiate a crack of unit length. It can be estimated using the work of Wu *et al.* (2001) using Equation 3.2, as:

$$G_f = \frac{{P_{max}}^2}{2 \times {b_f}^2 \times E_f \times t_f} \qquad (3.2)$$

where Gf = interfacial fracture energy (N/mm)

P_{max} = ultimate load (N)

b_f = FRP laminate width (mm)

E_f = tensile modulus of FRP laminate (N/mm^2)

t_f = thickness of FRP laminate (mm)

The results of interfacial fracture energy for each batch are summarized in Table 3.2.The fracture energy of Group-I is found to be almost twice that of Group-II specimens, which indicates higher bond toughness (Figure 3.12). The fracture of Group-I specimens was observed inside the concrete prisms in a very brittle manner because of brittleness of the concrete in tension (Fig. 3.13(a)), while in Group-II specimens, fracture initiated from the bonded aggregates because the reinforcement in concrete prisms delayed concrete cracking and transferred the stresses to the bonded depth of the FRP-concrete interface, allowing it to absorb more energy before final fracture.

In Group-I specimens, cracking initiated from the separation surface and propagated along the length of the plate, outside the bonded depth of the pre-glued aggregates. The failure was almost identical in all specimens in Group-I, except for specimen G1S2, in which the failure plane initiated from the bonded aggregates, as shown in Figure 3.12, leaving a thin layer of the aggregate particles acting as ‘shear keys’.

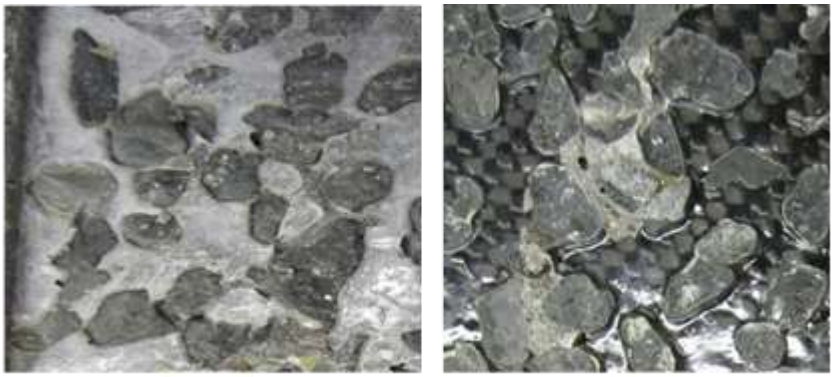

Figure 3.12 Failure from the Bonded Aggregates in Specimen G1S2 (a) view from the concrete prism (b) view from the FRP laminate

Failure of Group-II specimens were extremely brittle, accompanied by a large release of energy. The catastrophic failure was observed inside the unreinforced concrete prisms in a very brittle manner, by pulling out of a piece of a concrete with the FRP plate before bond began to fail at the epoxy-concrete interface, or epoxy-FRP plate interface (Figure 3.13). The failure was less brittle in the reinforced specimens as compared with the unreinforced specimens, and the reinforced concrete prism failed near the FRP-concrete interface which was a few millimetres from the interface of the bonded depth of the pre-glued aggregates.

Figure 3.13 Double-lap pull-off specimen (a) initial split between two concrete prisms at separation line (b) dislodged piece of concrete with FRP laminate after failure (c) FRP laminate with big chunk of concrete

3.5 Finite Element Modeling

Finite element analysis (FEA) can be very useful to evaluate the nonlinear behavior of the FRP-concrete interface and the associated slip phenomenon. A finite element study was conducted to investigate the properties and bond behavior at the FRP-concrete interface, and to understand the different influencing parameters and effective geometry of the double lap pull-off specimens (Minouei 2013).

The numerical analysis of the bond behavior at the FRP-concrete interface was performed using the commercially available ABAQUS^{TM} Software.

The objectives of this study were to develop a FE model for bond at the FRP-concrete interface, and to perform a comparison of numerical results with the experimental data to verify the accuracy of the FEM. The effect of different parameters on bond behavior was also examined.

3.5.1 Elements and their Properties

The FRP-concrete interface was modeled by defining a layer of adhesive resin between the FRP and concrete.

Three types of elements, based on their characteristics, were used to model the bond behavior at the FRP- concrete interface - solid elements, shell elements and cohesive elements.

1. Concrete and steel – solid elements were used to model both concrete and steel, because they have the closest similarity with the experimental behavior of concrete, and steel.
2. FRP laminates – shell elements were used because of the FRP geometry with negligible thickness. The shell elements have different characteristics in the thickness direction compared with that in the in-plane direction.
3. Adhesive epoxy-based resin layer – a cohesive element with ability to define traction-separation is used for modeling the epoxy layer.

Each part (concrete prisms, FRP laminates, steel rods and epoxy layers) was modeled separately, after assigning their mechanical properties, and then they were assembled into the final configuration. The discretization of the domain into smaller subdomains was performed manually to mesh each component of the model independently. The discretization process consisted of two steps. In the first step, seeds were assigned to the edge of each component. In the next step, meshes were assigned to the component of the model. The mesh size was optimized based on the desired level of accuracy and time. An optimum mesh size, 60×20, was used in modeling, which was determined after few iterations. In critical regions with a high failure risk, such as at the FRP-

concrete interface, a more refined mesh was assigned for increased accuracy. Details of the effect of mesh size on modeling are discussed elsewhere (Minouei 2013).

Following constitutive models available in ABAQUS^{TM} library were assigned for each material of the FE model:

- FRP laminates and load transferring steel rods - because of small deformations, linear elastic material properties were assigned.
- Bonding epoxy layer - elastoplastic model was assigned because of the large deformations before final failure. The von Mises model was assigned to the epoxy layer, in which the yield criterion is defined based on pure shear deformations with failure occurring when the effective shear stress reaches the critical value.
- Concrete - a damaged plasticity model was used, because it is more energy-based model than the other two (smeared cracking and brittle cracking) models available in the ABAQUS library; this property makes it a perfect choice for modeling the concrete in the double-lap pull-off test. The important parameters required to define the damaged plasticity model are the fracture energy (G_f), and the tensile strength of concrete, because it controls the initiation of crack and damage in concrete. The fracture energy (G_f) was determined using Equation 3.2 and summarized in Table 3.2. The tensile strength of the concrete was determined experimentally using Equation 3.1.

3.5.2 Comparison of Experimental and Numerical Results

The load-displacement responses were plotted to compare the maximum load capacity, deformation and stiffness of experimental tests with the FEA results for selected specimens from

both groups. Figures 3.14 and 3.15 present the comparison of load-displacement relationships for both experimental and FEA results.

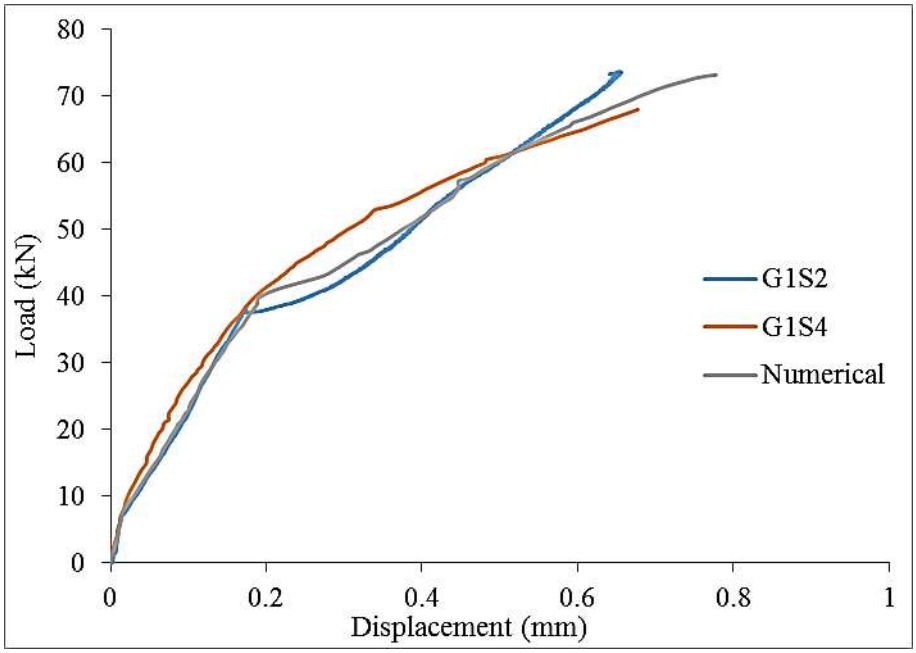

Figure 3.14 Comparison of load-displacement characteristics of double lab pull-off bond test for Group-I specimens

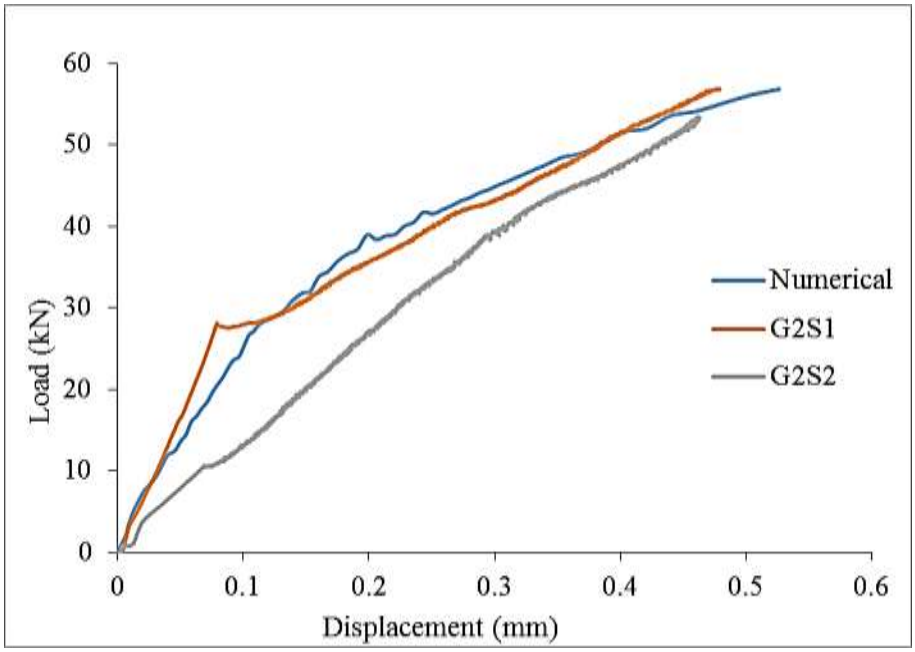

Figure 3.15 Comparison of load-displacement characteristics of double lab pull-off bond test Group-II specimens

The FEA results of both groups specimens showed that the average ultimate loads of 73.8 kN and 56.8 kN, and the final displacement of 0.78 mm and 0.53 mm, respectively, showing a difference of less than 5% in both the ultimate load and the displacement from the experimental results.

The stress distributions in different parts of the FE model are shown in Figures 3.16, 3.17, 3.18 and 3.19, which represent the left half of the specimen, with the right side representing the plane of specimen symmetry C. The colour spectrum shows the stress variation in the left half of the specimen. The blue color means lowest stress values, and the red color implies highest stress values.

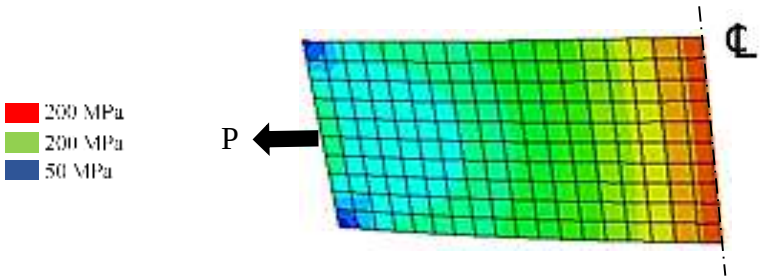

Figure 3.16 Stress distribution in FRP laminates up to the middle of laminate for Group-I specimens

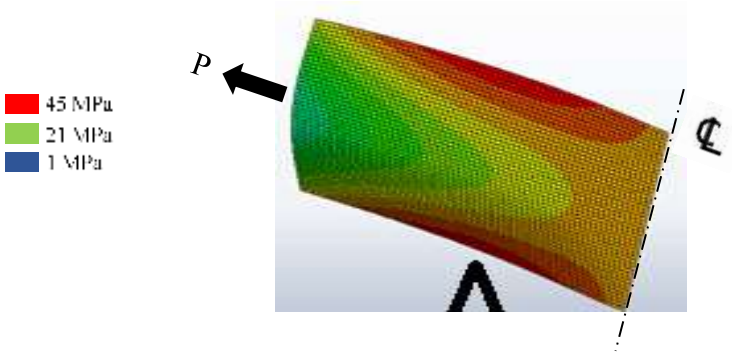

Figure 3.17 Stress distribution in the epoxy layer in Group-I specimen

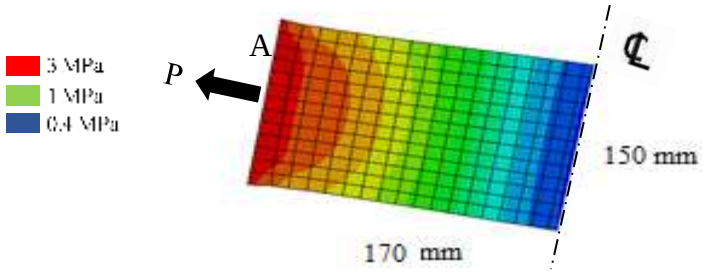

Figure 3.18 Stress distribution in the concrete prism Group-I specimen

The following important observation can be made from these spectra:

1. The stress reaches its maximum value at the middle of laminate and the stress concentration can be observed around the edge of the epoxy layer (Figures 3.16 and 3.17).

2. The epoxy layer is working as a bonding agent between FRP and concrete, and the load is transferred through the epoxy layer. In the second batch, the stress distribution in epoxy layer was much more severe.
3. The load increased gradually through the concrete block and reaches its maximum value around the middle, and the stress reaches its maximum value (Figure 3.18).
4. The stress distribution in the concrete at the specimen extremity A, where almost the entire load is carried by the steel bar, the amount of load and the resulting stress in concrete are negligible. The load is transferred to concrete from the steel bar, and the stress increases, but in the second batch the concrete, the damage does not take place in concrete.
5. Most of the FRP laminate length remains in the low stress range and only around the middle of the FRP laminate, where the most of the load is transferred through the laminate, the stress increases (Figure 3.19).

Figure 3.20 presents the strain distribution in the FRP laminate along the length at the ultimate load and compares the experimental results with the computed values. It can be observed that the strain increases and reaches its maximum value at the center, and then it decreases. The load transfer increases gradually along the along the FRP laminate, and at the center of the laminate, the entire applied load is transferred through the FRP laminate, which dictated by equilibrium conditions.

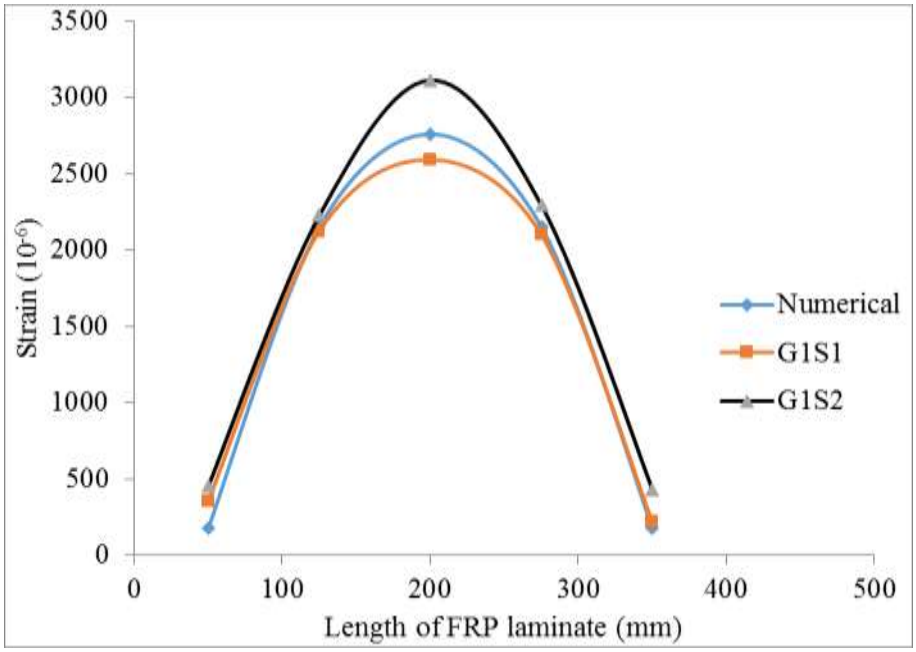

Figure 3.19 Strain distribution along the length of FRP laminate at ultimate load

Figure 3.21 presents the load transfer through the different elements at the ultimate load. For the 140 mm, extension of the steel rod out of the specimen, the load is constant at 73.2 kN, then the load is transferred to the concrete through the steel-concrete interface along the remaining length of the steel rod. This load transfer along the steel rod decreases, but it does not reduce to zero because the end of the bar is attached to a plate.

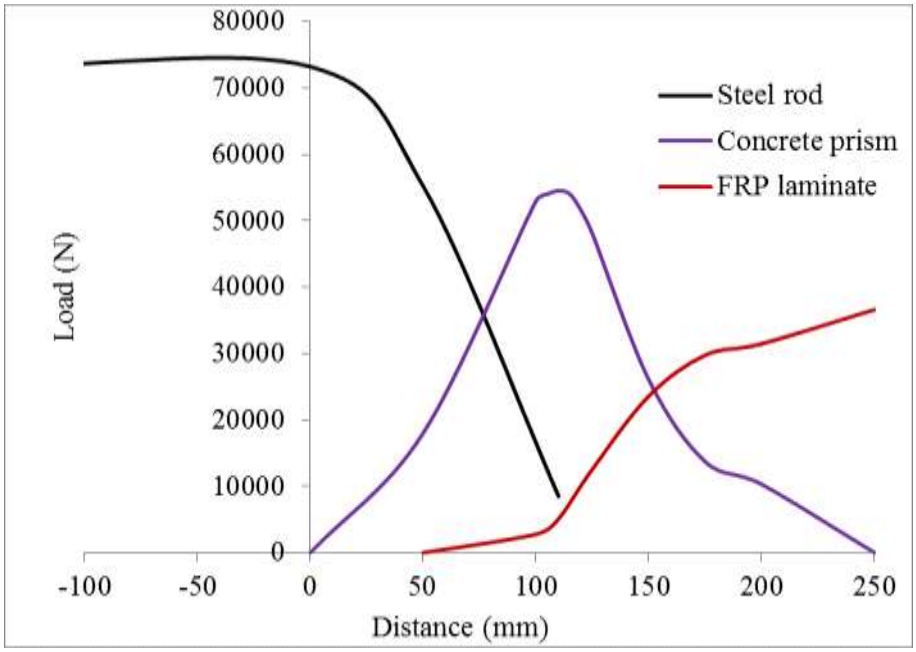

Figure 3.20 Load variation in different component elements along the length of the specimen at ultimate load

The FRP laminate is located at 50 mm from the edge of the concrete block. As the load in the steel rod decreases, the load in the FRP laminate increases slowly and the load in concrete reaches its maximum value around the middle of the concrete prisms. At the middle of the specimen, by equilibrium conditions, the entire load is transferred through the FRP laminates. The load transfer was slow for the first 50 mm, and then it increases and finally reaches its maximum value at 200 mm which is the center of FRP laminate.

Figure 3.22 also presents that the load distribution along the FRP laminate. In the first 50 mm length of the FRP laminate, the load increases slowly and then the slope of the curve increases significantly, and remains almost constant leading to the maximum value.

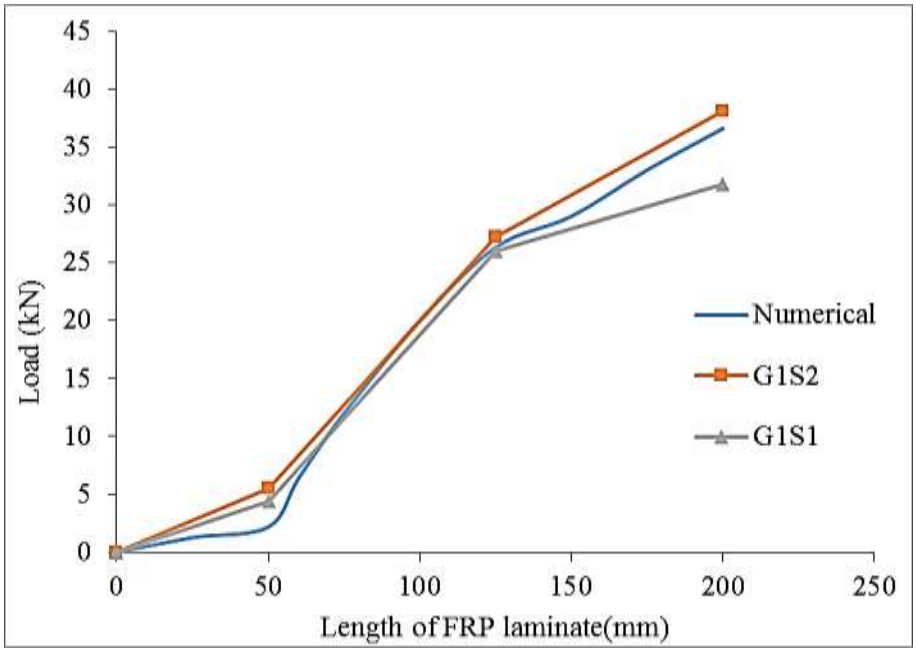

Figure 3.21 Strain variation in FRP laminate

3.6 Summary

The bond between FRP laminates and cast-in-place concrete was investigated using double lap pull-off bond tests. The hybrid FRP laminates were prepared, combining glass and carbon fibers in an epoxy resin based matrix, to enhance the durability of prestressed concrete girders, serving as a barrier against the ingress of the various aggressive elements into the concrete. These laminates were bonded to the cast-in-place concrete using pre-glued coarse aggregates with epoxy resin on the contact surface of the laminates.

Eight double lap pull-off specimens were constructed and tested. These specimens were instrumented to record the strain variation, slip at the FRP-concrete interface, and the interfacial bond stress between the FRP laminates and the cast-in-place concrete.

The interfacial bond stresses, using pre-glued aggregate technique, were found to be about 1.80 MPa, with a coefficient of variation of 3.3%. The interfacial shear stress and slip characteristics

were noted to be bi-linear, with higher bond stiffness (680 kN/mm) in the first part of the curve up to about 55% of the maximum load and then gradually decreasing near failure.

The final failure was less brittle in the reinforced specimens as compared with the unreinforced specimens. The failure plane in the reinforced concrete prisms occurred near the FRP-concrete interface which was observed a few millimetres inside the bonded depth of the pre-glued aggregates.

Numerical analysis results are compared with the experimental results. Both sets of curves reflected similar responses. The ultimate load, ultimate displacement and the associated strain were close to each other.

More experimental work is needed with different geometric and material properties to examine their effect on bond behavior and to ensure the accuracy of numerical results on parametric study. Also, in modeling the bond at the FRP-concrete interface, the effect of coarse aggregates was neglected, which can be considered in any future analysis.

CHAPTER 4 BEHAVIOR OF PRESTRESSED TENSION MEMBERS WITH FRP COMPOSITE LAMINATES

4.1 Introduction

Precast, pre-stressed concrete girders are normally considered to be durable; however, chloride ingress from de-icing salts used on bridge decks for traction during winters, can cause corrosion of the prestressing tendons, which has become a very serious problem in terms of safety, serviceability, reduced service life, expensive maintenance and very costly rehabilitation. Some of the present national codes and standards deal prescriptively with bridge durability issues, when subjected to aggressive environments (Sarja and Vesikari 1996; JSCE 1996; ACI-440 2008; CHBDC 2010). Structural concrete members, protected against aggressive environments can be more durable. Durability of prestressed concrete girders can be enhanced by eliminating, or avoiding the various deterioration reactions, and/or by providing multiple protective barriers, including protective coatings on steel, good quality concrete cover to the reinforcement, and external protective coatings or barriers on the concrete surfaces (Wu *et al.* 2003; Mirza 2007).

Bond characteristics between the FRP composite laminates and cast-in-place concrete (with and without prestressing) were investigated in this experimental study. To evaluate the effectiveness of FRP composite laminates in prestressed concrete construction, 12 prestressed FRP - reinforced tension specimens were prepared and tested. The prefabricated FRP composite laminates, with pre-glued aggregates, were placed symmetrically in a mold, which was later filled with cast-in-place concrete. Subsequently, these specimens were subjected to uniaxial tension; the experimental data were analyzed, and the stress and strain distributions at different load levels were evaluated.

4.2 Objectives of the Study

To evaluate the contribution of the FRP composite laminates to the structural strength and overall behavior of prestressed concrete tension members, this chapter focuses on following objectives:

- Evaluation of bond characteristics between FRP composite laminates and cast-in-place concrete before and after prestressing.
- Application of FRP composites to new prestressed concrete construction, including the effect of prestressing on FRP composite laminates and their bond with the concrete substrate.
- Development of construction procedures for composite beams with an FRP composite shell, and evaluation of their strength and durability characteristics.

4.3 Experimental Program

4.3.1 Materials

The FRP composite laminates were designed to act as a barrier against ingress of the various aggressive elements, such as moisture and chlorides into the concrete cover. The hybrid FRP composite laminates were fabricated in the Structures and Composites Laboratory of the Department of Mechanical Engineering at McGill University. Two 100 x 700 mm size hybrid FRP composite laminates plates were installed with a 1.0 mm thick uniform epoxy resin film applied on the surface of the FRP composite plate (with 10 mm maximum size coarse aggregates evenly broadcast over the entire surface). The fabrication details and mechanical properties results are summarized in Chapter 3.

A concrete mixture was designed, considering its workability, specimen size and minimum compressive strength. The same mixture was used to construct the specimens for other phases of this research project (Details in Chapter 3).

A 9.5 mm (3/8”) diameter, 1860 MPa grade, low relaxation seven-wire prestressing steel strand was used for pre-tensioning. Tension tests were performed on the prestressing steel strands to verify the mechanical properties provided by the manufacturer. Special couplers were designed to grip the strand during the tension test which was also instrumented with 2 mm long strain gauges to evaluate the stress-strain characteristics.

4.3.2 Specimen Preparation

Twelve prestressed FRP-reinforced tension specimens (two for each group, Table 4.1) were constructed to investigate the response of the prestressed concrete with FRP composite bonded laminates. These specimens were used to study the bond characteristics at the FRP composite laminate-concrete interface, and its strength and stiffness contribution in tension. A prestressing bed was prepared for the pre-tensioning operations to accommodate two specimens at a time. Two channel sections, back-to-back connected with a steel plate, with a central hole to allow the strand to pass, was fixed at both bed ends. Different level of prestressing force were applied, using a hydraulic jack at the active end and a load cell was installed to measure the applied load at the dead end of the bed. Pre-tensioning force was also monitored through bonded strain gauges on the strand surface before the concrete was poured into the oil coated surface wooden forms.

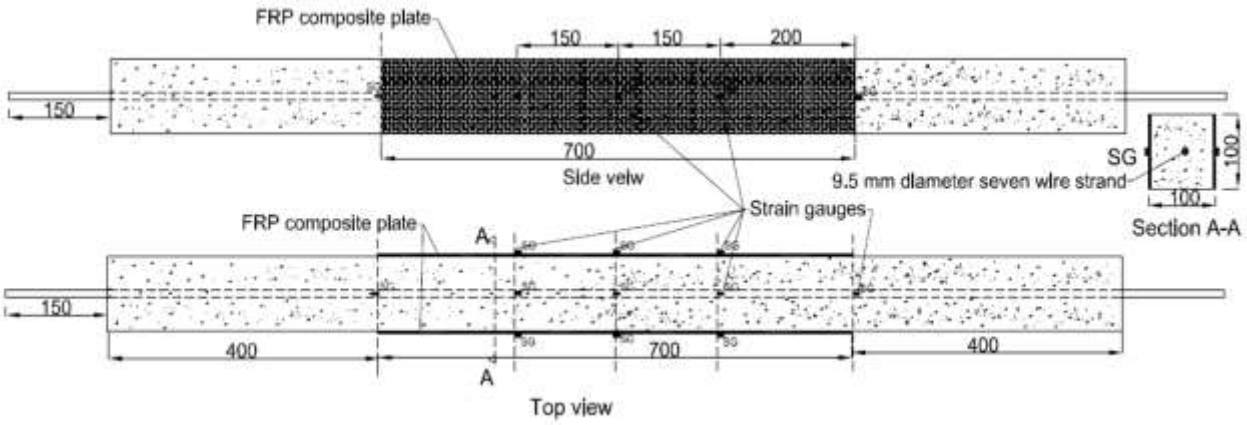

Figure 4.1 Details of FRP-reinforced prestressed concrete tension specimen

A 1500 mm long, prestressed concrete prism, 100 x 100 mm in cross-section, reinforced with a symmetrically placed 9.5 mm (3/8") diameter seven-wire, prestressing steel strand, and with 700 mm long FRP composite laminates placed on two opposite faces of the specimen (Figure 4.1), were cast and tested. The specimens were also reinforced longitudinally at both ends, using four 6 mm diameter steel bars, and with three 6 mm diameter ties at 180 mm spacing as transverse reinforcement, to prevent any splitting failure in the concrete during the prestressing operation and to ensure that the final failure would occur in the 700 mm long FRP-reinforced length of the specimen. As part of the construction procedure, the prestressing strand was pre-tensioned with varying levels of prestressing (0, 25, 50, 75, and 100% of total prestressing force). The FRP composite laminates were then placed symmetrically on opposite sides of the mold, and concrete was cast into the mold. The prestressing force was calculated based on the ultimate strength of the strand. The pre-tensioning force for specimens P100 (100% level of prestressing) was 80 kN, which corresponded to 74% of ultimate strength of the strand, and for P75, P50, and P25, it was 60, 40 and 20 kN, respectively (Table 4.1). For comparison purposes, four control specimens (P0-C and P100-C) were also prepared, which were constructed without the FRP composite laminates.

Table 4.1 Prestressing data

Specimen	No.	Level of prestressing (%)	Prestressing force (kN)			
			Design Force (kN)	Jacking force (kN)	Force before release (kN)	Effective prestressing force (kN)
P0	2	0	0	5	0	0
P25	2	25	20	25.1	24.6	23.8
P50	2	50	40	45.8	43.9	43.6
P75	2	75	60	65	61.6	60.5
P100	2	100	80	86	79.9	78.3
P100-C	2	100	80	86	79.9	77.9
P0-C	2	0	0	5	0	0

4.3.3 Test Setup and Instrumentation

The prestressed FRP-reinforced tension specimens were instrumented to monitor the strain variation in the 700 mm long FRP composite laminates and the prestressing steel strand, at different loading stages, such as jacking, releasing of prestressing force after construction and during the testing of the specimens. The strain variation in the prestressing steel strand was monitored using 2 mm long electrical resistance strain gauges (SG), with gauge resistance of 120± 0.3 Ω and a gauge factor of 2.11. These SG were installed on the surface of the prestressing steel strand, at spacings of 400, 600, 750, 900 and 1100 mm from active end, along the length of the specimen. The strain variation in the FRP composite laminates was monitored using six 10 mm long electrical resistance strain gauges (SG), three on each plate, installed along the plate centerline at spacings of 200, 350, and 500 mm from one end of the FRP composite laminate (Figure 4.1). Four 10V Linear Variable Differential Transformers (LVDT) sensors were installed on the opposite faces of the specimen (2 LVDTs for 700 mm gauge length and 2 LVDTs for 1500 mm

specimen length), to record the average elongation during testing. All sensors were connected to the data acquisition system (VISHAY 5100B series), which was connected to the computer to record the test data (Figure 4.2).

The specimens were tested using a displacement-controlled tension force, applied through the prestressing strand gripped in the machine jaws using special couplers. A slow uniform deformation rate of 0.001 mm/s was used to detect the first crack and then the deformation rate was increased to 0.01 mm/s until the end. The outputs from the load cell and the testing machine were also directly connected to the data acquisition system to collect all of the data in one file.

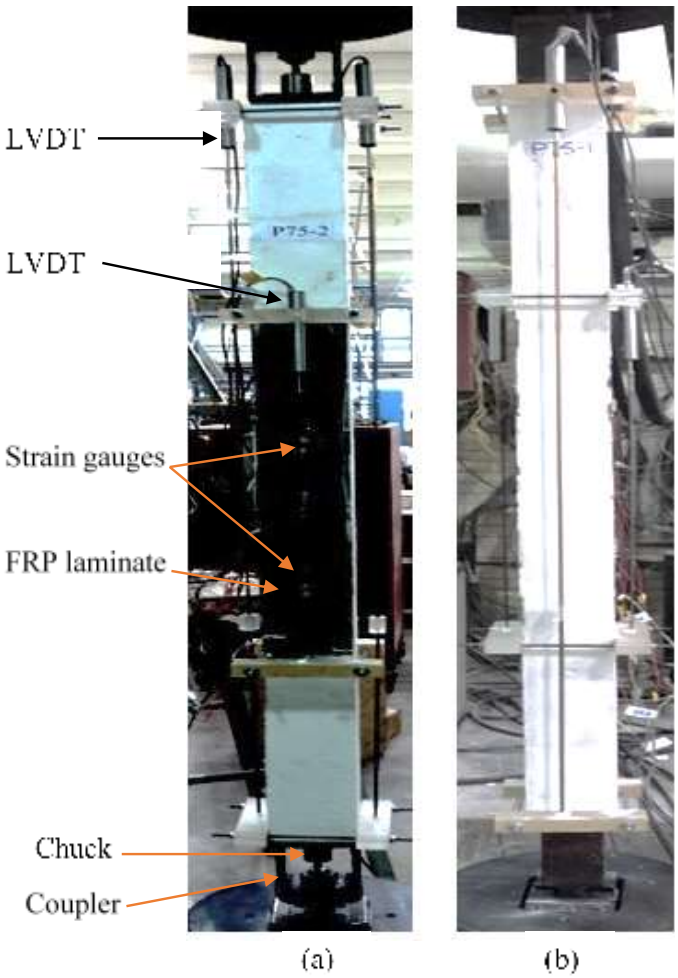

Figure 4.2 Test setup (a) front view (b) side view)

4.4 Results and Discussion

The test results from tension tests on FRP-reinforced prestressed concrete specimens are summarized in Table 4.2.

Table 4.2 Summary of prestressed tension member test results

Specimen	Level of prestressing	At first crack			At ultimate load		
		Load (kN)	Strain (με)		Load (kN)	Strain (με)	
			FRP laminates	Strand		FRP laminates	Strand
P0	0%	33.5	65	948	91.5	67	2128
P25	25%	39.76	155	176	102.29	1491	8144
P50	50%	56.54	178	162	106.81	1090	3740
P75	75%	75.5	203	178	109.71	1648	3141
P100	100%	83.93	224	270	112.52	773	9265
P100-C	100%	78.81	---	2120	98.48	---	8776
P0-C	0%	18.78	---	189	100.37	---	4223

Figure 4.3 presents the relationship between the applied load and the axial deformation in the 1500 mm length of the specimen. The behavior of prestressed tension specimens was linear up to the first crack, irrespective of the level of prestressing, with an average stiffness of about 1080 kN/mm for the FRP-reinforced prestressed and 544 kN/mm for the simple prestressed (specimen P100 and P100-C) without the FRP reinforcement; thus the stiffness of the uncracked FRP-reinforced specimen was about twice that of the specimen without the FRP reinforcement. The cracking load was a function of the level of prestressing, which was basically the pre-tensioning load plus the additional load required to crack the concrete cross-section. After initial cracking of the specimens with 100% level of prestressing, the applied load decreased slightly and then increased again, until

the peak load was attained just prior to failure. After cracking, the slope of the curve (axial stiffness of the specimen) decreased to 305 kN/mm. The experimental results showed that the axial stiffness of the specimen, after cracking, increased with the level of prestress. This stiffness of the cracked specimen increased from 180 kN/mm for specimen P0 to 305 kN/mm for specimen P100.

The specimen P0 cracked at 33.50 kN, while the control specimen P0-C cracked at 18.78 kN; thus FRP-reinforcement resulted in an increase of 80% in the cracking strength. An examination of the load-deflection curves for all of the specimens shows an increase in the cracking load and the axial stiffness after cracking, depending on the level of prestress and of the FRP reinforcement.

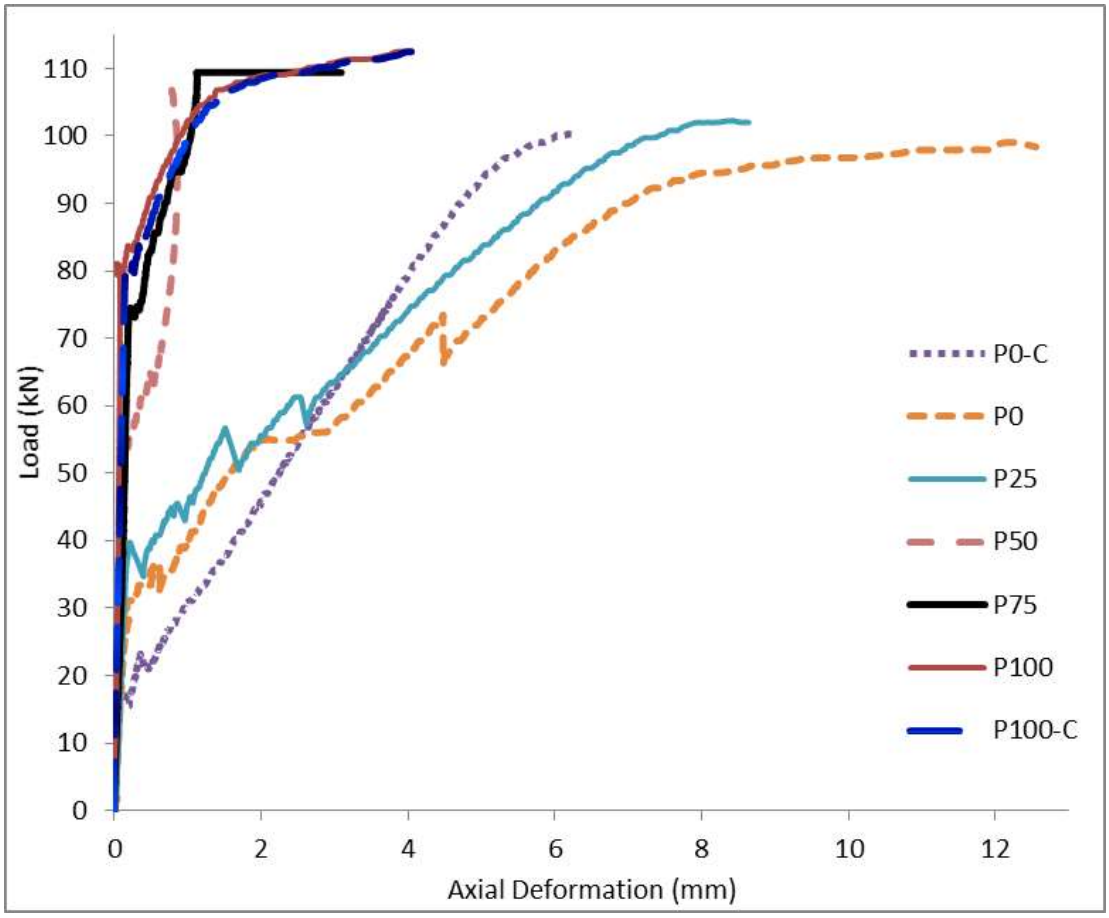

Figure 4.3 Load–Deformation curve for FRP-reinforced prestressed tension specimens

The strains in the FRP composite laminates and prestressing strand were recorded during the test, at specific locations; however, only the strain values in the FRP composite laminates and prestressing steel strand, measured at the middle (at 750 mm) of the specimens, are summarized in Figure 4.4 and Figure 4.5. The load – strain curves for the prestressing steel and the FRP reinforcement show the same trends as those observed for the load – axial deformation characteristic for all of the specimens. Again, the beneficial effects of the level of prestressing and the FRP reinforcement are noted.

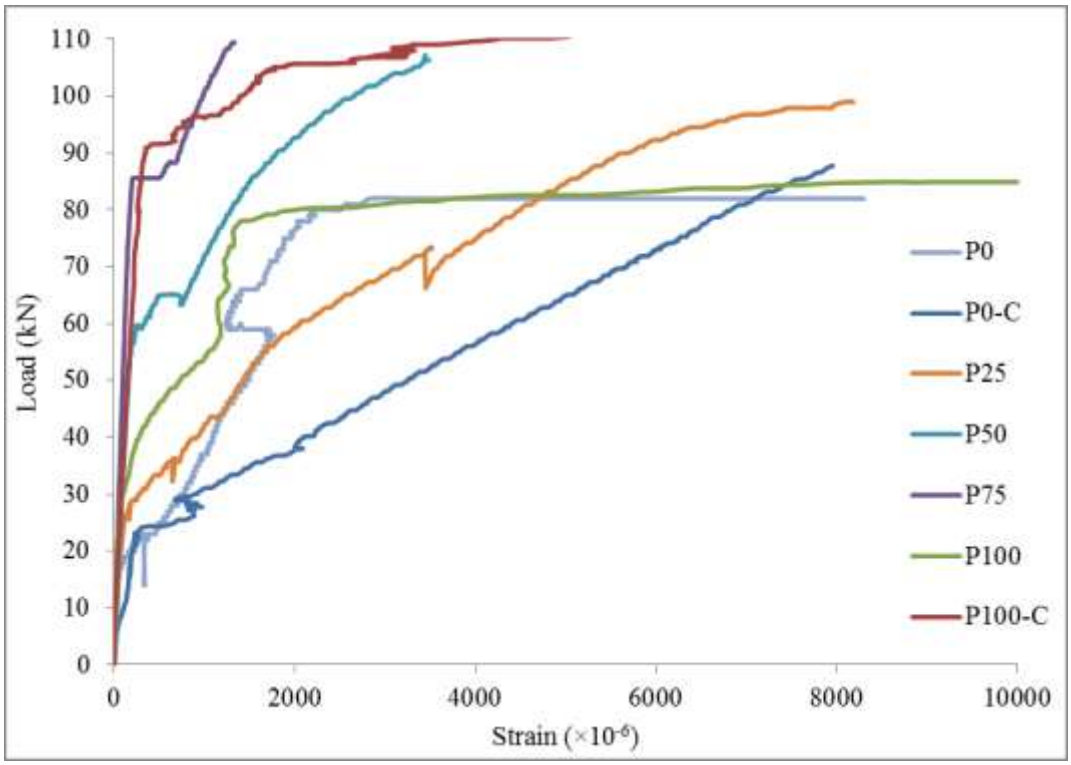

Figure 4.4 Strain variation at different load levels in prestressing steel strand

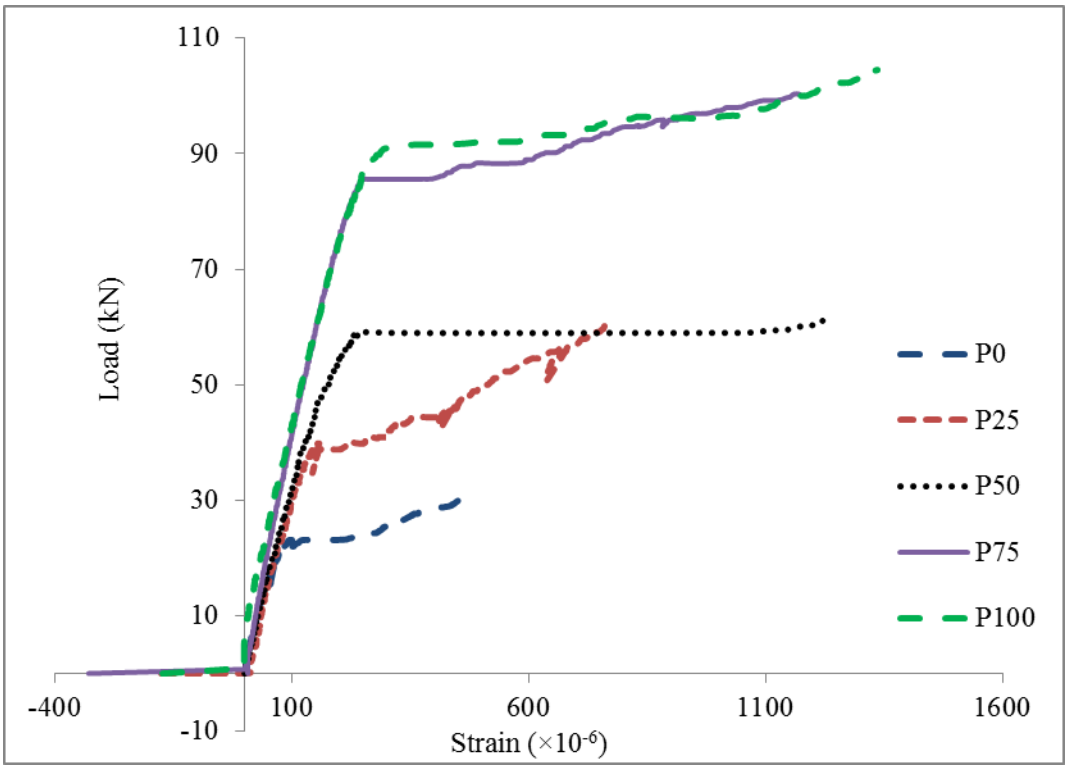

Figure 4.5 Strain variation at different load levels in FRP laminates

4.5 Summary

This paper summarizes the experimental work on FRP-reinforced prestressed concrete tension specimens. These tests were performed to determine the contribution of the bonded FRP composite laminates to the strength and stiffness of the prestressed concrete tension members.

Concrete prisms, with externally-bonded FRP laminates, using pre-glued aggregates to the FRP laminates and FRP-reinforced prestressed tension specimens with five different levels of prestressing (0, 25, 50, 75 and 100%) were prepared and tested.

The tensile strength of the simple FRP-reinforced specimen at initial cracking was almost twice that of the control specimens (without FRP composite laminates). The FRP composite laminates

and the prestressing force (at different levels) provided additional strength and stiffness to the system and enhanced the cracking strength and stiffness.

CHAPTER 5 FLEXURAL CHARACTERISTICS OF REINFORCED CONCRETE BEAMS WITH FRP COMPOSITE SHELL

5.1 Introduction

Structural steel embedded in structural concrete can corrode when exposed to chloride from de-icing salts used on bridge decks for traction during winters. Corrosion of reinforcing and prestressing steel has become a very serious and costly problem in terms of safety, serviceability, reduced service life, expensive maintenance and costly rehabilitation of infrastructure, and in extreme cases requiring its replacement at an exorbitant cost. However, when properly designed, constructed and maintained reinforced concrete member(s) are protected against any aggressive environments, and they can be sustainable and durable. Durability of concrete beams can be enhanced by eliminating or avoiding the various deterioration reactions, and/or by providing multiple barrier protection, including protective coatings on steel, high quality concrete cover to the reinforcement, and external protective coatings or barriers on the exposed concrete surfaces.

For the past two decades, application of FRP materials for construction of new bridges or strengthening, rehabilitation, and retrofitting of existing deteriorated structures, has proved to be an efficient solution. FRP composite systems have been successfully used for flexural strengthening and rehabilitation of existing reinforced concrete structures. For example, CFRP strips can be bonded mechanically or adhesively to the concrete surface and/or wrapped with GFRP wet lay-up fabric with epoxy based resins. The FRP composite materials are commonly used to reinforce bridge girders because of their light weight, easy installation, very low permeability and lower maintenance requirements, as compared with the traditional materials, such

as steel and concrete. Application of the FRP composite materials to hardened concrete for structural repair and upgrading of existing concrete structures over the past two decades has been studied by several researchers. However, application of FRP composite materials to new concrete construction is a relatively new area of research.

Integrated FRP stay-in-place forms is an other way to support the newly placed concrete, act as external reinforcement, and in some cases, provide confinement for the concrete. Concrete-filled FRP tubes is can be used as piles in corrosive marine environments and as bridge girders, piers, or columns.

The combination of FRP composite materials with concrete results in composite structural members for which FRP composites contribute to the tensile and shear strengths of the member, while the concrete provides the compressive strength along with additional stiffness. These composite members can be composite shell systems filled with concrete for columns and composite bridge decks, beams and girders with varying geometry. Other advantages of this type of composite member are their high quality and good dimensional stability because of the automated manufacturing process, such as pultrution and filament winding. CFRP, hybrid CFRP-GFRP composites can be used for FRP composite concrete beams. Hybrid FRP-concrete members, subjected to transverse loadings, such as beams, slabs or bridge decks, have been investigated by Deskovic *et al.* (1995), Dieter *et al.* (2002), Fam and Rizkalla (2002), Banthia (2003), Ferreira *et al.* (2004), Hejll *et al.* (2005), Cheng and Karbhari (2008), and Elmahdy *et al.* (2008). The results showed a significant imporvement in both strength and stiffness of these composite members.

This chapter deals with a detailed experimental program to investigate the flexural behavior of reinforced concrete (RC) beams with an FRP composite shell in the tension zone. To evaluate the

effectiveness of an FRP composite shell in reinforced concrete construction, eight simple reinforced concrete beams were constructed with and without an FRP composite shell. The prefabricated U-shaped FRP composite shells, with pre-glued aggregates for improved bond resistance, were filled with concrete. These beams were then tested under four point monotonically increasing loads until failures to study their complete behavior. The experimental data were analyzed; the results included the load-deflection relationships, along with the stress and strain distributions at different load levels, the cracking patterns and the modes of failure along with the cracking, yielding and ultimate strengths. The response of the FRP composite shell and the FRP-concrete interface were examined in detail.

5.2 Experimental Procedure

5.2.1 Materials and Properties

5.2.1.1 FRP Shell

The hybrid FRP U-shaped composite shells were fabricated in the Materials Laboratory of the Department of Civil Engineering and Applied Mechanics at McGill University. Two 2.3-metre long, aluminum angle sections (100 x 75 x 6 mm) were used to form the required U-shaped mold to fabricate the FRP composite shell. These angle sections were held together transversally with inverted 50 mm by 100 mm channel sections. The inner surface of the aluminum U-shape mold was prepared in three steps for smooth and easy demolding. The inner surface of the mold was polished using different grades of sand paper; this was followed by thorough cleaning of the mold using commercially available mold cleaner. Finally, a demolding treatment (sealant and mold release agent) was applied to the surface and left to dry for two hours. After this treatment, the mold was ready for fabrication of the FRP U-shaped composite shell.

The hybrid FRP composite shells were a combination of 2 plies of glass fabric and 2 plies of carbon fabric, saturated in epoxy-based resin, using the hand lay-up method, and vacuum bagging. Details of mechanical properties of glass and carbon fibers, epoxy-based resin and the FRP composite shell are presented in Chapter 3. Each layer was separately saturated with resin and rolled, with specially prepared rollers, on the wet lay-up bed. After saturating and rolling, all plies were placed carefully into the U-shape mold; fabrication setup and other details are shown in Figure 5.1(a). These resin-saturated plies were then rolled again in the mold to ensure correct placing of the wet plies within the mold walls. After placing and rolling of the saturated FRP plies in the U-shape mold, a perforated plastic film was applied to help hold the resin in the plies under a high vacuum pressure. On top of the perforated plastic film, a layer of a breather (or bleeder) cloth was placed to permit air flow by providing a slight air space between the bag and the laminate. A vacuum bag was used to create an airtight envelope around the mold. A sealant gum tape was used to provide a continuous airtight seal between the vacuum bag and the mold, around the perimeter of the mold. A piston type vacuum pump with hose and suction valve were used to create the vacuum. After 24 hours when the resin cured, the FRP U-shape composite shell was demolded and cut into required size of 2 meters length and 80 mm height U-shaped segments.

The bond between the FRP stay-in-place shell and the concrete core is very important, especially in flexural members because of slipping or sliding between the concrete and the surrounding FRP composite shell (Bank 2006). Aggregates pre-glued on the surface of the FRP composite shell provided adequate bond through the mechanical interlocking between the cast-in-place concrete and the FRP composite shell. A 1.0 mm thick uniform epoxy resin film was applied to the surface

of the FRP U-shaped composite shell and coarse aggregates with a maximum size of 10 mm, were evenly broadcast over the entire surface (Figure 5.1(b)).

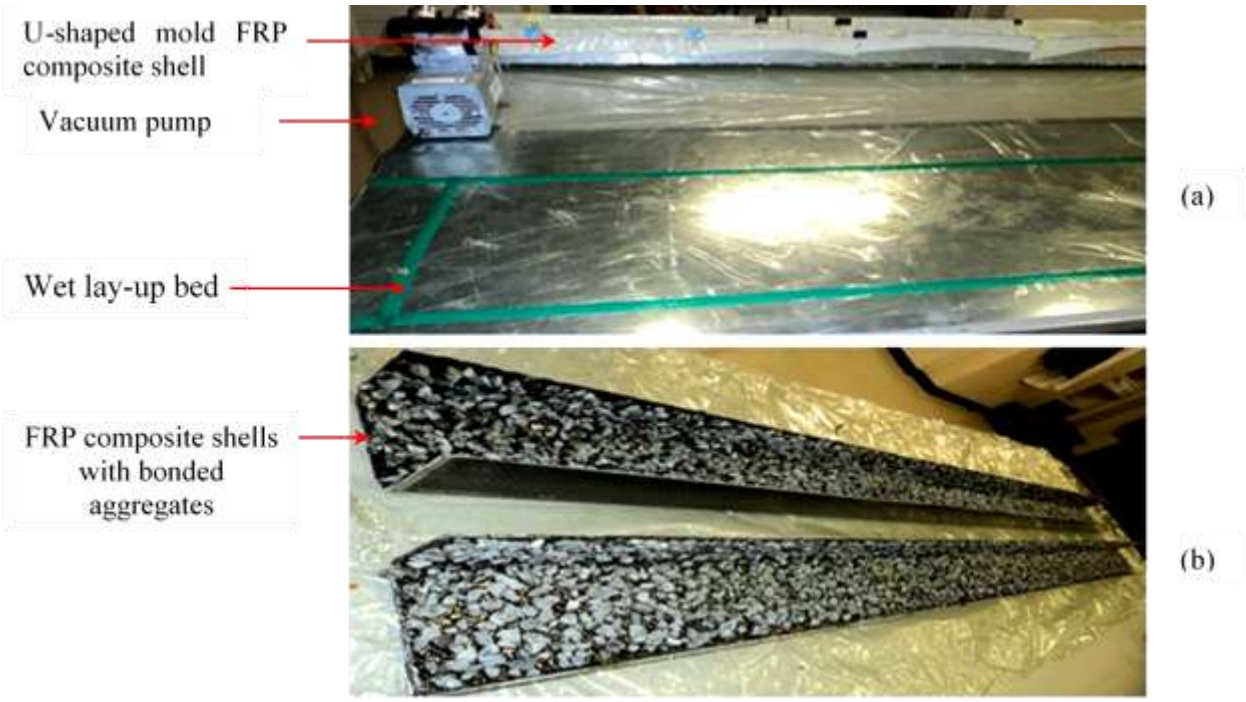

Figure 5.1 Preparation of FRP composite shell (a) vacuum hand molding wet lay-up setup (b) u-shape FRP composite shells with bonded aggregate.

5.2.1.2 Reinforcing Steel

Commercially available reinforcing steel was used to reinforce the concrete section. Standard tension tests (ASTM A615M), were performed on a minimum of three steel specimens from each size bar to determine the stress-strain relationships and other mechanical properties. The test results are summarized in Chapter 3.

5.2.1.3 Concrete

The concrete mixture was designed for workability, smaller specimen size and minimum compressive strength. The same mixture was used to construct specimens for all phases of this

research project. All composite beam specimens were cast using two batches, because of the limited capacity of the mixer. A minimum of three 100 x 200 mm concrete cylinders were cast from each batch, and cured under the same conditions as the beam specimens. These concrete cylinders were tested under uniaxial compression using the Rockwell Compression Testing Machine. An extensometer, with a gauge length of 100 mm, was installed on each test cylinder to determine its axial deformation. The concrete mixture had a slump of 75-100 mm, an average compressive strength of 61.3 MPa, with a coefficient of variation of 2.7% and one hour working time.

Table 5.1 Concrete cylinders testing data

Batch	f_c' (MPa)	standard error (MPa)
1(B1, B2)	61.17	±1.37
2 (B3, B4)	61.47	±1.08

5.2.2 Specimen Details

The FRP composite shell was assumed to act as a barrier or protection against the harsh environment. The contribution of the FRP composite shell to flexural and shear strengths were not considered in the design process, to ensure the beam would be able to develop its full load carrying capacity, if it deteriorated over time.

Eight 2-metres long, 132 x 200 mm in cross-section, reinforced concrete beams, reinforced with FRP shell, were constructed. The specimens were divided into four groups based on their steel reinforcement ratios *(ρ)* – 0.8, 1.6, 2.4, and 4.8%. Each group consisted of two specimens, one specimen reinforced with the FRP composite shell and the second without the FRP composite

shell. The length, width, and height of the beams were 2000 mm, 135 mm, and 150 mm, respectively. The ρ values for Group I specimens was almost equal to ρ_{min} (= 0.5%), whereas for Group IV, it was 75% of the balanced steel reinforcement ratio (ρ_b= 6.4%). Each beam in Group I was reinforced with two 10M bars as tension reinforcement, which made steel ratios ρ, equal to 0.8 %. In Group II, III and IV, each beam was reinforced with two 15M bars, three 15M and three 20M bars, respectively (Table 5.2). In addition, all beams were also reinforced with two 10M bars as hanger bars in the compression zone. All beams had shear reinforcement in excess of the minimum amount required to avoid shear failure (Figure 5.2).

Table 5.2 Specimens details

No.	Beam	Description	Reinforcement	ρ
Group I	B1F	With FRP composite shell	2-10M	0.8%
	B1S	Without FRP composite shell	2-10M	0.8%
Group II	B2F	With FRP composite shell	2-15M	1.6%
	B2S	Without FRP composite shell	2-15M	1.6%
Group III	B3F	With FRP composite shell	3-15M	2.4%
	B3S	Without FRP composite shell	3-15M	2.4%
Group IV	B4F	With FRP composite shell	3-20M	4.8%
	B4S	Without FRP composite shell	3-20M	4.8%

The first letter in specimen nomenclature represents beam specimen (B); the following number is the specimen number and the last letter distinguishes the specimen without (S) and with FRP composite shell (F). For example, B1F is Beam 1, reinforced with the FRP composite shell.

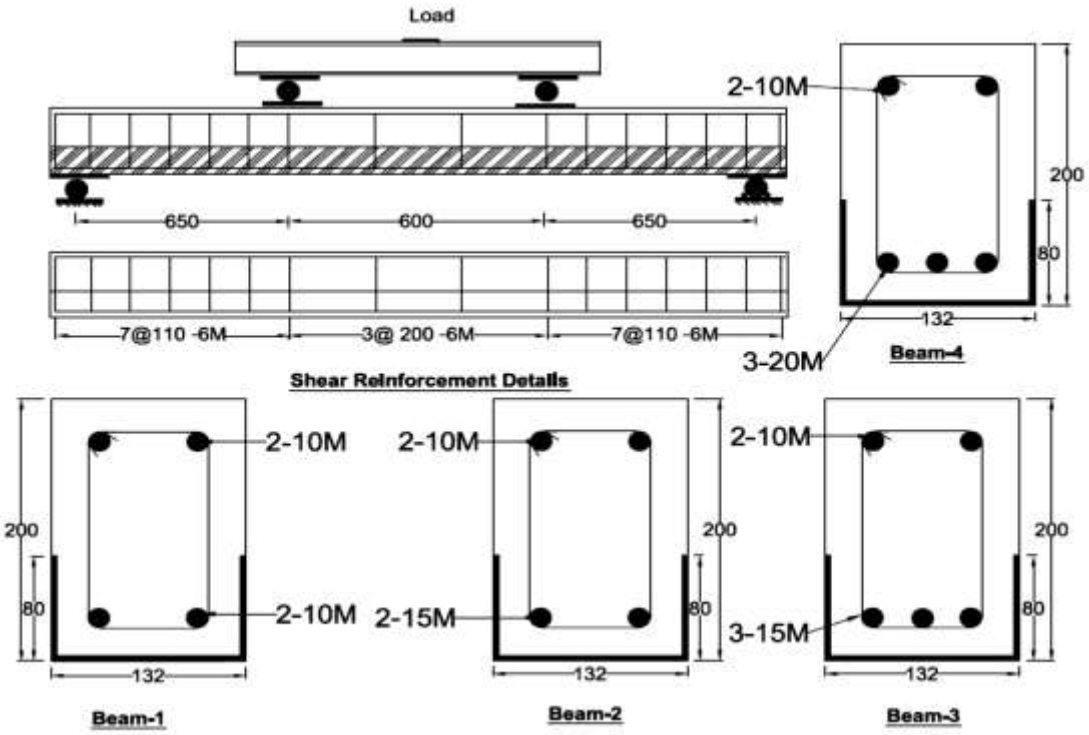

Figure 5.2 Specimen geometry and reinforcement details

The specimens were cast in two batches. The four wooden molds with steel reinforcement cages were placed directly on a vibrating table (Figure 5.3). These specimens were demolded on the following day and cured. The wooden molds were reassembled and reused for the next batch of specimens.

Figure 5.3 Specimens construction (top views) (a) ready for concrete casting (b) during pouring of concrete

5.3 Structural Testing

5.3.1 Instrumentation and Test Setup

The loading setup and instrumentation are shown in Figures 5.4 and 5.5. The specimens reinforced with the FRP composite shell "BF" from the each group were instrumented with four 20 mm long electrical resistance strain gauges, with gauge factor = 2.12 and electrical resistance =120±0.3 ohm (F1, F2, F3, and C1). Three strain gauges were installed on the FRP composite shell - one at the tension face (bottom), F1, one at the rebar level (35 mm from the bottom), F2, and one near the top edge of the FRP composite shell (75 mm from the bottom), F3. One strain gauge (C1) was installed on the concrete surface on the compression face of the beam.

Six 10V linear variable differential transformers (LVDTs) with a range of ±25 mm, were installed on the opposite vertical faces of the specimen, two at the center (TL2 and TR2) and two at each load point (TL1 and TL3 on the left side and TR1 and TR3 on the right side) to record the vertical deflections. These six LVDTs were clamped with adjustable plexiglass holders, into a rectangular frame, which was connected to rigid supports of the test setup (Figure 5.5) to eliminate any possible support settlement.

The mid-span LVDTs (TL2 and TR2) were supported on a pre-glued thin aluminum strip on the top surface of the beam. The LVDTs (TL1, TL3, TR1 and TR3) at the loading points were placed directly on the top surface of the bearing plates, underneath the loading rollers.

Two LVDTs (TS1 and TS2), with a range of ±15 mm, were also installed to measure the relative slip between the concrete and the FRP composite shell. These LVDTs (TS1 and TS2) were attached with clamps and holders, which were drilled into the concrete on both faces of the specimen. The LVDTs TS1 and TS2 were supported on an angle section, glued on the surface of the FRP composite shell. The position and location of these sensors are shown in Figures 5.4 and 5.5.

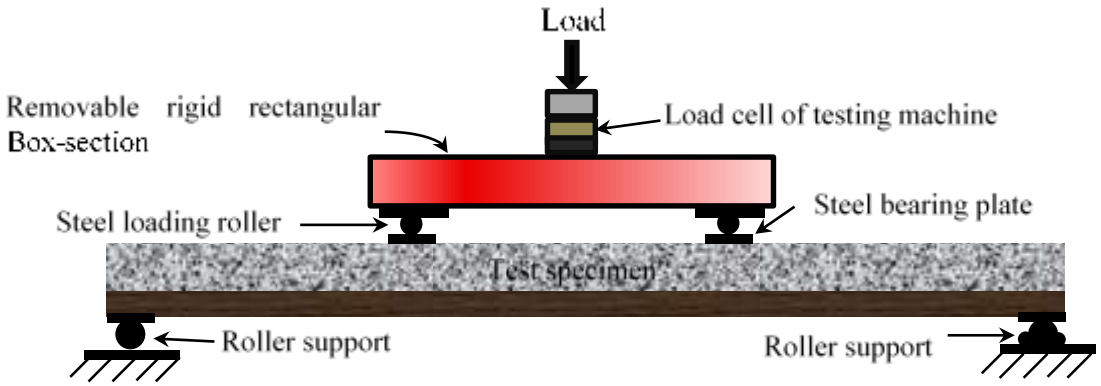

Figure 5.4 Schematic diagram of test setup

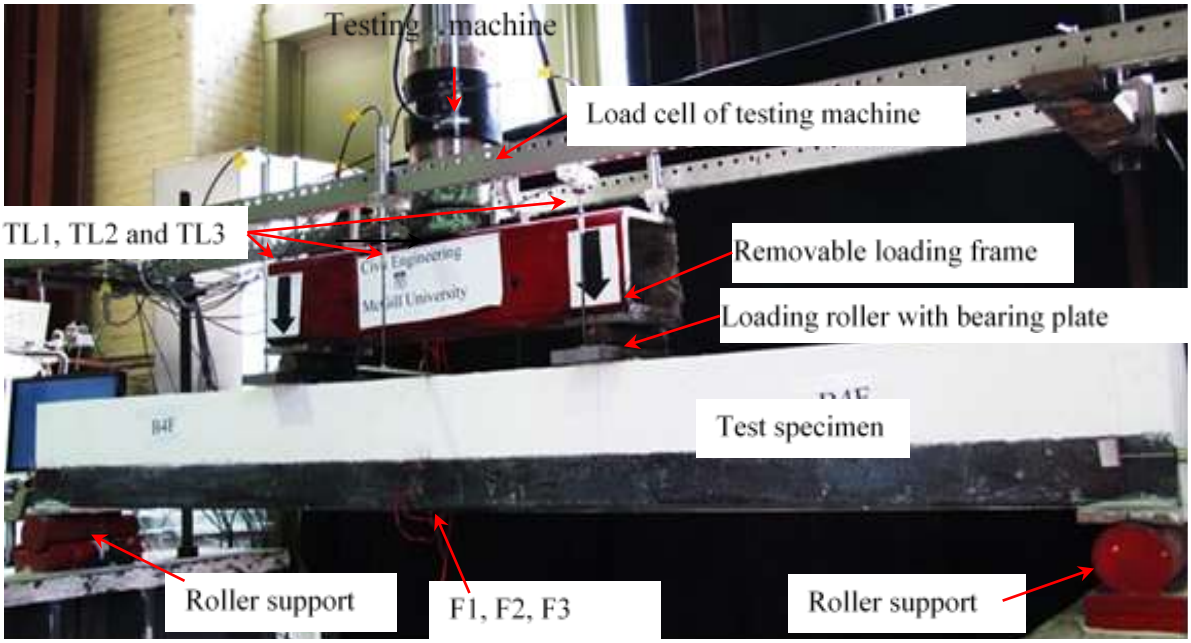

Figure 5.5 Four points loading setup with instrumentation

All sensors were connected directly to a data acquisition system (VISHAY 5100B Series) with Strain Smart software, which was connected to a computer to record the test data. The frequency of the recorded data was 2 scans/sec. The final instrumentation setup is shown in Figure 5.5.

Each specimen was subjected to flexural loading, using a four point loading arrangement, and was loaded using deflection control. Each specimen was loaded in two steadily applied deflection rate increments. A slow uniform deformation rate of 0.2 mm/min was applied transversely to the specimens until yielding of the tension reinforcement and then the deformation rate was doubled until the end of the test. The outputs from the load cell and the testing machine were also directly transmitted to the data acquisition system. The duration of the tests ranged between 4 to 6 hours depending on the deformability and the load carrying capacity of the specimen. The specimens were continuously monitored for cracking and any other phenomenon during the test and were photographed after every 10 kN loading interval.

Table 5.3 Data summary for the beam tests

Loading stages	Parameters	Group I		Group II		Group III		Group IV	
		B1F	B1S	B2F	B2S	B3F	B3S	B4F	B4S
At first crack	P_{cr} (kN)	22.5	14.1	25.9	14.8	34.3	21.0	37.1	22.7
	Δ (mm)	1.2	1.2	1.73	1.2	1.7	1.2	1.7	1.2
	S1 ($\varepsilon\times10^{-6}$)	538	649	378	324	448	299	426	210
	S2 ($\varepsilon\times10^{-6}$)	485	466	428	303	379	318	373	321
	C1 ($\varepsilon\times10^{-6}$)	-250	-	-258	-	-261	-	-283	-
	F1 ($\varepsilon\times10^{-6}$)	514	-	486	-	434	-	494	-
	F2 ($\varepsilon\times10^{-6}$)	412	-	434	-	404	-	408	-
	F3 ($\varepsilon\times10^{-6}$)	271	-	241	-	186	-	197	-
At yielding	P_y (kN)	75.7	49.5	101.2	91.7	153.8	135.0	181.5	197.4
	Δ (mm)	7.1	7.6	9.3	9.7	10.75	11.2	10.2	13.5
	S1 ($\varepsilon\times10^{-6}$)	2596	3901	2086	3358	D	2861	2513	3613
	S2 ($\varepsilon\times10^{-6}$)	2523	2887	2498	2472	2500	3265	2384	3403
	C1 ($\varepsilon\times10^{-6}$)	-1147	-	-1145	-	-1723	-	-1497	-
	F1 ($\varepsilon\times10^{-6}$)	3576	-	2403	-	3873	-	2786	-
	F2 ($\varepsilon\times10^{-6}$)	2055	-	1744	-	2305	-	2306	-
	F3 ($\varepsilon\times10^{-6}$)	1627	-	1230	-	1552	-	1137	-
At peak load	P_u (kN)	161.0	65.0	192.0	106.7	213.8	148.9	244.3	209.1
	Δ (mm)	25.6	42.6	25.4	41.4	19.0	29.7	16.5	20.7
	S1 ($\varepsilon\times10^{-6}$)	8233	D	6069	D	D	5138	10643	4284
	S2 ($\varepsilon\times10^{-6}$)	6729	D	8444	5720	10176	4840	13431	3735
	C1 ($\varepsilon\times10^{-6}$)	-3319	-	-2837	-	-3156	-	-2512	-
	F1 ($\varepsilon\times10^{-6}$)	3504	-	7503	-	8503	-	5458	-
	F2 ($\varepsilon\times10^{-6}$)	7080	-	4698	-	4992	-	4500	-
	F3 ($\varepsilon\times10^{-6}$)	5162	-	3273	-	3405	-	2103	-
At failure	P_{fail} (kN)	142.6	60.7	186.3	98.5	174.3	130.9	233.2	171.5
	Δ (mm)	36.2	66.9	27.1	50.5	20.3	48.3	16.9	28.8
	S1 ($\varepsilon\times10^{-6}$)	8251	D	6134	D	6394	D	4766	D
	S2 ($\varepsilon\times10^{-6}$)	6013	D	8635	D	9235	7397	6189	D
	C1 ($\varepsilon\times10^{-6}$)	-3130	-	-2843	-	-2884	-	-2521	-
	F1 ($\varepsilon\times10^{-6}$)	2915	-	D	-	7584	-	5573	-
	F2 ($\varepsilon\times10^{-6}$)	6812	-	4723	-	4633	-	4594	-
	F3 ($\varepsilon\times10^{-6}$)	4858	-	3281	-	3145	-	2114	-

D = strain gauge debonded

5.4 Results and discussion

All 8 specimens were loaded to failure, using displacement control, which allowed observation of both the pre-peak (just before the ultimate load) and post-peak behavior. The experimental data obtained and analyzed, included load-deflection relationships, along with stress and strain distributions at different load levels, the cracking patterns and the mode of failure along with the cracking, yielding and ultimate strengths. All of the RC beams with the FRP composite shell exhibited significantly higher flexural load-carrying capacity at first cracking, yielding and at ultimate loads, and a higher stiffness than that of the associated control beam. However, higher deformability was observed in the control RC beams as compared to RC beams with the FRP composite shell. The details of the test results for each specimen are summarized in Table 5.3.

5.4.1 Flexural Characteristics and Cracking of Beam Specimens

During the initial loading stage, the beam with FRP composite shell behaved differently as compared with the corresponding control specimen. Under increased loading, the beam's stiffness started to deteriorate and the load-deflection response was nonlinear due to cracking. On further loading, cracking propagated and the stiffness continued to decrease until failure. Specimens with FRP shell showed a stiffer response as compared with the specimens without the FRP shell because of the contribution of the FRP shell. A brief description of the response of the beams in the various groups, as they are loaded from zero load until failure follows:

5.4.1.1 Group I

The Beam B1S was loaded at a constant rate of 0.2 mm/min. It cracked at midspan at a load of 14.1 kN and at the loading points, on the tension face of the beam. With an increase in the applied load, the beam cracked further, with cracks at approximately equal distance of 10 cm apart in the

pure bending zone (Figure 5.6). The beam behaved nonlinearly until the applied load reached values of 49.5 kN, when the longitudinal tensile steel started yielding. The cracks propagated with the increase in the applied load, accompanied by an increasing central deflection. The beam demonstrated some increase in the load resistance after yielding of reinforcing steel along with substantial increase in the midspan deflection (Figure 5.6 and Appendix A). Near the ultimate load, the beam cracked extensively, with a very large deflection, and the neutral axis shifted upwards beyond the compression reinforcement (hanger bars). The concrete in the compression zone started crushing when the applied load reached the maximum values, which was followed by a decrease in the applied load. The final failure of the beam occurred with flexural cracks penetrating deep into the concrete compression zone. The crack patterns were continuously traced and photographed during the test. Figure 5.6 shows these cracks on one side of the beam.

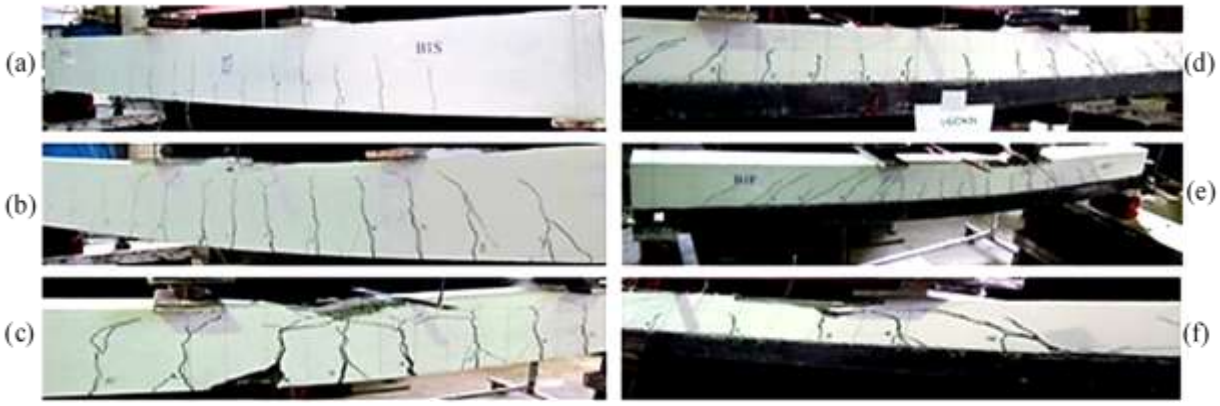

Figure 5.6 Cracking and failure sequence of Group II beam specimens (a) Beam B1S at yielding stage (b) Beam B1S at ultimate stage (c) Beam B1S at failure (d) Beam B1F at yielding stage (e) Beam B1F at ultimate stage (f) Beam B1F at failure stage

The Beam B1F exhibited different behavior as compared with the associated control Beam B1S. After experiencing the first cracking at midspan and load points, at an applied load of 22.5 kN, the

beam load-deflection response was nonlinear until a load of 75.7 kN, when the longitudinal tensile steel started yielding. After yielding of the reinforcing steel, the Beam B1F demonstrated a significant increase in the load resistance until the ultimate load (161 kN). After yielding of reinforcing steel, the flexural shear cracks appeared outside the pure bending zone. These cracks propagated, both in length and width, more than the flexural cracks in the pure bending zone. The concrete started crushing from the compression zone, as the applied load decreased to 142.6 kN. The final failure of the beam occurred because of flexural-shear cracks penetrating into the concrete compression zone, at a very large midspan deflection (36 mm), as shown in Figure 5.6. There was a debonding of the FRP composite shell near the tip of the widely opened diagonal crack; it extended toward the right side support.

Before initial cracking and prior to the yielding of the reinforcing steel, both beams exhibited considerably different flexural stiffnesses. The Beam B1F had a pre-cracking and pre-yielding flexural stiffnesses of 18.3 kN/mm and 8.8 kN/mm, respectively (Figure 5.9). The associated Beam B1S had a pre-cracking flexural stiffness of 9.3 kN/mm and pre-yielding flexural stiffness of 6.0 kN/mm for midspan deflection for the loading pattern used. The Beam B1F had 97% higher pre-cracking and 47% higher pre-yielding flexural stiffnesses than the Beam B1S, as indicated by the slopes of the load-deflection curve in Figure 5.9 and 5.10. As expected, the Beam B1F displayed stiffer response as compared with the associated control Beam B1S, because of the contribution of the FRP shell.

5.4.1.2 Group II

The Beam B2S initially cracked at midspan and loading points on the tension face at a load of 14.8 kN. This was followed by cracking in the pure flexure zone. The load-deflection relationship was

almost linear before cracking and became non-linear from the first cracking to the pre-yielding region, before yielding of tension steel at a load of 91.7 kN. There was a gradual increase (16%) in resistance from yield load until the ultimate load (106.7 kN), with a significant increase in the central deflection (Figure 5.9 and Appendix A). After reaching the ultimate load, the beam cracked extensively throughout its length, with the cracks growing in length and width, with gradual upward shifting of the neutral axis up to the level of the compression reinforcement. The concrete in compression started crushing, followed by a crack at the end of the hanger bars. After reaching the ultimate load, a piece of concrete separated from the compression face with a strength decrease (load = 98.5 kN). The final failure of the beam occurred with flexural cracks penetrating into the concrete compression zone and crushing of the concrete.

The Beam B2F exhibited almost similar behavior as beam B1F, the significant differences being a higher ultimate load value as expected, and lower deformations. The beam cracked just outside the FRP composite shell in the pure flexural region at a load of 31 kN. With a gradual increase in applied loading, flexural shear cracks appeared outside of the pure flexural zone. These flexural-shear cracks propagated more than the pure flexure cracks. The concrete started crushing in compression when the load reached a maximum value at 192 kN (Figure 5.10). The final failure of the beam occurred when flexural-shear cracks penetrated into the concrete compression zone accompanied by a very large midspan deflection (27.1 mm). The final failure of the specimen was in shear along with debonding of FRP composite shell.

Both beams exhibited notably different flexural stiffnesses before initial cracking and prior to yielding of the reinforcing steel. The Beam B2F had pre-cracking and pre-yielding flexural stiffnesses of 19.4 kN/mm and 10.0 kN/mm, respectively. The associated Beam B2S had pre-

cracking and pre-yielding flexural stiffnesses of 10.9 kN/mm 8.9 kN/mm, respectively; the Beam B2F displayed 78% higher stiffness compared with the Beam B2S before cracking, and 12% higher stiffness prior to the yielding respectively.

5.4.1.3 Group III

The Beams B3S and B3F cracked initially at mid-span and loading points on the tension face at loads of about 21 kN and 34.3 kN, respectively. In Beam B2S, these cracks were observed at midspan and at the loading points, accompanied by cracks in the pure bending zone. In Beam B3F, the initial cracking was detected from the load-deflection response, before these cracks appeared physically outside the FRP composite shell. With a gradual increase in the applied loading, flexural-shear cracks appeared outside the pure flexural zone in both beams. However, in Beam B3F, these flexural-shear cracks propagated more rapidly than the pure flexural cracks. There was not a clear indication of the beam yield strength. When the applied loading reached the maximum value, it failed suddenly without any significant post-ultimate deformation. The final failure of the beam was due to flexural-shear cracks penetrating into the concrete compression zone and crushing of the concrete. There was debonding of FRP composite shell from the widely opened crack at an angle of approximately 45 degrees from the loading point, penetrating into the concrete compression zone (Figure 5.7). The sequence of the final failure of the specimen was crushing of concrete, accompanied by debonding of the FRP composite shell, leading to the shear failure.

By contrast, the Beam B3S demonstrated a very gradual increase in the load resistance from the yield load to the ultimate load, with a significant increase (165%) in deflection. However, this increase in the applied load from the yield load to the ultimate load was not very significant as was observed in Beams B1S and B2S. After reaching the ultimate load capacity, the beam cracked

extensively throughout its length. These cracks propagated in length and in width, with gradual upward shifting of the neutral axis to the level of the compression reinforcement. The concrete started crushing at an ultimate load of 213.8 kN (Figure 5.7 and Appendix A).

The beam with FRP composite shell (B3F) exhibited a relatively higher stiffness (13.3 kN/mm) as compared with Beam B3S (11.4 kN/mm) prior to the yielding of the steel, as can be seen in the load-deflection curve (Figures 5.10 and 5.11). The difference in flexural stiffness of these two beams, with the same steel reinforcement ratio, was relatively small (16%) as compared to Group I and Group II specimens.

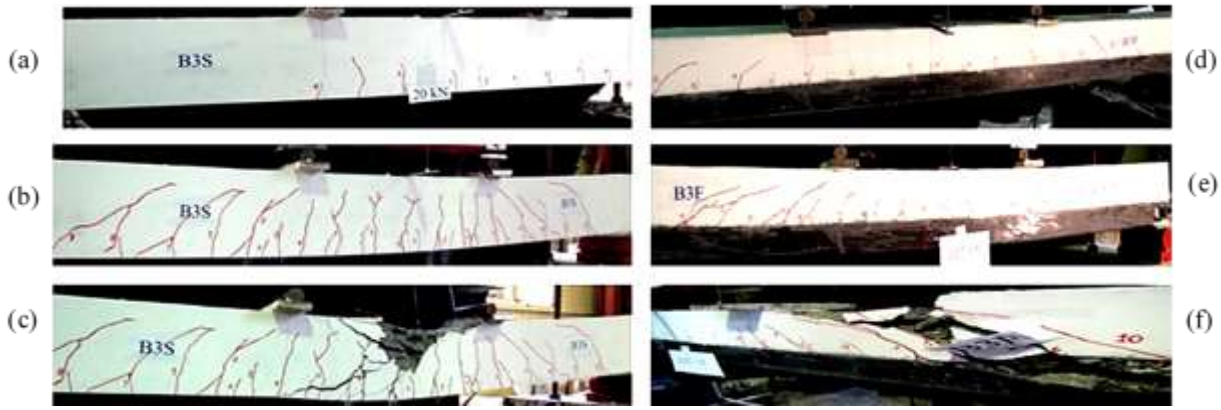

Figure 5.7 Cracking and failure sequence of Group III beam specimens (a) Beam B3S at initial cracking (b) Beam B3S at ultimate stage (c) Beam B3S at failure (d) Beam B3F after initial cracking and prior to yielding stage (e) Beam B3F at ultimate stage (f) Beam B3F after failure

5.4.1.4 Group IV

The load-deflection characteristics of Beams B4S and B4F were almost similar to the Group III beams. In Group IV, the initial cracking load was 37.1 kN for the Beam B4F and 22.7 kN for the associated Beam B4S, which were determined from the data analysis results. The initial cracks in

Beam B4S appeared in the pure bending zone, whereas this cracking of the Beam B4F was determined from the load deflection-curve (Figure 5.9 and Appendix A). Cracks appeared outside the FRP composite shell, within and outside the pure flexural region. In Beam B4F, the flexural cracks outside the pure flexural zone were accompanied by the flexural-shear cracks, and propagated more than the pure flexural cracks because of the higher reinforcement ratio, which made the beam stronger in flexure. There was no clear indication of yielding of steel in the load-deflection curve until the applied load attained the maximum value. The beam suddenly failed at the ultimate load (244.3 kN), without any significant gain in the midspan deflection from the ultimate load to the failure load (Figure 5.10). The final failure of the beam was similar to that of Beam B3F, due to flexural-shear cracks penetrating into the concrete compression zone. The final failure of the beam specimen was due to crushing of concrete in compression, accompanied by debonding of the FRP shell, leading to shear failure (Figure 5.8).

In Beam B4S, there was a very gradual and insignificant increase in the applied loading after tension steel yielding, accompanied by a significant increase in the midspan deflection. At ultimate load, the beam experienced extensive cracking in the pure flexural zone, flexural-shear cracking outside the loading points and diagonal shear cracks near the beam supports. The final failure of the beam resulted from crushing of concrete at an ultimate load of 209.1 kN (Figure 5.8).

The Beam B4F exhibited higher flexural stiffness (21.7 kN/mm) than the associated control Beam B4S (16.4 kN/mm), prior to initial cracking (Figures 5.9 and 5.10). The Beam B4F was much stiffer after yielding of the tension reinforcement than the Beam B4S because of the contribution of the FRP shell in flexural stiffness, after yielding of the reinforcing steel.

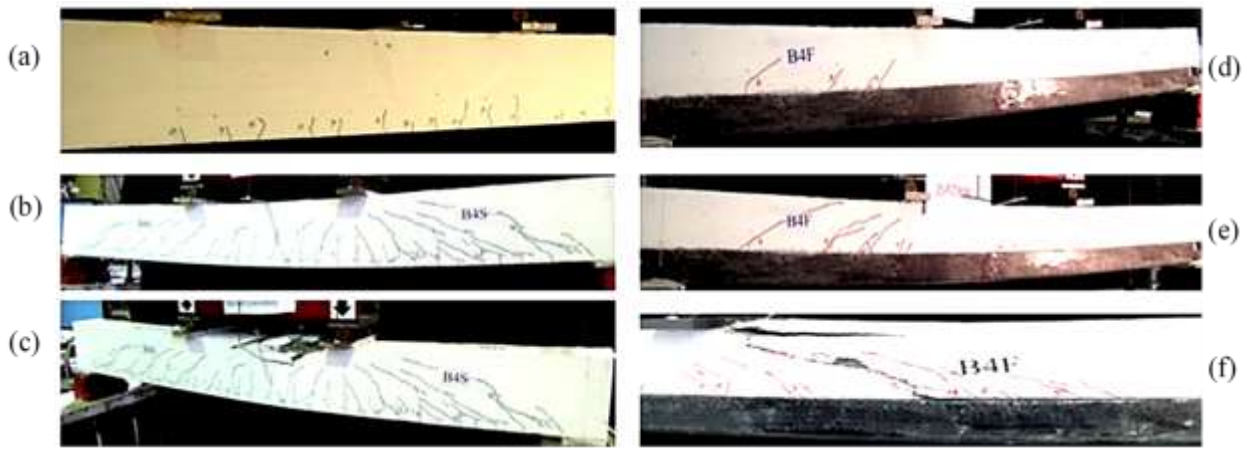

Figure 5.8 Cracking sequence and failure modes of Group IV beam specimens at different loading stages a) Beam B4S at initial cracking (b) Beam B4S at ultimate stage (c) Beam B4S after failure (d) Beam B4F at initial cracking stage (e) Beam B4F after failure

5.4.2 Comparison of Responses in all Four Groups

5.4.2.1 Load – Deflection Characteristics

Figures 5.9, 5.10 and 5.12 illustrates complete load-deflection responses of all test specimens at various loading stages. Irrespective of the beam types and failure modes at ultimate load, the load-deflection response of the beams can be divided into pre-cracking, yielding, pre-ultimate and ultimate and post-ultimate stages. All beams with the FRP composite shell exhibited almost similar behavior with a significant difference of higher ultimate load values and lower midspan deflection than the beam specimens without the FRP composite shell. The tension reinforcement ratios and the cracking pattern define modes of the final failure of the beam specimens.

All beams with the FRP shell exhibited almost similar behavior, with significantly higher cracking loads than the beams without the FRP shell. The average initial cracking load of the specimens with the FRP shell was about 70% higher than that of the associated control beams; however, the average midspan deflection was about 25% higher than that of the associated control beams.

The control beams of each group cracked on the tension face, at mid-span and at the loading points, followed by cracking in the pure flexural zone. The beam specimens with the FRP shell showed higher post-cracking stiffness, as indicated by the lower value of the steel strain at the same load level, compared with the associated control beam specimens, with the same reinforcement ratios. The post-cracking flexural stiffnesses were found to be 8.8, 10.0, 13.3 and 16.6 kN/mm for Beams B1F, B2F, B3F and B4F and 6, 8.9, 11.5, and 16.5 kN/mm for the associated control Beams B1S, B2S, B3S and B4S, respectively (Figure 5.10).

The load-deflection responses of the control beams (without the FRP shell) from each group were nonlinear before yielding of tension steel. The yield load values were very clearly followed by a yield plateau and a very gradual increase in the applied loading up to the ultimate loads. The yielding loads for specimens B1S, B2S, B3S and B4S were 49.5, 91.5, 135.0, and 197.4 kN, respectively (Figure 5.9).

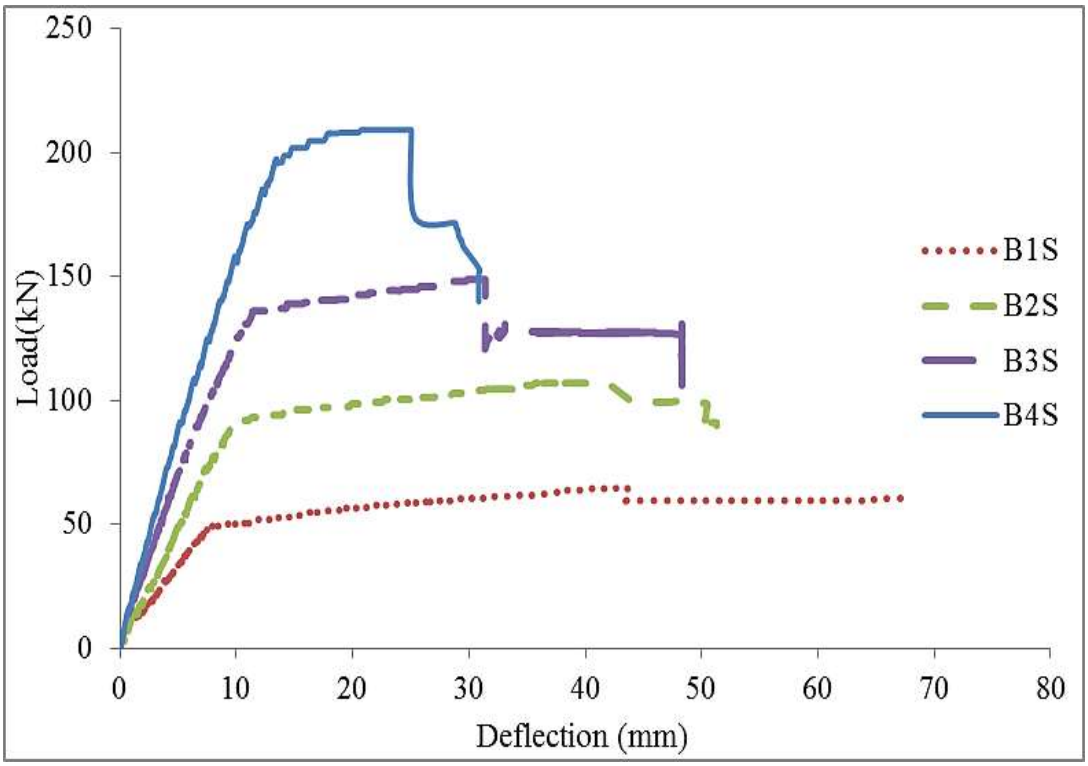

Figure 5.9 Load-deflection response of specimens without FRP shell.

The beam specimens with the FRP shell also behaved nonlinearly before yielding of the tension reinforcement. The yield loads were determined from the reinforcing steel strains readings. The yield loads for beam specimens B1F, B2F, B3F and B4F were found to be 75.7, 101.2, 153.8, and 181.5 kN, respectively (Figure 5.10).

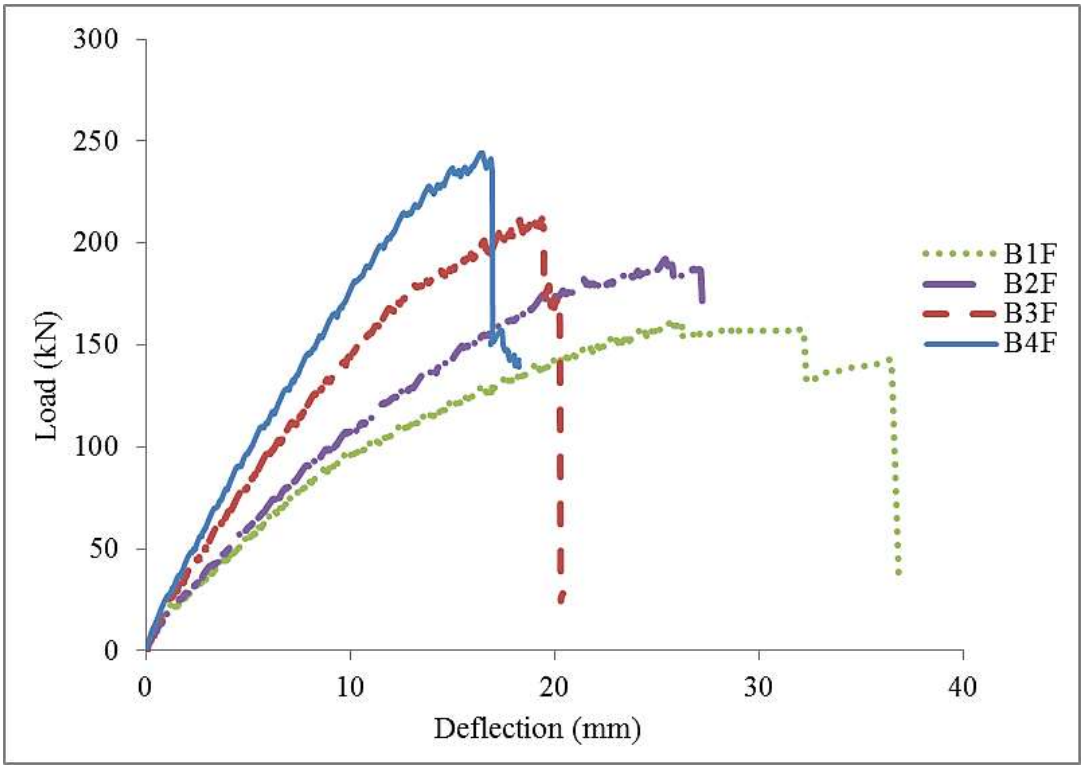

Figure 5.10 Load-deflection response of specimens with FRP composite shell

In beam specimens with the FRP shell, there was a significant increase in the applied loads, with a steeper slope of the load-deflection curves, from the yield load up to the ultimate load. The ultimate load values for Beams B1F, B2F, B3F and B4F were observed to be 161 kN, 192 kN, 213.8 kN and 244.3 kN, respectively. After reaching the ultimate load, these beams with the FRP shell failed suddenly, without any significant post-ultimate midspan deflection.

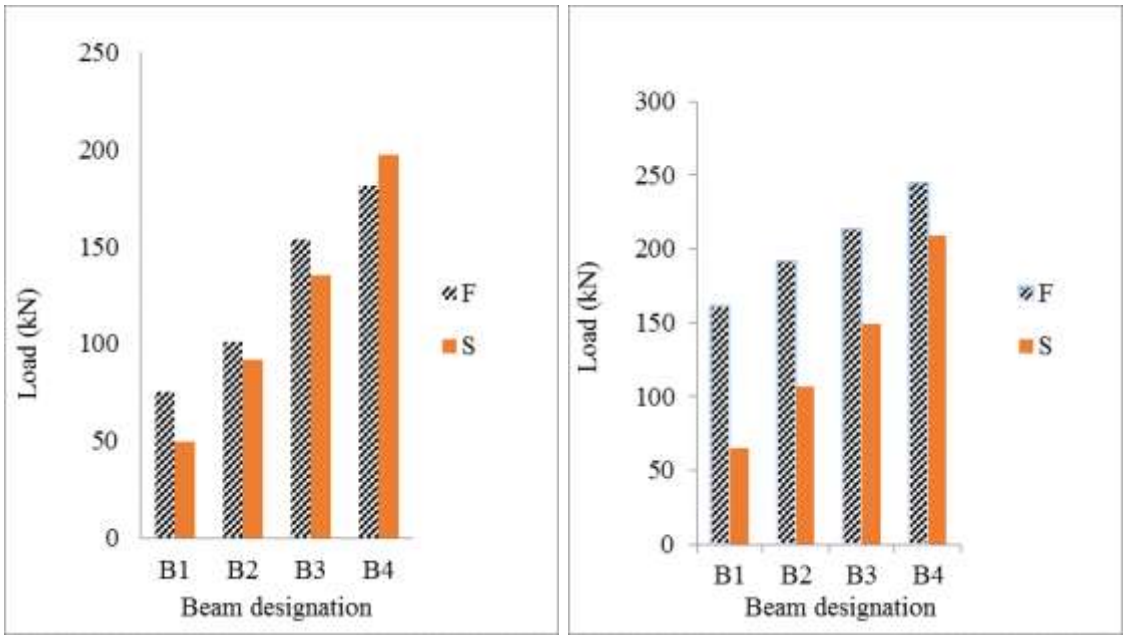

(a) *(b)*

Figure 5.11 Comparative improvement of beam strengths (a) in yielding (P_y) (b) at ultimate load (P_u)

By contrast, the associated control beam specimens demonstrated a very gradual increase in the applied load in the yield plateau to reach the ultimate load, with a significant increase in the midspan deflection. However, this increase from the yield load to the ultimate load was not significant as was observed in the beam specimens with the FRP shell. The ultimate load values for Beams B1S, B2S, B3S and B4S were 65 kN, 106.7 kN, 148.8 kN, and 209.1 kN, respectively (Figure 5.10 and 5.11(b)).

The post-ultimate behavior is distinguished by the residual resistance and deformability of the specimens. In both types of beams, the response varied depending on the steel reinforcement ratios and the effect of the FRP shell. In specimens without the FRP shell, the post-ultimate response, characterized by a gradual reduction in the beam resistance, initiated just after reaching the

ultimate load, leading to the final failure. However, in beams with the FRP shell, this decrease in the applied load was gradual for the ρ values from 0.8% to 1.6% and it was abrupt for ρ values from 2.4% to 4.8%. The post-ultimate midspan deflection of Group I and Group II beam specimens was larger, which failed pre-dominantly in flexure, as compared with the beam specimens which failed in combined flexure and shear (Group III and Group IV). The beams with the FRP shell, except for the Beam B1F, had a sudden decrease in resistance, after reaching the ultimate load, due to the development of the flexural-shear cracks, propagating into the compression zone, over the loading points and crushing of the concrete, followed by debonding of the FRP shell. Whereas, in Beam B1F, it was crushing of the concrete, followed by the flexural-shear cracks penetrating into the concrete compression zone, accompanied by a large deflection. The post-ultimate deformation response of beam specimens with the FRP shell were lower as compared with the beams without the FRP shell, which failed without a significant midspan deflection, after reaching the ultimate load. Figure 5.12 summarizes the load-deflection characteristics of all beam specimens.

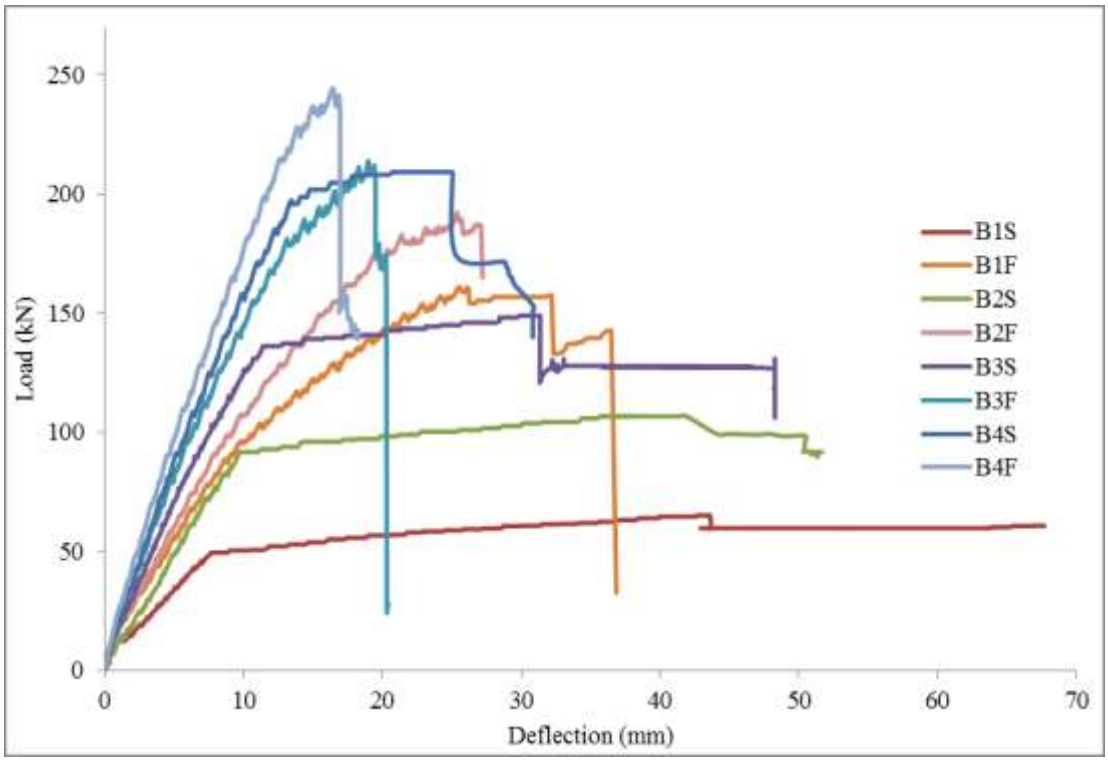

Figure 5.12 Load-deflection response of all specimens without and with FRP shell

5.4.2.2 Stiffness Characteristics

The flexural stiffness (K) is defined as a load corresponding to a unit midspan deflection for the loading pattern used. The flexural stiffness is the slope of the load-deflection curve before the initial cracking load (K1) and pre-yielding (from cracking to yield load) (K2). In general, the beam specimens with the FRP shell showed higher average stiffness than those of the associated control beams. This increase in flexural stiffnesses K1 and K2 due to the FRP shell and the different steel percentages, ρ, are summarized in Table 5.4.

Table 5.4 Pre-cracking (K1) and pre-yielding (K2) flexural stiffnesses of beam specimens.

Groups	Specimen	Flexural stiffness (kN/mm)			
		Pre-cracking (K1)	Difference (%)	Pre-yielding (K2)	Difference (%)
Group I	B1S	9.3	96%	6	47%
	B1F	18.3		8.8	
Group II	B2S	10.9	78%	8.9	12%
	B2F	19.4		10	
Group III	B3S	16.4	20%	11.5	16%
	B3F	20.4		13.3	
Group IV	B4S	18.4	18%	16.5	2%
	B4F	21.7		16.8	

The average increase in K2 for the beams with FRP shell was about 15% over that of the associated control beams, varying among 13% for Group I beams to 18% for Group IV beams (Figure 5.13)

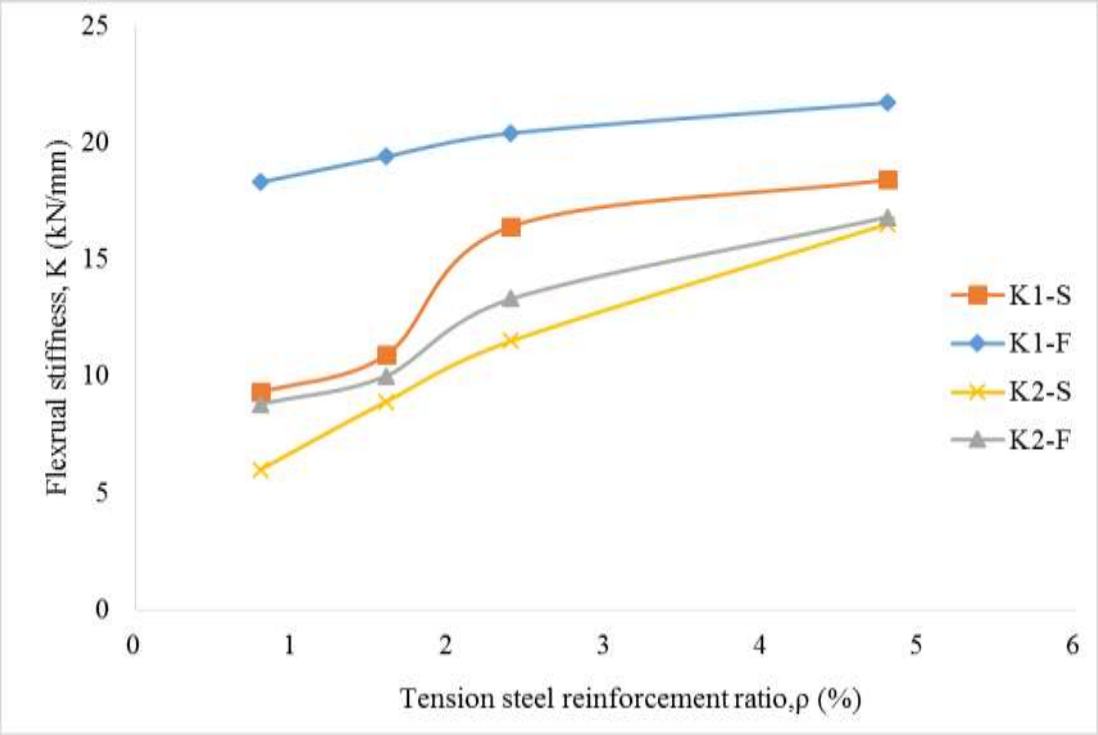

Figure 5.13 Effect of steel reinforcement ratio on pre-cracking (K1) and pre-yielding (K2) flexural stiffnesses of beam specimens with (F) and without (S) FRP shell.

5.4.2.3 Ductility and Energy Absorption Characteristics

The displacement ductility ratio (μ) is defined as the ratio of the ultimate deflection (Δ_u) to the deflection at yield load (Δ_y), when the beam is subjected to the loading pattern used. The beam specimens with FRP shell behaved in a brittle manner as compared to the associated control beams in all groups. From Group I to Group IV, there was a significant decrease in the μ values (59%) specimens without FRP composite shell and 200% in the specimens with FRP composite shell, when the steel reinforcement ratio increased from 0.8% to 4.8%. The average ratio of the total deflection at peak loads among all beams with FRP composite shell and the associated control beams decreased from 3.7% to 0.4%. The average values of ductility ratio (μ) corresponds to ultimate deflection and ultimate load are summarized in the Table 5.5.

Table 5.5 Comparison of displacement ductility ratio (μ) of all beam specimens

Groups	Specimen	Ductility ratio (μ)			
		Corresponds to ultimate deflection	Difference (%)	Corresponds to ultimate load	Difference (%)
Group I	B1S	8.8	-42%	5.6	-35%
	B1F	5.1		3.6	
Group II	B2S	5.2	-44%	4.3	-37%
	B2F	2.9		2.7	
Group III	B3S	4.3	-58%	2.7	-33%
	B3F	1.9		1.8	
Group IV	B4S	2.1	19%	1.6	0%
	B4F	1.7		1.6	

The energy absorption (E) is defined as the area under the load-deflection curve. The results showed that an increase in the steel reinforcement ratio from 0.4% to 4.8%, the E value decreased significantly (37%) in the specimens with the FRP composite shell. The beam specimens with FRP composite shell absorbed a smaller amount of energy as compared with their associated control beams in most of the cases; however, in Group I specimens, the energy absorbed by the Beam B1F was 12% more than the associated Beam B1S. This difference is due to the added FRP composite shell. However, for the same steel reinforcement ratio, the energy absorption capacity drastically decreased (37%) for the beam specimens with FRP composite shell because of their lower deformability, after the post-peak. The average values of energy absorption (E) are summarized in the Table 5.6.

Table 5.6 Comparison of energy absorption of all beam specimens

Group	Specimen	Energy absorption, E (kN.mm)	Difference (%)
Group I	B1S	3711	-12%
	B1F	4159	
Group II	B2S	4718	29%
	B2F	3329	
Group III	B3S	5611	52%
	B3F	2666	
Group IV	B4S	4816	46%
	B4F	2620	

5.4.2.4 Effect of Steel Reinforcement Ratio

Steel reinforcement ratio had a significant effect on the initial cracking strength of the beam specimens, both with and without the FRP shell. With an increase in the steel reinforcement ratio from 0.4% to 4.8%, the cracking strength increased by 64.4% for the beam specimens with the FRP shell and 53.3% for the associated control beam specimens. Again, this was due to the additional contribution of the FRP shell which delayed this cracking by contributing to increased flexural strength of the reinforced concrete beam.

With an increase in the steel reinforcement ratio, there was a notable increase in the yield load for the beams with the FRP shell and their associated control beam specimens. The yield strength gain in the control specimens from Group I to Group IV was consistent with the steel reinforcement ratio increase. However, the beam specimens with the FRP shell, the yield strength increased by a factor of 2.6 when the steel reinforcement ratio increased by a factor of 6 times. The FRP shell

contributed to the flexural strength of the beam specimens which enhanced the yield strength of the beams. The summary of results is presented in Figure 5.14.

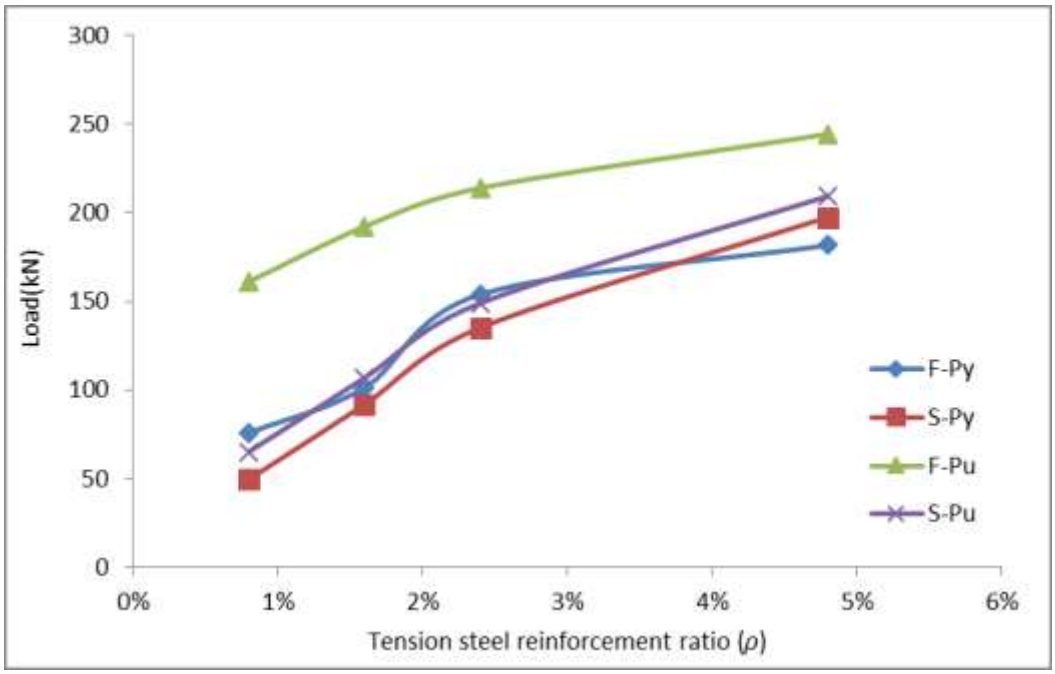

Figure 5.14 Effect of tension steel reinforcement ratio on yield and ultimate loading of beam specimens

The ultimate strength gain was higher between the beam specimens and their associated control beams in groups with lower reinforcement ratios and substantially decreased from 147% to 16.8% for groups with higher reinforcement ratios, because the beam specimens behaved as over-reinforced and the FRP shell strength was not fully utilized.

5.4.3 Strain Distributions

The strains in the concrete in compression, reinforcing steel and FRP composite shell were measured until debonding of the strain gauges, or failure of the beam specimens, whichever occurred first. Figure 5.15 presents the measured strain variation versus the applied load in the

concrete in compression, reinforcing steel and FRP shell. The trends of strain variation with the applied loads were almost similar as in the load-deflection curves of the beam specimen.

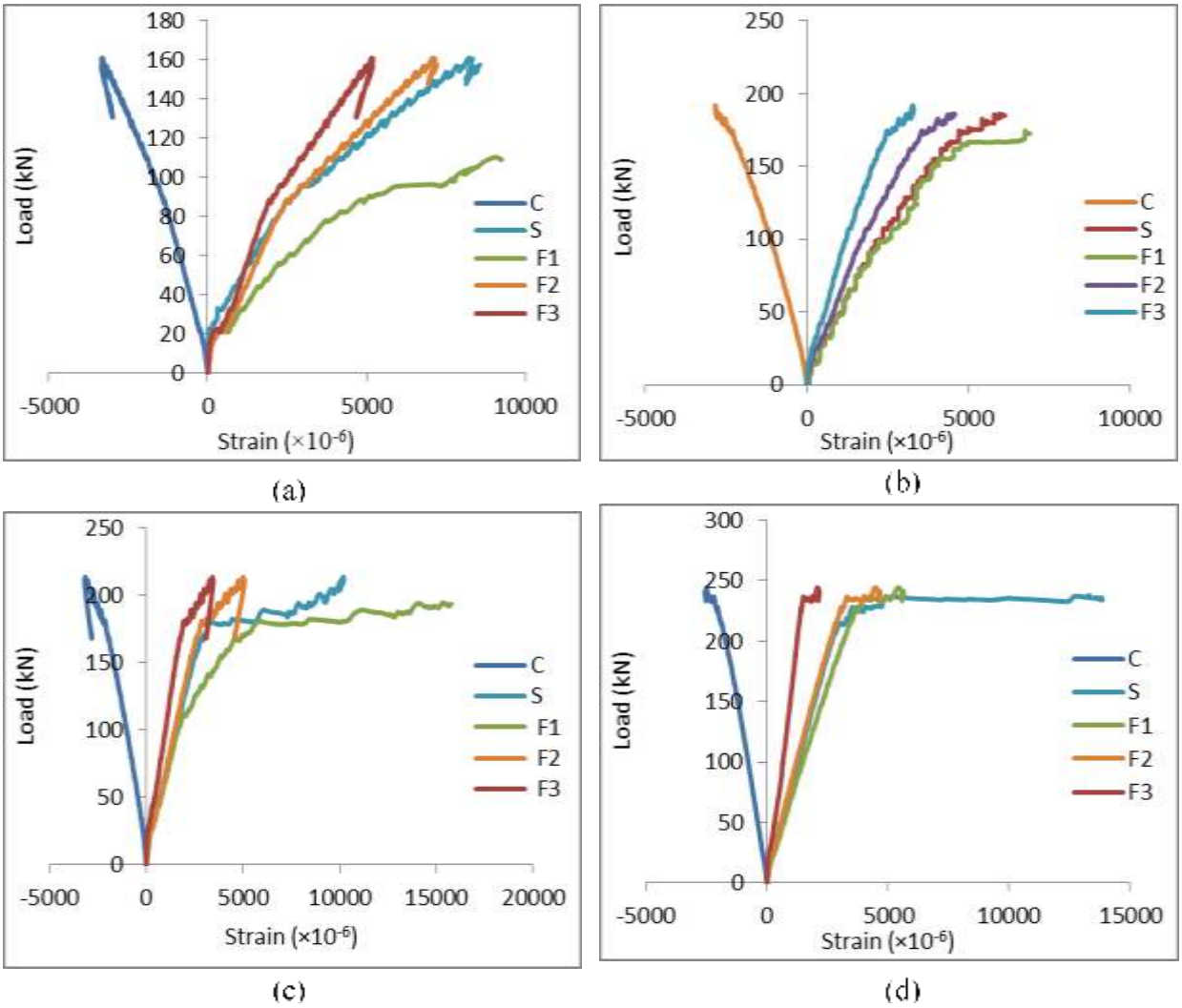

Figure 5.15 Strain variation in the FRP shell, reinforcing steel and concrete with applied load (a) Beam B1F (b)Beam B2F (c) Beam B3F (d) Beam B4F

5.4.4 Slip between the FRP Shell and the Concrete Interface

The slip between the FRP shell and the concrete interface was recorded using LVDTs (TS1 and TS2) at both ends. The results showed that there was no slip until the beams with the FRP

composite shell failed and debonding of FRP composite shell occurred. This implies that a perfect bond exists between the FRP shell and the cast-in-place concrete.

5.4.5 Modes of Failure

In each group, the control beam specimens were designed as under-reinforced sections to fail in flexure as the steel reinforcement reached and exceeded the yield strength, followed by crushing of the concrete, with a large associated deflection. The modes of failure varied depending on the different steel reinforcement ratios and the effect of the FRP shell in beams with and without the FRP shell.

Three types of failure mechanisms were observed in all of the beam specimens, as summarized in Table 5.7. Flexural compression failure was the most common failure mode, which occurred in all control beam specimens and in Beam B1F. In Groups II, III and IV, the beam specimens with the FRP shell finally failed due to flexural-shear, as these cracks penetrated into the concrete compression zone and crushing of the concrete. There was a debonding of the FRP shell from the tip of the wide diagonal cracks, under the loading points, penetrating into the concrete compression zone, to the beam supports.

Table 5.7 Summary of beam failure modes

Group	Beam	Failure sequence	Failure mode(s)
Group I	B1F	• Flexural cracking • Concrete crushing • FRP shell debonding	Flexural cracks penetrated into the concrete compression zone at the loading point, followed by debonding of the FRP shell.
	B1S	• Tension steel yielding • Concrete crushing at midspan.	Yielding of tension steel followed by crushing of the concrete at a large midspan deflection.
Group II	B2F	• Flexural cracking • Concrete crushing • FRP shell debonding.	Flexural-shear cracks penetrated into the concrete compression zone at the loading point, followed by debonding of the FRP shell.
	B2S	• Flexural cracking • Concrete crushing at midspan.	Yielding of tension steel followed by crushing of the concrete at a large midspan deflection.
Group III	B3F	• Concrete crushing • Steel stirrup fracture • Debonding of FRP shell • Shear failure.	Fracture of one steel stirrup along the diagonal tension cracks (shear failure)
	B3S	• Flexural cracking • Concrete crushing at midspan.	Yielding of tension steel followed by crushing of the concrete at a large midspan deflection.
Group IV	B4F	• Concrete crushing • Debonding of FRP shell • Shear failure.	Diagonal tension cracks (shear failure)
	B4S	• Flexural cracking • Concrete crushing at midspan.	Flexural cracks penetrated into the concrete compression zone at a large midspan deflection and crushing of concrete.

5.5 Summary

This chapter examines the flexural behavior of simple reinforced concrete beams with the cast-in-place U-shaped FRP shell. This external FRP shell or membrane around the lower part of the concrete beams can eliminate, or significantly reduce the ingress of chloride, and consequently

help to enhance its service life. The flexural characteristics of the FRP shell-concrete interface along with the effect of the steel reinforcement ratio were studied experimentally to evaluate the flexural and shear behaviors of the FRP shell-reinforced concrete beams.

Simple reinforced concrete beams, consisted of cast-in-place concrete with an externally-bonded U-shape FRP shell, were constructed. These beams were designed for four different reinforcement ratios – 0.8, 1.6, 2.4, 4.8 %, - to examine their flexural characteristics. These U-shaped FRP shells were pre-glued with 10 mm maximum size aggregates to improve the bond mechanically with the cast-in-place concrete. The specially designed U-shaped FRP shell demonstrated a significant enhancement in both the strength and stiffness as well as higher ductility and energy absorption capacities of the FRP-reinforced beams, as compared with the associated control beams.

These beams were tested under four point loading. The recorded data were analyzed and the load-deflection responses of all specimens were plotted. Irrespective of the beam types and failure mode, the load-deflection response of the beams can be divided into initial cracking, pre-yielding, pre-ultimate, ultimate, and post-ultimate stages. The first part of the load-deflection curve was almost linear; however, the second part of the load-deflection curve was nonlinear, the beam stiffness continued to decrease due to cracking, along with high reinforcing steel strains until failure occurred. The beam specimens with the FRP shell showed a significant enhancement in the strength, stiffness and energy absorption capacity as compared with the associated control beams. The mode of failures varied depending on the steel reinforcement ratios, along with the effect of FRP shell.

CHAPTER 6 FLEXURAL CHARACTERISTICS OF PRESTRESSED CONCRETE BEAMS WITH FRP COMPOSITE SHELL

6.1 Introduction

This chapter deals with an experimental program to investigate the flexural behavior of prestressed concrete beams with an FRP composite shell in the tension zone. To evaluate the effectiveness of the FRP composite shell in prestressed concrete construction, ten prestressed concrete beams were constructed with and without a FRP composite shell. These beams consisted of pretensioned high strength strands, along with prefabricated U-shaped FRP composite shells, with pre-glued aggregates for improved bond resistance, which were later filled with concrete. These beams were tested under four point monotonically increasing loads until failure to study their complete behavior. The experimental data were analyzed; the results included load-deflection relationships, stress and strain distributions at different load levels, flexural stiffnesses, ductility, energy absorption, cracking patterns and the modes of failure along with the initial cracking, yielding and ultimate strengths. The response of the FRP composite shell and the FRP- prestressed concrete interface were examined in detail.

6.2 Research Significance

To evaluate the contribution of the FRP composite shell to the structural strength and the overall behavior of prestressed concrete beams, this chapter focuses on following objectives:

- Application of FRP composite shells to new prestressed concrete construction, including the effect of prestressing on FRP composite shell and its bond with the concrete substrate.

- Development of construction procedures for composite beams with an FRP composite shell, and evaluation of their strength and stiffness characteristics.
- Evaluation of flexural characteristics of FRP composite shell and cast-in-place concrete before and after prestressing.

6.3 Experimental Procedure

6.3.1 Materials and Properties

6.3.1.1 FRP Shell

The hybrid FRP U-shape shells were fabricated in the Materials Laboratory of the Department of Civil Engineering and Applied Mechanics at McGill University. The detailed fabrication procedure is presented in Chapter 5. The design details and mechanical properties of the FRP U-shape shell are described in Chapter 3.

6.3.1.2 Reinforcing Steel

A 9.5 mm (3/8") diameter, 1860 MPa grade, low relaxation seven wires prestressing steel strand was used for prestressing the beam specimens. Tension tests were performed on prestressing steel strands to evaluate their mechanical properties, and compared with those provided by the manufacturer. Special couplers were designed to grip the strand during the tension test; detailed procedure and mechanical properties are summarized in Chapter 4.

Commercially available 10M reinforcing steel bars were was used as hanger bars and 6 mm diameter deformed steel bars were used for shear reinforcement. The results of these flexure tests are summarized in Chapter 3.

6.3.1.3 Concrete

The beam specimens for all phases of this research project were constructed using the same concrete mixture. Two prestressed composite beams were cast at a time. The concrete mix had a compressive strength of 55.45 (±1.04) MPa. The average compressive strength (f_c') of the concrete from each batch is summarized in Table 6.1.

Table 6.1 Concrete compressive strength data

Group	Beam	Description	Prestress level	f_c' (MPa)
P0	P0F	With FRP composite shell	0%	55.1
	P0S	Without FRP composite shell		
P25	P25F	With FRP composite shell	25%	55.7
	P25S	Without FRP composite shell		
P50	P50F	With FRP composite shell	50%	56.2
	P50S	Without FRP composite shell		
P75	P75F	With FRP composite shell	75%	55.0
	P75S	Without FRP composite shell		
P100	P100F	With FRP composite shell	100%	55.3
	P100S	Without FRP composite shell		

6.4 Design of Beams Specimens

As mentioned earlier, ten prestressed concrete beam specimens, reinforced with FRP composite shell, were constructed to investigate the response of cast-in-place prestressed concrete with the bonded FRP composite shell. These specimens were tested to study the flexural characteristics of prestressed concrete beams reinforced with the FRP composite shell and its strength and stiffness characteristics. The contribution of the FRP composite shell to flexural and shear strengths were

not considered in the design process, to ensure the beam would be able to develop its full load carrying capacity, if it deteriorated over time.

For analysis and design of prestressed concrete beams, commercially available software 'Concise Beam' version 4.58f was used. This software package is based on procedures outlined in the CPCI Design Manual, PCI, and NPCAA (Black Mint Software).

The beam specimens were divided into five groups, based on level of prestress – 0, 25, 50, 75 and 100% of total prestressing force. Each group consisted of two specimens, one specimen reinforced with an FRP composite shell and the second without the FRP shell, as an associated control beam specimen. The 'P' value (prestressing force percentage) for the first group specimens was zero, which simulated a complete loss of prestressing force over the service life of the structural member; whereas, the group P100 beams had 'P' force values equal to the maximum allowed value of pre-tensioning force (P_{max}) that can be applied to the prestressing strand (Table 6.1).

The first letter in the specimen nomenclature represents a prestressed concrete beam specimen (P); the following number is the level of prestressing expressed as a percentage of total pretensioning force and the last letter distinguishes presence (F) or absence (S) of the FRP composite shell, with letter being the associated control beam specimen. For example, P25F is a prestressed concrete beam, with 25% level of prestressing force, reinforced with the FRP composite shell.

6.5 Specimen Preparation

A 2-metre long, prestressed concrete beam, 132 x 200 mm in cross-section, reinforced with two 9.5 mm (3/8") diameter seven-wire prestressing steel strands, four 10M (one in each corner) and

with the top bars acting as hanger bars, with the FRP composite shell installed along with the form work (Figure 6.1) were cast and tested.

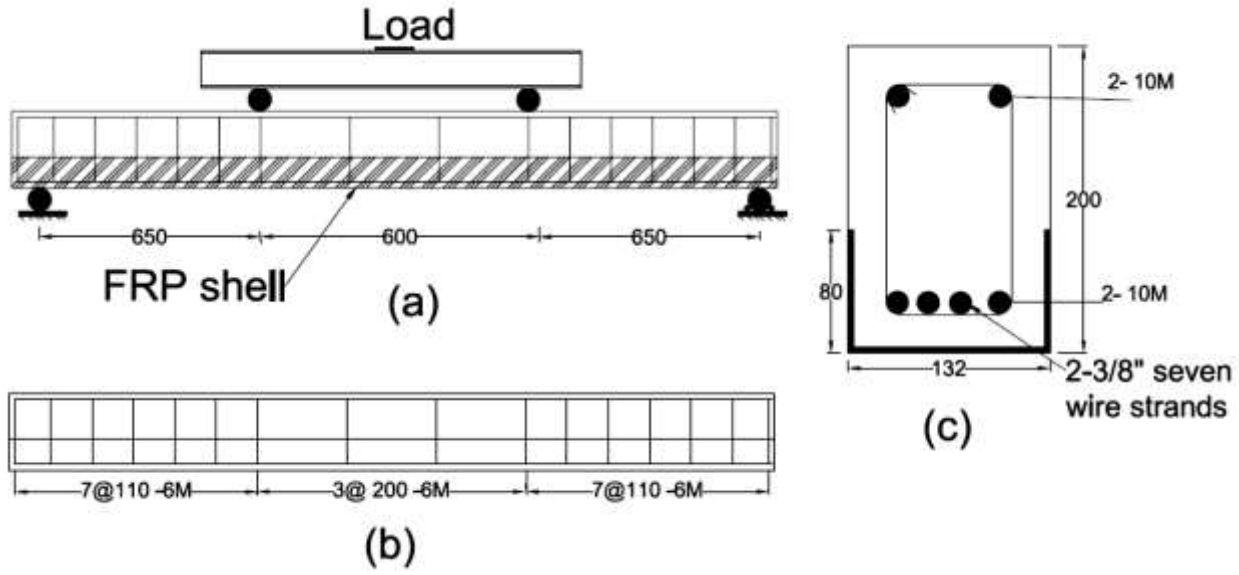

Figure 6.1 Specimen geometry and reinforcement details of simple reinforced beam with FRP shell (a) elevation (b) shear reinforcement detail (c) cross-section

The prestressing force was calculated based on the ultimate strength of the strand. The pre-tensioning force for specimens P100 (100% level of prestressing) was 160 kN, which corresponded to 74% of the ultimate strength of the strand (f_{pu}). For P75, P50, and P25 specimens, the prestressing forces were 120, 80 and 40 kN, respectively (Table 6.3). For comparison purposes, five associated control specimens (P0S, P25S, P50S, P75S and P100S) were also constructed without the FRP composite shell.

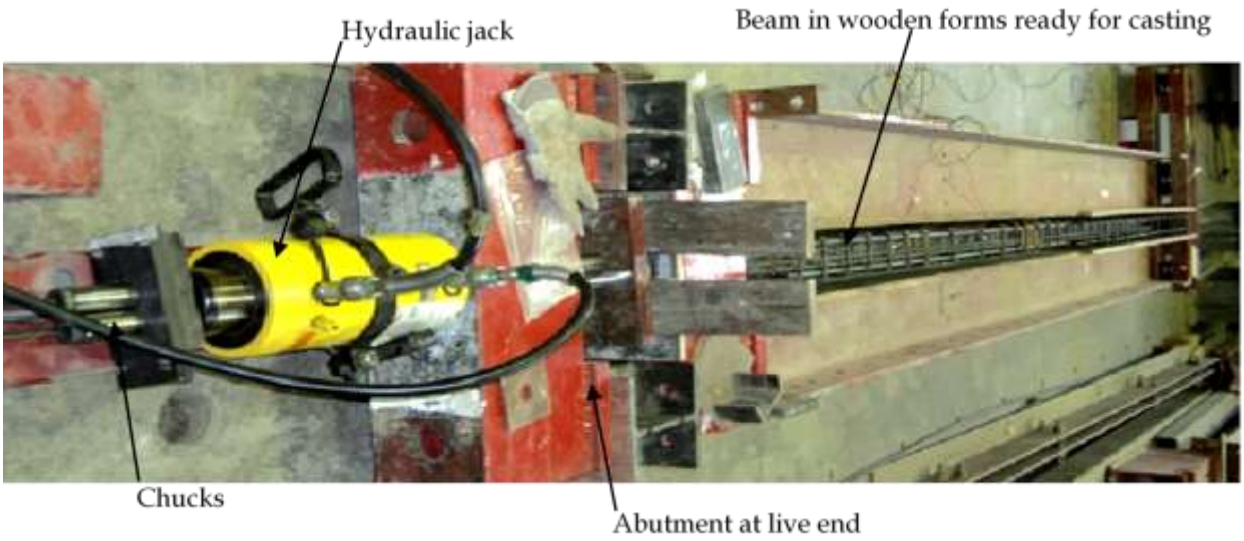

Figure 6.2 Prestressing bed with pre-tensioning setup and beam construction arrangement

A prestressing bed was prepared for the pre-tensioning operation to accommodate two specimens at a time. Two channel sections, placed back-to-back and connected with a steel plate, with a central hole to allow the strands to pass in-between, were fixed at each end of the bed. The pre-tensioning force corresponding to the different levels of prestressing was applied using a hydraulic jack at the active end, and one load cell was installed on each strand at the dead end of the bed to measure the pre-tensioning force. The required pre-tensioning force was monitored using three different methods - load cells installed at the dead end of the prestressing bed, effective elongation in the prestressing strand (measured at the live end of the prestressing bed) and bonded strain gauges on the prestressing steel strand - before the concrete was poured into the wooden forms, with the surface coated with oil to facilitate removal of the beams from the form. After every 10 kN increment of the pre-tensioning force, the readings from the three methods were monitored simultaneously and the prestressing bed was monitored carefully to avoid any accident. The prestressing bed and the pretensioning setup is shown in Figure 6.2.

The beam specimens were instrumented to monitor the strain variation in the FRP composite shell and the prestressing steel strand, at different loading stages, such as jacking of the prestressing strand, releasing of the prestressing force after concrete hardening and during the testing of the specimens. The strain variation in the prestressing steel strand was monitored using two 2 mm long electrical resistance strain gauges (SG), with a gauge resistance of (120± 0.3) Ω and a gauge factor of 2.11. One 20 mm long electrical resistance strain gauge (gauge factor = 2.12) was installed on the FRP composite shell, before the concrete casting, to measure the strain during the preparation procedure, as shown in Figure 6.2.

Table 6.2 summarizes the prestressing data at jacking and release stages. The jacking force was the maximum load applied to the prestressing steel strands by the hydraulic jack during the pre-tensioning operation. During the pre-tensioning operation, there was a slight loss in the prestressing force because of locking and seating of chucks, and elastic shortening of the concrete. After completion of the pre-tensioning operation, the concrete was cast. The concrete shrinkage, along with other time dependent factors, also contributed to the losses in the pre-tensioning force.

Table 6.2 Prestressing data of prestressed concrete beams

Group	Specimen	Level of prestressing	Prestressing force (kN)		
			Designed (P_d)	Jacking (P_j)	Effective (P_e)
P0	P0F	0%	0	5	0
	P0S				
P25	P25F	25%	40	43	39.8
	P25S				
P50	P50F	50%	80	83	80.2
	P50S				
P75	P75F	75%	120	124	119.5
	P75S				
P100	P100F	100%	160	164	158.6
	P100S				

6.6 Structural Testing of Specimens

6.6.1 Instrumentation and Test Setup

All beams were subjected to four point monotonically increasing transverse loads. The loading setup was similar to the one used for testing of simple reinforced concrete beams; the loading setup details are presented in Chapter 5. The load, midspan and load points deflections, strains in the prestressed steel strands and the concrete compression fibers at midspan, strain variation in the FRP composite shell at midspan, and the slip between the concrete and FRP composite shell interface at both ends, were recorded during testing. Cracks were also monitored and marked during the test. The loading setup and instrumentation are shown in Figure 6.3.

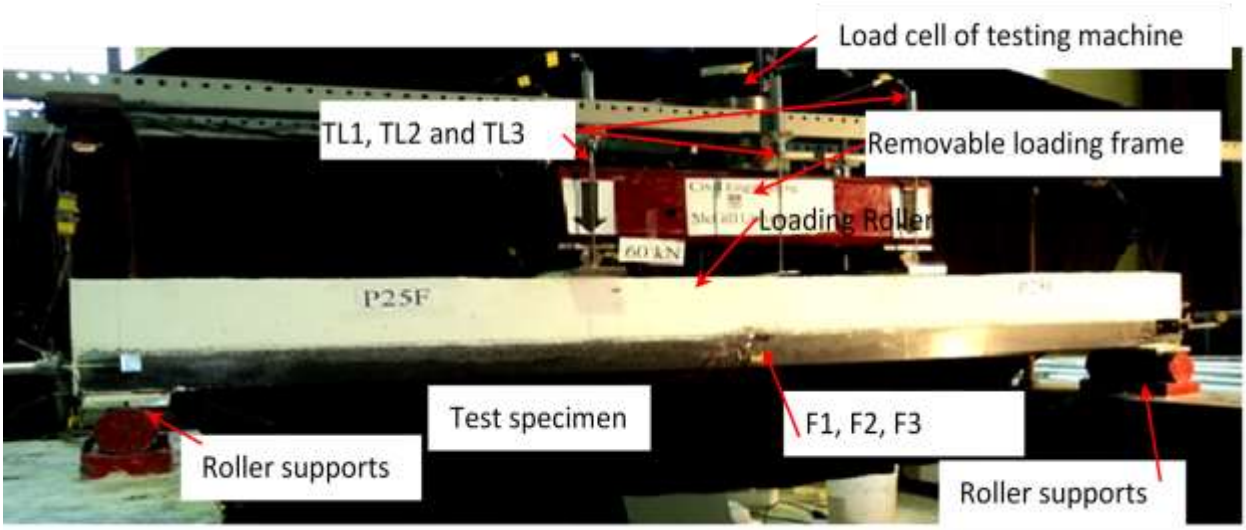

Figure 6.3 Four point loading test setup with instrumentation

6.7 Results and Discussion

All ten specimens were loaded to failure using displacement control, which allowed observation of the specimen behavior during all loading stages, from zero load until failure. All of the prestressed concrete beams with FRP composite shell exhibited significantly higher flexural load-carrying capacity before cracking, pre-yielding and at ultimate load, and a higher stiffness compared with the associated control beams. Higher deformation in the form of midspan deflection was observed in the control beams as compared with the beams with the FRP composite shell. The details of the test results for each specimen are summarized in Table 6.3.

Table 6.3 Data summary for the prestressed concrete beam tests

Loading stages	Parameters	Prestressing %									
		0		25		50		75		100	
		P0F	P0S	P25F	P25S	P50F	P50S	P75F	P75S	P100F	P100S
First crack	P_{cr} (kN)	27.6	13.3	35.7	13.9	50.6	36.4	50.2	42.9	67.8	62.3
	Δ (mm)	2.1	1.0	2.0	0.8	2.9	2.8	2.3	2.8	2.5	5.1
	S_1 ($\varepsilon \times 10^{-6}$)	654	395	D	D	727	647	456	476	D	D
	S_2 ($\varepsilon \times 10^{-6}$)	622	219	468	D	702	776	531	592	401	870
	C_1 ($\varepsilon \times 10^{-6}$)	-346	-	-391	-	-529	-	-377	-	-260	-
	F_1 ($\varepsilon \times 10^{-6}$)	740	-	486	-	964	-	577	-	471	-
	F_2 ($\varepsilon \times 10^{-6}$)	518	-	281	-	760	-	410	-	389	-
	F_3 ($\varepsilon \times 10^{-6}$)	341	-	137	-	364	-	169	-	141	-
Yield load	P_y (kN)	93.5	76.9	108.1	89.3	114.7	99.9	115.1	99.1	121.3	102.7
	Δ (mm)	7.7	9.3	9.9	12.2	9.9	12.5	9.1	10.3	9.8	14.5
	S_1 ($\varepsilon \times 10^{-6}$)	2500	3348	D		2506	3751	2007	1623	D	D
	S_2 ($\varepsilon \times 10^{-6}$)	2439	3403	2500		D		2501	2611	2500	2078
	C_1 ($\varepsilon \times 10^{-6}$)	-1518	-	-1608	-	-1432	-	-1287	-	-1104	-
	F_1 ($\varepsilon \times 10^{-6}$)	2968	-	3282	-	2964	-	2418	-	2456	-
	F_2 ($\varepsilon \times 10^{-6}$)	2016	-	2190	-	2295	-	1842	-	1788	-
	F_3 ($\varepsilon \times 10^{-6}$)	1345	-	1233	-	1233	-	1072	-	917	-
Ultimate load	P_u (kN)	165.0	104.4	185.0	118.1	183.1	120.8	184.8	125.7	192.3	134.1
	Δ (mm)	19.9	35.6	31.9	29.1	24.0	21.6	25.8	37.1	29.5	37.5
	S_1 ($\varepsilon \times 10^{-6}$)	5900	9886	D	D	D	6847	2605	2454	D	D
	S_2 ($\varepsilon \times 10^{-6}$)	5783	8358	5714	D	D	D	7813	5779	8601	D
	C_1 ($\varepsilon \times 10^{-6}$)	-3743	-	-3758	-	-2572	-	-2851	-	-2814	-
	F_1 ($\varepsilon \times 10^{-6}$)	D	-	D	-	6366	-	5550	-	6511	-
	F_2 ($\varepsilon \times 10^{-6}$)	5473	-	5348	-	4831	-	4547	-	4957	-
	F_3 ($\varepsilon \times 10^{-6}$)	3430	-	3394	-	2752	-	2556	-	2948	-
Failure load	P_{fail} (kN)	109.9	122.5	135.2	96.2	173.4	119.8	181.2	129.6	163.1	96.9
	Δ (mm)	21.0	36.5	35.1	36.7	29.3	41.5	25.3	37.4	32.0	37.5
	S_1 ($\varepsilon \times 10^{-6}$)	4825	10801	D	D	D	D	2534	2188	D	D
	S_2 ($\varepsilon \times 10^{-6}$)	4390	D	4431	D	D	D	7699	5506	7614	D
	C_1 ($\varepsilon \times 10^{-6}$)	-2524	-	-2957	-	-2511	-	-2802	-	-2328	-
	F_1 ($\varepsilon \times 10^{-6}$)	D	-	D	-	6292	-	5439	-	6475	-
	F_2 ($\varepsilon \times 10^{-6}$)	D	-	4282	-	4751	-	4455	-	4739	-
	F_3 ($\varepsilon \times 10^{-6}$)	4256	-	2600	-	2715	-	2500	-	2627	-

D= Strain gauge debonded

6.8 Load – Deflection Characteristics

Figures 6.8, 6.9 and 6.10 present the load-deflection responses of all the beam specimens by distinguishing the various stages of flexural loading. The load-deflection responses for all beams were non-linear, with a smooth transition before yielding to the ultimate load stages. The nearly linear initial part of the load-deflection curves had a steep slope, which corresponds to the uncracked stiffness. In the second part, the beam stiffness decreased as a result of flexural cracking and higher strain values in the prestressing steel strands. Irrespective of the beam types and failure modes, the load-deflection response of the beams can be divided into four stages: initial cracking, pre-yielding and ultimate, and post-ultimate/failure stages.

6.8.1 Initial Cracking

All beams with an FRP shell exhibited almost similar behavior at initial cracking, with a significant difference in the higher ultimate load values and lower deformability than the associated control beams (without FRP shell). For the beams with FRP shell, the initial cracking was deduced from their load-deflection curves and when cracks appeared outside the FRP shell in the pure bending region. The cracking in all of the control beams appeared on the tension face at midspan and loading points, followed by further cracking in the pure bending region. At higher load levels, the previously formed cracks propagated, along with the appearance (formation) of new cracks between the major cracks at approximately equal spacings regardless the location of the shear reinforcement.

The initial cracking loads of all beams along with their comparisons with the associated control beam from each group are summarized in Table 6.4. In general, the average initial cracking loads increased by 108% to 410% with the level of prestressing from 0% to 100%, in the beam specimens

with FRP shell as compared with their associated control beams (Table 6.4). However, this enhancement in the initial cracking load was reduced from 108% to 9% within the same group beams, when the level of prestress increased from 0% to 100%.

Table 6.4 Comparison of initial cracking loads for all specimens

Groups	Specimen	Initial cracking loads ($P_{initial}$)	
		$P_{initial}$ (kN)	Difference (%)
Group P0	P0S	13.3	108%
	P0F	27.6	
Group P25	P25S	13.9	156%
	P25F	35.7	
Group P50	P50S	36.4	39%
	P50F	50.6	
Group P75	P75S	42.9	17%
	P75F	50.4	
Group P100	P100S	62.3	8%
	P100F	67.8	

6.8.2 Pre-Yielding and Pre-Ultimate Load Characteristics

The initial linear part of the load-deflection curves in Figures 6.4, 6.5 and 6.6, with a steep slope, corresponds to uncracked flexural stiffness for the midspan deflection for the loading condition used for this beam. The flexural stiffness decreased as a result of increased flexural cracking with an increase in the applied load. At ultimate load, the flexural cracks propagated both in length and width gradually from the tension face towards the compression face of the beam; finally, the

concrete crushed at the beam top, accompanied by large deflections in the beam (Appendix B). The specimens with FRP shell showed higher post-cracking flexural stiffness, as indicated by the low value of the steel strain, at the same load level, and as compared with the specimens without the FRP shell, for the same level of prestress. A detailed comparison of the flexural stiffnesses is presented in Section 6.8.5.

The yield loads were deduced from the strain value of 2500×10^{-6} in the prestressing steel strands, which were found from the simple tension test on the prestressing steel strand. These yield load values for all specimens and their percentage increase or decrease are summarized in Table 6.5.

Table 6.5 Comparison of yield loads for all beam specimens

Groups	Specimen	Yield loads ($P_{y)}$	
		P_y(kN)	Difference (%)
Group P0	P0S	76.6	22%
	P0F	93.9	
Group P25	P25S	89.3	21%
	P25F	108.1	
Group P50	P50S	99.9	15%
	P50F	114.7	
Group P75	P75S	99.1	16%
	P75F	115.1	
Group P100	P100S	102.7	18%
	P100F	121.3	

In Group P0 (0% prestress level), the Beam (P0F) had an increase of 23% in the yield load, along with a significant increase in the flexural stiffness (Figure 6.4(a)).

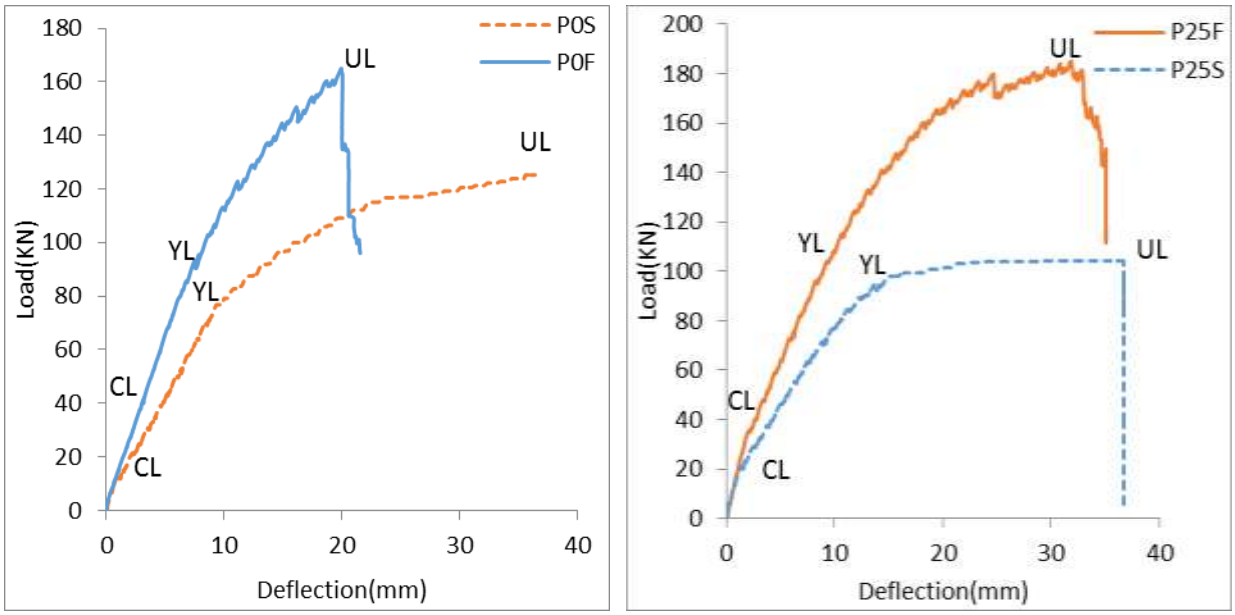

(a) (b)

Figure 6.4 Load-deflection characteristic of prestressed concrete beams (a) 0% level of prestress (b) 25% level of prestress

The associated control Beam P25S from Group P25 (prestressed to 25%), initially cracked at the tension face at midspan and at the loading points at a load of 13.6 kN. The prestressing steel strands started yielding at load P_y = 89.3 kN. After yield load, there was a small gradual increase in the load, along with a significant increase in the deflection up to the ultimate load (P_u = 118.1 kN). The beam cracked extensively throughout its length, with a gradually upward shifting of the neutral axis, to the level of the compression reinforcement, and the concrete started crushing. The Beam P25F exhibited different behavior compared with the associated control Beam P25S, with a significantly higher (21%) yield load and smaller (18%) midspan deflection (Figure 6.4(b)).

In Group P50 (Figure 6.5(a)), the Beam P50F (50% prestress level) had 15% higher yield strength than the associated control Beam P50S. In both beams P50S and P50F, flexural-shear cracks appeared outside of the pure flexural region, in addition to the flexural cracks. However, in the Beam P50F, these flexural-shear cracks propagated more than the primary flexural cracks, which caused failure of the beam (Appendix B).

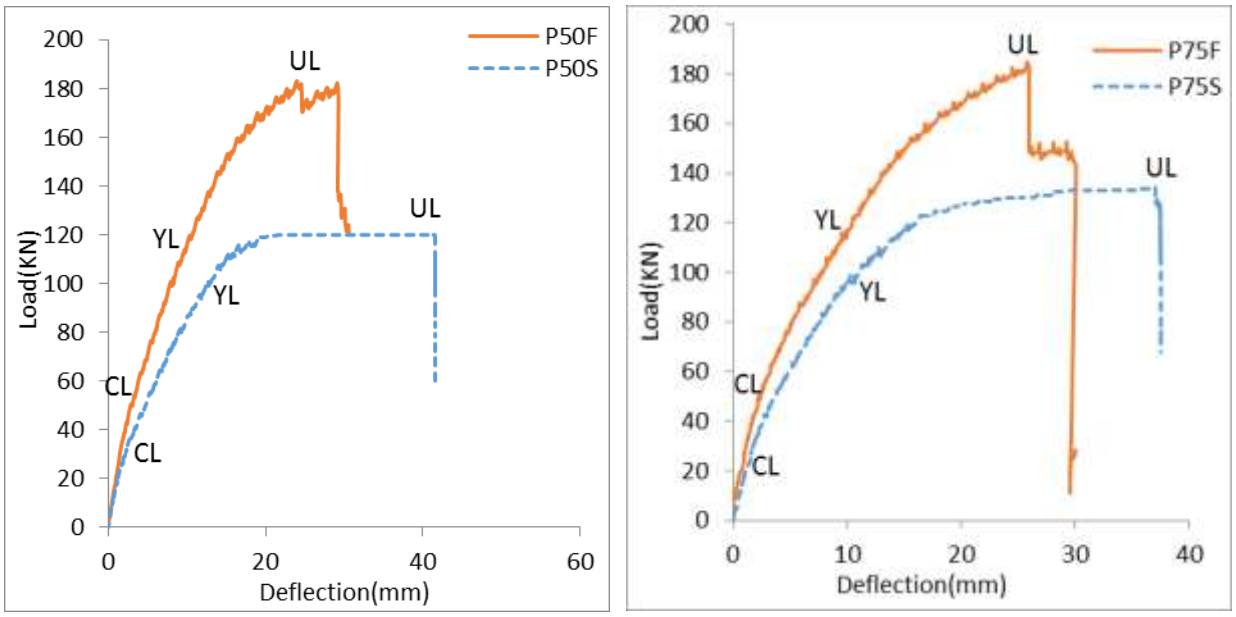

(a) *(b)*

Figure 6.5 Load-deflection characteristic of prestressed concrete beams (a) 50% level of prestress (b) 75% level of prestress

The load-deflection characteristics of Group P75 (75% prestress level) specimens were similar to those of the Group P50 specimens (Figure 6.5(b)). The yield strength was 16% higher than for the Beam P75F, as compared with the associated control beam P75S. Beam P75S demonstrated a gradual increase in strength at ultimate load (from an applied load of 99.1 kN to 125.7 kN), after

yielding of the prestressing steel strands. This was accompanied by a significant increase (by a factor of 2.6) in the midspan deflection.

The load-deflection characteristics of the beams for Group P100 (100% prestress level) are shown in Figure 6.6. An 18% yield load enhancement was observed in the Beam B100F as compared with the associated control Beam B100S.

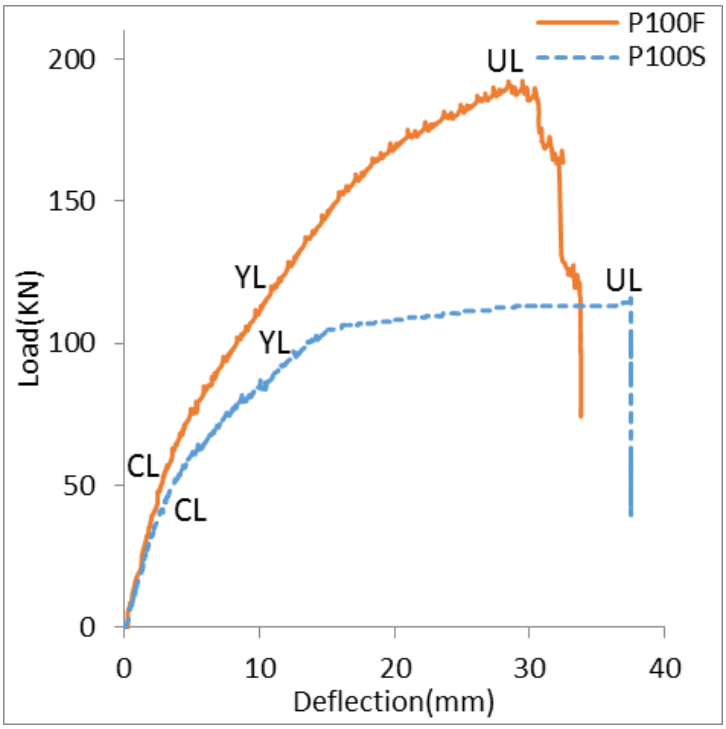

Figure 6.6 Load-deflection characteristic of prestressed concrete beams with 100% level of prestress

Figure 6.7 (a) and (b) shows comparative enhancement in the yield (P_y) and ultimate load (P_u) the beam specimens in all five groups, along with their associated control beam specimens.

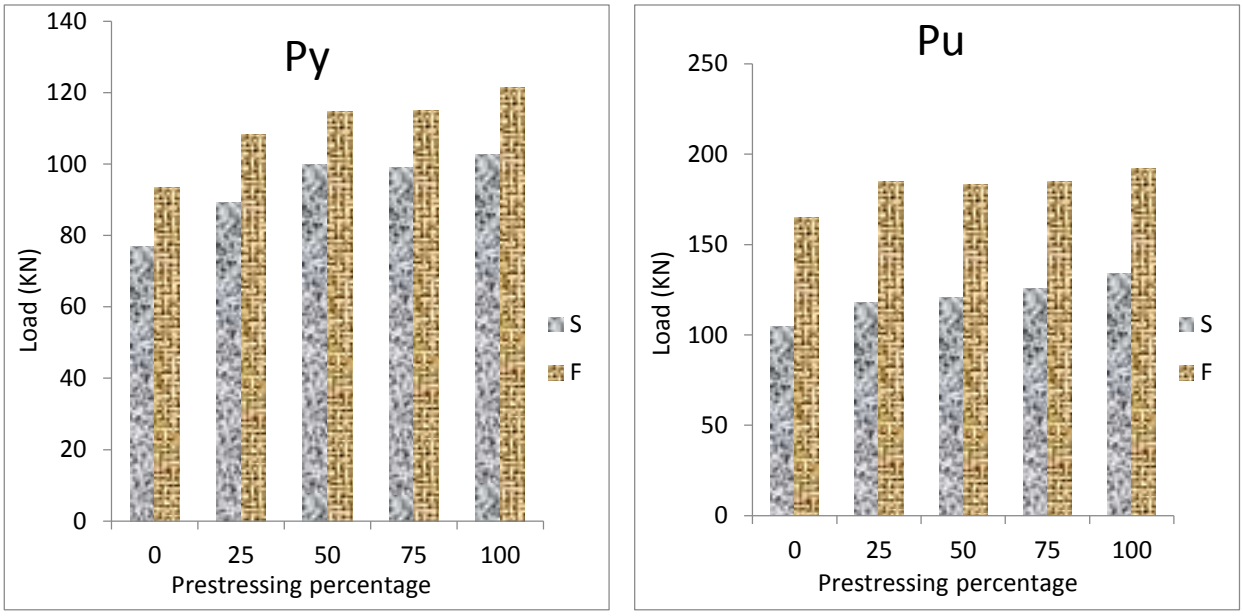

(a) (b)

Figure 6.7 Comparative enhancement in the beam specimens with different level of prestress along with their associated control beam (a) yield load (P_y) (b) ultimate load (P_u)

6.8.3 Ultimate Load Behavior

There was a significant increase in the ultimate loads for beam specimens with FRP shell in all groups, with a steeper slope of the load-deflection curve, from yield load to the ultimate load (Figures 6.8 and 6.9). The ultimate loads for Beams P0F, P25F, P50F, P75F and P100F were 58%, 57%, 52%, 47%, and 43%, respectively, higher than those of the associated control beams P0S, P25S, P50S, P75S and P100S (Table 6.6). This noticeable improvement in the ultimate load value decreased from 58% to 43% when prestress of level increased from 0% to 100% (Table 6.6). This percentage decease in the ultimate load can be observed from the load-deflection curves (Figure 6.8). In beams with 50% or higher prestress level, bond between the FRP shell and the concrete interface depleted before the ultimate load was attained. These beams (P50F, P75F and P100F) failed suddenly without any significant increase in the midspan deflection. The associated control

beams demonstrated a gradual increase in strength after the yield load until the ultimate load, accompanied by a significant increase in the midspan deflection (Figure 6.8). However, this increase in the load from the yield load to the ultimate load was not significant in the associated beams, as was observed in the beams with FRP shell (Figure 6.9).

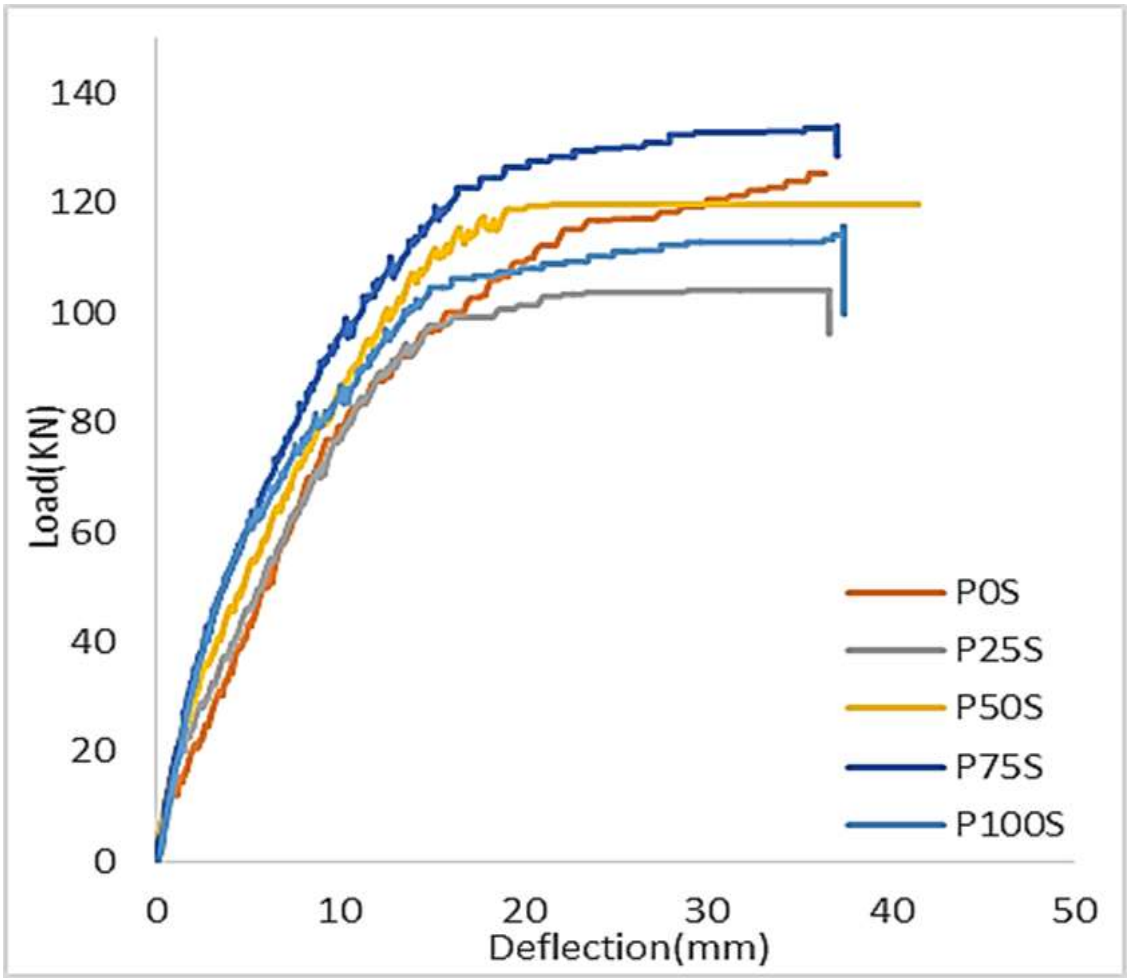

Figure 6.8 Load-deflection response of prestressed concrete specimens without FRP shell

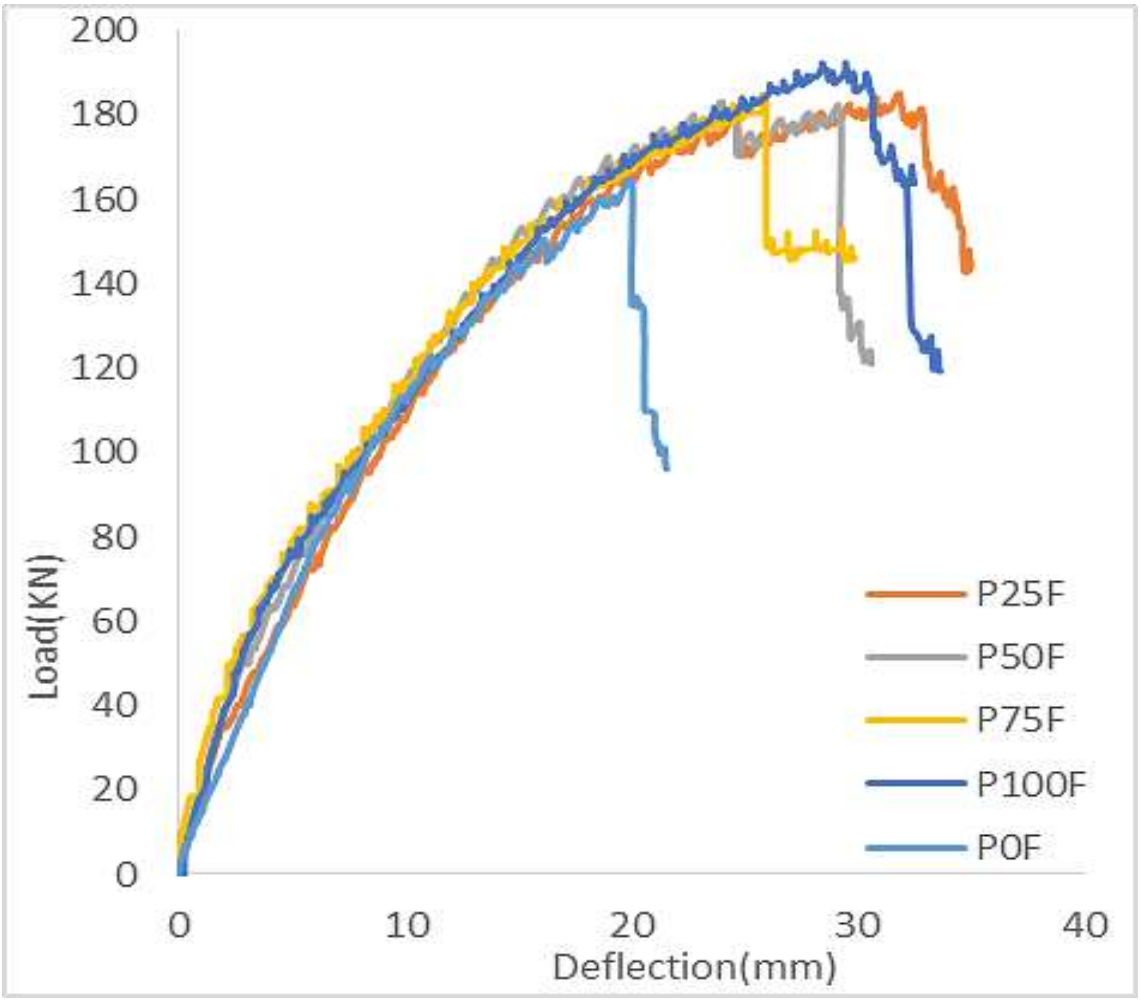

Figure 6.9 Load-deflection response of prestressed concrete specimens with FRP shell

Table 6.6 Comparison of ultimate loads for all beam specimens

Groups	Specimen	Ultimate loads ($P_{u)}$	
		P_u (kN)	Difference (%)
Group P0	P0S	104.4	58%
	P0F	165	
Group P25	P25S	118.1	57%
	P25F	185	
Group P50	P50S	120.8	67%
	P50F	183.8	
Group P75	P75S	125.7	47%
	P75F	184.8	
Group P100	P100S	134.1	43%
	P100F	192.3	

6.8.4 Post-Ultimate Behavior

The post-ultimate load-deflection behavior of the beams can be distinguished by the differences in residual resistance and deformability after reaching the ultimate load. The post-ultimate load-deflection for each group varied, depending on the level of prestress and the effect of the FRP shell (Figures 6.8, 6.9 and 6.10). All control specimens failed just after reaching the ultimate load. Reduction in the load resistance from the ultimate load to the failure load in the beam specimens with FRP shell was gradual to abrupt, depending on level of prestressing force; however, the load decreased very gradually in all associated control beam specimens. The post-ultimate midspan deflection was large in the beams (P0F and P25F), which failed predominantly in flexure as

compared to the beams (P50F, P75F and P100F), which failed in combined flexure and shear. The beams with FRP shell, except for the Beam P75F, had a sudden decrease in the load resistance after the ultimate load. This sudden decrease in the load resistance was because of the flexure-shear cracks which developed and penetrated into the concrete compression zone, at the load pints and crushed the concrete, followed by debonding of the FRP shell (Appendix B). In Beam P75F, the concrete in the compression zone initially started crushing and then the flexural-shear cracks penetrated into the concrete compression zone, accompanied by a large deflection, which prolonged the post-ultimate part of the load-deflection curve (Figure 6.10).

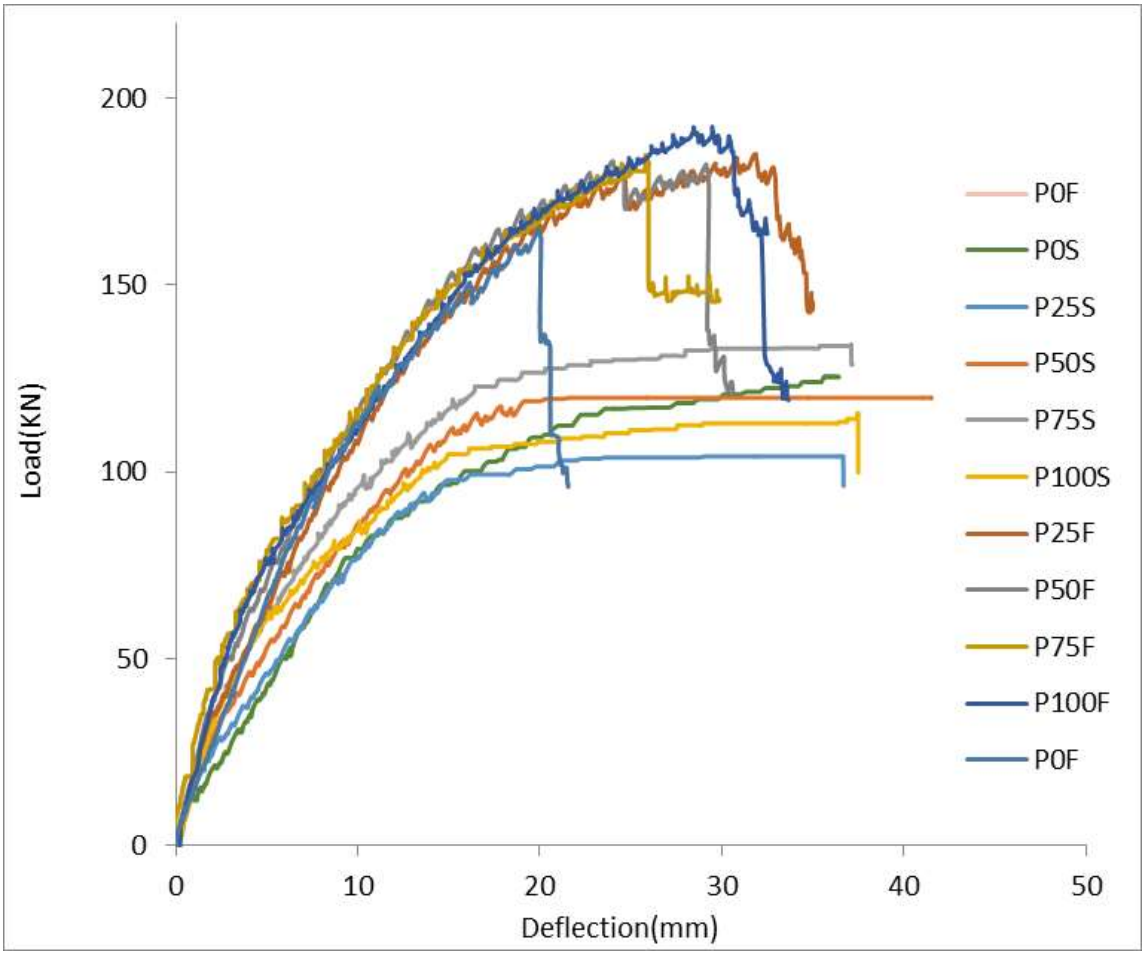

Figure 6.10 Load-deflection response of all prestressed concrete specimens

6.8.5 Stiffness Characteristics

Flexural stiffness (K) is the slope of midspan deflection for the loading pattern used, before the first cracking load (K1), and from cracking to the yield load (K2). The increase in K1 were 9% in Group P0, 17% in Group P25, 20% in the Group P50, 17 % in Group P75 and 20% in Group P100 specimens (Table 6.7). Among all five groups, the flexural stiffness enhancement due to the FRP shell varied from 17% to 20% when the level of prestress increased from 25% to 100%. In beam specimens with FRP shell, stiffness increased by 28%, with an increase in the level of prestressing force from 0 to 100%.

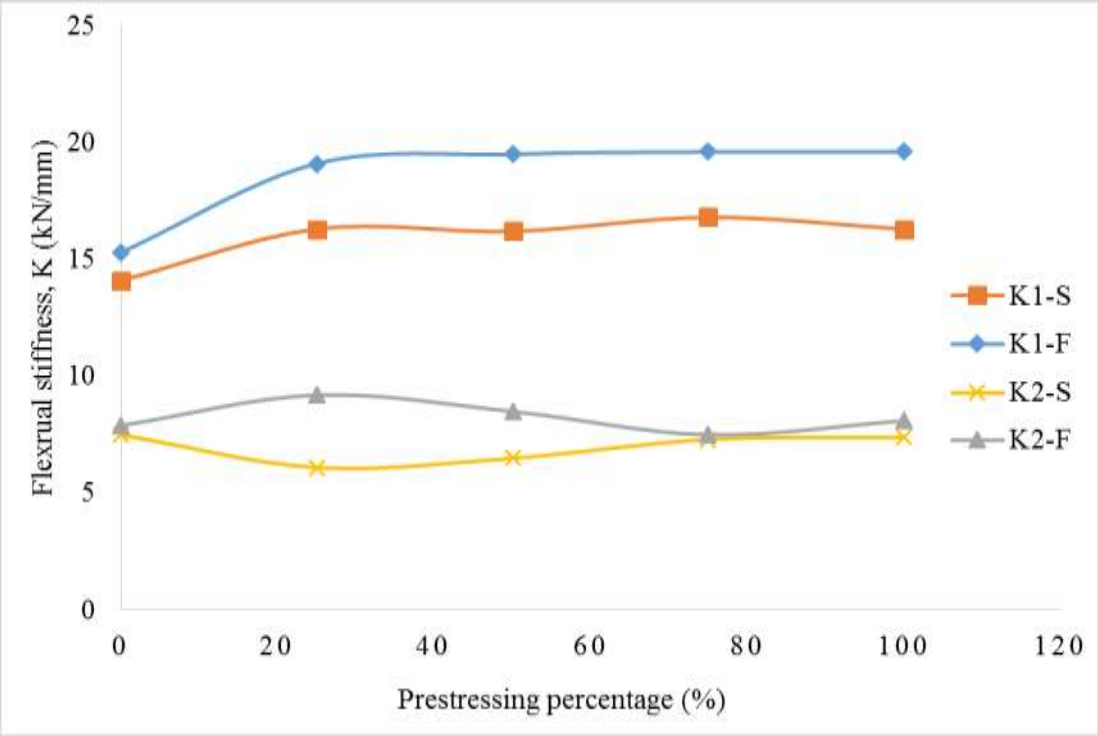

Figure 6.11 Effect of prestressing level on flexural stiffness of prestressing concrete beams with FRP shell

The specimens with FRP shell showed higher post-cracking stiffness (K2), as compared with the associated control beam specimens, when subjected to the same level of prestress. Table 6.7

compares the pre-yielding flexural stiffnesses (K2) for the all beams within the same group as well as with all other groups.

Table 6.7 Comparison of uncracked flexural stiffnesses (K) of the all beam specimens

Groups	Specimen	Flexural stiffnesses (kN/mm)			
		Uncracked (K1)	Difference (%)	Cracked (K2)	Difference (%)
Group P0	P0S	14.1	9%	7.5	5%
	P0F	15.3		7.9	
Group P25	P25S	16.3	17%	6.1	50%
	P25F	19.1		9.2	
Group P50	P50S	16.2	20%	6.5	31%
	P50F	19.5		8.5	
Group P75	P75S	16.8	17%	7.3	3%
	P75F	19.6		7.5	
Group P100	P100S	16.3	20%	7.4	10%
	P100F	19.6		8.1	

6.8.6 Ductility and Energy Absorption Characteristics

The displacement ductility ratio (μ) is defined as the ratio of the ultimate deflection (Δ_u) to the deflection at yield load (Δ_y), when the beam is subjected the loading pattern used. The beam specimens with FRP shell behaved in a brittle manner as compared to the associated control beams in all groups. The difference in the μ values was -17% in Group P0, -19% in Group P25, -21% in Group P50, -12% in Group 75, and -37% in Group P100 beams, which reflects the ductile behavior of the associated control beams. These results showed that the beam specimens with FRP shell

were less ductile than the associated control beams when the prestressing level varied from 0% to 100%. The averages values and percentage comparison of the displacement ductility ratios (μ) of beams are summarized in the Table 6.8.

Table 6.8 Comparison of displacement ductility ratio (μ) of the all beams

Groups	Specimen	Ductility ratio, μ			
		Corresponds to ultimate deflection	Difference (%)	Corresponds to ultimate load	Difference (%)
Group P0	P0S	9.3	-17%	3.8	-32%
	P0F	7.7		2.6	
Group P25	P25S	12.2	-19%	3.4	-6%
	P25F	9.9		3.2	
Group P50	P50S	12.5	-21%	2.9	-17%
	P50F	9.9		2.4	
Group P75	P75S	10.3	-12%	2.6	8%
	P75F	9.1		2.8	
Group P100	P100S	15.5	-37%	2.3	30%
	P100F	9.8		3	

It is also important to analyze displacement ductility at the ultimate load to the yield load in the strength based design method because it not only results in warning before ultimate failure but also indicates energy dissipation, and the level of damage at the ultimate load. Table 6.8 summarizes the values and percentage comparison of displacement ductility corresponding to the ultimate load.

The energy absorption capacity (E) is defined as the area under the load-deflection curve. No clear trend existed, as the level of prestress increased from 0% to 100%. In Group P0, the Beam P0F absorbed 34% lower energy as compared with the associated control beam (P0S). However, there was a notable difference (46% higher) in the energy absorption for the Beam P25F than the associated control beam (P25S). The Group P50 beams absorbed almost the same amount of energy. The energy absorption capacity was 18% lower for Beam P75F as compared with the corresponding control Beam P75S. The Beam P100F absorbed 42% higher energy as compared with the associated control beam P100S. The average values and percentage comparison of energy absorption (E) of all beams are summarized in the Table 6.9.

Table 6.9 Comparison of energy absorption capacity (E) of the all beams

Groups	Specimen	Energy absorption capacity (E)	
		E (kN.mm)	Difference (%)
Group P0	P0S	3312	-34%
	P0F	2194	
Group P25	P25S	3125	-46%
	P25F	4569	
Group P50	P50S	4200	-7%
	P50F	3913	
Group P75	P75S	3945	-18%
	P75F	3239	
Group P100	P100S	3175	42%
	P100F	4514	

6.8.7 Effect of Prestressing

The level of prestress had a significant effect on the initial cracking strength of all of the beams (Figure 6.12). As the prestressing level increased from 0% to 100%, the initial cracking strength improved by 59% for the beam specimens (with FRP shell) and 79% for the control beam specimens because of the contribution of the FRP shell to the strength and confinement of the system which delayed initial cracking.

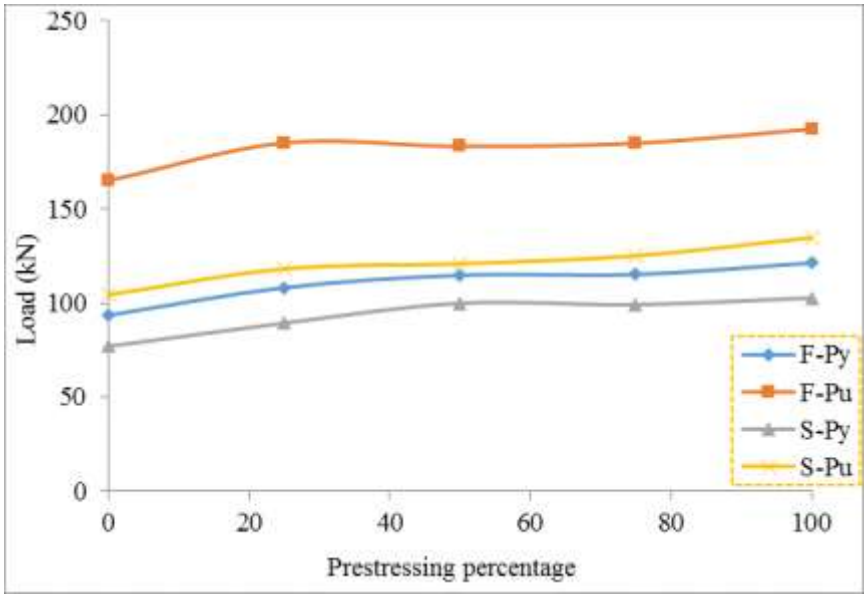

Figure 6.12 Effect of prestressing level on yield and ultimate strengths

As the prestressing level increased from 0% to 100%, there was a significant increase (23%) in the yield strength for the specimens in all groups. This increase in yield strength was quite consistent from one group to another. Again, the FRP shell enhanced the yield strength of the beams. Similarly, there was an increase in the ultimate strength from 58% to 43% when the level of prestress varied from 0% to 100%.

The results showed that when the level of prestress increased from 0% to 100%, the difference in the midspan deflection among the beams as compared with associated control beams decreased from 44% to 21% at ultimate load. In the beams with FRP shell, the midspan deflection decreased by 25% at ultimate load, when the prestressing level was increased from 25% to 50%; however, the midspan deflection increased by 14% when the level of prestress was increased from 75% to 100% and the ultimate load value increased by 4%.

6.8.8 Strain Characteristics

Strains in the prestressing steel strand, concrete and FRP shell were recorded during the tests at different beam locations; the measured strain values of the beam specimens are presented in Figure 6.13.

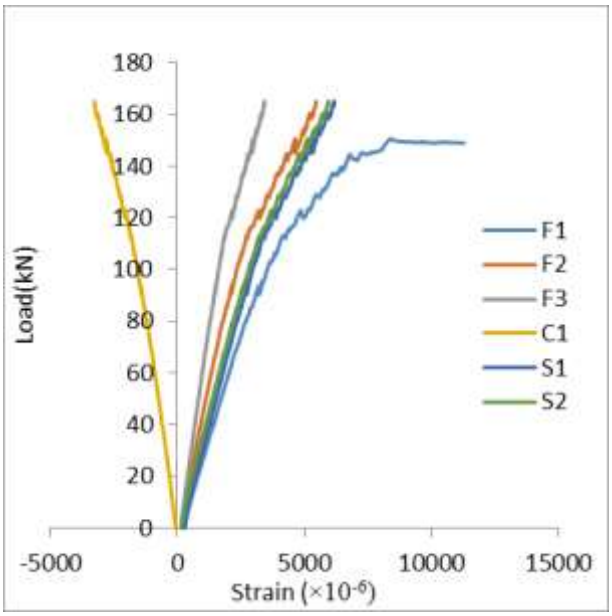
Load(kN)
Strain (×10⁻⁶)
F1
F2
F3
C1
S1
S2

(a)

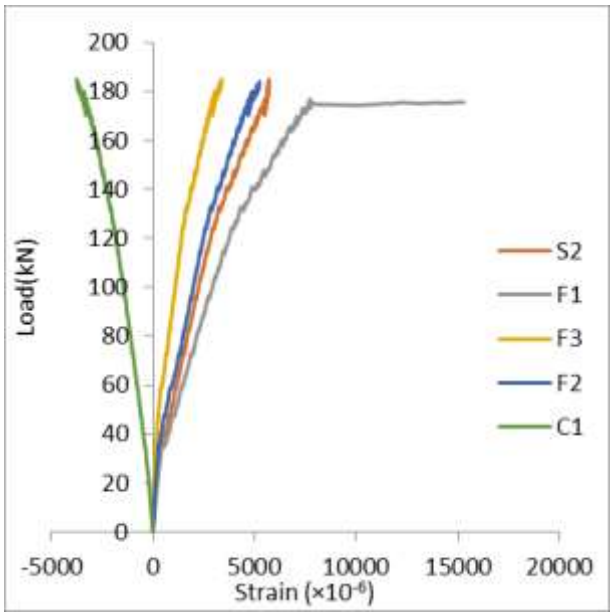
Load(kN)
Strain (×10⁻⁶)
S2
F1
F3
F2
C1

(b)

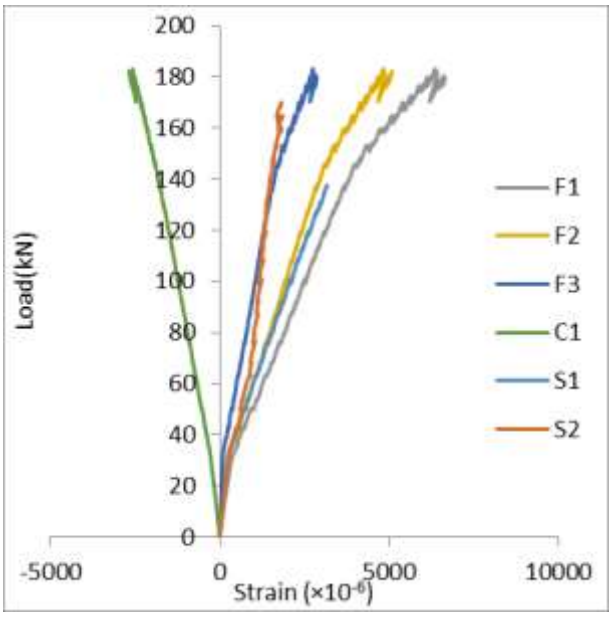
Load(kN)
Strain (×10⁻⁶)
F1
F2
F3
C1
S1
S2

(c)

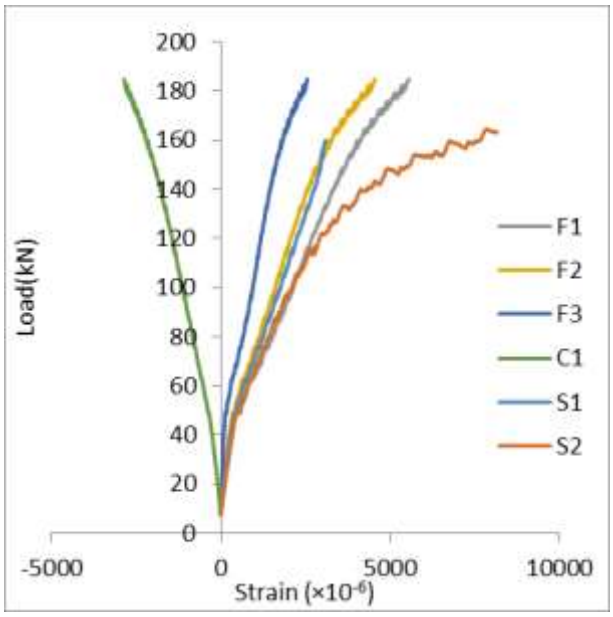
Load(kN)
Strain (×10⁻⁶)
F1
F2
F3
C1
S1
S2

(d)

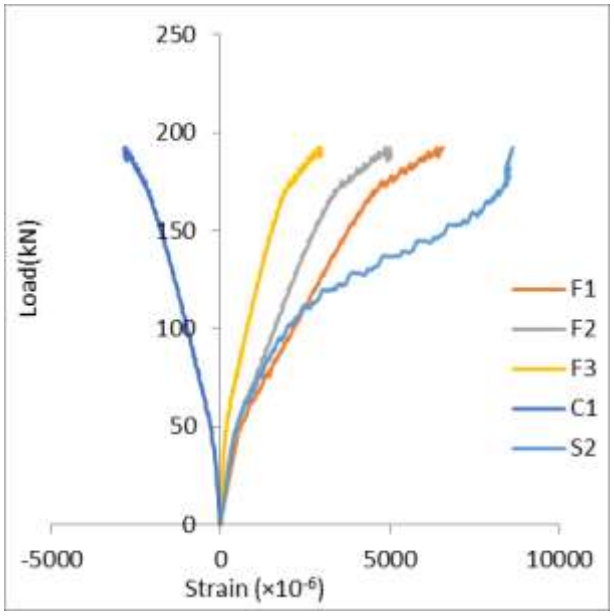

(e)

Figure 6.13 Strain variation in the FRP shell, concrete and prestressing steel strands (a) Beam P0F (b) Beam P25F (c) Beam P50F (d) BeamP75F (e) Beam P100F

6.8.9 Slip between FRP Shell and Concrete Interface

The slip between the FRP shell and the concrete interface was recorded using of LVDTs (TS1 and TS2) at both ends. The results showed that there was no slip until the prestressed concrete beams (with FRP shell) failed and the FRP shell debonded. This implies that a perfect bond existed between the FRP shell and the cast-in-place prestressed concrete.

6.8.10 Modes of Failure

The control beams in each group were designed to fail in flexure as the prestressing steel strands reach and/or exceed their yield strength, followed by the crushing of concrete, associated with large deflections. However, with the addition of the FRP shell, the beam specimens failed in a different manner as compared with their associated control specimens. The modes of failure varied

depending on the level of prestress (from 0% to 100%) and the effect of the FRP shell (Appendix B).

Flexural-shear cracks appeared outside the pure bending region in the beams specimens with FRP shell, after yielding of the prestressing strands. These cracks propagated both in length and width more than the flexural cracks. The concrete crushed in the compression zone at the ultimate load. The beam specimens failed finally due to the flexural-shear cracks penetrating into the concrete compression zone and crushing of the concrete. There was debonding of the FRP shell from the widely opened cracks at an approximately 45 degree angle, starting from the load point and penetrating towards the support. The general modes and sequence of failure are presented in Figure 6.14.

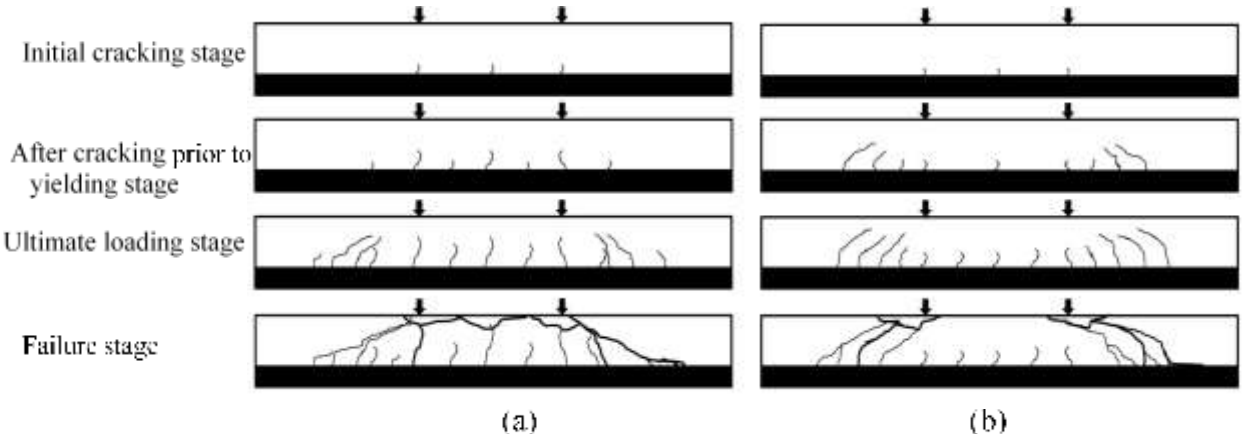

Figure 6.14 Typical cracking and failure modes of beams (a)low to medium prestress level (Groups P0, P25 and P50)(b) high presress level (Groups P75 and P100)

6.9 Summary

The flexural behavior of prestressed concrete beams with cast-in-place FRP shell is studied in this chapter. Flexural tests were performed to examine the contribution of the bonded FRP shell in the

strength, stiffness, ductility and energy absorption capacity of the prestressed concrete beam specimens along with the effect of five levels of prestressing (– 0, 25, 50, 75, 100%).

The initial cracking, yield and ultimate strengths in the beam specimens with FRP shell were significantly higher than those associated with the control beam specimens (without the FRP shell). The prestressed beams with FRP shell demonstrated a significant enhancement in both the strength and stiffness as well as higher ductility and energy absorption capacities, as compared with the associated control beams.

The beam specimens with FRP shell failed in a different manner as compared with their associated control beams, the modes of failure varied depending on the level of prestressing and the effect of the FRP shell.

CHAPTER 7 DURABILITY OF PRESTRESSED CONCRETE GIRDERS REINFORCED WITH FRP SHELL

7.1 Introduction

Durability of FRP composites and concrete is well documented individually; however, data on durability of composite FRP-structural concrete are lacking, and the system needs to be evaluated for its long-term behavior. The FRP-concrete interface is the critical component to ensure the effectiveness of FRP composites in structural applications as this interface can be exposed to aggressive environments. The durability of FRP-reinforced concrete composites is influenced by several factors, such as the quality and durability of concrete, the quality and durability of the FRP and the resin; all other factors are summarized in Chapter 1. To act as a barrier against penetration of injurious elements, such as ingress of moisture or chlorides, the durability of the FRP shell and that of the entire system needs to be examined in detail (fib 2001).

This chapter presents a preliminary attempt made to determine the durability of the proposed FRP shell and that of the FRP-concrete system. The main objective of this study was to investigate the effectiveness of the FRP shell against ingress of moisture and chlorides into concrete with externally bonded FRP shell-concrete specimens. The experimental results of water absorption tests, chloride penetration tests and scanning electronic microscope (SEM) tests are presented. Based on the available information in the literature, an attempt is made to predict the profile of chlorides for a bridge girder subjected to an aggressive environment, considering the effectiveness of the FRP shell and its performance over the design service life; this would also help with projection of the service life of the girder.

7.2 Durability of FRP Shell against Water

7.2.1 Moisture Diffusion

Moisture absorption in polymeric materials can be described as the process of diffusion, involving small molecules of water migrating though the concentration gradient. Fick's Second Law of diffusion can be used, assuming unidirectional diffusion normal to the plane of the FRP shell and assuming the diffusing species to be independent of the concentration gradient (Crank 1975). Assuming the diffusion coefficient and the boundary conditions to remain constant, Fick's Second Law of diffusion requires:

$$\frac{\partial c}{\partial t} = D\frac{\partial^2 c}{\partial x^2} \tag{7.1}$$

where *C* is water concentration, and *D* is diffusivity at time '*t'* at distance '*x'* from the face.

When the polymers are exposed to moisture, the mass gain can be obtained by solving Equation 7.1, using the relevant constant boundary conditions (Crank, 1975), as:

$$\frac{M_t}{M_\infty} = \left[1 - \sum_{n=0}^{\infty} \frac{8}{(2n+1)^2} exp\left[\frac{-D_{frp}(2n+1)^2\pi^2 t}{4\lambda^2}\right]\right] \tag{7.2}$$

where M_t = mass gain (%) at time 't' (s),

M_∞ = mass gain at steady state (%),

2λ= FRP shell thickness (mm), and

D_{frp} = diffusion coefficient (m^2/s).

If $\frac{D_{frp}t}{4\lambda^2} < 0.05$, Equation 7.2 can be simplified as:

$$\frac{M_t}{M_\infty} = 4 \times \sqrt{\left[\frac{D_{frp}t}{\pi(2\lambda^2)}\right]} \qquad (7.3)$$

For short time exposure, the coefficient of diffusion can be calculated using Equation (7.4) by plotting the mass gain as a function of time according to Fick's theory of diffusion (Karbhari 2007).

$$D_{frp} = \left(\frac{M_t}{M_{max}}\right)^2 \times \left(\frac{\pi\lambda^2}{4t}\right) \qquad (7.4)$$

7.2.2 Water Absorption Tests

Accelerated water absorption tests were conducted to determine the moisture absorption rate through the FRP shell, and indirectly the penetration rate of chloride Cl^- and hydroxide OH^- ions into the FRP shell. Tap water was used in immersion test, because Kouadio (2001) found that the moisture absorption was higher with tap water than with salt water.

The samples were immersed in water at the following three temperatures:

- 6°C (annual average temperature in Montreal ≈ 5.9°C)
- 25°C (room temperature 23±2°C)
- 70°C (a selected higher temperature)

7.2.3 Preparation of Test Samples

Five specimens, 75 mm long and 25 mm wide, were cut from the FRP laminate, and their edges were smoothened using sand paper. The same epoxy resin, as used in the preparation of the FRP shell, was applied to the edges of the FRP samples to eliminate the edge effect on absorption of water. Another set of polymeric matrix samples, of the same size (75 x 25 mm), was prepared from the cured resin (Figure 7.1).

The initial conditioning was performed according to the ASTM Standard D 570 (ASTM, 2010). The samples were placed in an oven at 50°C for 24 hours. The samples were then enclosed in a climatic chamber at a temperature of 35°C and 90% humidity for a period of 96 hours ± 2 hours. Immediately after conditioning; the test samples were then placed in a sealed polythene bag to stabilize them before immersion. The initial dry mass of each sample was recorded using an electronic scale with an accuracy of 0.001g. The samples were then placed in sealed plastic containers maintained at one of the three temperatures mentioned earlier (6°C, 25°C and 70°C).

Figure 7.1 Samples for water absorption test (a) epoxy-based resin (matrix) (b) FRP shell

The first step involved obtaining the moisture uptake readings. The samples were removed from their respective containers, and the surface was dried using a dry towel and then using a hot air blower. After the drying process, the specimens were weighed using the electronic scale. The drying and weighing procedure was conducted within a short period of time to prevent the specimens from being affected by the surrounding environment. After weighing, the samples were placed back in their respective exposure environments, and the procedure was repeated for every reading at time intervals of 24 hours for a period of 100 days.The moisture absorption of the FRP shell and resin samples was determined until a steady state was attained (ASTM 2010). The

percentage mass increase of the sample at any time of immersion (W_w) was calculated using Equation 7.5 as:

$$W_w\% = \frac{w_t - w_d}{w_d} \times 100 \qquad (7.5)$$

where W_t and W_d are the masses of the sample after immersion time 't' and in the conditioned state, respectively.

The percentage moisture uptake was calculated and the mass gain was corrected to take into account of the possible mass loss of the specimens because of various dissolution or leaching phenomena after depolymerisation, during the immersion procedure as compared with their initial masses, using equation 7.6.

$$W_{loss},\% = \frac{w_{d1} - w_{d2}}{w_d} \times 100 \qquad (7.6)$$

where W_{loss} = mass loss (%)

W_{d1} = mass of initial conditioned specimen

W_{d2} = mass of the reconditioned sample after immersion.

7.2.4 Water Immersion Test Results and Discussion

Water immersion resulted in mass gain over time at all three temperatures; Table 7.1 summarizes the results of mass gain and diffusion coefficients for both FRP shell and resin samples. The moisture mass gain of the FRP shell samples, at steady state saturation, were lower than the resin samples because the fibers did not absorb any moisture. The moisture mass gains were 0.27%, 0.36% and 0.52% after immersion in water at 6°C, 25°C and 70°C temperatures for 100 days,

respectively. The results are the average values obtained from five samples each of FRP and resin immersed in water.

Using equation 7.4 and the absorption test data, the coefficient of diffusion for both FRP shell and resin were determined; the results are summarized in Table 7.1.

Table 7.1 Mass gain and diffusion coefficients of FRP shell and resin at different temperatures

Temperature	Mass gain (%)		Diffusion coefficient, D (mm^2/s)	
	Resin	FRP shell	Resin	FRP shell
6°C	0.19	0.23	1.35×10^{-6}	1.19×10^{-6}
25°C	0.36	0.33	2.26×10^{-6}	1.51×10^{-6}
70°C	2.30	0.53	5.99×10^{-6}	3.38×10^{-6}

Figure 7.2 presents the moisture uptake characteristics of the FRP shell samples at different temperatures; these are the average values obtained from five specimens of both FRP shell and matrix immersed in water as a function of time up to a steady state.

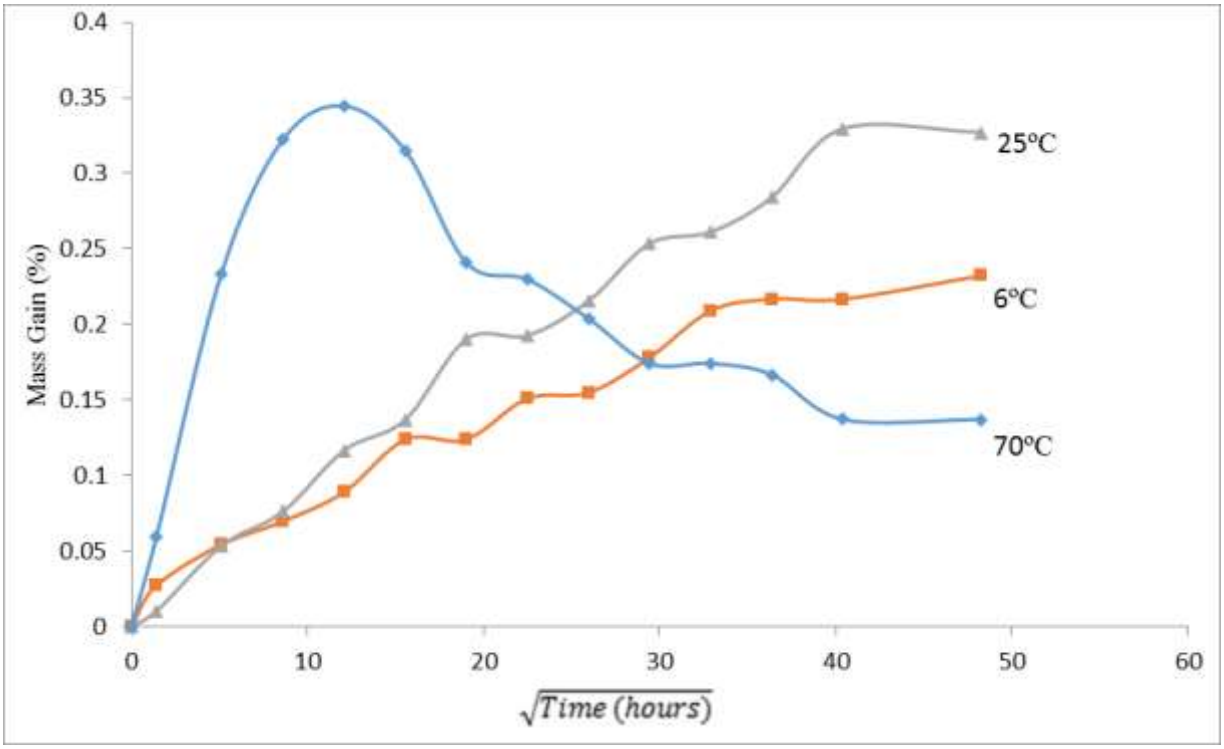

Figure 7.2 Moisture uptake curves for FRP shell samples at different temperatures

After 100 days of exposure at 6°C and 25°C, the absorption curves showed continued mass gain up to the saturation states, although at a gradually slowing rate. Both curves showed similar trends; however, the moisture absorption rate was higher at 25°C than at 6°C, as can be observed from the initial part of the curve.

The moisture absorption behavior of the FRP shell at 70°C was quite different from that at the other two temperatures (Figure 7.2). The moisture absorption rate was highest at 70 C, involving a steady increase until it reached the maximum value; after that the absorption rate decreased rapidly, indicating that the FRP shell samples had aged in water at 70°C after about 100 days of exposure, because of depolymerisation and leaching out of the polymeric matrix. This ageing phenomenon in this exposure condition was quite visible from the micrographs of the samples

from the Scanning Electron Microscope (SEM) (see Figure 7.10). Although there was no significant mass loss observed in the samples exposed to moisture at 6°C and 25°C temperatures.

The moisture uptake at the steady state equilibrium for the resin samples at 70°C increased the most but the mass loss was also the largest because of degradation and de-polymerization of the epoxy resin (Figure 7.3).

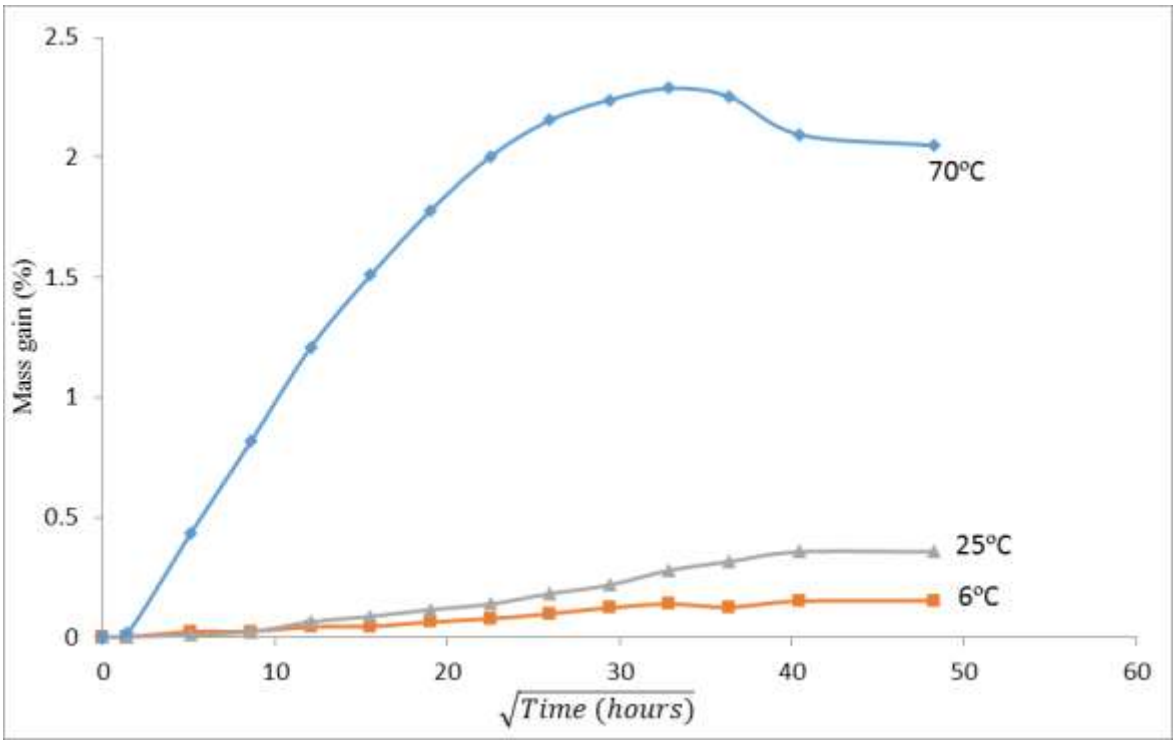

Figure 7.3 Moisture uptake curves of epoxy-based resin (matrix) samples at 6°C, 25° and 70°C temperatures

7.3 Permeability of Concrete Reinforced with FRP Shell for Chlorides Ingress

7.3.1 Transportation of Aggressive Elements and Mechanisms

Transport of chlorides in concrete is dependent on the continuity of the pore network, porosity of the aggregates and the hydrated cement paste (hcp), the interfacial transition zone (ITZ) between them and any existing micro-cracks at the hcp-aggregate interface. Depending on the driving force,

normally governed by the environmental conditions, such as humidity and temperature levels, and the internal concrete moisture content, capillary absorption of a salt-containing liquid or diffusion of free chlorides may prevail or act simultaneously in some combination. Mixed modes of chloride transport into the concrete are common in practice, such as capillary absorption, hydrostatic pressure, and diffusion. (Rosenberg 1989).

Permeation is "flow" of liquids or gases caused by a pressure head; the ingress and transport of chlorides occurs by convective flow of chloride ions and is dependent on the concrete pore structure and viscosity of the salt solution. Therefore, long-term durability of concrete structures exposed to chloride carrying liquids is strongly dependent on the permeation characteristics of the concrete cover zone. However, this mechanism is relevant only in rare cases, such as marine structures under a high hydrostatic pressure, or for seepage of solution through retaining structures (RILEM 1995).

Capillary absorption can be defined as the transport of chloride-containing liquids in concrete due to the surface tension acting in the capillaries, and is predominant in porous media. It is basically a convective phenomenon and is influenced by the viscosity and density of the fluid, the pore structure of the medium (radius, tortuosity and continuity of capillaries), and the surface tension and the surface energy within the capillaries.

Transportation by diffusion is governed by the concentration gradient across the member. While diffusion does not depend on the flow of a fluid, it requires an adequate level of moisture to create a continuous path for the chlorides to migrate into the concrete. In dry concrete, these "liquid paths" become discontinuous, resulting in considerable lowering or arresting of diffusion. The highest rates of diffusion occur in saturated concretes, and the lower moisture limit allowing

diffusion to occur is at a relative humidity (RH) of 60-80%. This range also coincides with the upper RH limit allowing free diffusion of gases, such as oxygen and carbon dioxide. In addition, the hygroscopic nature of salts reduces the rate of evaporation of water in the concrete, resulting in increased moisture content in salt-contaminated concretes. Since only the chlorides freely dissolving in the pore solution can be involved in the corrosion process, temperature can play a large role in corrosion, especially in warm and humid climates.

These three mechanisms can transport chlorides into the concrete to the rebar level; however, diffusion is the most common mechanism.

Diffusion of chlorides into the concrete has been used by several investigators to assess the service life of a concrete structure at risk of deterioration due to corrosion of the embedded reinforcing steel. Transport of chemicals into porous media is considered to be predominantly a diffusion process and Fick's laws, which consider the driving force for diffusion through a thin film is a concentration gradient. An appropriate modification can be used to idealize migration of chlorides through FRP-reinforced concrete composites.

There are several standard tests available in the literature to measure chloride penetration into the concrete, such as electrical indication of concrete's ability to resist chloride ion penetration (ASTM C 1202), rapid chloride permeability test (AASHTO T277), and resistance of concrete to chloride penetration, also referred as salt ponding test (AASHTO T259).

Comprehensive literature is available on the subject of moisture diffusion into both the FRP materials and the concrete separately; however, the knowledge of diffusion of chloride ion laden moisture into the concrete with an externally bonded FRP shell is very limited (Lin et al. 2006). Moisture can be transported into the FRP composite due to either capillary action along the

longitudinal axis of the fibres, or at the resin-fibre interface, or transfer through cracks and voids in the structure, or diffusion through the polymeric matrix, or a combination of all of the above modes (Karbhari 2007). The transport mechanism through the concrete with the FRP shell is dominated by the diffusion process because in the long-term, it is generally controlled by transport through the gel pores, and moisture diffusion, which is driven by a concentration gradient (Karbhari 2007).

The objective of the diffusion tests in this research program was to investigate the effectiveness of the FRP shell against chloride solution ingress into the concrete specimens. An experimental method, for the rapid chloride solution penetration into the FRP bonded concrete specimen, was developed. The results from these tests are evaluated in the following section.

7.3.2 Measuring Chloride Penetration

To accelerate the penetration of chloride ions into the concrete with an FRP shell, an exterior face of the sample, with the FRP shell, was exposed to 3.5% sodium chloride solution under pressure, using a specially designed diffusion cell. The chlorides were transported into the sample due to convection and diffusion processes, and the tests were aimed at determining the chloride penetration rate, chloride concentration profile and the diffusion coefficient of the samples.

7.3.2.1 Diffusion Cell

A pressure based diffusion cell was developed in this study as shown in Figure 7.4. This test setup is a modified form of the existing systems described in the literature (ASTM-2002 2005; Trefry 2001; Khoe *et al.* (2009). The diffusion cell consisted of two, 25 mm thick, rectangular (250 mm x 100 mm) aluminum plates, and a 150 mm square and 15 mm thick plexiglass plate. The central part of the plexiglass plate was machined to create a diffusion chamber and a 5 mm deep groove

for a rubber O-ring to provide an airtight seal, along with a threaded inlet hole at the centre of the plate. The diffusion chamber was 100 mm in diameter and 15 mm in depth, as shown in Figure 7.4.

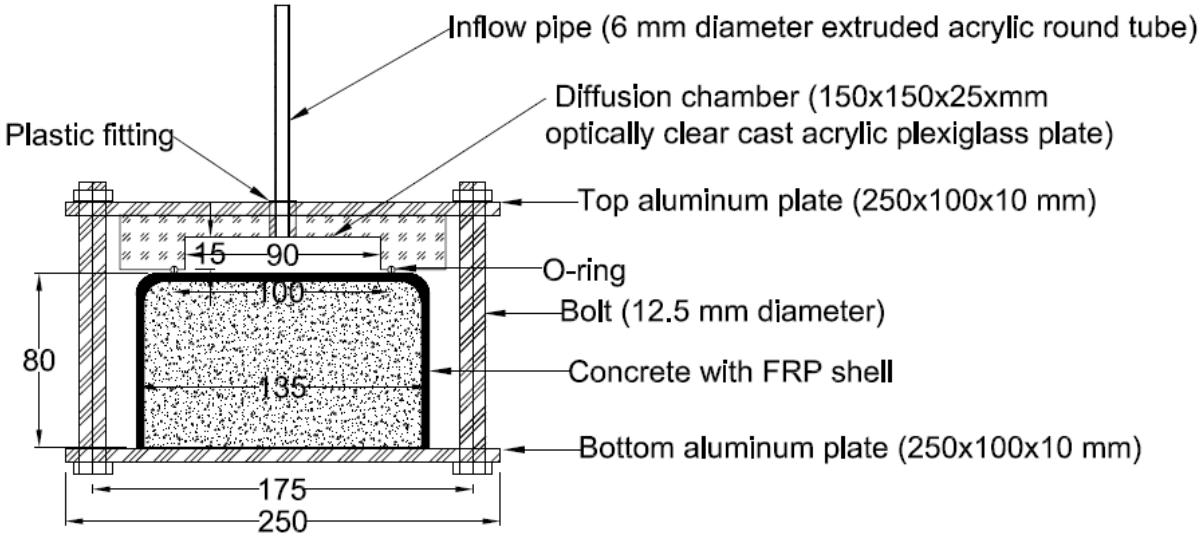

Figure 7.4 Schematic diagram of the diffusion cell

The test sample was positioned between the two aluminum plates and the top plexiglass plate in such a way that the black rubber O-ring would be at the center of the sample, as shown in Figure 7.5. The two parts of the diffusion cell were assembled using four durable stainless steel bolts with nuts and washers. All connections were made leak-proof using Teflon tape.

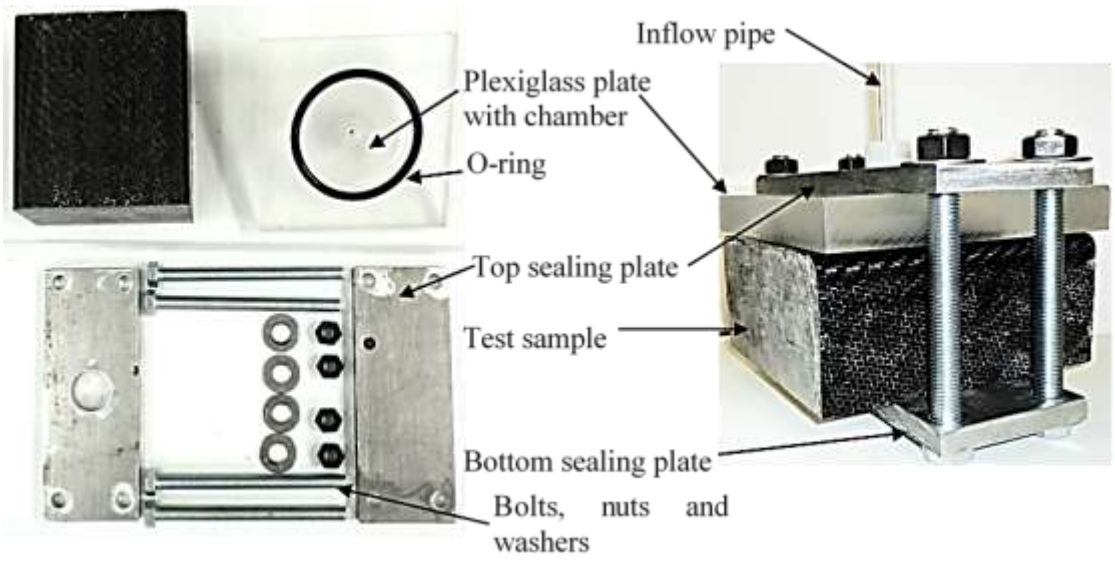

Figure 7.5 Diffusion cell setup

7.3.2.2 Specimen Preparation

The specimens were cast in 150 mm long FRP shell and were moist cured for two weeks, followed by four weeks of drying at room temperature. The samples were then sealed with an epoxy resin, around the two exposed concrete faces, to avoid evaporation or any other atmospheric effects. After sealing the faces, the specimens were conditioned, followed by the procedure described in the Standards for chlorides resistivity of the concrete (ASTM C 1202 and AASHTO T277). The specimens were placed in the environmental control oven at a temperature of 50°C and relative humidity of 80% for 72 hours and then placed in an oven at a temperature of 50°C. After conditioning, the samples were placed in plastic zip bags for spatial equilibration of the moisture distribution within the samples until they were installed in the diffusion cells.

7.3.2.3 Measuring Chloride Diffusion

The test samples were exposed to 3.5% NaCl solution at room temperature (23°C) for more than 100 days. Based on the exposure conditions, the samples were divided into two groups – P-specimens and H-specimens. In P-specimens, chloride solution was injected under a constant pressure of 550 kPa (Figure 7.6), to accelerate the chloride transportation process. The H-specimens were exposed to a one metre height of chloride solution column. This pressure was maintained constant until the test samples were removed from the diffusion cell and analysed for chloride ion diffusion rate and concentration.

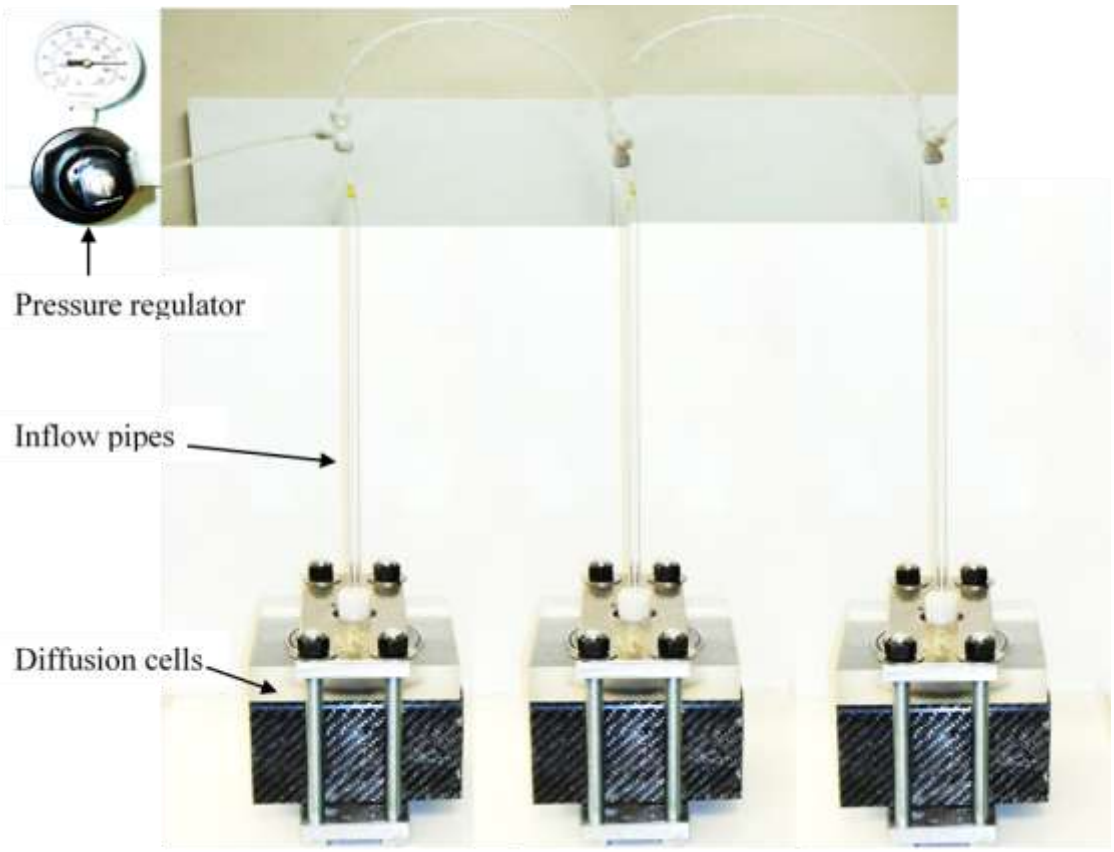

Figure 7.6 Rapid chloride penetration test setup

The chloride penetration depths and concentration levels were measured and analyzed using the following three techniques:

(a) Inflow Measurement

The amount of chloride solution penetrating into the samples was recorded from the difference in the levels of the solution in the inflow pipes, assuming that no leakage or evaporation occurs. A few drops of oil were added, on top of the chloride solution in the inflow pipes, to avoid evaporation of the solution. Periodic readings of the solution level drop were taken from the paper scales attached to the inflow pipes.

The reading remained constant for the exposure period, which indicated that the FRP shell did not allow any chloride to travel into the concrete. Although there was a very small lowering of the oil meniscus during the initial 24 hours of the test. This initial drop in the level could be due to the trapped air in the chamber and its fittings. However, the readings remained constant for the rest of the exposure period.

(b) Colorimetric Technique

After each specified exposure duration, the specimens were removed from the diffusion cells and immediately cut into half with a diamond saw. The cut surfaces were machined to remove any chloride movement or contamination because of the cutting process (Figure 7.7). The chloride penetration depth was determined using a colorimetric technique in which a 0.1 N silver nitrate solution was used as a colorimetric indicator (Tang and Nilsson 1991). When the silver nitrate solution was sprayed on the concrete cut surface, the chlorides in the concrete reacted with the silver and produced silver chloride, a whitish substance. At the concrete surface with no chlorides, the silver in the silver nitrate solution reacted with the hydroxides present in the concrete and a dark brownish color appeared.

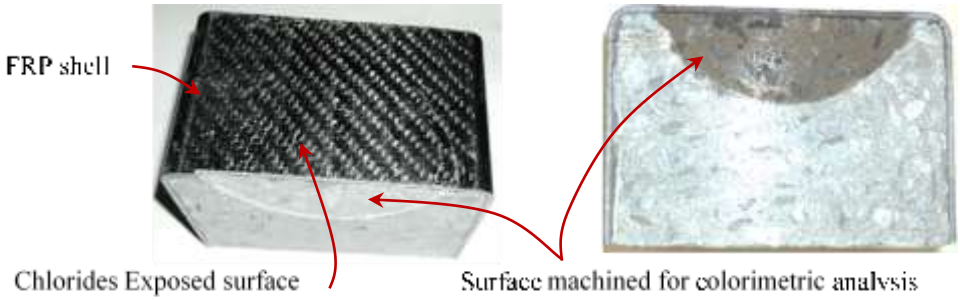

Figure 7.7 Sample prepared and tested for colorimetric test

When a silver nitrate solution was sprayed on the concrete exposed surface of the samples with FRP composite shell, the colour changed to dark brown (Figure 7.7), which indicated absence of any chlorides. Whereas, the samples without FRP composite shell, a portion of concrete penetrated by chlorides turned into whitish color, which indicated the thickness of the concrete affected by chlorides. In both exposure conditions, the FRP shell acted as an impervious barrier against the penetration of chlorides.

(c) Profile Drilling Technique

The samples were removed from the diffusion cells after the required exposure period of 100 days. A 12.5 mm diameter diamond tip drill bit was used to collect the drill dust or powder from layers at every 3 mm depth from the surface. The dust from every layer depth was collected and preserved separately for further chemical analysis. To verify the drilled depth recorded from the drilling machine after completion of the drilling process, the drilled hole depth was measured with a digital caliper.

The ASTM Standard method of titration (ASTM C 114) was used for chemical analysis of the collected dust samples to determine the chloride concentration. All chemical analyses results

showed absence of chlorides in the collected dust samples, which proved that the FRP shell did not allow any penetration of chlorides into the concrete.

7.4 Scanning Electron Microscopy

7.4.1 Environmental Scanning Electron Microscope (ESEM)

The ESEM Quanta 200 FEG has a Schottky field-emission source gun and three modes of imaging and analysis - high vacuum for characterization of conductive, low vacuum (<200 Pa) for non-conductive, and environmental (ESEM) mode (<4000 Pa) for wet organic or inorganic materials. High vacuum operation mode was used in this study.

The ESEM has several advantages over the SEM, such as the specimens do not need to be coated with a conductive film because the gas ionization in the sample chamber eliminates the charging effects, which can be seen typically with nonconductive samples. It can capture image of wet, dirty and oily samples. It can acquire electron images from samples as hot as 1000°C, because the Gaseous Secondary Electron Detector (GSED) is insensitive to heat.

Figure 7.8 shows the laboratory configuration of the ESEM equipment available in the Biomaterials and Cartilage Laboratory (BCL) in the Department of Chemical Engineering at Ecole Polytechnique, Montreal.

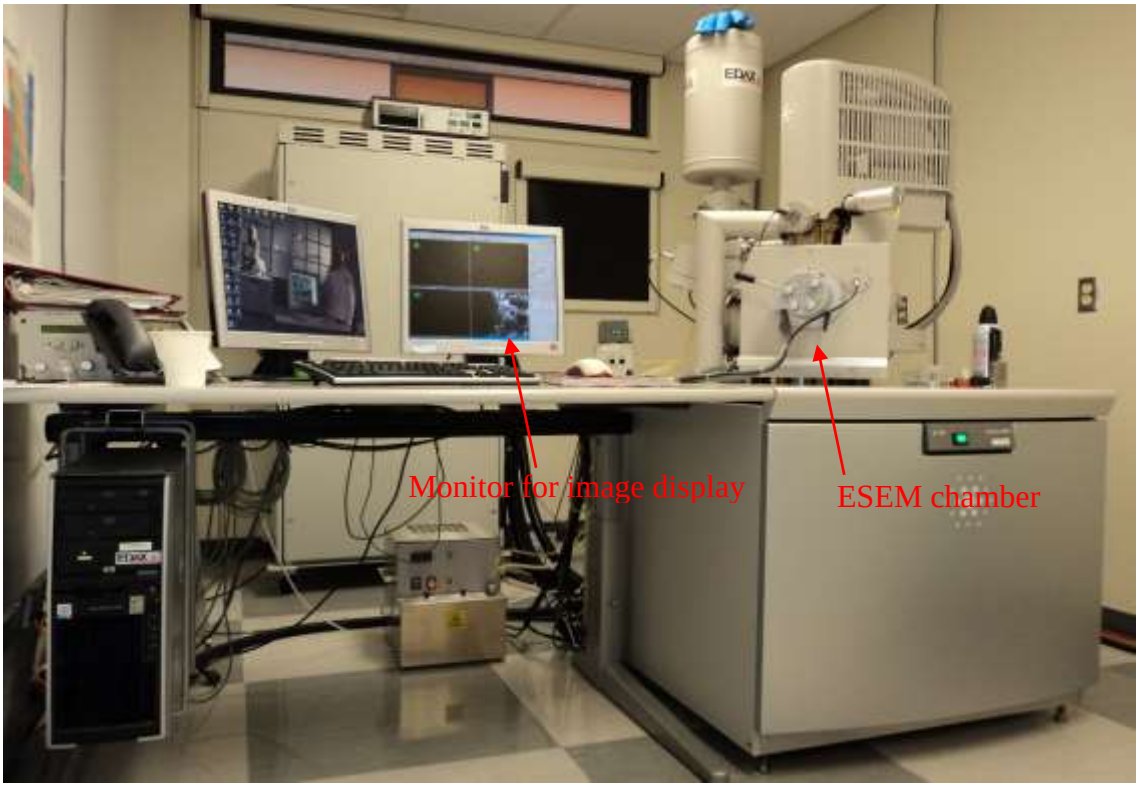

Figure 7.8 Environmental scanning electron microscope – model Quanta 200 FEG

7.4.2 Objectives of ESEM Tests

The objectives of the ESEM were as follow:

- To examine the arrangement of fibers and plies in a cross-section of the FRP composite shell.
- To examine the manufacturing defects, such as micro-cracks and pores.
- To observe the micro-structure of the FRP composite shell before and after exposure to chloride solution at a high pressure.
- To examine the degradation of the FRP composite shell and resin as a result of moisture absorption at different temperatures.

7.4.3 Sample Preparation

The first set of the samples was taken from the unexposed specimens and the specimens exposed to moisture absorption at three temperatures (6°C, 25°C and 70°C); details of the exposure conditions are presented in Sections 7.2 and 7.3. These samples were cut into pieces of 50 mm by 25 mm to fit into the ESEM chamber, and the samples were coated with a thin layer of gold-palladium by a vapor-deposit process to eliminate the charging effects of the non-conductive materials used in the ESEM environment.

The second set of samples was taken from the unconditioned (control) specimens and from the specimens which were previously exposed to the chloride solution at a pressure of 550 kPa (80 psi) and one metre high column of chloride solution for more than 100 days. The details of the exposure conditions are presented in Sections 7.2 and 7.3. Three samples of 25 mm square in size and 15 mm in thickness were cut, perpendicular to the fiber axis, using a diamond blade saw, from the exposed part of the each specimen. These cut samples were then smoothened using different grit size sandpapers, and were also coated later with a thin film of gold-palladium by a vapor-deposit process to eliminate the charging effects.

7.4.4 Microscopic Imaging

After surface coating, the microstructural observations were performed using the ESEM - Quanta 200 FEG. These observations were conducted to examine the fiber arrangements, and any potential degradation of the fibers, matrix, or interfaces due to moisture and chloride exposure.

The ESEM was set to 10 kV voltages and 380 μA emission current. The brightness and contrast for each image was adjusted manually, before acquiring images. Figure 7.9 shows the scanned results for the physical arrangement of the fibres in the FRP shell sample. The composite lay-up

of the plies, and voids, or any other manufacturing flaws were identified using a relatively low magnification in the ESEM, so that they could be clearly noted. The ESEM micrographs of the fibers appeared brighter than the matrix in the sample.

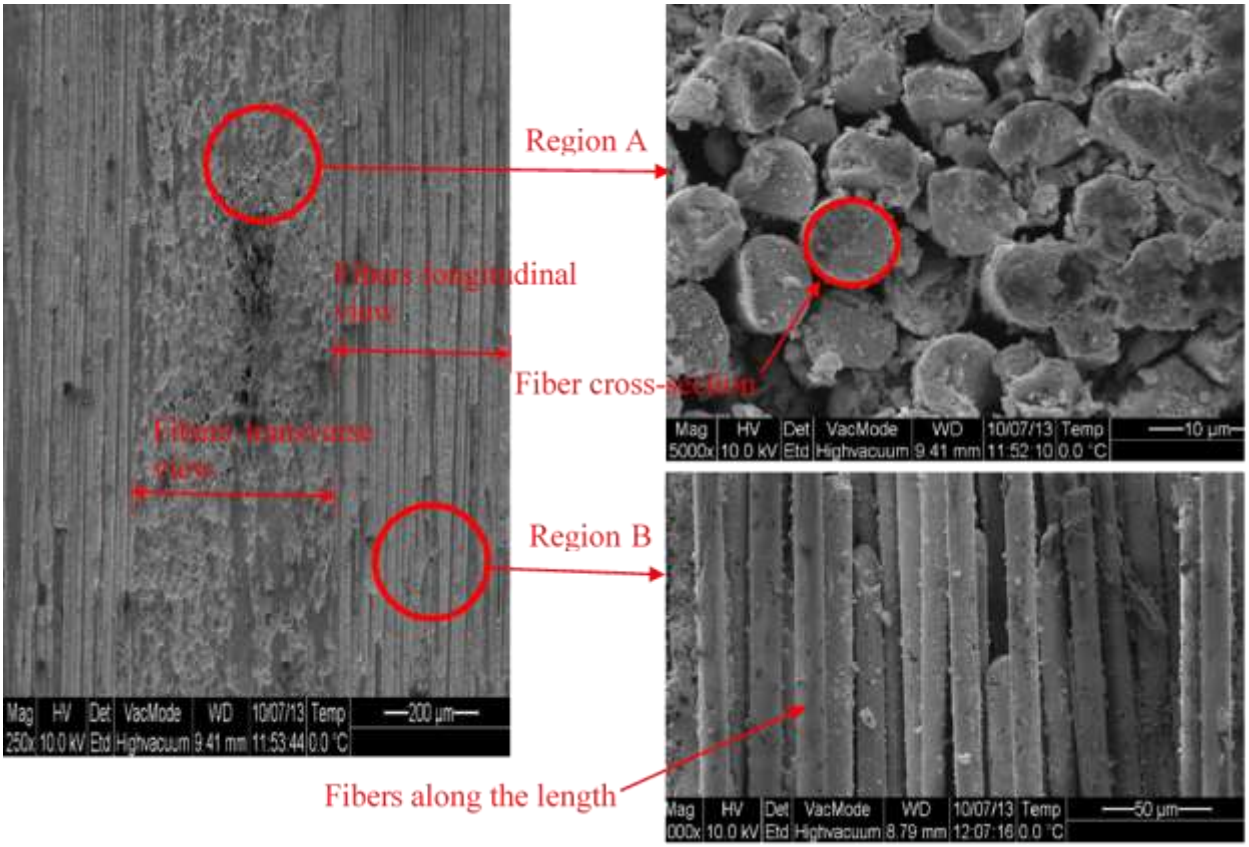

Figure 7.9 ESEM micrograph of physical arrangement of fibers in the FRP shell sample

The weakest links in the FRP shell are the interfacial bond between the fibers and the matrix, and between the laminates, which can deteriorate before the fibers and/or the matrix. The ESEM micrographs of the samples from the side surfaces can reveal flaws, or defects between the fibers and matrix, as well as voids or discontinuities among the consecutive plies of the lamina (Figure 7.10). A large void was detected between two plies, as shown in Figure 7.10.

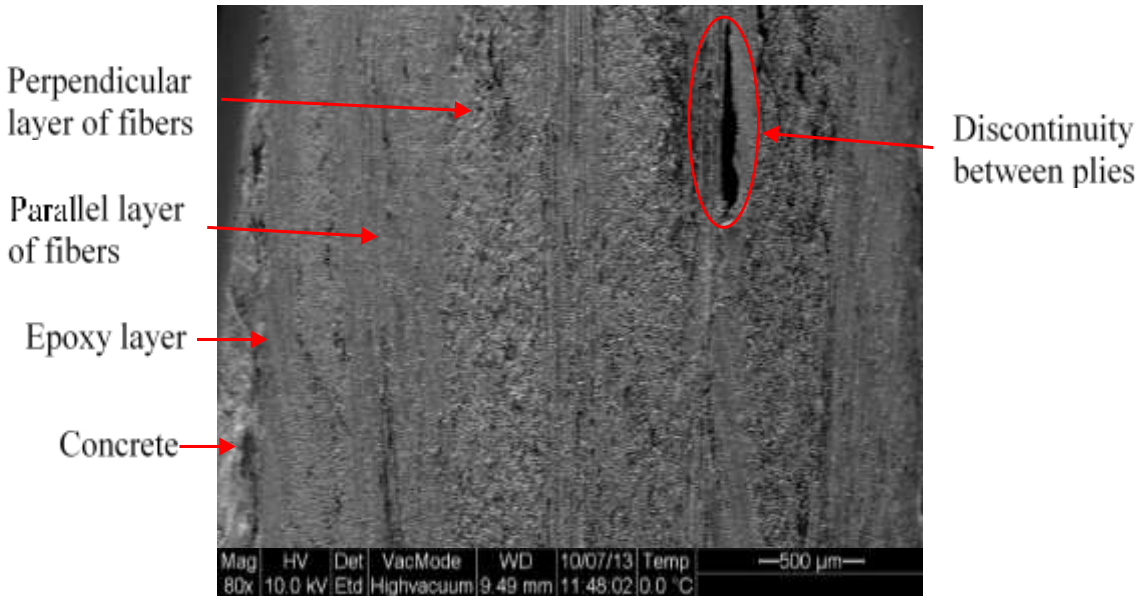

Figure 7.10 ESEM micrograph of microstructure of FRP shell bonded with concrete surface

7.4.5 ESEM Results and Discussion

7.4.5.1 Effect of Moisture

The microstructural observations showed no damage after 100 days of immersion in water at 6°C and 25°C temperatures; however, some micro-cracking and leaching of polymeric matrix due to moisture absorption was observed at 70°C. Figure 7.11 presents micrographs of the reference specimen and specimens immersed in water for more than 100 days at 6°C, 25°C and 70°C temperatures.

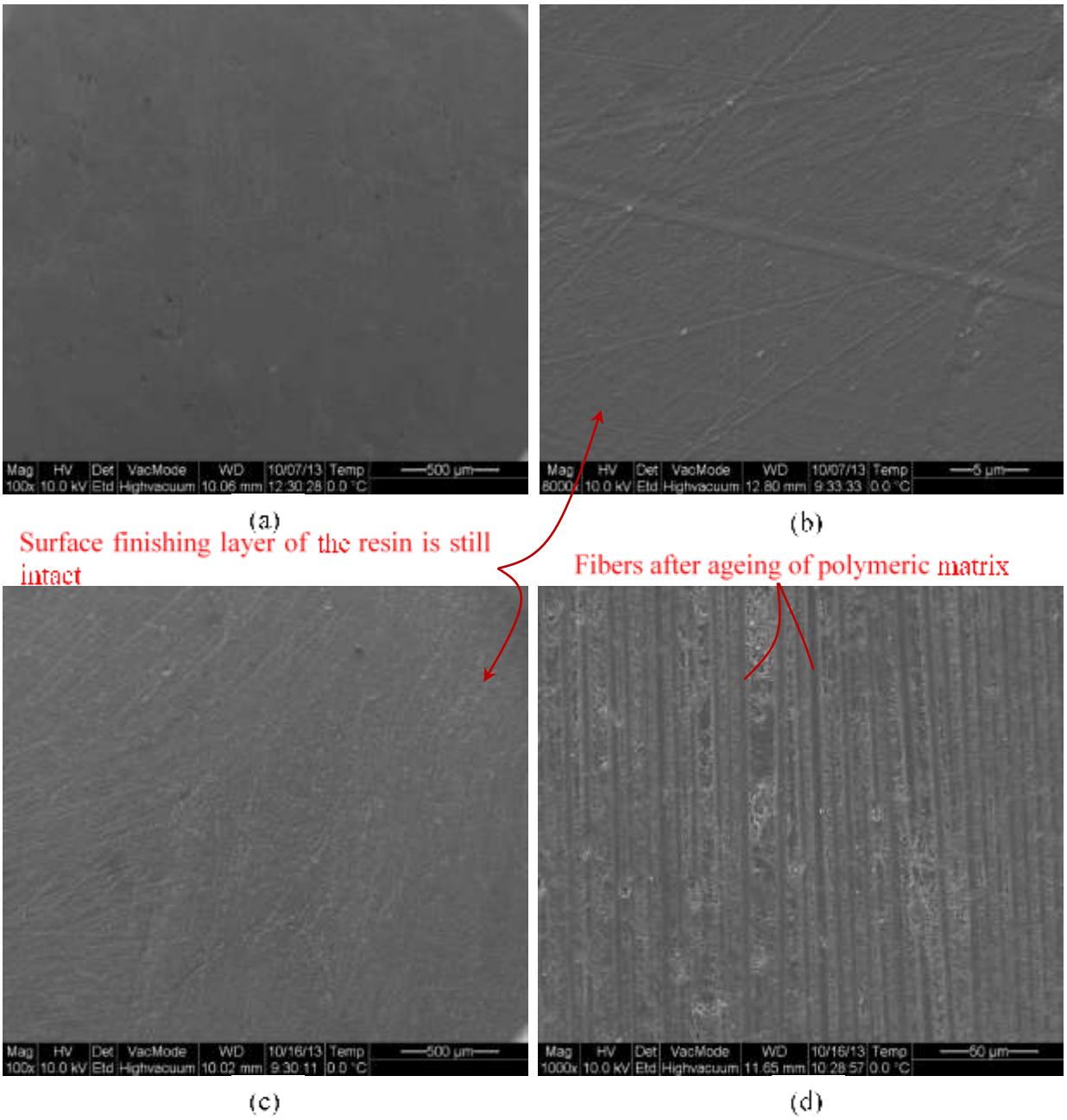

Figure 7.11 ESEM micrograph of ageing of FRP shell due to moisture absorption at different temperatures (a) reference sample (b) at 6 ºC (c) at 25 ºC (d) at 70 ºC

Similarly, the matrix (epoxy-based resin) microstructure observations demonstrated that the water absorption did not influence their microstructural properties at 6°C and 25°C temperatures;

however, the matrix samples immersed in water at 70°C, suffered from serious degradation due to depolymerization, as clearly spotted at high magnification micrograph in Figure 7.12.

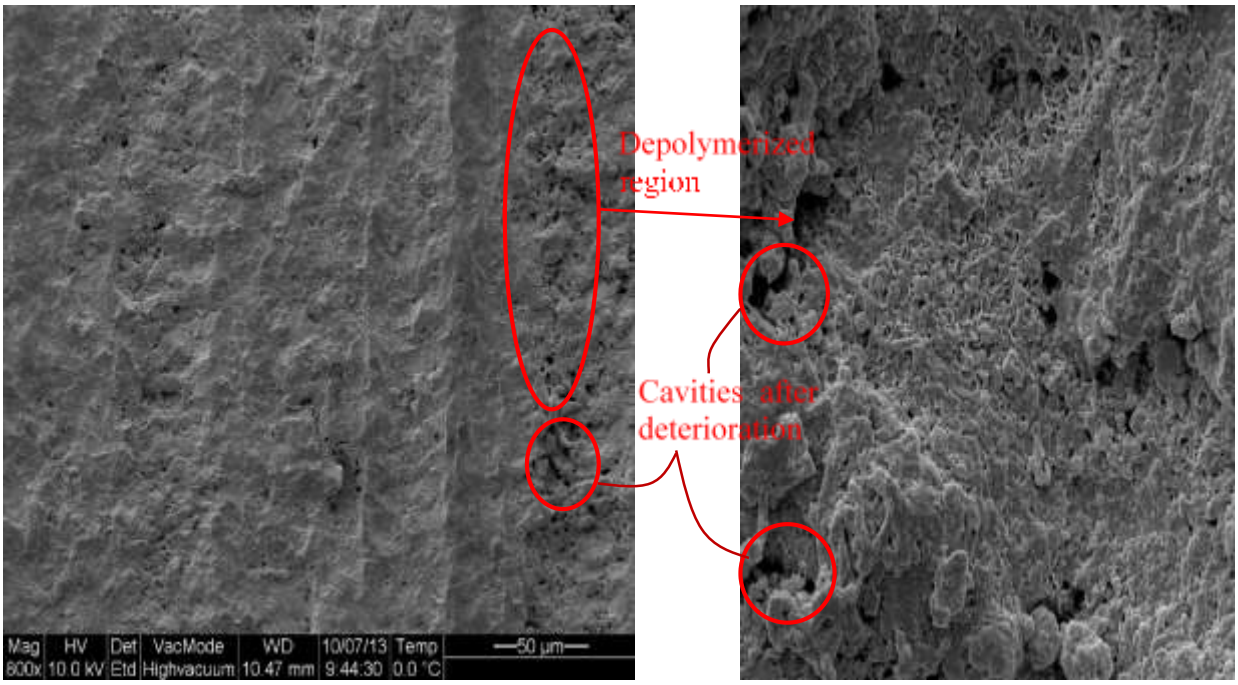

Figure 7.12 ESEM micrograph of ageing of polymeric matrix due to moisture absorption at 70ºC

7.4.5.2 Effect of Chloride Penetration

The ESEM micrograph showed that proper surface finishing is very important to prevent chloride penetration. The chloride deposits were spotted at the surface and in the cavities because of poor surface finish and microscopic pockets. The depth of chlorides in these cavities in the P-specimens were approximately 20 µm (Figure 7.13). However, no physical damage was detected after more than 100 days of exposure period. Figure 7.13 shows micrographs of H-specimens; there were no chlorides or physical damage observed. From these test results, it can be concluded that the FRP shell performed well as an impervious barrier against the penetration of chlorides and moisture.

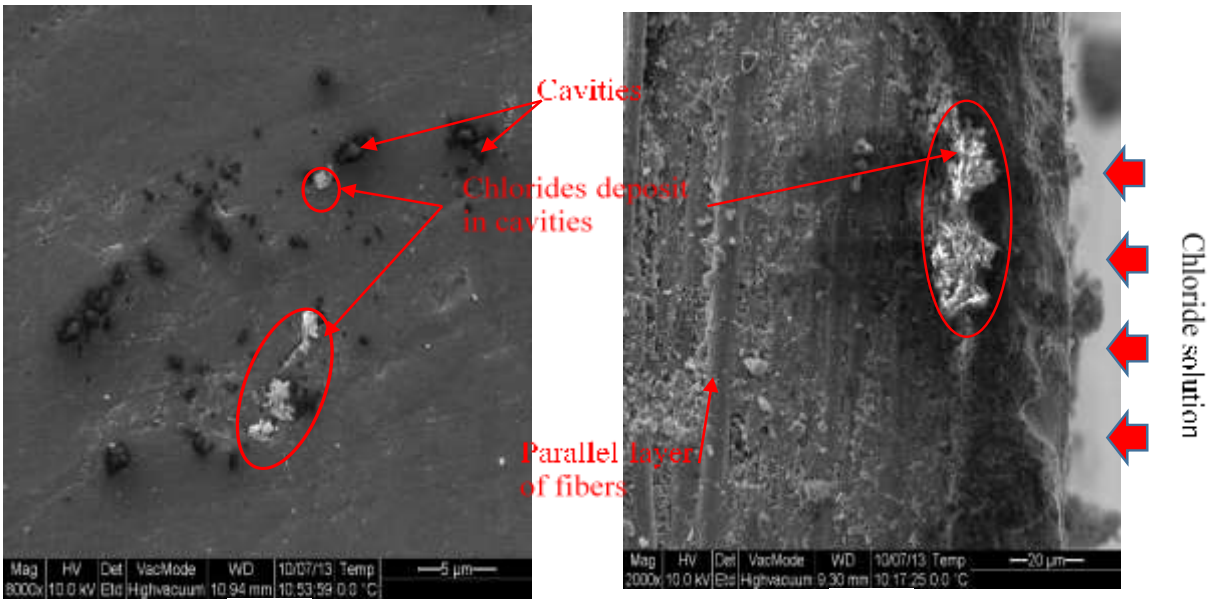

Figure 7.13 ESEM micrograph of rapid chloride penetration in P-specimen (a) top view (b) cross-sectional view

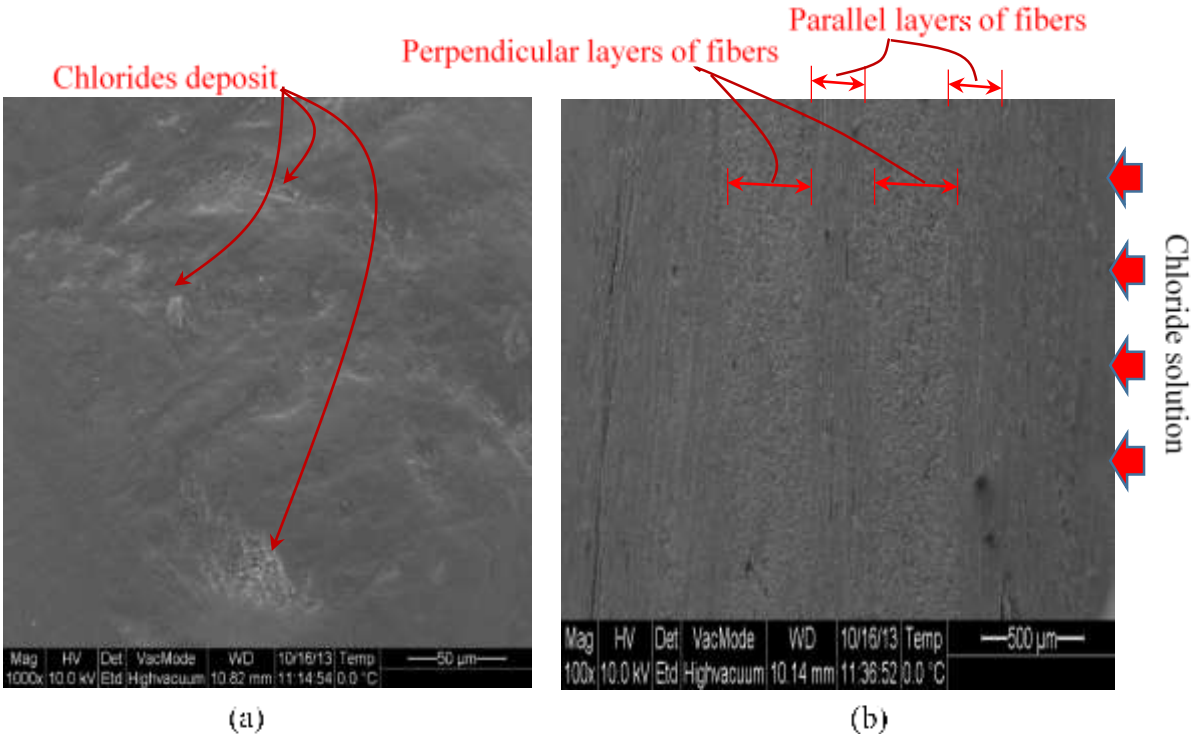

Figure 7.14 ESEM micrograph of rapid chloride penetration in H-specimen (a) top view (b) cross-sectional view

7.5 Projected Long-Term Behavior of Prestressed Concrete Girders with FRP shell on the Bottom Flange

7.5.1 Basics of Deterioration in Prestressed Concrete

The system of three materials - FRP composites, concrete and prestressing steel, when combined in a structural member, performs together differently as compared with the performance of the individual materials, under different types of loading and environmental conditions over a certain time period. These materials have their individual durability problems and the associated deterioration mechanisms, which can range from superficial surface problems to disintegration of the FRPs, concrete and prestressing steel within the member, the latter resulting principally from moisture (wetting and drying), freezing and thawing cycle, corrosion of reinforcing steel, alkali-aggregate reactivity, sulphate attack and other physical, chemical, mechanical and biological causes (Mirza 2005). To identify the main mechanisms of deterioration, it is important to evaluate its driving mode, such as the relationship of chloride ingress to chloride induced corrosion. The principal mechanisms which must be considered during the design for durability of prestressed concrete bridge girders are corrosion of reinforcing and prestressing steel and freezing and thawing cycles.

This section provides a brief summary of design of bridge girders for durability, when subjected to an aggressive environment, considering the effectiveness of the FRP shell and its performance over the design service life.

7.5.1.1 Corrosion of Reinforcing and Prestressing Steel

Corrosion deterioration and the associated cracking cause an increase in the stresses in bridge members and a decrease in the bridge strength and stiffness, resulting in larger deflections and significant changes in the bridge dynamic response. Durability against corrosion can be controlled

by ambient temperature, relative humidity, chloride content, degree of exposure to CO_2, concrete mix design, type of cement, and degree of exposure to severe and aggressive micro-climates, among other factors (Sarja and Visakari 1996; Richardson 2002; Ji 2003; Amleh and Mirza 2004; Mirza *et. al* 2005).

Cyclic loadings applied on a bridge structure located in a corrosive environment can result in corrosion fatigue problems. Fatigue causes cracking and the rate of fatigue cracking increases in the presence of a corrosive environment. Different types of corrosion (surface pitting and crevice corrosion) can reduce the fatigue resistance of some structural members. Other detrimental effects include the loss of local member stability and damage to bridge bearings, leading to their locking (Mirza 2006).

Chlorides present in de-icing salts can penetrate into the reinforced concrete elements. The time required for the critical chloride level to reach and depassivate the protective layer around the reinforcing and prestressing steel elements is normally defined as the corrosion incubation and initiation period (t_0). After the initiation period, the rate of corrosion accelerates. A modified version of Tuutti's two-stage model of service life from a structural concrete element exposed to chlorides, can be used to model the initiation and propagation periods for the time of construction and initiation of operations to the onset of corrosion to failure of a reinforced concrete element (Figure 7.15).

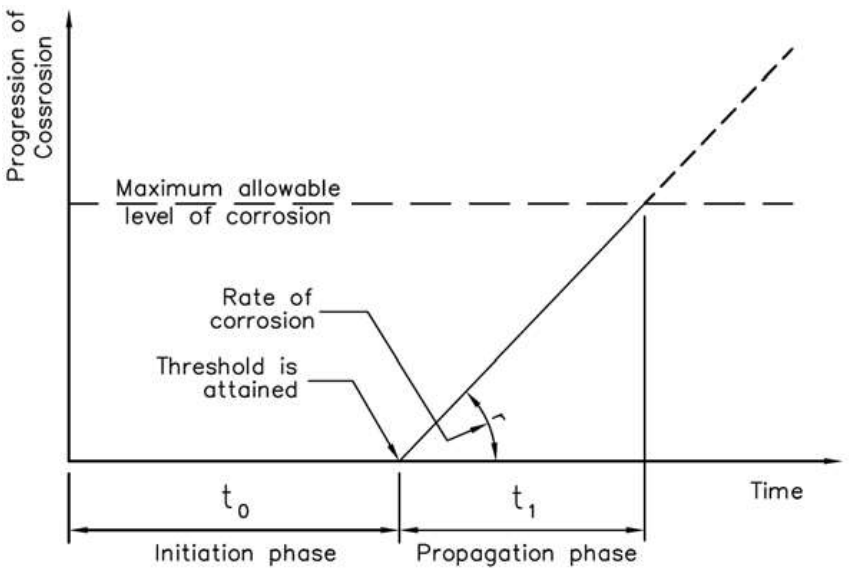

Figure 7.15 corrosion of reinforcement stages (Sarja and Vesikari 1996)

Carbon dioxide (CO_2) from the air penetrates into the concrete and decreases the alkalinity of the pore solution of the concrete microstructure which results in formation of a carbonation front that progressively penetrates into the reinforced concrete element. After reaching the steel reinforcement level, this carbonation front reacts and dissolves the passive protective layer of oxides of iron around the surface of the steel reinforcement, which leads to initiation of corrosion in the presence of moisture and oxygen.

The phenomenon of corrosion of prestressing steel strands in prestressed concrete is significantly different from that of the reinforcing steel. The prestressing strands are normally made of smaller size individual wires. Any reductions in the wire cross-section due to corrosion can lead to brittle wire fracture, which can cause a brittle failure without any warning, and can have serious consequences. Presence of corrosive agents (chlorides, water and oxygen, etc.) near the strands surface, depassivates the protective layer due to a decrease in the alkalinity of the surrounding

concrete. Corrosion in prestressed concrete can be uniform, pitting and stress-corrosion cracking, or a combination of these.

Pitting corrosion is associated with the depassivation of the protective layer, and it is characterized by a highly localized loss of steel, resulting in a deep and tiny holes termed the pits. The pit acts as a notch, and high tensile stresses (three-dimensional) concentrate at the edge of the pit in the remaining cross-section, which can lead to a brittle failure of the member, without any warning. Pitting corrosion is a more serious form of corrosion as compared with uniform corrosion.

The stress-corrosion cracking phenomenon exists only in prestressing steel strands subjected to aggressive elements. The tensile stresses in prestressing strands are normally quite high, therefore, any reduction in the cross-sectional area is quite dangerous. Surface corrosion involves the risk of stress corrosion cracking, leading to brittle failure. Stress-corrosion is incubated in very small surface cracks and needs local depassivation of steel surface to produce surface cracks. It is very important to protect the prestressing steel from aggressive elements over their service life. For obvious reasons, corrosion in prestressing steel is normally always limited to the initiation period; it can be calculated using similar chloride diffusion equations as for reinforcing steel (Sarja and Vesikari 1996).

7.5.1.2 Freezing and Thawing Cycles

Bridge structures exposed to extreme temperatures on a cyclic basis are at greater risk of durability distress problems and failure in extreme cases. The problem stems from freezing of water inside the capillary pore system, which is accompanied by expansion (about 9% of its volume), inducing internal pressure inside the pore system (similar to a pipe under pressure), which is eventually dissipated through cracking of concrete. Concrete subjected to a significant number of freezing

and thawing cycles permits penetration of increasing amounts of moisture during thawing and as a result an increasing volume demand during freezing. After a prolonged period of exposure, freezing and thawing cycle decreases the concrete strength, generate an eventual disruption and a complete loss of material near the surface of the structural member.

The degradation process due to freeze/thaw cycling is very complex. The rate of deterioration depends mainly on the quality of the concrete and the number of freezing and thawing cycles imposed on the element. The other factors which can influence freeze/thaw behavior and damage are the degree of saturation, available water volume, pore structure, concrete age, climatic conditions, aggregate characteristics, and the effect of de-icing salts (Richardson 2002).

7.5.1.3 Prediction against Deterioration

Statistical analysis of empirical data from the various laboratory and field tests for durability of materials have been used to develop mathematical models of the different degradation modes that influence the durability of structural concrete systems. These models are used to estimate any projected deterioration in the structures that could be used to approximate its service life. To design a bridge girder for durability, an evaluation of the possible environmental effects, and material and structural performance over the design service life needs to be considered. This requires an extrapolation of the current knowledge about macro- and micro-climate, material properties, as well as the available models that describe the different mechanisms of deterioration.

Ji (2003) developed a method to assess corrosion of steel in reinforced concrete elements by direct integration of the durability parameters into the structural design equations (Ji 2003; Mirza *et. al* 2005). Figure 7.16 presents the definition of such a model. The reinforced concrete section can be analyzed by considering a unit width, when the concrete covers on both sides are subjected to

different mechanisms of deterioration, such as interior and exterior faces of exterior girders (Figure 7.16 (a)). The active corrosion process starts once the initiation period for corrosion is over after the concrete cover becomes ineffective (Figure 7.16. (b)). Figure 7.16 (c) represents the stage when corrosion starts at the most exposed location of the reinforcing bar and then continues around the perimeter of the bar. Once corrosion occurs over the entire perimeter, it continues toward the inside of the rebar, reducing the cross section of the bar in proportion to the rate of corrosion (Figure 7.16 (d)).

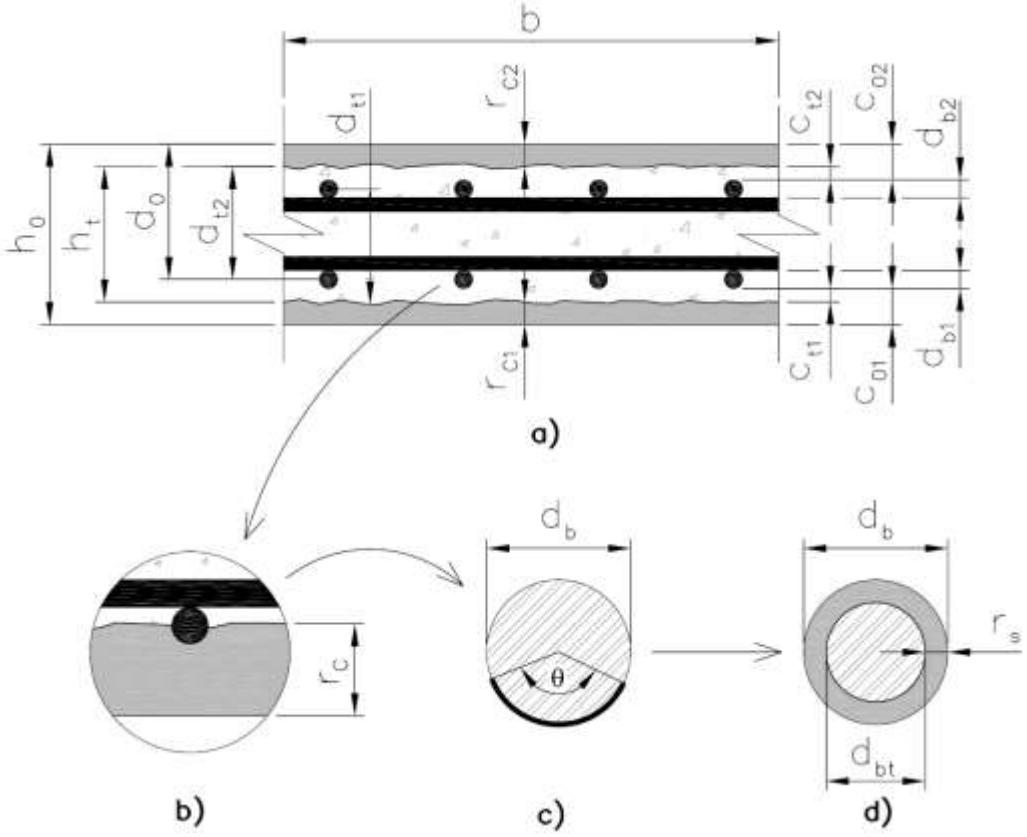

Figure 7.16 Reinforced concrete section parameters for the structural and durability design (Ji 2003)

In Figure 7.16, the suffices 1 and 2 referred to internal and external faces of the reinforced concrete element being analyzed, respectively, such as the internal or external layers of reinforcing steel.

The parameters involved in the resistance of this reinforced concrete section are:

b = reinforced concrete section width
h_0 = reinforced concrete section initial thickness
d_0 = initial effective depth of the section
h_t = height of the section being affected by the deterioration rate, rc_1 and rc_2
d_{t1} = effective height of the section being affected by the deterioration rate, rc_1.
d_{t2} = effective height of the section being affected by the deterioration rate rc_2.
c_{t1} = concrete cover of the section affected by the deterioration rate rc_1.
c_{t2} = concrete cover of the section affected by the deterioration rate rc_2.
c_{01} = initial concrete cover at the internal face.
c_{02} = initial concrete cover at the external face.
r_{c1} = depth of deterioration of concrete at the internal face.
r_{c2} = depth of deterioration of concrete at the external face.
d_{b1} = initial diameter of the rebar near the internal face.
d_{b2} = initial diameter of the rebar near the external face.
d_{bt1} = diameter of the rebar affected by corrosion rs_1.
d_{bt2} = diameter of the rebar affected by corrosion rs_2.
r_{s1} = depth of corrosion at the internal layer of rebars.
r_{s2} = depth of corrosion at the external layer of rebars.

Using the latest available models of the relevant deterioration modes, a bridge structure was designed for a service life of 150 years in a cold climate region near Montreal (Macia 2011; Macia and Mirza 2012). They determined the macro-climate at the bridge site, and based on the site location and the bridge location, they defined the micro-climates around each defined member of the bridge, or its parts where necessary. They incorporated the effects of the various deterioration modes on the behavior of bridge structure over its entire service life. The designed bridge was subjected to the various mechanical, natural and man-made loads and an aggressive environment, considering the performance of the various materials and structural components over the design

service life. The proposed design for durability procedure was illustrated with a detailed worked out example.

The environmental conditions around the bridge girders induce certain physical, chemical and biological processes responsible for the different mechanisms of deterioration that can occur and affect the different composing elements, depending on their degree of exposure. Figures 7.17 and 7.18 show the rates of deterioration for frost attack, surface deterioration due to the different weathering mechanisms, carbonation and chloride induced corrosion of the edge and internal girders of a prestressed concrete bridge, respectively. Based on the field experience, suitable assumptions were made about the materials, and the concrete cover thickness was determined based on the severity of the deterioration modes, which was 75 mm. The combined effect of these modes of deterioration over time simulates the progressive deterioration of the bridge girders and their corresponding loss of strength and stiffness; details can be found elsewhere (Macia, 2011; Macia and Mirza 2012).

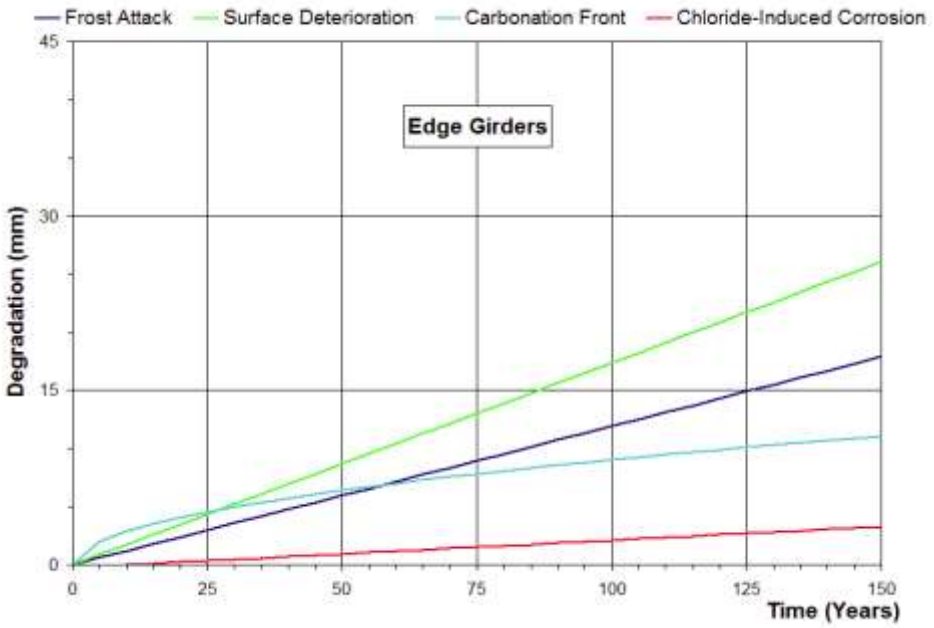

Figure 7.17 Rate of degradation of prestressed concrete bridge edge girders (Macia, 2011; Macia and Mirza 2012)

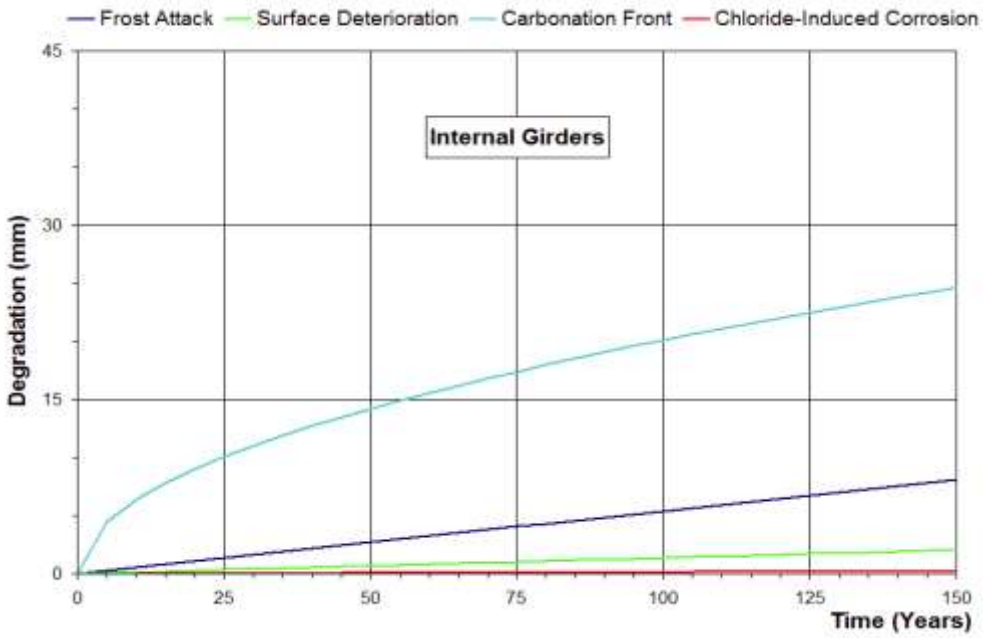

Figure 7.18 Rate of degradation of prestressed concrete bridge internal girders (Macia 2011; Macia and Mirza 2012)

7.5.2 Projected Ingress of Injurious Elements into the System

Diffusion of injurious element, such as moisture, chlorides and CO_2 into the concrete and FRP materials have been used by several investigators to assess the service life of a concrete structure which is subjected to deterioration due to corrosion of the embedded reinforcing steel. As mentioned earlier, transport of chemicals into porous media is predominantly a diffusion process and Fick's laws, which consider the driving force for diffusion through a thin film to be the concentration gradient, or an appropriate modification thereof can be used to idealize migration of chlorides through FRP-reinforced concrete members; details are presented in Section 7.3.

As mentioned earlier, moisture absorption in an FRP shell, can be described as a process of diffusion involving small molecules of water migrating though a concentration gradient. Fick's Second Law of diffusion can be used, assuming unidirectional diffusion normal to the plane of the FRP shell and the diffusing species being independent of the concentration gradient (Crank, 1975); details are presented in Section 7.2.

Based on inspection of bridges operating in aggressive environments, the surface of the concrete around the lower flange on the girders is more susceptible to deterioration due to corrosion of prestressing steel as compared with the other parts of the girders. In this proposed FRP-concrete system, the lower flange is protected by an FRP shell.

Prediction of ingress of injurious elements (moisture and chlorides) over the service life is complicated by the variety of complex mechanisms involving penetration through the FRP shell, bonding epoxy-based resin and the concrete cover, to reach the prestressing steel strands (Figure

7.19). To make the problem simpler, prediction of chloride ingress can be made in the FRP composite shell and concrete separately. Both set of water absorption in the FRP shell and chlorides diffusion for the concrete data can be used for the preliminary long-term prediction of chloride ingress into the FRP-concrete system.

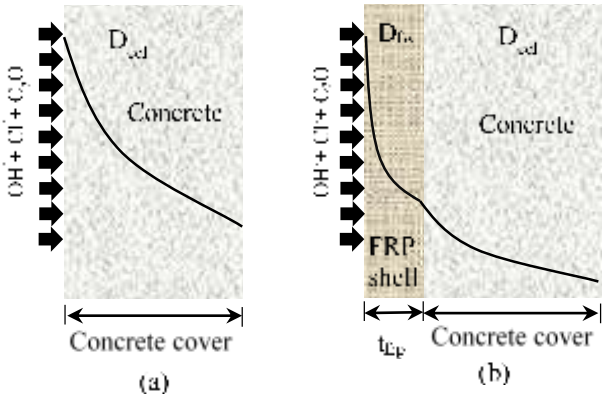

Figure 7.19 Schematic mass concentration profiles (not to scale) (a) without FRP shell (b) with FRP shell

Crank's error function solution of Fick's second law of diffusion (Equation 7.1) can be restated as a function of diffusion coefficient:

$$C_x = C_s\left(1 - erf\left(\frac{x}{\sqrt{4D_{ccl}t}}\right)\right) \qquad (7.7)$$

where C_x = chloride concentration at depth *x* at time 't',

C_s= surface chloride concentration,

t = time of exposure,

erf = error function, and

D_{ccl} = apparent diffusion coefficient

For this preliminary study on prediction of chloride ingress over time into the prestressed concrete girder with an FRP shell over its bottom flange, a few assumptions were made. The chloride content at the reinforcing steel surface to initiate correction was considered to be the critical chloride content or chloride threshold value. A wide range of chloride threshold values exit in the literature, from a minimum of 0.06% to a 2.5% by the weight of cement. The chloride threshold value was assumed to be 0.4% by weight of cement in the prestressed concrete (Angst *et al.* 2009; Richardson 2002).

Similarly, the value of the surface chloride level, C_s, depends on many factors, such as the environmental conditions and the chloride absorption ability of the concrete with different compositions. Although the value of C_s is variable during the life of the concrete; however, a constant value of C_s = 3.5% by the weight of cement was considered in this preliminary analysis, which was based on application of de-icing salt on bridges at an annual dosage rate of about 250 grams/m^2 (Li, 2005; Richardson, 2002). The coefficient of diffusion was assumed to be constant at 0.54×10^{-12} m^2/s for the prediction model , calculated as a function of the w/c ratio = 0.37, using Equation 7.9 (Richardson, 2002).

$$D_{ccl} = 0.04\left(1166^{\frac{w}{c}}\right) \times 10^{-12} \qquad (7.9)$$

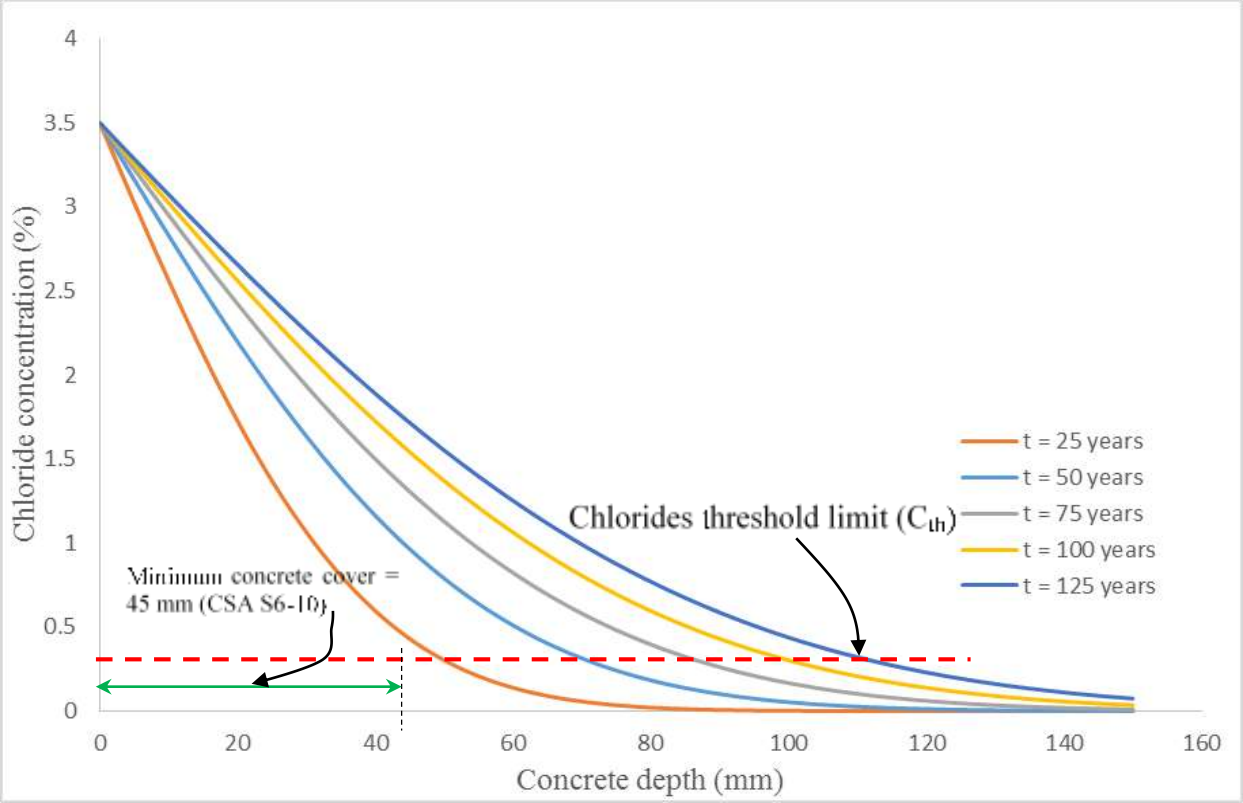

Figure 7.20 Predicted chlorides ingress profile for the prestressed concrete girder (without FRP shell)

Figure 7.20 presents the predicted chloride ingress profile during the service life of the bridge girder. If the concrete cover thickness for the girders is assumed to be 75 mm, the predicted profile showed that chloride ingress from the exterior surface would reach the prestressing strands within an exposure period of 45 years, as shown by a dashed line in Figure 7.20. As mentioned earlier, the corrosion initiation period is the time required for the steel to depassivate by the penetration of chloride ions which can be assumed equal to the time for chloride to reach prestressing steel, which is 45 years in this case.

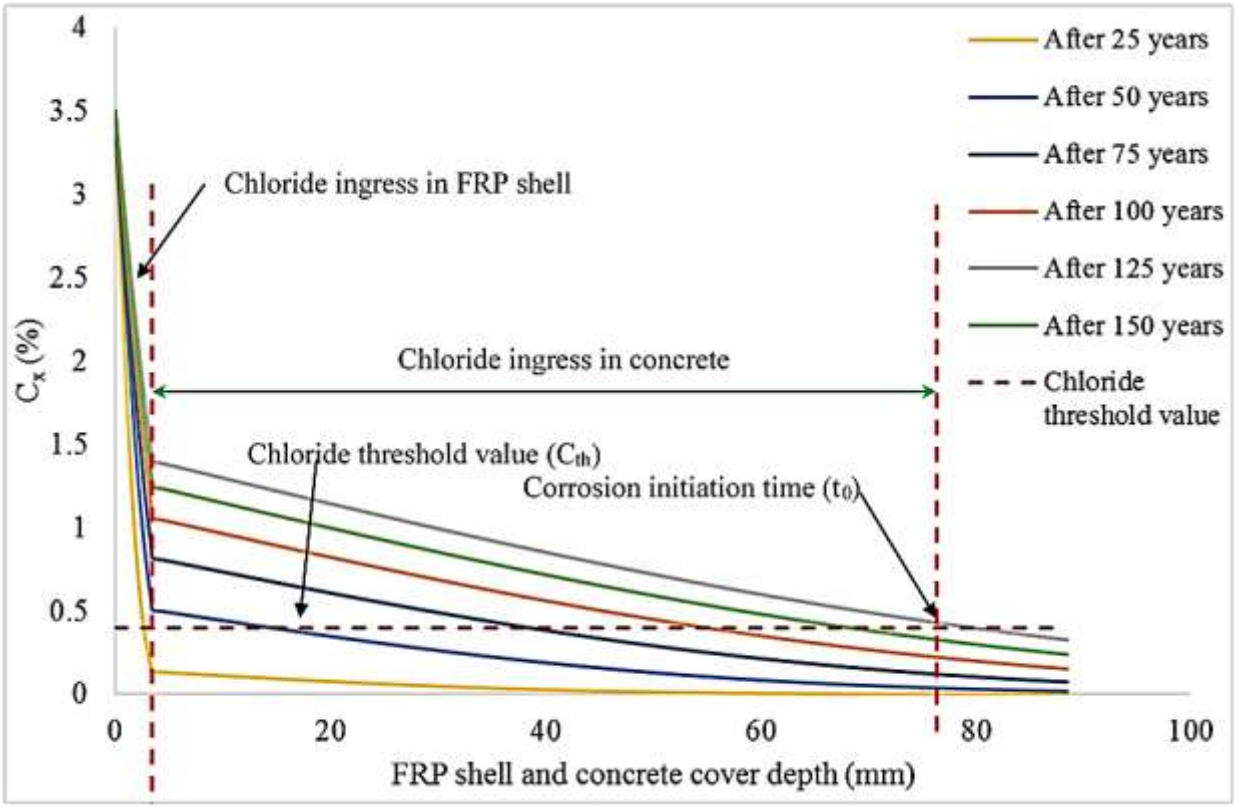

Figure 7.21 Predicted chlorides ingress profile for the prestressed concrete girder with FRP shell

Figures 7.21 presents the predicted chlorides ingress profiles during the service life of the prestressed concrete bridge girder with an FRP shell. The FRP shell, as a barrier, showed great resistance against the chloride ingress by significantly slowing down the chlorides ingress rate and the amount of chloride ions. For a prestressed concrete girder with an FRP shell, the accumulated time of chloride penetration from the surface of the concrete to reaching the prestressing steel stands level was predicted to be about 135 years. If the required time for chloride penetration is **conservatively** assumed to be equal to corrosion initiation period (t_0), the overall service life of this proposed system can be calculated by adding time associated with an "acceptable" deterioration of the prestressed concrete girder, which would be twice of the suggested design

service life by the Canadian Highway Bridge Design Code (CHBDC 2010). It can be concluded that the FRP shell can be quite effective in improving durability of the girders, i.e. to significantly extend service life of the prestressed concrete girders.

Overall performance of the prestressed concrete girders needs to be evaluated over the entire service life of the bridge structure, considering all limit states, which will be the future work in this research program. With the addition of an FRP shell, the selection of construction materials, careful design, construction and maintenance are also equally important for a satisfactory performance of the bridge girder over its entire service life.

7.6 Summary

The long-term durability of the FRP shell to act as a barrier against penetration of injurious elements, and the proposed FRP shell-concrete system, were examined experimentally. The experimental results of water absorption tests, chloride penetration tests and electronic scanning microscope are presented.

Water immersion test were conducted at three different temperatures of 6°C, 25°C and 70°C; the results of mass gain and diffusion coefficients for both FRP shell and resin samples were determined. The moisture mass gains of the FRP shell samples, at steady state, were lower than that of the resin samples because the fibers did not absorb any moisture. The moisture absorption behavior of the FRP shell at 70°C was different from the samples at the two lower temperatures. After the maximum absorption level, the absorption rate decreased rapidly in these samples, showing that the FRP shell samples aged in water at 70°C after about 100 days of exposure because of depolymerisation and leaching out of the polymeric matrix.

To investigate the effectiveness of the FRP shell against chloride solution ingress in the concrete specimens, an experimental method, for rapid chloride solution penetration into the FRP bonded concrete specimen, was developed. The specimens were exposed to sodium chloride solution under a pressure of 550 kPa, using a specially designed diffusion cell. The chloride penetration depth and the concentration level were measured and analyzed using three techniques - inflow measurement, colorimetric technique, and profile drilling technique. The results showed absence of chlorides in the concrete samples which demonstrated that the FRP shell did not allow any chlorides to penetrate into the concrete, and acted as an impervious barrier against the penetration of chlorides.

The microstructural observations were performed using the Environmental Scanning Electron Microscope (ESEM - Quanta 200 FEG) to examine the arrangement of fibers and plies in a cross-section of the FRP composite shell, manufacturing defects (micro-cracks and pores), effects of chloride exposure, and degradation due to moisture absorption at different temperatures. The microstructural observations showed no damage after 100 days of immersion in water at 6°C and 25°C temperatures; however, some micro-cracking and leaching out of the polymeric matrix due to moisture absorption was noted at 70°C. Similarly, the matrix (epoxy-based resin) microstructural observations demonstrated that the water absorption did not affect their microstructural properties at 6°C and 25°C temperatures; however, the matrix samples immersed in water at 70°C, suffered from serious degradation due to depolymerisation. The ESEM micrograph also showed that proper surface finishing is very important against chloride penetration. The chloride deposits were noted on the surface and in the cavities because of poor surface finishing and microscopic pockets. The average depth of chlorides in these cavities in the

P-specimens was approximately 20 μm. However, no physical damage was detected after more than 100 days of exposure. From these test results, it can be concluded that the FRP shell performed satisfactorily as an impervious barrier against the penetration of chlorides and moisture.

The effectiveness of the FRP composite shell, as a barrier against chloride and moisture ingress, was evaluated. The FRP shell, acting as a barrier, showed a significant resistance against chloride ingress by significantly slowing down the chlorides ingress rate and the total amount of chloride ions. The predicted profiles showed that chloride ingress from the exterior surface can reach the prestressing steel strands within a period of 45 years. For a prestressed concrete girder with an FRP shell, the accumulated time of chloride penetration reaching up to the prestressing steel strand level was predicted to be about 135 years. It can be concluded that an FRP shell is quite effective in improving the durability characteristics of a prestressed concrete girder and can significantly extend service life of the prestressed concrete girders.

Since this was a preliminary study, more work is required to evaluate the overall performance of prestressed concrete girders with FRP shell on the bottom flange, considering all of the pertinent limit states over the entire service life of the bridge structure. This research work can be improved further, combining the research work by Macia and Mirza (2012) and by incorporating all possible modes of deterioration and their effects on structural integrity over time.

CHAPTER 8 SUMMARY, CONCLUSIONS AND RECOMMENDATIONS

8.1 Summary and Conclusions

The results of the studies in this research program can be summarized and conclusions drawn as follows:

8.1.1 Bond Characteristics

The bond between FRP laminates and cast-in-place concrete was investigated using eight double lap pull-off bond tests. The hybrid FRP laminates were prepared, combining glass and carbon fibers in an epoxy-based resin matrix. These laminates were bonded to the cast-in-place concrete using pre-glued coarse aggregates with epoxy-based resin on the contact surface of the laminates. The interfacial bond stresses were found to be about 1.80 MPa. The interfacial shear stress and the slip characteristics were noted to be bi-linear, with a higher bond stiffness (680 kN/mm) in the first part of the curve up to about 55% of the maximum load and then gradually decreasing near failure. The failure surface in the composite prism occurred in the concrete a few millimetres inside the concrete from the bonded pre-glued aggregates.

8.1.2 Behavior of FRP-Reinforced Prestressed Concrete Tension Members

Experimental work on the FRP-reinforced prestressed concrete tension specimens, with five different levels of prestressing (0, 25, 50, 75 and 100%), was performed to determine the contribution of the bonded FRP composite laminates to the strength and stiffness of the prestressed concrete tension members. These specimens were reinforced externally with bonded FRP laminates, using aggregates pre-glued to the FRP laminates. The tensile strength at initial cracking

in the FRP-reinforced concrete specimen was almost twice that of the control specimens (without FRP composite laminates). The FRP composite laminates and the prestressing force (at different levels) provided additional strength and stiffness to the system and enhanced the cracking strength and stiffness.

8.1.3 Flexural Behavior of Simple Reinforced Concrete Beams with FRP Shell

The flexural characteristics of the FRP shell and the concrete interface along with the effect of the steel reinforcement ratio were studied experimentally to evaluate the flexural and shear behavior of simply supported FRP shell-reinforced concrete beams. These beams were designed for four different reinforcement ratios – 0.8, 1.6, 2.4, 4.8 %, - to examine their flexural characteristics. The beam specimens with the FRP shell showed a significant enhancement in the strength, stiffness and energy absorption capacity as compared with the associated control beams. The modes of failure varied depended on the steel reinforcement ratio, and in both beams with and without the FRP shell.

8.1.4 Flexural Behavior of Prestressed Concrete Beams with FRP Shell

The flexural behavior of cast-in-place prestressed concrete beams with FRP shell was studied to examine the contribution of the bonded FRP shell to the strength, stiffness, ductility and energy absorption capacity of prestressed concrete beam specimens, for five level of prestressing (0, 25, 50, 75, 100%). The initial cracking, yield and ultimate strengths of the beam specimens with FRP shell were significantly higher than those of the associated control beam specimens (without FRP shell). The FRP shell and the prestressing force (at different levels) enhanced the strength and stiffness of the beams. The beam specimens with FRP shell failed in a different manner as

compared with the associated control beams; the modes of failure varied depending on the level of prestressing and the effect of the FRP shell.

8.1.5 Durability of Reinforced Concrete with FRP Shell

The long-term durability of the FRP shell to act as a barrier against penetration of injurious elements, such as moisture and chlorides, and the proposed FRP shell-concrete system, was examined experimentally to obtain a preliminary knowledge of the effects of ingress of moisture and chloride ions into the system. The experimental results of water absorption tests, chloride penetration tests and scanning electronic microscope are presented.

Water immersion tests were conducted at three different temperatures of 6°C, 25°C and 70°C; the results of the mass gain and diffusion coefficients for both FRP shell and resin samples were determined. The moisture absorption behavior of the FRP at 70°C was different from the samples at the two lower temperatures. After the maximum absorption level, the absorption rate decreased rapidly in these samples, showing that the FRP shell samples aged in water at 70°C after about 100 days of exposure because of depolymerisation and leaching out of the polymeric matrix.

To investigate the effectiveness of the FRP shell against chloride solution ingress into the concrete specimens, an experimental method for rapid chloride solution penetration into the FRP bonded concrete specimen, was developed. The specimens were exposed to sodium chloride solution under a pressure of 550 kPa, using a specially designed diffusion cell. The chloride penetration depth and the concentration level were measured and analyzed using three techniques - inflow measurement, colorimetric technique, and profile drilling technique. The results showed absence of chlorides in the concrete samples which proved that the FRP shell did not allow any chlorides

to penetrate into the concrete, and acted as an impervious barrier against the penetration of chlorides.

The microstructural observations were performed using the Environmental Scanning Electron Microscope (ESEM - Quanta 200 FEG) to examine the arrangement of fibers and plies in a cross-section of the FRP composite shell, manufacturing defects (micro-cracks and pores), effects of chloride exposure, and degradation due to moisture absorption at different temperatures. The microstructural observations showed no damage after 100 days of immersion in water at 6°C and 25°C temperatures; however, some micro-cracking and leaching out of polymeric matrix due to moisture absorption were noted at 70°C. Similarly, the matrix (epoxy-based resin) microstructural observations demonstrated that the water absorption did not affect their microstructural properties at 6°C and 25°C temperatures; however, the matrix samples immersed in water at 70°C, suffered from serious degradation due to depolymerisation. The ESEM micrograph also showed that proper surface finishing is very important to inhibit chloride penetration. Chloride deposits were noted on the surface and in the cavities because of poor surface finishing and microscopic pockets. The average depth of chlorides in these cavities in the P-specimens was approximately 20 μm. However, no physical damage was detected after more than 100 days of exposure.

The effectiveness of FRP composite shell, as a barrier against chloride and moisture ingress, was evaluated. The FRP shell, acting as a barrier, showed a significant resistance against chloride ingress by significantly slowing down the chlorides ingress rate and the total amount of chloride ions. The predicted profiles for a prestressed concrete girder without FRP shell suggested that chloride ingress from the exterior surface can reach the prestressing steel strands in about 45 years. For a prestressed concrete girder with an FRP shell, the accumulated time for chloride penetration

and reaching the level of prestressing steel strands was predicted to be about 135 years. These results suggest that the FRP shell is quite effective in improving the durability characteristics of prestressed concrete girders and can significantly extend their service life.

More work is needed to evaluate the overall performance of the prestressed concrete girders with an FRP shell, considering all limit states, over the entire service life of the bridge structure.

8.2 Original Contributions

The original contributions of this research program are:

- Development and behavior of hybrid FRP laminates
- Evaluation of bond characteristics between FRP shell and cast-in-place concrete, before and after prestressing
- Application of FRP shell to new prestressed concrete construction, including the effect of prestressing on FRP and their bond with the concrete substrate
- Development of construction procedure for composite beams with an FRP shell, and evaluation of their strength and durability characteristics
- Needed changes in structural design and construction of prestressed concrete bridge girders for achieving a specific service life using the multiple protection technique, aimed at significantly enhancing the service life
- Preliminary evaluation of durability of FRP composite shell-concrete systems

8.3 Future Recommendations

This research program was aimed at enhancement of the service life of prestressed concrete girders with an FRP composite shell. Further research will help to refine and improve future applications to prototype girders and monitoring, evaluation and enhancement of their durability. The following fundamental and applied research is recommended:

- Development of techniques for plant application of FRP shell to prototype prestressed concrete girders
- Development of design guidelines for this proposed construction technique
- Finite element modeling of the FRP girder with the FRP shell
- The results obtained from durability testing of FRP composite shell prompted further investigations that would complement the first step undertaken here. The proposed recommendations for future work include determination of the nature of the mass loss of the epoxy-based resin in a high temperature water absorption tests and to perform a salt water absorption test at high temperature to determine the moisture saturation
- Evaluation of service life performance of prestressed concrete FRP girders with an FRP shell, using stochastic methods of assessing degradation of the structural components over time
- Overall performance of the prestressed concrete girders needs to be evaluated over the entire service life of the bridge structure, considering all limit states, which will constitute the future work in research program. With the addition of an FRP shell, the selection of the

construction materials, careful design, construction and maintenance are equally important for a satisfactory performance of the bridge girder during its entire service life

- Application of the FRP shell to other civil infrastructure assets

REFERENCES

Abanilla, M. A., Li, Y. and Karbhari, V. M., (2005), "Durability characterization of wet layup graphite/epoxy composites used in external strengthening", Composites Part B: Engineering 37(2-3): 200-212.

ABAQUS, (2010), "A General-Purpose Finite Element Program", Pawtucket, USA. Karlsson & Sorensen.

American Concrete Institute (ACI-440.3R), (2004), "Guide Test Methods for Fiber-Reinforced Polymers (FRPs) for Reinforcing or Strengthening Concrete Structures", American Concrete Institute, Farmington Hills, MI.

American Concrete Institute (ACI-440), (2004), "State-of-the-art Report on Fibre Reinforced Plastic Reinforcement for Concrete Structures", American Concrete Institute, Farmington Hills, MI.

American Concrete Institute (ACI-440.2R), (2008), "Guide for the Design and Construction of Externally Bonded FRP system for Strengthening Concrete Structures", Farmington Hills, MI.

Aldajah, S., Alawsi, G. and Rahmaan, S. A. (2009), "Impact of Sea and Tap Water Exposure on the Durability of GFRP Laminates" Materials & Design 30(5): 1835-1840.

Ali, M. S., Mirza, M. S. and Lessard, L., (2012), "Bond Characteristics between Hybrid FRP Laminates and Cast-In-Place Concrete –an Experimental Study", International Conference on Advanced Concrete Technology & its Applications (ACTA-2012), Islamabad, Pakistan.

Amleh, L. and Mirza, M. S., (2004), "Corrosion Response of a Decommissioned Deteriorated Bridge Deck", Journal of Performance of Constructed Facilities 18(4): 185-194.

Canadian Highway Bridge design code (CHBDC), (2006), "Commentary on CAN/CSA-S6-10", Canadian Standards Association. Toronto.

ASTM D570, (2010), "Standard Test Method for Water Absorption of Plastics", West Conshohocken, PA.

ASTM C1202, (1999), "Standard Test Method for Electrical Indication of Concrete's Ability to Resist Chloride Ion Penetration," West Conshohocken, PA.

ASTM D3039 (2008), "Standard Test Method for Tensile Properties of Polymer Matrix Composite Materials.

Attari, N., Amziane, S. and Chemrouk, M., (2012), "Flexural Strengthening of Concrete Beams Using CFRP, GFRP And Hybrid FRP Sheets", Construction and Building Materials 37(0): pp 746-757.

Aydin, F. and Sarıbıyık, M. (2013), "Investigation of Flexural Behaviors of Hybrid Beams Formed with GFRP Box Section and Concrete", Construction and Building Materials 41(0): 563-569

Bakis, C. E., Bank, L. C., Brown, V. L., Cosenza, E., Davalos, J. F., Lesko, J. J., Machida, A., Rizkalla, S. H. and Triantafillou, T. C., (2002), "Fiber-Reinforced Polymer Composites for Construction-State-of-the-Art Review", Journal of Composites for Construction 6(2): 73-87.

Bank, L. C., (2006), "Composite for Construction: Structural Design with FRP Materials", Canada, John Wily & Sons, Inc.

Bank, L. C., Barkatt, A. and Gentry, T. R., (1995), "Accelerated Test Methods to Determine the Long-term Behavior of FRP Composite Structures: Environmental Effects", Journal of Reinforced Plastics and Composites 14(6): 559-587.

Banthia, P. N., (2003), "FRP-concrete bond in structural strengthening and rehabilitation", 2009, from://www.rilem.net/tcDetails.php?tc=FRP.

Belingardi, G., Cavatorta, M. P. and Frasca, C., (2006), "Bending fatigue behavior of glass-carbon/epoxy hybrid composites", Composites Science and Technology 66(2): pp 222-232.

Benachour, A., Benyoucef, S., Tounsi, A. and Adda bedia, E. A., (2008), "Interfacial stress analysis of steel beams reinforced with bonded prestressed FRP plate", Engineering Structures 30(11): 3305-3315.

Benzarti, K., Chataigner, S., Quiertant, M., Marty, C. and Aubagnac, C., (2011), "Accelerated ageing Behaviour of the Adhesive Bond between Concrete Specimens and CFRP Overlays", Construction and Building Materials 25(2): 523-538.

Brant, O., (2008), “Combined Effects of Freeze-Thaw and Sustained Loads on Reinforced Concrete Beams Strengthened with FRPS”, M.Eng. Thesis Queen's University, Kingston.

Cardon, A. H., Qin, Y. and Van Vossole, C., (2000), "Durability Analysis of Polymer Matrix Composites for Structural Applications”, Computers & Structures 76(1-3): 35-41.

Canadian Highway Bridge Design Code (CHBDC) CAN/CSA-S6-10 (2010), “National Standard of Canada. Canadian Standards Association (CSA)”, Mississauga, Ont., Canadian Standards Association.

Cheng, L. and Karbhari, V. M., (2006), "New Bridge Systems using FRP Composites and Concrete: A State-of-the-Art Review”, Progress in Structural Engineering and Materials 8(4): 143-154.

Cheng, L. and Karbhari, V. M., (2008), “Efficient use of CFRP Stay-in-place Form for Durable Concrete Bridge Decks. FRP Stay-in-place Forms for Concrete Structures”, session at the ACI spring convention. A. Z. Fam. Los Angeles, California, USA, ACI. SP-257: 1-14.

Black Mint Software, Inc. Ottawa, ON, CANADA, website: http://www.blackmint.com/CB_Home.html

Crank. J., (1975), "The Mathematics of Diffusion". Clarendon Press. Oxtè. Jrd

David, E., Ragneau, E. and Buyle-Bodin, F., (2003), "Experimental Analysis of Flexural Behaviour of Externally Bonded CFRP Reinforced Concrete Structures”, Materials and Structures 36(4): 238-241.

Demers, M., Labossière, P. and Mercier, C., (2006), “Glass FRP Jacketing of Prestressed Concrete Beams”, 7th International Conference on Short and Medium Span Bridges

Diab, H., Wu, Z. and Iwashita, K., (2009), "Short and Long-term Bond Performance of Prestressed FRP Sheet Anchorages”, Engineering Structures 31(5): 1241-1249.

Dieter, D. A., Dietche, J. S., Bank, L. C., Oliva, M. G. and Russell, J. S., (2002), “Concrete Bridge Decks Constructed with Fiber-Reinforced Polymer Stay-In-Place Forms and Grid Reinforcing”, Washington, DC, ETATS-UNIS, National Research Council.

El-Hacha, R. and Omran, H. Y., (2012), “Reinforced Concrete Beams Strengthened Using Prestressed NSM CFRP Reinforcement - Effects of CFRP Geometry and Freeze-Thaw Exposure”, 6th International Conference on Advanced Composite Materials In Bridges and Structures, Kingston, Ontario.

El-Hacha, R., Wight, R. and Green, M., (2001), "Prestressed Fibre-reinforced Polymer Laminates for Strengthening Structures”, Progress in Structural Engineering and Materials 3(2): 111-121.

Elmahdy, A., El-Hacha, R. and Shrive, N., (2008), “Flexural Behavior of Hybrid Composite Girders for Bridge Construction”, ACI Spring Convention 2008. A. Z. Fam. Los Angeles, California, USA, ACI. SP-257: 15-32.

Egypt Concrete Design Code (ESCC), (2005), “The Use of Fiber Reinforced Polymer (FRP) In the Construction Fields”. Egypt.

Fam, A. Z. and Rizkalla, S. H., (2002), "Flexural Behavior of Concrete-Filled Fiber-Reinforced Polymer Circular Tubes”, Journal of Composites for Construction 6(2): 123-132.

Ferreira, A. J. M., Ribeiro, M. C. S. and Marques, A. T., (2004), "Analysis of hybrid beams composed of GFRP profiles and polymer concrete”, International Journal of Mechanics and Materials in Design 1(2): 143-155.

Ferrier, E., Si Larbi, A., Georgin, J. F. and Ambroise, J., (2012), "New hybrid cement-based composite material externally bonded to control RC beam cracking”, Construction and Building Materials 36(0): 36-45.

fib, (2001). "Design and use of Externally Bonded Fibre Reinforced Polymer for Reinforcement (FRP EBR) for Reinforced Concrete Structures″. Lausanne, Switzerland: International Federation for Structural Concrete (fib), Bulletin 14.

Figeys, W., Verstrynge, E., Brosens, K., Van Schepdael, L., Dereymaeker, J., Van Gemert, D. and Schueremans, L., (2011), "Feasibility of a novel system to prestress externally bonded reinforcement”, Materials and Structures 44(9): 1655-1669.

GangaRao, H. V. S., Taly, N. and Vijay, P. V., (2007), "Reinforced Concrete Design with FRP composites". New York, Taylor & Francis.

Green, M. F., Bisby, L. A., Beaudoin, Y. and Labossière, P., (2000), "Effect of Freeze–thaw Cycles on the Bond Durability Detween Fibre Reinforced Polymer Plate Reinforcement and Concrete", Canadian Journal of Civil Engineering 27: 949-959.

Hejll, A., Täljsten, B. and Motavalli, M., (2005), "Large Scale Hybrid FRP Composite Girders For Use In Bridge Structures-Theory, Test And Field Application", Composites Part B: Engineering 36(8): 573-585.

Helbling, C., Abanilla, M., Lee, L. and Karbhari, V. M., (2006), "Issues of Variability and Durability under Synergistic Exposure Conditions Related to Advanced Polymer Composites in the Civil Infrastructure", Composites Part A: Applied Science and Manufacturing 37(8): 1102-1110.

Hollaway, L. C., (2010), "A Review of the Present and Future Utilization of FRP Composites in the Civil Infrastructure with Reference to their Important In-service Properties", Construction and Building Materials 24(12): 2419-2445.

Hollaway, L. C. and Head, P. R., (2000), "Composite Materials and Structures in Civil Engineering. Comprehensive Composite Materials. K. Editors-in-Chief", Anthony and Z. Carl. Oxford, Pergamon: 489-527.

Homam, S. M., (2000), "Durability of Fibre Reinforced Polymers (FRP) used in Concrete Structures", M.A. Sc. Thesis, Department of Civil Engineering. Toronto, University of Toronto

Honorio, U., Wight R.G., Erki, M.A., (2002), "CFRP Sheets for Strengthening Full-Scale Severely Damaged Concrete Structures", 4th Structural Specialty Conference of the Canadian Society for Civil Engineering Montreal, Quebec, Canada.

ISIS, (2001), "Strengthening Reinforced Concrete Structures with Externally-Bonded Fibre Reinforced Polymers", Design Manual No. 4. Winnipeg, MB, Canada, ISIS Canada Research Network.

Japan Society of Civil Engineers (JSCE), (1997), “Recommendation for Design and Construction of Concrete Structures Using Continuous Fiber Reinforcing Materials”, Concrete Engineering Series No. 23, Tokyo, Japan Society of Civil Engineers.

Ji, C. H., Jefremczuk, S. and Mirza, M.S., (2005), “Design of Reinforced Concrete Elements for Durability Against Corrosion”, First Canadian Conference on Effective Design of Structures - Transferring Research into Practice, Hamilton, Canada.

Ji, C. H., (2003), “Design of Reinforced Concrete Elements for Durability against Corrosion”, M. Eng. Thesis, Department of Civil Engineering and Applied Mechanics, McGill University, Montreal, Canada

Kachlakev, D. and McCurry, D. D., (2000), "Behavior of Full-Scale Reinforced Concrete Beams Retrofitted for Shear and Flexural with FRP Laminates”, Composites Part B: Engineering 31(6–7): 445-452.

Karbhari, V. M. (2007),"Fiber Reinforced Composite Bridge Systems -Transition from the Laboratory to the Field”, Composite Structures 66(1-4): 5-16.

Karbhari, V. M., (2004), “E-Glass/Vinylester Composites in Aqueous Environments: Effects on Short-Beam Shear Strength”, Journal of Composites for Construction 8(2): 148-156.

Karbhari, V. M., Ed., (2007), “Durability of Composites for Civil Structural Applications”, Cambridge, England, CRN Press Woodhead publishing limited.

Karbhari, V. M. and Abanilla, M. A., (2007), "Design factors, reliability, and durability prediction of wet layup carbon/epoxy used in external strengthening”, Composites Part B: Engineering 38(1): 10-23.

Karbhari, V. M., Seible, F., Burgueño, R., Davol, A., Wernli, M. and Zhao, L., (2000), "Structural Characterization of Fiber-Reinforced Composite Short- and Medium-Span Bridge Systems”, Applied Composite Materials 7(2): 151-182.

Karbhari, V. M. and Zhang, S., (2003), "E-Glass/Vinylester Composites in Aqueous Environments – I: Experimental Results”, Applied Composite Materials 10(1): 19-48.

Karbhari, V. M. and Zhao, L., (2000), "Use of Composites for 21st Century Civil Infrastructure", Computer Methods in Applied Mechanics and Engineering 185(2-4): 433-454.

Keller, T., (2003), "Use of Fibre Reinforced Polymers in Bridge Construction", Switzerland, IABSE-AIPC-IVBH ETH Honggerberg, CH-8093 Zurich, Switzerland

Khoe C., F.ASCE, R. S., and Bhethanabotla V. R., (2011) "Oxygen Permeability of Fiber-Reinforced Polymers", ASCE Journal of Composites for Construction. JULY/AUGUST 2011, pp 513-521

Kouadio K. S. P. (2001), "Durability of Fiberglass Composite Sheet Piles in Water", M. Eng. Thesis, Department of Civil Engineering and Applied Mechanics, McGill University, Montreal, Canada.

Kim, H.-Y., Park, Y.-H., You, Y. J. and Moon, C.-K., (2008), "Short-term Durability Test for GFRP Rods under Various Environmental Conditions", Composite Structures 83(1): 37-47.

Konecny, P., Tikalsky P.J. and Tepke D.G., (2007), "Performance Evaluation of Concrete Bridge Deck Affected by Chloride Ingress Simulated-Based Reliability Assessment and Element Modeling", Journal of Transportation Research Board 2028, Washington, D.C.: 6.

Lai, W. L., Kou, S. C., Poon, C. S., Tsang, W. F. and Lai, C. C., (2009), "Effects of Elevated Water Temperatures on Interfacial Delamination, Failure Modes and Shear Strength in Externally-Bonded CFRP-concrete Beams using Infrared Thermography, Gray-scale Images and Direct Shear Test", Construction and Building Materials 23(10): 3152-3160.

Li, L., Shao, Y., and Wu, Z., (2010), "Durability of Wet Bond of Hybrid Laminates to Cast-in-Place Concrete", Journal of Composite Construction, 14(2): 209–216.

Li, L. (2007), "Durability of Wet-Bond between Hybrid FRP Laminate and Cast-In-Place Concrete", Master of Engineering Thesis, Department of Civil Engineering and Applied Mechanics. McGill University, Montreal.

Liao, K., Schultheisz, C. R. and Hunston, D. L., (1999), "Long-term Environmental Fatigue of Pultruded Glass-Fiber-Reinforced Composites under Flexural Loading", International Journal of Fatigue 21(5): 485-495.

Marshall, J. M., Marshall, G. P. and Pinzelli, R. F. (1982), "The Diffusion of Liquids into Resins and Composites", Polymer Composites 3(3): 131-137.

Macía, J.M. and Mirza, M.S., (2012) "Design of Concrete Bridges for Sustainability and Durability", 8th International Conference – Concrete in the Low Carbon Era, Dundee, U.K.

Macia, J. M., (2011), "Design of Concrete Bridges for Sustainability and durability", M. Eng. Thesis, Department of Civil Engineering and Applied Mechanics, McGill University, Montreal, Canada.

McSweeney, B. M. and Lopez, M. M., (2005), "FRP-Concrete Bond Behavior: A Parametric Study through Pull-Off Testing", ACI Special Publication Series SP-230, 7th International Symposium on Fiber Reinforced Polymer Reinforcement for Reinforced Concrete Structures. C. K. Shield. Kansas, Missouri, ACI. 230: 441-460.

Menegotto, M., Monti, G. and Liotta, M. A., (2012), "Prestressed FRP Fabrics for Flexural Strengthening of Concrete", Innovative Materials and Techniques in Concrete Construction. M. N. Fardis, Springer Netherlands: 267-282.

Mirmiran, A., Samaan, M., Cabrera, S. and Shahawy, M. (1998), "Design, manufacture and testing of a new hybrid column", Construction and Building Materials 12 (Compendex): 39-49.

Mirmiran, A. and Shahawy, M. (1997), "Behavior of concrete confined by fiber composites", Journal of structural engineering 123(5): 583-590.

Mirza, M.S., (2013), "A Tentative National Infrastructure Policy For Canada", Canadian Society for Civil Engineering 2013 Annual Conference and General Meeting, Montreal, Canada, May. Paper No. GEN-232.

Mirza, M.S., (2006), "Durability and Sustainability of Infrastructure – A State-of-the-Art Report", National Research Council of Canada, Canadian Journal of Civil Engineering: 33(6), 639-649.

Mirza, M.S., (2007), "Design of Durable and Sustainable Concrete Bridges", Department of Civil Engineering and Applied Mechanics, McGill University, Montreal, Canada. CBM-CI International Workshop, Karachi, Pakistan.

Mirza, M. S.; Jefremczuk, S.; Ji, C., (2005), "Design of Reinforced Concrete Elements for Durability against Corrosion", 1st Canadian Conference on Effective Design of Structures. McMaster University. Hamilton, Ontario, Canada. July 10 – 13.

Mirza, M. S. and Amleh, L., (2004), "Corrosion Response of a Decommissioned Deteriorated Bridge Deck". Journal of Performance of Constructed Facilities, American Society of Civil Engineers (ASCE):18(4), 185 -194

Moy, S., Ed., (2001), "FRP Composites - Life Extension and Strengthening of Metallic Structures", Thomas Telford.

Mufti A. A., (2007), "State-of-the-Art of FRP and SHM Applications in Bridge Structures in Canada", Composites & Polycon, American Composites Manufacturers Association, October 17-19, Tampa, FL USA.

Mufti, A., Onofrei, M., Benmokrane, B., Banthia, N., Boulfiza, M., Newhook, J., Bakht, B., Tadros, G., and Brett, P., (2005), "Studies of Concrete Reinforced with GFRP Specimens from Field Projects", ISIS Canada Research Network Technical Report. Winnipeg, Manitoba, Canada.

Mufti A., Onofrei, M., Benmokrane, B., Banthia N., Boulfiza, M., Newhook, J., Bakht, B., Tadros G., and Brett P., (2005), "Durability of GFRP Reinforced Concrete in Field Structures": SP-230-77, 1361-1378.

Mufti A. A., Bakht B., and Jaeger L. G, (1996), "Bridge Superstructures: New Developments", National Book Foundation, Technology & Engineering, 480.

Mukherjee, A. and Arwikar, S. J., (2007), "Performance of Externally Bonded GFRP Sheets on Concrete in Tropical Environments. Part I: Structural Scale Tests", Composite Structures: 81(1), 21-32.

Nikopour, H., (2012), "Mechanics of Fibre Reinforced Composite Plates: Experiments and Computational Modelling", Ph.D. Thesis, Department of Civil Engineering and Applied Mechanics, McGill University, Montreal.

Nanni, A., Huange, P. C. and Tumialan, J. G., (2001), “Strengthening of Impact-Damaged Bridge Girder Using FRP Laminates” 9th Int. Conference, Structural Faults and Repairs, London, UK, Engineering Technology Press.

Pendhari, S. S., Kant, T. and Desai, Y. M. (2008), "Application of Polymer Composites in Civil Construction: A General Review”, Composite Structures: 84(2), 114-124.

Podolka, L. a. K., J. (2005), “Experience with strengthening structures using the prestress FRP materials”, International Symposium on Bond Behavior of FRP in Structures (BBFS 2005),

Pulngern, T., Chimkhlai, A., Rosarpitak, V. and Sombatsompop, N. (2013), "Analytical, numerical and experimental investigations on flexural strengthening for wood/PVC composite members using flat bar strips”, Construction and Building Materials: 41(0), 545-556.

Purnell, P., Cain, J., van Itterbeeck, P. and Lesko, J., (2008), "Service life modelling of fibre composites: A unified approach”, Composites Science and Technology: 68(15-16), 3330-3336.

Richardson, M. G., (2002), “Fundamentals of Durable Reinforced Concrete”, Modern Concrete Technology 11. Spon Press. Taylor & Francis Group. London.

Robert, M. and Benmokrane, B., (2013), "Combined effects of saline solution and moist concrete on long-term durability of GFRP reinforcing bars”, Construction and Building Materials: 38(0), 274-284.

Rosenboom, O., Walter, C. and Rizkalla, S., (2009), "Strengthening of Prestressed Concrete Girders with Composites: Installation, Design and Inspection”, Construction and Building Materials: 23(4), 1495-1507.

Rosenboom, O. A. and Rizkalla, S. H., (2005), "Fatigue Behavior of Prestressed Concrete Bridge Girders Strengthened with Various CFRP Systems”, Construction and Building Materials 230 (Special Publication): 597-612.

Rousakis, T. C., Karabinis, A. I., Kiousis, P. D. and Tepfers, R. "Analytical modelling of Plastic Behaviour of Uniformly FRP Confined Concrete Members”, Composites Part B: Engineering: 39(7-8), 1104-1113.

Saadatmanesh, H., Tavakkolizadeh, M. and Mostofinejad, D. (2010), "Environmental Effects on Mechanical Properties of Wet Lay-up Fiber-Reinforced Polymer", ACI Material Journal: 107(3), 267-274.

Samaan, M., Mirmiran, A. and Shahawy, M., (1998), "Model of Concrete Confined by Fiber Composites", Journal of Structural Engineering: 124 (Compendex) 1025-1031.

Sarja, A; Vesikari, E., (1996), "Durability Design of Concrete Structures", Report of RILEM Technical Committee 130-CSL. RILEM (The International Union of Testing and Research Laboratories for Materials and Structures), Technical Research Centre of Finland. VTT Building Technology. Espon, Finland. E & FN SPON.

Savastano Jr, H., Santos, S. F., Radonjic, M. and Soboyejo, W. O., (2009), "Fracture and Fatigue of Natural Fiber-Reinforced Cementations Composites", Cement and Concrete Composites: 31(4), 232-243.

Schutte, C. L. (1994), "Environmental Durability of Glass-Fiber Composites", Materials Science and Engineering: R: Reports: 13(7), 265-323.

Setunge, S. (2002), "Review Of Strengthening Techniques Using Externally Bonded Fiber Reinforced Polymer Composites", CRC for Construction Innovation.

Shan, Y. and Liao, K. (2002), "Environmental Fatigue Behavior and Life Prediction of Unidirectional Glass-Carbon/Epoxy Hybrid Composites", International Journal of Fatigue: 24(8), 847-859.

Sheikh, S., Pantazopoulou, S., Bonacci, J., Thomas, M., and Hearn, N., (1997), "Repair of Delaminated Circular Pier Columns with Advanced Composite Materials." Ontario Joint Transportation Research Rep. No 31902. 1, Ministry of Transport, Ontario.

Shao, Y., and Kouadio, S., (2002), "Durability of Fiberglass Composite Sheet Piles in Water." Journal of Composite Construction, 6(4), 280-287.

Shao, Y., Wu, Z.S. and Zhu, H.T., (2005), "FRP-concrete Composite Beams using Wet-bond Technology", Annual Conference of Japan-SAMPE, Tokyo, December, CDROM.

Shao, Y., Wu, Z. S. and Bian, J., (2005), “Wet-Bond between FRP Laminates and Cast-in-Place Concrete”, Proceedings of the International Symposium on Bond Behavior of FRP in Structures (BBFS 2005), International Institute for FRP in Construction.

Silva, M. A. G. (2007), "Aging of GFRP Laminates and Confinement of Concrete Columns”, Composite Structures: 79(1), 97-106.

Sims, G. D. and Broughton, W. R., (2000), “Glass Fiber Reinforced Plastics-Properties. Comprehensive Composite Materials”, K. Anthony and Z. Carl. Oxford, Pergamon: 151-197.

Siva, P., Varma, I., Patel, D. and Sinha, T. (1994), "Effect of Structure on Properties of Vinyl Ester Resins”, Bulletin of Materials Science: 17(6), 1095-1101.

SP Systems, G. U. (2010), "Resin Properties for Composite Materials”, from http://www.azom.com/Details.asp?ArticleID=997.

Springer, C.-H. S. a. G. S. (1977), "Effect of Moisture and Temperature on the Tensile Strength of Composite Materials”, Journal of Composites Materials: 11, 2-16.

Subramaniam, K., Ghosn, M. and Ali-Ahmad, M. (2007), “Impact of Freeze-Thaw Degradation on FRP-Concrete Interface Fracture”. Advances in Construction Materials 2007. C. U. Grosse, Springer Berlin Heidelberg: 419-426.

Van Den Einde, L., Zhao, L. and Seible, F. "Use of FRP Composites in Civil Structural Applications”, Construction and Building Materials: 17(6-7), 389-403.

Walker, R. A. and Karbhari, V. M., (2007), "Durability based design of FRP jackets for seismic retrofit”, Composite Structures: 80(4), 553-568.

Wang, X.-G. and Zhou, C.-Y., (2009), "Calculation of load-carrying capacity of RC beams externally bonded with prestressed composite laminate under sustaining load”, Harbin Gongye Daxue Xuebao/Journal of Harbin Institute of Technology: 41(4), 159-163.

Wight, R. G., Green, M. F. and Erki, M.-A., (2001), "Prestressed FRP Sheets for Post strengthening Reinforced Concrete Beams”, Journal of Composites for Construction: 5(4), 214-220.

Wight, R. G., Green, M. F. and Erki, M. A., (2001), "Prestressed FRP Sheets for Post strengthening Reinforced Concrete Beams", Journal of Composites for Construction: 5(4), 214-220.

Wu, H.-C., Fu, G., Gibson, R. F., Yan, A., Warnemuende, K. and Anumandla, V., (2006), "Durability of FRP Composite Bridge Deck Materials under Freeze-Thaw and Low Temperature Conditions", Journal of Bridge Engineering: 11(4), 443-451.

Wu, Z. and Shao, Y. (2008), "Wet-Bond of Concrete to FRP Framework using Epoxy Adhesive", ACI Spring Convention, Los Angeles, California, USA, American Concrete Institute.

Wu, Z., Yuan, S., Yoshizawa, H. and Kanakubo, T., (2001), "Experimental/Analytical Study on Interfacial Fracture Energy and Fracture Propagation along FRP-Concrete Interface", ACI Spring Convention. Los Angeles, California, USA, American Concrete Institute: SP-201-8, 133-152.

Wu, Z. S., Iwashita, K., Hayashi, K., Higuchi, T., Murakami, S. and Koseki, Y., (2003), "Strengthening Prestressed-Concrete Girders with Externally Prestressed PBO Fiber Reinforced Polymer Sheets", Journal of Reinforced Plastics and Composites: 22(14), 1269-1286.

Yang, D.-S., Park, S.-K. and Neale, K. W., (2009), "Flexural Behaviour Of Reinforced Concrete Beams Strengthened with Prestressed Carbon Composites", Composite Structures: 88(4), 497-508.

Yang, Q.-S., Qin, Q.-H. and Zheng, D. H., (2002), "Analytical and Numerical Investigation of Interfacial Stresses of FRP-Concrete Hybrid Structure", Composite Structures: 57(1-4), 221-226.

Zhou, J., Chen, X. and Chen, S. (2011), "Durability and Service Life Prediction of GFRP Bars Embedded in Concrete under Acid Environment", Nuclear Engineering and Design: 241(10), 4095-4102.

Zhuo, J., Wang, F. and Li, T., (2009), "Application of FRP Strap in an Innovative Prestressed Method", Journal of Materials in Civil Engineering: 21(4), 176-180.

Appendix A: Load-Deflection Curves for Simple Reinforced Beams With FRP Shell

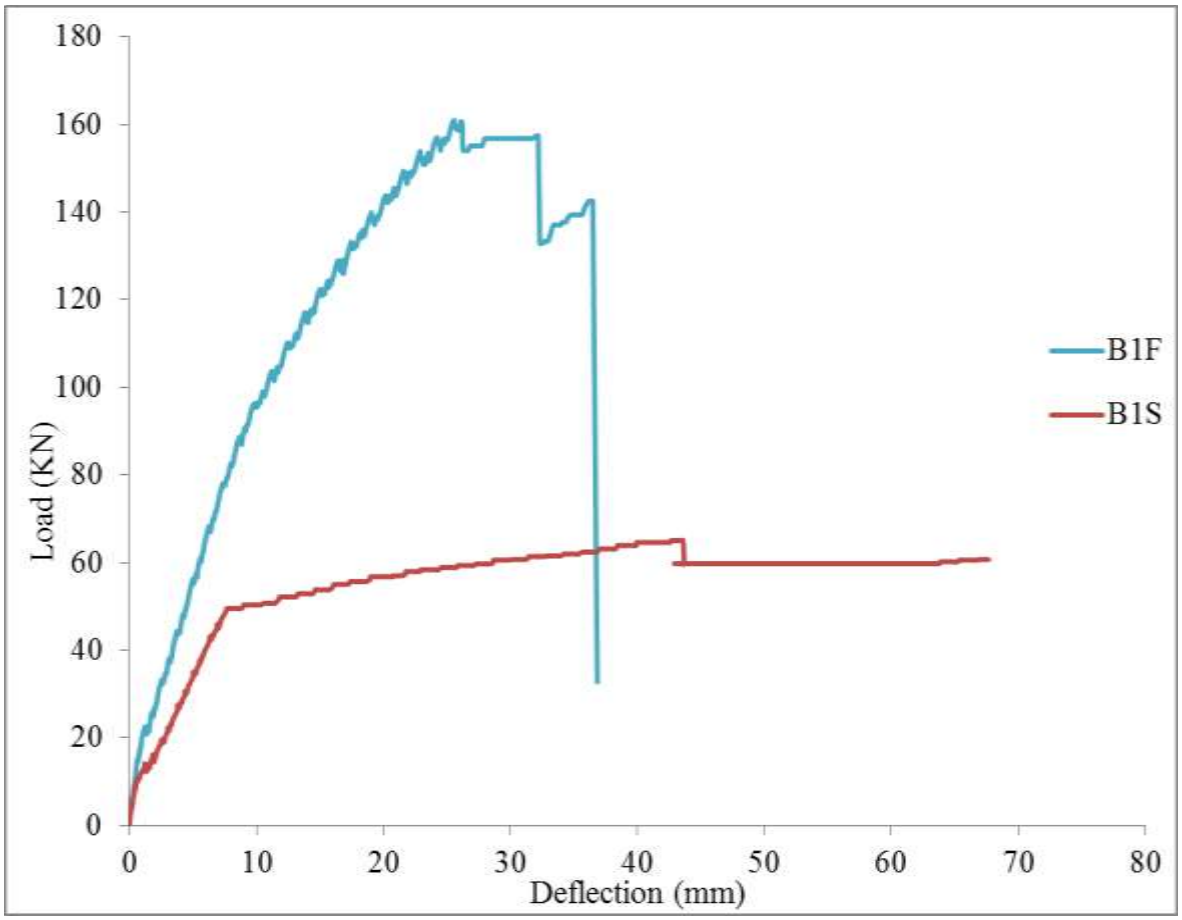

Figure A.1 load-deflection response of simple reinforced beams with FRP shell (Group I)

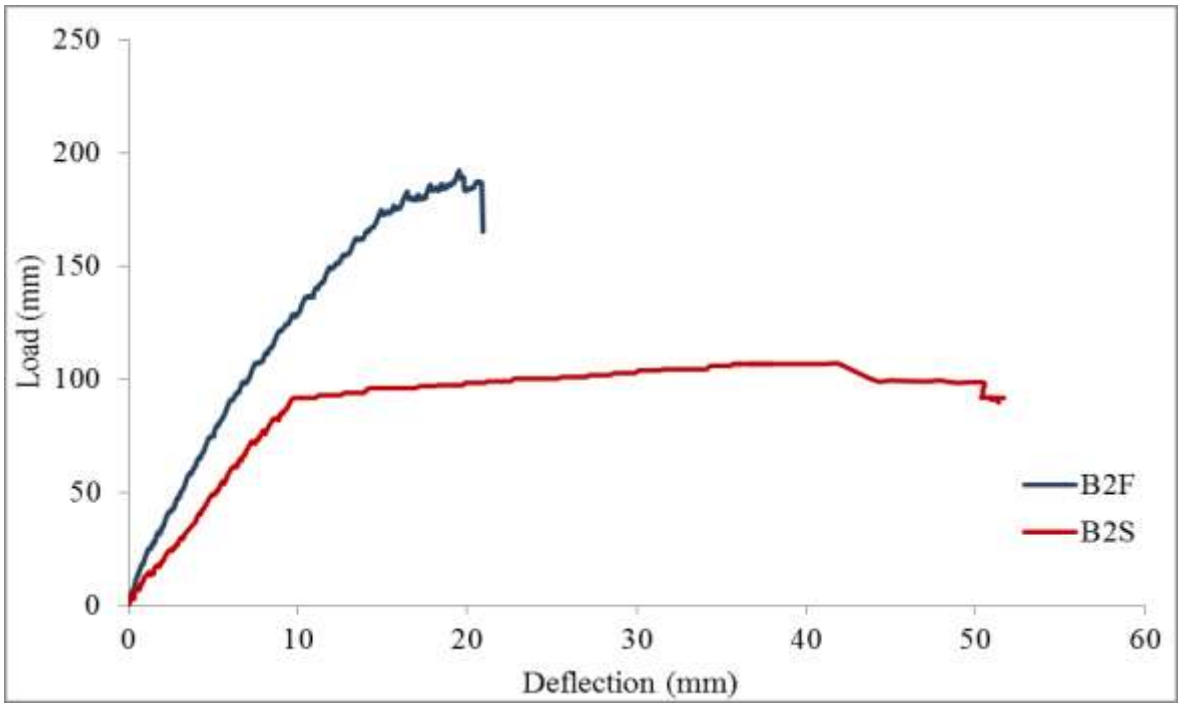

Figure A.2 Load-deflection response of simple reinforced beams with FRP shell (Group II)

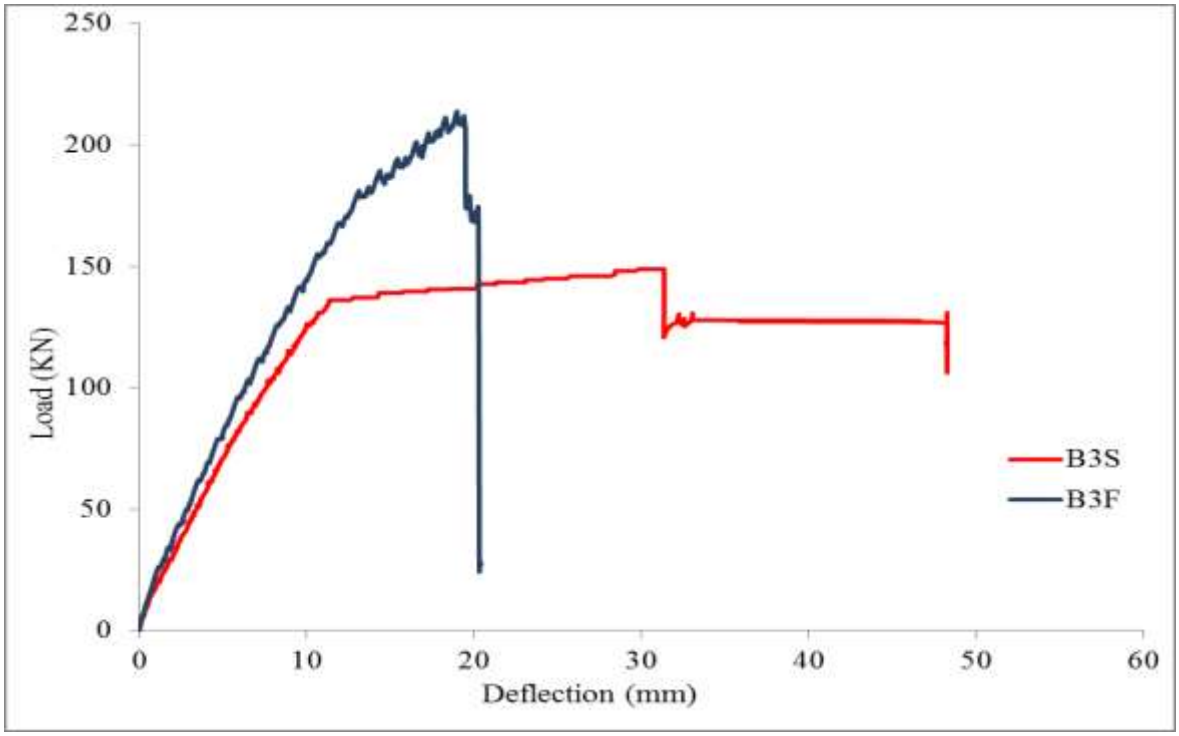

Figure A.3 Load-deflection response of simple reinforced beams with FRP shell (Group III)

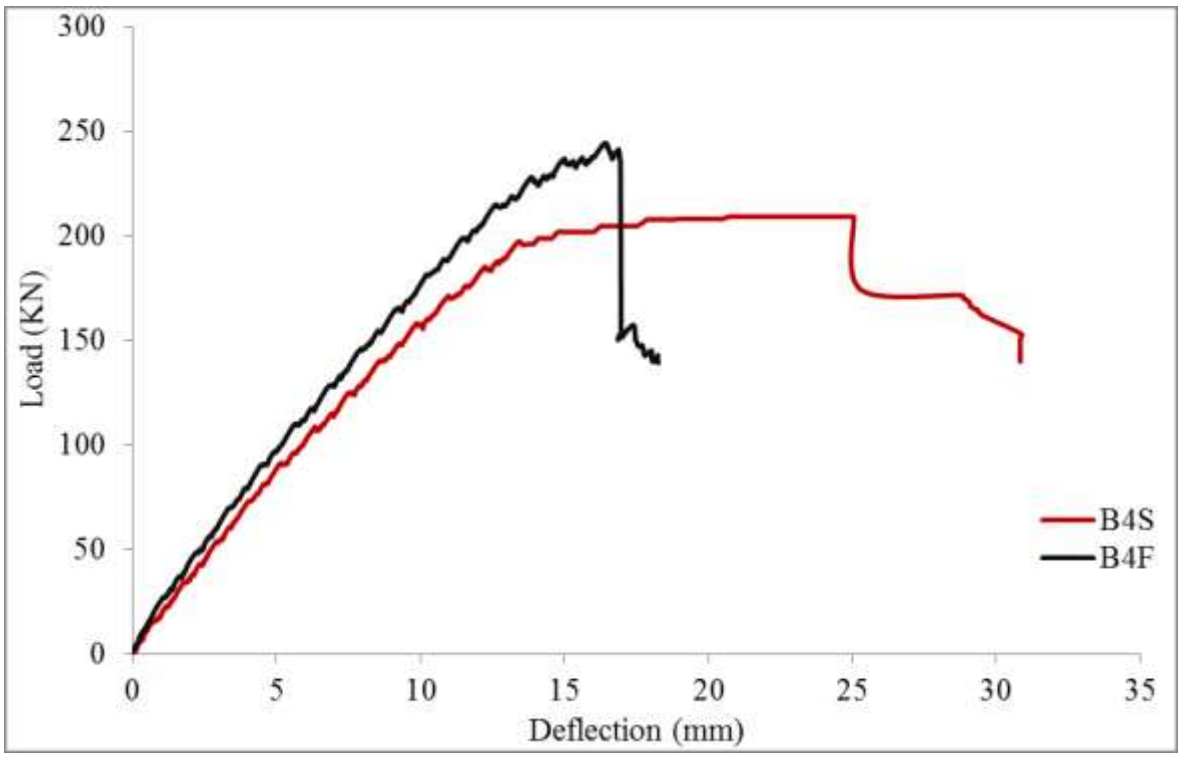

Figure A.4 Load-deflection response of simple reinforced beams with FRP shell (Group IV)

Appendix B: Failure Modes Of Prestressed Concrete Beams with FRP Shell

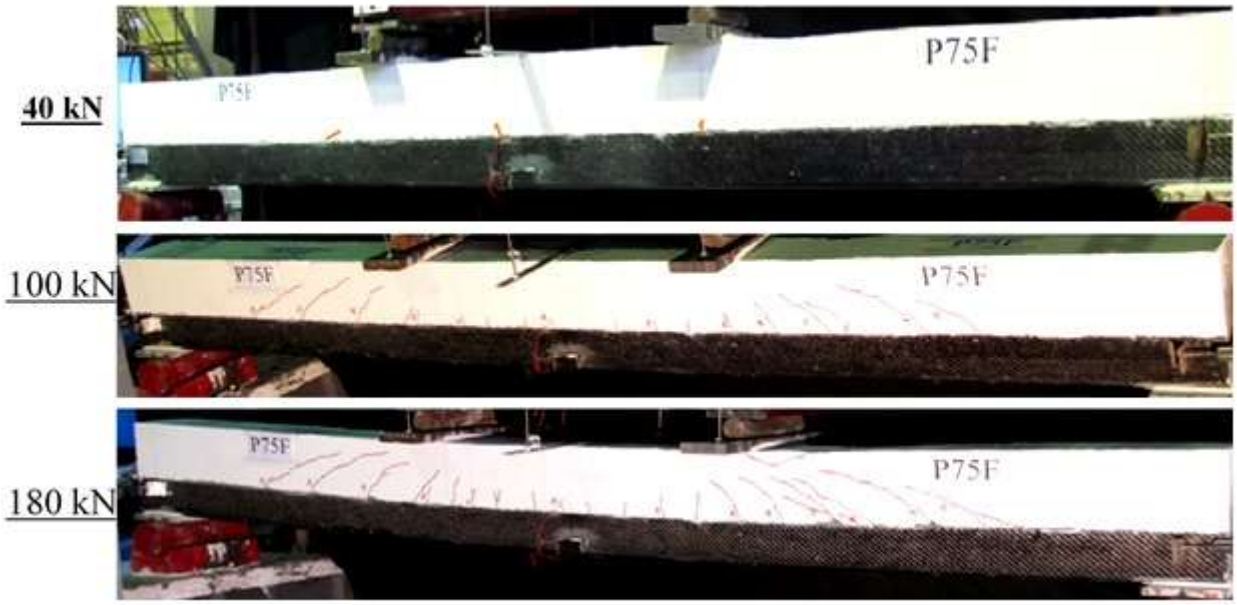

Figure B.1.1 Failure modes of Beam P75F

Figure B.1.2 Failure modes of Beam P100F